Univerzita Karlova v Praze

Přírodovědecká fakulta

Biochemie

RNDr. Kamila Burdová

Studium molekulárních mechanismů udržujících stabilitu genomu

Molecular mechanisms underlying maintenance of genome stability

Disertační práce

Školitel: RNDr. Pavel Janščák, CSc.

Prague, 2014

Declaration:

I declare I wrote this doctoral thesis by myself and all the informational sources and literature are properly cited. The thesis has not been submitted, either whole or in part, for a degree at this or any other university.

Prague, October 21st 2014

Signature:

ACKNOWLEDGEMENT

I would like to thank to all people that have helped me and supported during the years. Foremost, I would like to thank my supervisor, Pavel, for giving me the opportunity to work on interesting research topics in his lab. I appreciate his support and encouragement all the time and valuable discussions. Next, I would like to acknowledge all my colleagues from the lab of genome integrity and the lab of cancer cell biology. Last but not least, I would like to thank to my family and friends, and especially my beloved boyfriend for his endless support and understanding.

ABSTRACT

Cells in our body are challenged every day by DNA damage arising as a result of both endogenous and exogenous insults. The ability of cells to repair DNA lesions is essential for correct propagation of genetic information. The most cytotoxic DNA lesion is DNA double-strand break (DSB) while oxidative DNA damage is one of the most frequent lesions. The aim of this thesis was to improve current the knowledge of the molecular mechanisms underlying the repair of DSBs and oxidative DNA damage.

The major source of oxidative damage in cells are reactive oxygen species that are constantly generated as by-products of cell metabolism. One of the most frequent lesions is 7,8-dihydro-8-oxo-guanine (8-oxo-G) that gives rise to 8-oxo-G:A mispairs during DNA replication and if left unrepaired, results in accumulation of DNA mutations. We found that Werner helicase (WRN) physically interacts with DNA polymerase λ (Polλ) and stimulates DNA gap-filling by Polλ opposite to 8-oxo-G followed by strand displacement synthesis in MutY DNA glycosylase homolog (MUTYH) initiated base excision repair (BER) of 8-oxo-G:A mispairs.

There are two major pathways involved in repair of DSBs: homologous recombination (HR) and non-homologous end joining (NHEJ). NHEJ is highly error-prone while HR is error-free. There are two subpathways of HR, namely synthesis-dependent strand annealing (SDSA) and canonical double strand break repair (DSBR). DSBR results in both crossovers (CO) and non-crossover (NCO) products while SDSA yields only NCOs. Undesired CO formation may lead to chromosomal rearrangements and loss of heterozygosity. Thus, in mitotic cells, majority of HR events proceed via SDSA to avoid crossing-over.

The molecular mechanism underlying promotion of SDSA is not well studied in human cells. RECQ5 and FBH1 have been suggested to be functional orthologs of Srs2 helicase that promotes SDSA in yeast cells. We have demonstrated that RECQ5 can prevent illegitimate RAD51 nucleofilament formation during post-synaptic phase of SDSA to promote formation of NCO products. Thus we propose that RECQ5 is the functional ortholog of Srs2 in human cells.

In yeast, Exonuclease 1 (Exo1) and Dna2 in conjunction with Sgs1 represent two separate pathways of long-range DNA end resection. In human cells, Bloom helicase (BLM) has been suggested to cooperate with DNA2 to mediate long-range resection. We were

able to show that DNA2 cooperates with either BLM or WRN in human cells to mediate this process. In addition, our experiments suggest that BLM promotes DNA end resection in complex with TopIIIα-RMI1-RMI2.

Activation of *Ataxia telangiectasia* and Rad3 related (ATR) kinase upon DSB induction depends on DNA end resection. We have identified the mismatch recognition complex MSH2-MSH3 as a component of the ATR signalling pathway. We have shown that MSH2-MSH3 is recruited to sites of DSBs in a DNA end resection dependent manner and promotes DSB repair by HR. Moreover, our results suggest that the MSH2-MSH3 complex binds to DNA hairpin structures in replication protein A-coated ssDNA and recruits the ATR-ATRIP complex hence stimulating ATR activation and DNA repair.

ABSTRAKT

Buňky v našem těle jsou každý den vystaveny poškození DNA vlivem endogenních a exogenních faktorů. Schopnost buněk opravit poškozenou DNA je důležitá pro zachování genetické informace. Mezi nejvíce cytotoxické DNA léze patří dvojvláknové zlomy DNA. Oxidační poškození DNA je jednou z nejčastějších lézí. Cílem této práce bylo prohloubit stávající znalosti molekulárních mechanismů opravy dvojvláknových zlomů DNA a oxidačního poškození DNA.

Hlavním zdrojem oxidačního poškození buněk jsou reaktivní formy kyslíku, které jsou neustále generovány jako vedlejší produkty buněčného metabolismu. Jednou z nejčastěji vznikajících modifikací DNA je 7,8-dihydro-8-oxo-guanin (8-oxo-G), jež se během replikace chybně páruje s adeninem. Pokud toto poškození není opraveno, dochází k akumulaci bodových mutací. Oxidační poškození DNA je opravováno převážně vystřižením porušené báze, tzv. „base excision repair“ (BER). Při odstranění špatně inkorporovaného adeninu oproti 8-oxo-G dochází v prvním kroku k jeho vystřižení MutY DNA glykosylázou (MUTYH). Naše výsledky ukazují, že v následném kroku tohoto procesu opravy DNA WRN helikáza (WRN) fyzicky interaguje s polymerázou λ a stimuluje správné přiřazení cytosinu oproti 8-oxo-G a následnou syntézu DNA vedoucí k opravě poškozené DNA.

Oprava dvojvláknových zlomů DNA má dvě hlavní větve: homologní rekombinaci (HR) a nehomologní spojování konců (tzv. non-homologous end-joining, NHEJ). Zatímco HR je téměř bezchybný proces, NHEJ je proces vysoce náchylný k chybám. V rámci HR existují dvě paralelní dráhy, a to tzv. „synthesis-dependent strand-annealing“ (SDSA) a kanonická oprava dvojvláknových zlomů DNA (DSBR). Zatímto výsledkem DSBR může být tzv. „crossover“ (CO), kdy dochází k výměně části DNA mezi sesterskými chromatidami, nebo „non-crossover“ (NCO), kdy k této výměně nedochází, v případě SDSA jsou produkty vždy NCO. Tvorba CO je nežádoucí, protože může vést k přesmykům v chromozomech a ztrátě heterozygotnosti. V mitotických buňkách proto většina oprav probíhá mechanismem SDSA.

Molekulární podstata procesu, který napomáhá SDSA oproti DSBR není v lidských buňkách dobře prostudována. Lidské helikázy RECQ5 a FBH1 byly navrženy jako funkční orthology Srs2 helikázy, která podporuje SDSA v kvasinkách. Zjistili jsme, že RECQ5 helikáza dokáže zabránit nelegitimní tvorbě RAD51 nukleofilamentu během post-synaptické fáze

SDSA a tím podporuje tvorbu NCO produktů. Na základě tohoto zjištění navrhujeme, že funkčním orthologem Srs2 v lidských buňkách je práve RECQ5 helikáza.

V kvasinkách existují dvě oddělené dráhy resekce DNA závisející na exonukleáze 1 (Exo1) a Dna2 ve spojení s Sgs1. V lidských buňkách byla navržena Bloom (BLM) helikáza jakožto funkční ortholog Sgs1 helikázy spolupracující s DNA2 v tomto procesu. Naše výsledky ukazují, že DNA2 může spolupracovat v lidských buňkách jak s BLM, tak i s WRN helikázou. Další experimenty naznačují, že BLM helikáza je v tomto procesu vázána v komplexu s TopIIIα-RMI1-RMI2.

Aktivace *Ataxia telangiectasia* and Rad3 related (ATR) kinázy po indukci dvojvláknových zlomů v buňce je závislá na resekci DNA. Během našeho výzkumu jsme identifikovali MSH2-MSH3 komplex jako součást signální dráhy ATR. Ukázali jsme, že MSH2-MSH3 se váže na konce dvojvláknových zlomů DNA v závislosti na resekci a stimuluje opravu těchto dvojvláknových zlomů DNA homologní rekombinací. Naše výsledky naznačují, že MSH2-MSH3 komplex se váže na sekundární struktury přítomné v jednovláknové DNA i po navázání replikačního proteinu A a rekrutuje ATR-ATRIP komplex, čímž stimuluje aktivaci ATR a opravu DNA.

LIST OF PUBLICATIONS

Involvement of Werner syndrome protein in MUTYH-mediated repair of oxidative DNA damage.

Kanagaraj R, Parasuraman P, Mihaljevic B, van Loon B, Burdova K, König C, Furrer A, Bohr VA, Hübscher U, Janscak P.

Nucleic Acids Res. 2012 Sep 1; 40(17):8449-59.

IF: 8.808

Human RECQ5 helicase promotes repair of DNA double-strand breaks by synthesis-dependent strand annealing.

Paliwal S, Kanagaraj R, Sturzenegger A, Burdova K, Janscak P.

Nucleic Acids Res. 2014 Feb; 42(4):2380-90. doi: 10.1093/nar/gkt1263.

IF: 8.808

DNA2 cooperates with the WRN and BLM RecQ helicases to mediate long-range DNA-end resection in human cells.

Sturzenegger A*, Burdova K*, Kanagaraj R, Levikova M, Pinto C, Cejka P, Janscak P.

J Biol Chem. 2014 Sep 26;289(39):27314-26. doi: 10.1074/jbc.M114.578823.

IF: 4.651

A role for the mismatch-binding factor MutSβ as a mediator of ATR activation in response to DNA double-strand breaks.

Burdova K*, Mihaljevic B*, Janscak P

Mol Cell, submitted

IF: 14.464

* equal contribution

TABLE OF CONTENTS

List of Abbreviations

8-oxo-G	7,8-dihydro-8-oxo-guanine
AP site	abasic site
Alt-NHEJ	alternative end-joining
ATR	Ataxia telangiectasia and Rad3 related
ATM	Ataxia telangiectasia mutated
BER	base excision repair
BLM	Bloom helicase
BS	Bloom syndrome
CPT	camptothecin
CO	crossover
DNA	Deoxyribonucleic acid
D-loop	displacement loop
DNA-PKcs	DNA-protein kinase catalytic subunit
dHJ	double Holliday junction
dsDNA	double-stranded DNA
DSB	double-strand break
DSBR	double-strand break repair
EXO1	Exonuclease 1
FEN1	Flap endonuclease 1
HRDC	helicase and RNase D C-terminal
HR	homologous recombination
MMEJ	microhomology-mediated end-joining
MMR	mismatch repair
MRN	MRE11-RAD50-NBS1
MRX	Mre11-Rad50-Xrs2
MLH	MutL homolog
MSH	MutS homolog
MUTYH	MutY glycosylase homolog
NCO	non-crossover

NHEJ	non-homologous end-joining
Polß	DNA polymerase β
Polλ	DNA polymerase λ
PCNA	proliferating cell nuclear antigen
9-1-1	RAD9-HUS1-RAD1
RQC	RecQ C-terminal
RPA	Replication protein A
SSA	single strand annealing
SSB	single-strand break
ssDNA	single-stranded DNA
SCE	sister chromatid exchange
SF	superfamily
SDSA	synthesis-dependent strand annealing
Top3	topoisomerase 3
TopIIIa	topoisomerase IIIα
WRN	Werner helicase
WS	Werner syndrome

1 INTRODUCTION

Each cell in our body is everyday challenged by multiple deoxyribonucleic acid (DNA) damaging insults coming from both endogenous and exogenous sources. Endogenously, DNA damage comes from replication errors and oxygen radicals created by the cell metabolism. Exogenous sources include UV light, X-ray irradiation and genotoxic chemicals (Figure 1).

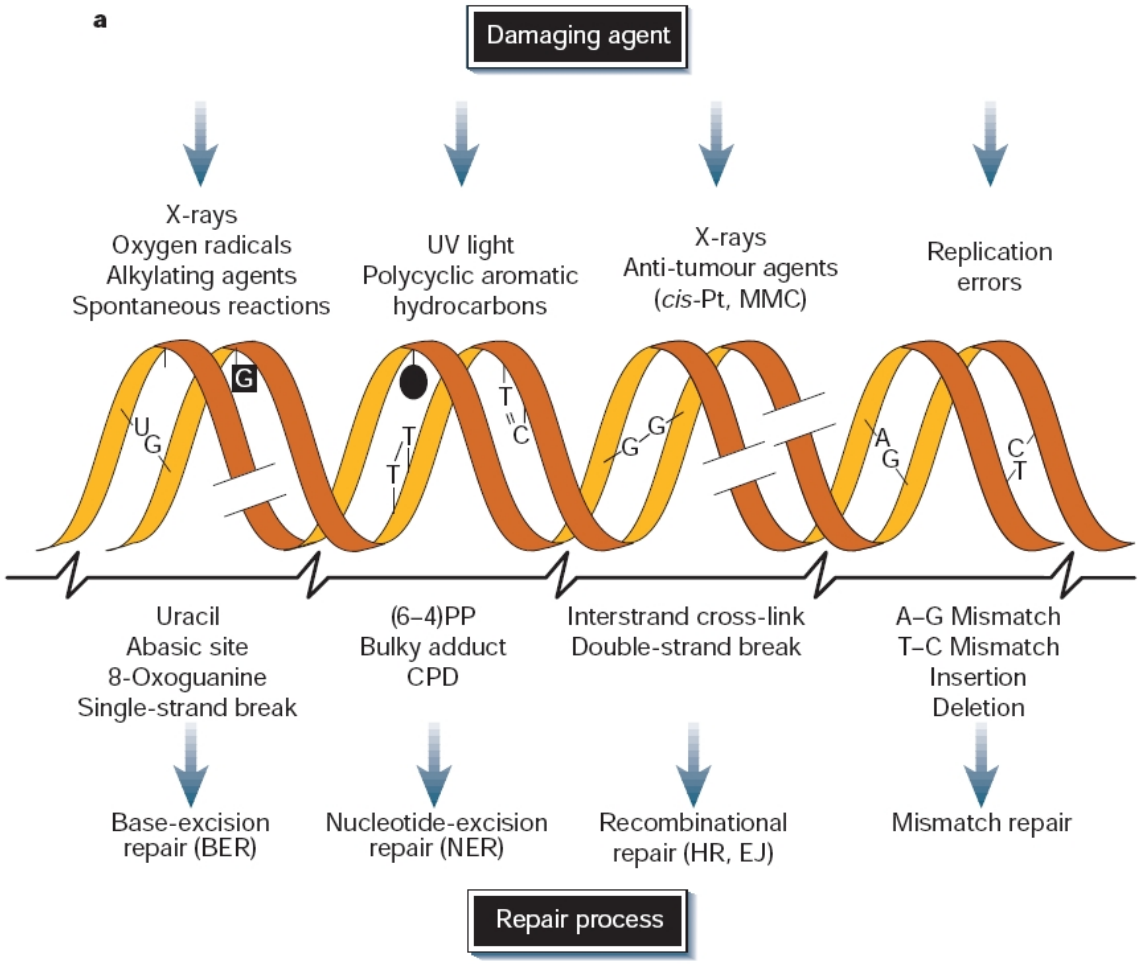

Figure 1. Common sources of DNA damage, types of DNA lesions and DNA damage repair pathways overview. Adapted from (Hoeijmakers, 2001).

DNA lesions can be divided to subgroups depending on their nature. These involve damage of single bases or nucleotides, crosslinks and single and double strand breaks. There are different DNA repair mechanisms dealing with different types of DNA damage. These mechanisms are highly conserved from bacteria to mammals (Hoeijmakers, 2001).

Eukaryotic cells respond to DNA damage by multiple mechanisms that influence the cell in short term and long term. In short term, cells inhibit DNA metabolism such as transcription, replication and chromosome segregation. In longer perspective, there is barrier for cells not to divide with damaged DNA. This mechanism called cell cycle checkpoint is activated by DNA damage at different stages of the cell cycle and leads to transient or permanent cell cycle arrest (senescence). If the cell is not capable of repair and DNA lesion persists, it would undergo apoptosis and thus be eliminated from the organism. If all these mechanisms fail, then cells would divide even in presence of DNA damage leading to undesired mutations and chromosomal aberrations inherited by daughter cells. These can subsequently lead to cancer or accelerate the onset of aging (Hoeijmakers, 2001).

1.1 Mismatch Repair

One of the most important DNA repair systems in the cell is mismatch repair (MMR) that deals mainly with replication errors such as adenine-guanine and thymidine-cytosine mismatches, and insertion – deletion loops (Jiricny, 2006). Mismatch repair is a multistep process involving mismatch recognition, excision, DNA resynthesis and ligation (Figure 2).

In the bacterium *Escherichia coli*, MutS homodimer binds to mismatch and recruits MutL homodimer that further recruits other factors needed to excise damaged DNA, fill-in the resulting DNA gap and ligate back to produce intact DNA molecule. In eukaryotes, five different MutS homologues (MSH) have been identified. Of these, MSH2, MSH3 and MSH6 were found to be present in heterodimeric complexes involved in the recognition of DNA lesions. Substrate specificities of these complexes are different but overlapping. MSH2-MSH3 complex (also named MutSβ) binds to loops of 1-14 extrahelical nucleotides while MSH2-MSH6 complex (also named MutSα) binds to base-base mismatches and single- and double-base insertions (Figure 2). All the MSH proteins are ATPases containing Walker ATP-binding motifs at their C-terminus. Nucleotide binding to MutS complexes is dispensable for binding to DNA substrates (DNA lesions) but necessary to proceed to further steps of DNA repair. Upon ATP binding, MutSα is released from the substrate and works as sliding clamp along the DNA. Only ATP binding but not hydrolysis is needed for this process (Jiricny, 2006).

MutL homologues (MLH) belong to gyrase/Hsp90/histidine-kinase/MutL (GHKL) family of ATPases with ATPase domain situated to its N-terminus and heterodimerization domain at their C-terminus. In humans, four different MLH proteins have been identified: MLH1, MLH3, post-meiotic segregation protein-1 (PMS1) and PMS2 that form 3 different heterodimers: MLH1-MLH3 (MutLγ), MLH1-PMS1 (MutLβ) and MLH1-PMS2 (MutLα). Of these the MLH1-PMS2 heterodimer is of the most importance (Jiricny, 2006).

The other factors needed for mismatch repair include homotrimeric proliferating cell nuclear antigen (PCNA), DNA polymerase δ and/or DNA polymerase ε and exonuclease 1 (EXO1).

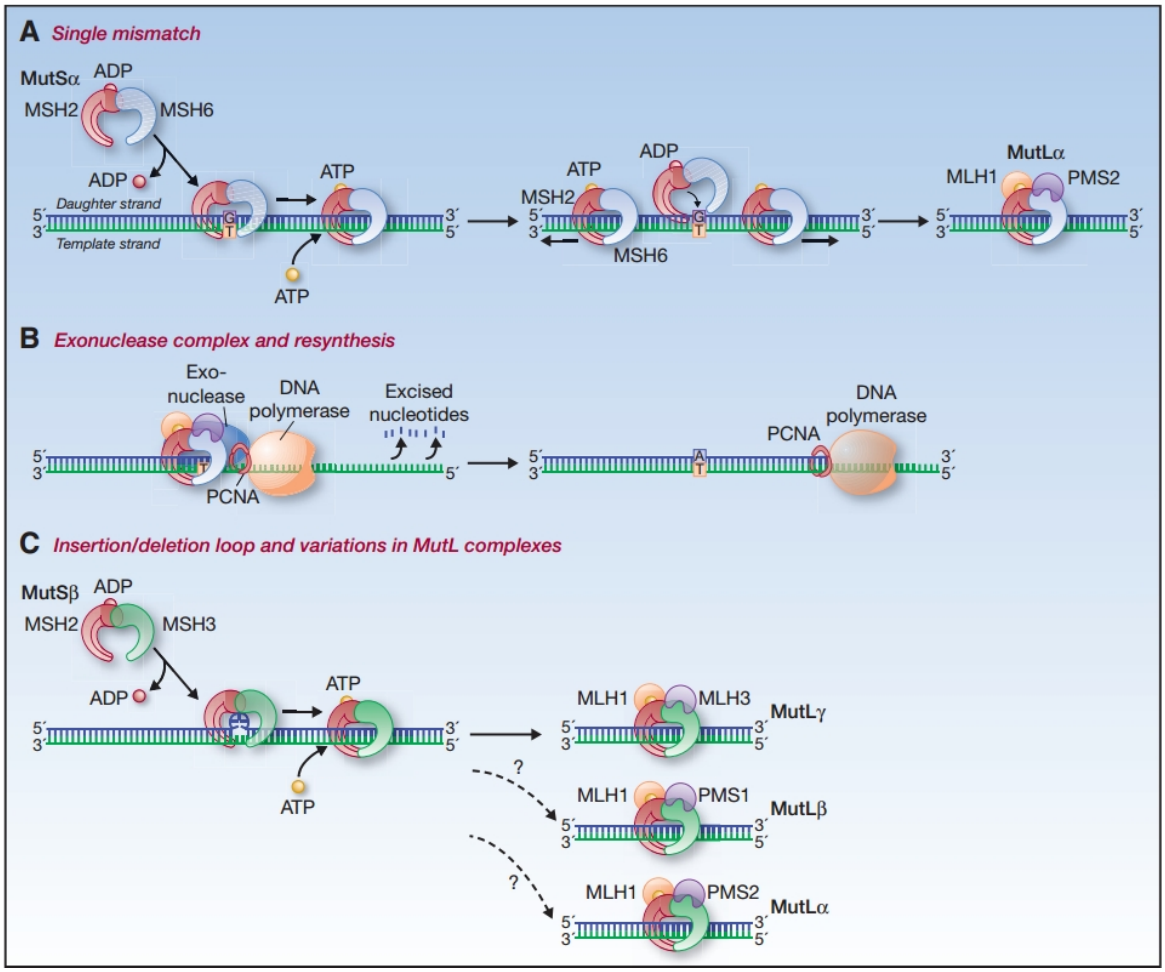

Figure 2. Protein complexes involved in mismatch repair in human cells. A. Mechanism of recognition of single mismatches by MutSα. After binding of MutSα to mismatched DNA, ATP is exchanged for ADP creating sliding clamp around the DNA. The MutSα complex is then bound by the MLH1-PMS2 (MutLα) complex B. Excision step of mismatch repair occurs when MMR protein sliding clamp interacts with exonuclease-1, proliferating cell nuclear antigen (PCNA), and DNA polymerase. The complex it released from

the DNA and resynthesis occurs. C. Mechanism of recognition of insertion-deletion loops by MutSβ showing potential interaction with MutL complexes. Adapted from (Sinicrope and Sargent, 2012).

Interestingly, the mismatch repair proteins MSH2, MSH3, MSH6 and MLH1 have been shown to be involved in the cellular response to DNA double strand breaks as they rapidly accumulate at sites of DNA damage caused by laser micro-irradiation (Hong et al., 2008; Liberti et al., 2010). As expected from canonical mismatch repair, MLH1 recruitment was found to be dependent on MSH2 (Jiricny, 2006). Experiments with *Msh2 -/-* mouse embryonic fibroblasts have shown potential role of MSH2 in homologous recombination (Bennardo et al., 2009). Moreover, MSH2 and MSH3 deficient cells were found to be more sensitive to DNA damage causing agents such as cis-platin, camptothecin and olaparib (Franchitto et al., 2003; Pichierri et al., 2001; Takahashi et al., 2011).

1.2 Base Excision Repair

Base excision repair (BER) is used when single base in DNA is damaged (e.g. alkylation, oxidation or deamination) and this base lesion is not distorting the DNA. More bulky base lesions that distort DNA helix are repaired by different mechanism called nucleotide excision repair.

First step of BER involves removal of damaged base by specific DNA glycosylase to create abasic site (AP site) in DNA and the phosphodiester bond 3’ or 5’ to the AP site is hydrolysed (Jacobs and Schar, 2012). This hydrolysis is catalysed by AP endonuclease 1 (APE1) or by DNA glycosylase itself if it possesses also AP lyase activity (such as OGG1) and leads to creation of e DNA single-strand break. There are at least two sub-pathways of BER that differ in the length of repaired DNA (Figure 3). In short-patch BER, only 1 nucleotide is replaced, while in long-patch BER, more than two nucleotides are replaced (Fortini and Dogliotti, 2007).

During short-patch BER, DNA polymerase β removes the sugar moiety through an associated lyase activity and incorporates one nucleotide to fill in the DNA gap. DNA ends are then ligated by Ligase III – XRCC1 complex. Strand displacement synthesis in long-patch BER is catalysed by DNA polymerase β, δ or ε along with PCNA, resulting 5’ flap is cleaved by flap endonuclease 1 (FEN1) and DNA is sealed by ligase I. The molecular mechanism

underlying the choice of long versus short patch BER is not fully understood but long-patch BER is known to be preferred if sugar moiety is also damaged (Fortini and Dogliotti, 2007).

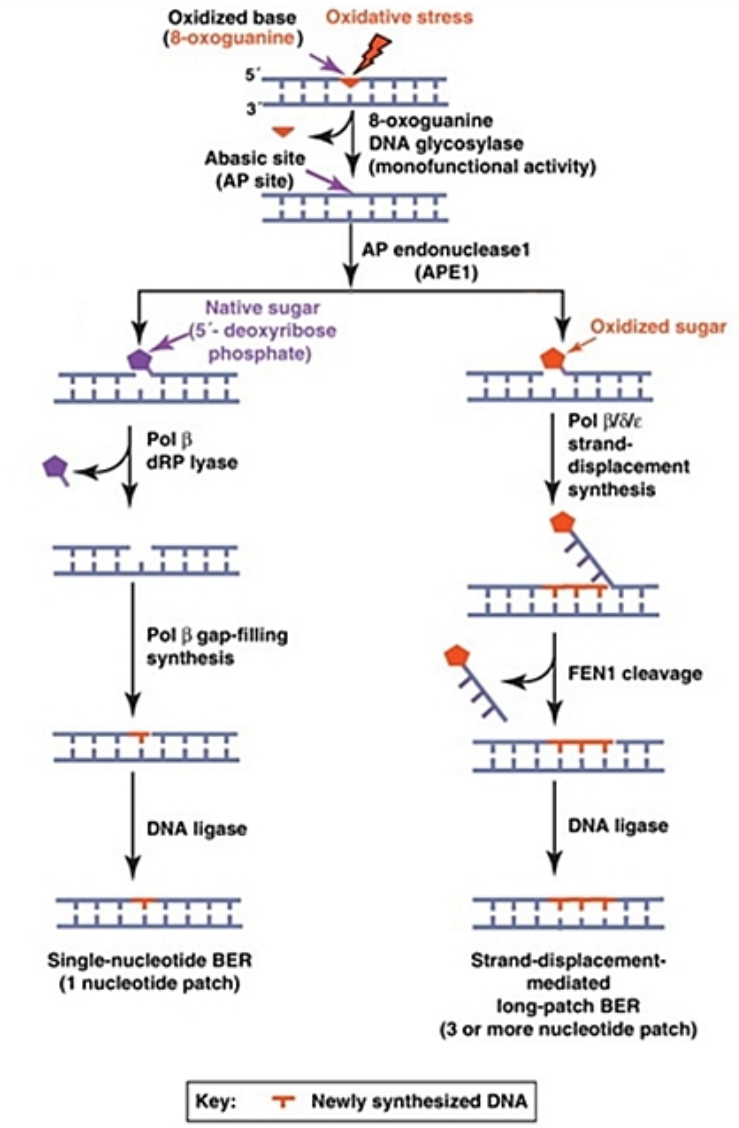

Figure 3. Scheme of long-patch and short-patch subpathways of base excision repair (BER). Oxidized base is excised by specific DNA glycosylase creating abasic site. The phosphodiester bond 3' or 5' to the AP site is hydrolysed. During short-patch BER, DNA polymerase β (Polβ) removes the sugar moiety, incorporates one nucleotide to fill in the DNA gap and DNA is ligated. Strand displacement synthesis in long-patch BER is catalysed by DNA polymerase β, δ or ε along with PCNA, resulting 5' flap is cleaved by flap endonuclease 1 (FEN1) and DNA is sealed by ligase I. Adapted from (Liu and Wilson, 2012).

Reactive oxygen species that are generated as by-products of cellular metabolism in living organisms or after exposure of organism to various agents attack DNA creating variety of oxidized DNA bases that are highly mutagenic due to possible mispairing during replication. One of the most common lesions is 7,8-dihydro-8-oxo-guanine (8-oxo-G) with

steady state level of about 10^3 lesions per cell per day in normal tissue (Klungland et al., 1999). If unrepaired, replication of DNA with these lesions frequently lead to 8-oxo-G:A mispair formation and subsequent G:C and T:A transversion mutations (Avkin and Livneh, 2002). Oxidized base lesions are predominantly repaired by BER (Hazra et al., 2007).

In human cells, 8-oxo-G:A mispairs are repaired by two subsequent BER events (van Loon et al., 2010). In the first step, excision of mispaired A base by MutY glycosylase homolog (MUTYH) in reaction coordinated with PCNA occurs and is followed by cleavage of AP site by APE1 (Hayashi et al., 2002; Takao et al., 1999; van Loon et al., 2010; Yang et al., 2001). Next, DNA polymerase λ (Polλ) incorporates dCTP opposite to 8-oxo-G site in the presence of PCNA and replication protein A (RPA) with subsequent strand-displacement synthesis. The resulting 5' ssDNA strand flap is cleaved by FEN1 that is recruited to the site of damage by. Finally, the nick in DNA generated by FEN1 cleavage is sealed by Ligase I (Maga et al., 2008; Maga et al., 2007; van Loon et al., 2010). 8-oxo-G:C mispair is predominantly recognized and 8-oxo-G is excised by OGG1 glycosylase during short patch BER event (Hazra et al., 2007).

1.3 Double Strand Break Repair

There are two major pathways involved in double strand break (DSB) repair: non-homologous end joining (NHEJ) and homologous recombination (HR) (Figure 4). Binding of MRE11- RAD50-NBS1/Xrs2 (MRN/X) complex to ends of DSB is the first step of DSB repair and is common to all pathways (Lisby et al., 2004). Following steps differ in each pathway and usually inhibit each other.

1.3.1 Non-Homologous End-Joining

In general, non-homologous end-joining involves direct ligation of free DNA ends or small alterations of DNA ends (excision and/or synthesis) prior to ligation if they cannot be directly re-ligated (Lieber, 2010; van Gent and van der Burg, 2007). Firstly KU70-KU80 heterodimer binds to DNA ends preventing their degradation and recruits DNA-protein kinase catalytic subunit (DNA-PKcs) forming DNA-PK holoenzyme and other end processing enzymes, such as Artemis, polynucleotide kinase, and terminal deoxynucleotidyl transferase (Lieber, 2010). The ligation step is performed by Ligase IV in complex with XRCC4 and XLF (Lieber, 2010; van Gent and van der Burg, 2007).

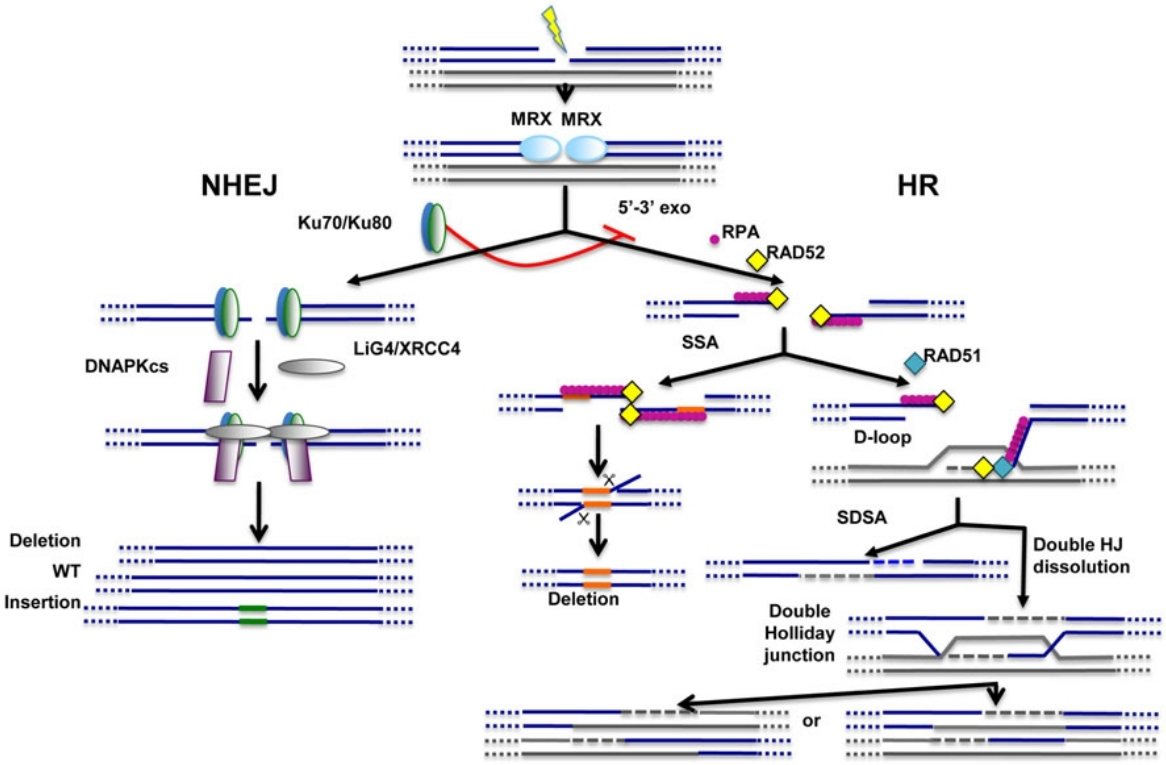

Figure 4. Major double-strand break repair pathways: Non-homologous end-joining (NHEJ) and homologous recombination (HR). MRE11/RAD50/XRS2 (MRX) complex is recruited at DNA ends. Ku70/Ku80 heterodimer is required for NHEJ and by inhibition of DNA end resection represses HR. 5'-3' resection is the first step of HR producing ssDNA that is coated by replication protein A (RPA). Single strand annealing (SSA) occurs only if direct repeats are present around the site of DSB resulting in loss of DNA. Further steps of HR involve exchange of RPA for RAD51, homology search and strand invasion. Two subpathways of HR represent synthesis-dependent strand annealing (SDSA) and canonical double-strand break repair. Adapted from (Decottignies, 2013).

Over last years, new pathway called alternative end-joining (alt-NHEJ) and microhomology-mediated end joining (MMEJ) were discovered and proven to play role in double-strand break repair in vivo (Decottignies, 2013; Mladenov and Iliakis, 2011). Both these pathways are repressed by KU70-KU80 heterodimer and involve 5' to 3' DNA end resection catalysed by MRN complex with CtIP and/or EXO1 (Figure 5). MMEJ needs presence of short homologous regions (microhomologies) around the site of DSB that are used for annealing. If annealing is stable, flap trimming, fill-in DNA synthesis and ligation occurs. Ligation in MMEJ is catalysed by Ligase III-XRCC1 complex (McVey and Lee, 2008; Mladenov and Iliakis, 2011). Alt-NHEJ pathway is not dependent on the presence of microhomologies and involves PARP-1, XRCC1 and Ligase I or Ligase III (Decottignies, 2013).

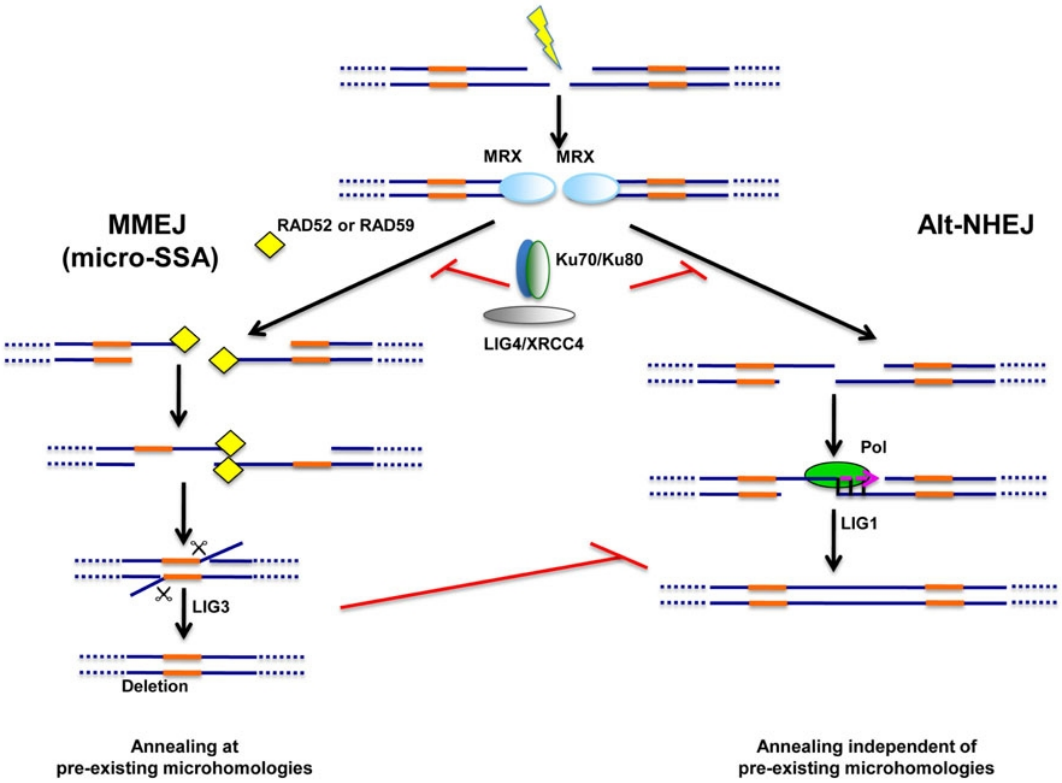

Figure 5. Alternative end joining pathways. Microhomology-mediated end-joining (MMEJ), relies on pre-existing microhomologies around the site of DSB. Mechanism of MMEJ is related to SSA. The second alternative pathway (Alt-NHEJ) does not require the presence microhomologies. Both these pathways are repressed by the NHEJ machinery (Ku70-Ku80, LigaseIV-XRCC4). The MRX complex is supposed to play important role in the initial DNA end trimming. Adapted from (Decottignies, 2013).

1.3.2 Homologous Recombination

Homologous recombination (HR) is most commonly used during replication promoting replication fork restart or one-ended DSB repair. However it is also used for repair of two-ended double strand breaks (Petermann and Helleday, 2010). HR begins with 5' to 3' DNA end resection mediated by MRN complex in conjunction with CtIP (Longhese et al., 2010; Sartori et al., 2007). The length of resected DNA is up to 100bp (Symington and Gautier, 2011). After this initial end trimming, which inhibits NHEJ, there is second step of resection (long range resection) that is in done by EXO1 exonuclease or by joint action of DNA2 endonuclease and a RecQ family helicase. In budding yeast the RecQ helicase Sgs1 exists in complex with Top3-Rmi1 (Cejka et al., 2010a; Mimitou and Symington, 2008; Nimonkar et al., 2011; Niu et al., 2010; Zhu et al., 2008). In human cells it has been suggested that Bloom helicase (BLM) is the Sgs1 ortholog mediating long range resection

as this protein interacts with the TOPIIIα-RMI1-RMI2 complex (Nimonkar et al., 2011). However in *Xenopus laevis* model organism, it has been shown that xWRN helicase interacts with DNA2 and promotes resection of DNA ends *in vitro* (Liao et al., 2008; Toczylowski and Yan, 2006; Yan et al., 2005). Resection of DNA yields long stretches of single stranded DNA (ssDNA) that need to be protected from nucleases. This is accomplished by binding of trimeric replication protein A (RPA) to these structures (San Filippo et al., 2008). RPA is then exchanged with help of BRCA2 for RAD51 recombinase forming RAD51-nucleofilament that conducts the search for homologous DNA sequence and catalyses the invasion to the donor sister chromatid at the site of homology, resulting in the formation of a joined DNA molecule termed displacement (D) -loop (Thorslund et al., 2010). When homologous sequence is found and annealing is stable, synthesis of DNA is primed by the invading DNA strand and repair synthesis takes place forming extended D-loop (San Filippo et al., 2008).

This structure can be resolved by two distinct mechanisms, namely synthesis dependent strand annealing (SDSA) and canonical double strand break repair (DSBR) (Heyer et al., 2010; San Filippo et al., 2008). During SDSA the extended D-loop is disrupted by action of helicase such as RTEL1, newly synthesized DNA strand is released and annealed back to the other end of damaged DNA (Kass and Jasin, 2010; Nassif et al., 1994; Paques and Haber, 1999; Uringa et al., 2011). Gaps are then filled by gap-filling DNA synthesis and DNA ends are ligated together (Nassif et al., 1994). SDSA yields only non-crossover products (Heyer et al., 2010).

The canonical DSBR starts if the second DSB end is captured by the D-loop to form an intermediate with two Holliday junctions, referred to as double Holliday junction (dHJ). This structure can be either resolved by specialized endonucleases including human GEN1, MUS81/EME1, SLX1/SLX4 or dissolved by concerted actions of the BLM helicase and the DNA topoisomerase IIIα (TOPIIIα) in complex with RMI1 and RMI2 (Cejka et al., 2010b; Wechsler et al., 2011). While resolution of dHJ can result both in crossovers (COs) and non-crossovers (NCOs), dissolution yields only non-crossovers (Heyer et al., 2010).

Mismatch repair proteins were also found to influence HR by discriminating homeologous (partly homologous) sequence from homologous one and thus increasing the recombination fidelity (Heyer et al., 2010).

The regulation of sub-pathway choice during HR is strict but not understood in detail. There is preference for crossover products in meiotic cells to ensure genetic diversity while their formation is suppressed in mitotic cells to prevent loss of heterozygosity and chromosomal rearrangements (Heyer et al., 2010; Matos et al., 2011). Lately, resolvases were found to be active only during mitosis in yeast and mammalian cells (Matos et al., 2011). The majority of non-crossover products are supposed to come from SDSA sub-pathway (Mitchel et al., 2010).

There are known DNA helicases from budding yeast that promote SDSA sub-pathway during HR: Mph1 and Srs2, both interfering with the role of RAD51 recombinase. Mph1 can disrupt Rad51 made D-loops while Srs2 can displace Rad51 from ssDNA but cannot disrupt Rad51 made D-loops (Ira et al., 2003; Krejci et al., 2003). In human cells, there are two candidates to be functional orthologs of Srs2: FBH1 and RECQL5 helicase. FBH1 has been shown to regulate HR at the step of RAD51 filament assembly while RECQL5 has been found to interact with RAD51 and to possess the ability to disrupt RAD51-ssDNA filament (Fugger et al., 2009; Hu et al., 2005; Hu et al., 2007; Islam et al., 2012; Schwendener et al., 2010; Simandlova et al., 2013; Wang et al., 2003).

Apart from HR, there is a more specific repair pathway called single strand annealing (SSA) that is used when direct repeats are present around the site of DSB. SSA involves long range resection of DNA ends that are subsequently coated by RPA (Cannavo et al., 2013). Annealing of complementary sequences with more than 30 nucleotides is mediated by RAD52, non-complementary 3’ overhangs are cleaved by ERCC1-XPF complex in conjunction with SLX4 and DNA is ligated resulting in one repeat deletion (Lyndaker and Alani, 2009; Sugawara et al., 2000). This process is RAD51 independent as no template DNA is used for repair.

1.3.3 Regulation of Double-Strand Break Repair

While NHEJ, SSA and MMEJ are error-prone mechanisms leading to insertions and/or deletions around the site of DSB, HR is mostly error-free (Karanam et al., 2012). Repair pathway choice is largely dependent on cell cycle phase and chromatin compaction at the site of DSB (Goodarzi et al., 2010; Kass and Jasin, 2010). NHEJ and MMEJ repair pathways are active throughout the cell cycle while HR is restricted to S phase and G2 phase cells due to the need of homologous sequence as a repair template that is preferably provided by

sister chromatid (Heyer et al., 2010; Kass and Jasin, 2010) (Figure 6). This is ensured by regulation of protein expression during cell cycle and by protein phosphorylations mediated by cyclin-dependent kinases that positively and negatively regulate HR (Heyer et al., 2010; Kass and Jasin, 2010). For example in S/G2, phosphorylated CtIP interacts with BRCA1 thus is recruited to the site of DSB and promotes HR (Heyer et al., 2010; Kass and Jasin, 2010). On the other hand, phosphorylated BRCA2 disrupts the interaction with RAD51 in mitosis and G1 phase to inhibit HR (Heyer et al., 2010).

The other important protein that regulate DSB repair is 53BP1 that binds to modified histones present on chromatin around double strand break where it promotes NHEJ in G1 cells and blocks DNA end resection thus inhibiting HR (Zimmermann and de Lange, 2014; Zimmermann et al., 2013). Recently discovered binding partner of 53BP1, Rif1 binds to 53BP1 and blocks binding of BRCA1 in G1 cells that is needed for homologous recombination to proceed (Chapman et al., 2013; Di Virgilio et al., 2013; Escribano-Diaz et al., 2013; Zimmermann and de Lange, 2014; Zimmermann et al., 2013). On the other hand recruitment of Rif1 is blocked by binding of phosphorylated CtIP to BRCA1, which promotes resection of DSBs for HR (Zimmermann and de Lange, 2014).

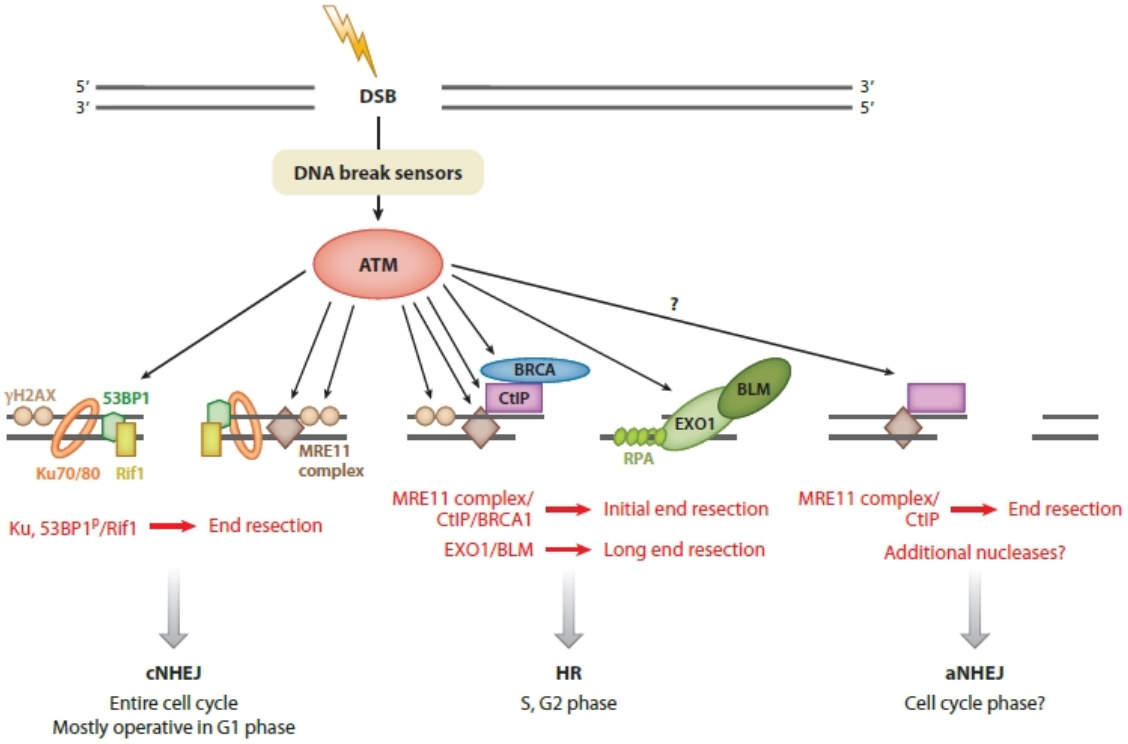

Figure 6. DSB repair pathway choice in different cell cycle phases. While canonical NHEJ (cNHEJ) is operative

throughout the cell cycle, HR is restricted to be active only in S and G2 phases of cell cycle. Alternative end-joining pathways (aNHEJ): MMEJ and alt-NHEJ are thought to be active throughout the cell cycle.

1.4 DNA DAMAGE RESPONSE SIGNALLING

Depending on type of DNA damage, different members of the family of phosphatidylinositol 3-like kinases are activated and their activity is usually enhanced by autophosphorylations. There are three members of this family: Ataxia telangiectasia mutated (ATM), Ataxia telangiectasia and Rad3 related (ATR) and DNA-PKcs. ATM kinase is of the most importance after DNA damage, however, ATR kinase can be also activated under certain circumstances.

During DSB repair, ATM is recruited to site of damage by MRN complex that is bound to blunt ended or minimally processed DSB ends (Figure 7). ATM then phosphorylates checkpoint kinase protein 2 (CHK2) and p53 leading to cell cycle arrest, activation of proteins involved in DNA damage repair and, in case of a high load of DNA damage, to apoptosis (Goodarzi and Jeggo, 2013). Other substrates of ATM are proteins involved in chromatin remodelling such as KRAB-associated protein-1 (KAP-1) or histones itself such as histone isoform H2AX at serine 139 (γ-H2AX). γ-H2AX signal spreads even a megabase away from DSB end and serves as a marker of DNA damage in cells (Goodarzi and Jeggo, 2013). In general, chromatin remodelling is important part of DNA repair as DSBs in heterochromatin are not accessible by DNA damage repair machinery (Goodarzi et al., 2010; Goodarzi and Jeggo, 2013).

During HR, resection of DNA leads to generation of ssDNA coated by RPA that recruits ATR kinase in complex with ATRIP (Cimprich and Cortez, 2008). Activity of ATR kinase is stimulated by its interaction with DNA topoisomerase 2-binding protein 1 (TopBP1) and RAD9-HUS1-RAD1 (9-1-1) complex that are bound to ssDNA-dsDNA junction and phosphorylates checkpoint kinase 1 (CHK1) that leads to cell cycle arrest through inhibition of CDC25 (Cimprich and Cortez, 2008). Replication stress as well as DNA crosslinks also lead to recruitment and activation of ATR kinase by its recruitment to RPA coated ssDNA in complex with ATR interacting protein (ATRIP) (Cimprich and Cortez, 2008; Zou and Elledge, 2003).

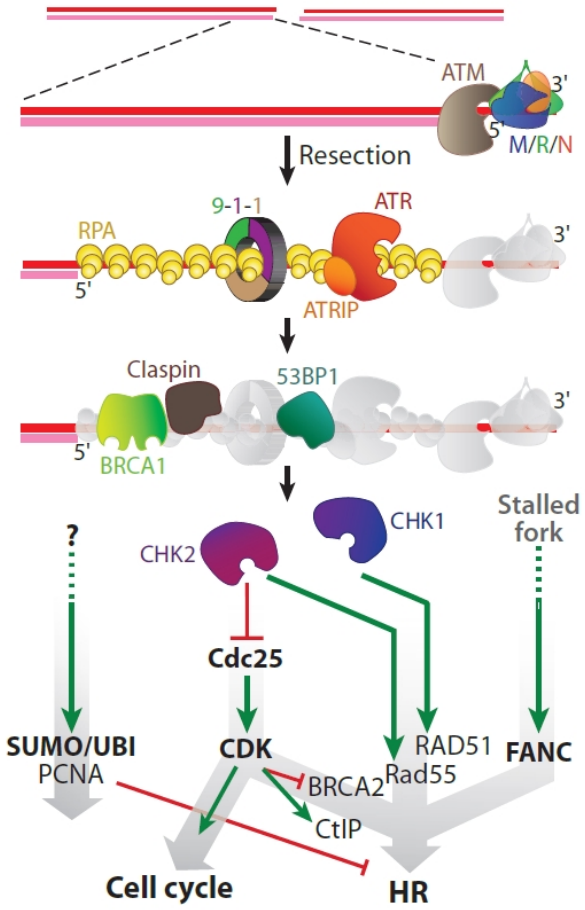

Figure 7. DNA damage response. After generation of DSB, MRN complex is bound to DNA ends and recruits ATM kinase. ATR kinase in complex with ATRIP and RAD9-HUS1-RAD1 (9-1-1) complex are then recruited to RPA-coated ssDNA created by DNA end resection. Finally, this signalling cascade leads to cell cycle arrest and DNA damage repair. Adapted from (Heyer et al., 2010).

Activation of ATR kinase is dependent on its interaction with TopBP1 that is recruited to sites of DSB and associates with 9-1-1 complex that is loaded at the ssDNA/dsDNA junction by RAD17-RFC clamp loader (Delacroix et al., 2007; Duursma et al., 2013; Kumagai et al., 2006; Lee et al., 2007; Mordes et al., 2008; Zou et al., 2002). Morever, there is recent indication that ATR can be also activated in 9-1-1/RAD17 independent manner by MRN dependent targeting or TopBP1 to RPA-coated ssDNA (Shiotani et al., 2013). *In vitro* experiments also show that TopBP1 can be recruited to RPA-coated ssDNA by its interaction with ATRIP and thus can activate ATR (Choi et al., 2010; Hashimoto et al., 2006; Kumagai et al., 2006).

1.5 RecQ Family of Helicases

Helicases are enzymes that catalyze unwinding of nucleic acid duplexes using energy derived from hydrolysis of nucleoside triphosphates (Singleton et al., 2007). There are two classes of helicases: type A that translocates in 3‘ to 5‘ direction and type B that translocates in opposite direction. Helicases have been also divided to six superfamilies (SF1-6) based on amino acid sequence homology (Singleton et al., 2007). RecQ helicases are highly conserved from bacteria to humans. They belong to the SF2 superfamily of helicases and are according to the *Escherichia coli* RecQ helicase. Most unicelullar organism have only one RecQ homolog (e.g. Sgs1 in *Saccharomyces cerevisiae*, while multicellular organisms express two and more RecQ homologues (Bernstein et al., 2010). In humans there are five members of RecQ family of helicases, namely RECQL1, WRN, BLM, RECQL4 and RECQL5β (Figure 8). They all contain a DEAH-type helicase domain that unwinds duplex DNA in ATP and Mg2+ dependent manner in 3‘ to 5‘ direction, a zinc-binding motif that is required for ssDNA binding, a RecQ C-terminal (RQC) domain that is responsible for binding to G quadruplexes (G4) and other DNA structures, a helicase and RNase D C-terminal (HRDC) domain that allows interaction with nucleic acid and a nuclear localization sequence (Croteau et al., 2014). Apart from these there are domains specific for each RecQ helicase. Werner helicase (WRN) is unique among RecQ helicases due to its N-terminal 3‘ to 5‘ exonucelase domain. However the *in vivo* role of this domain is still unclear (Croteau et al., 2014).

Mutations in three human RecQ helicases, namely WRN, BLM and RECQL4 have been found in hereditary genetic diseases that are characterized by cancer predisposition and/or premature aging (Bernstein et al., 2010). Werner syndrome (WS) is found in patients with mutation in *WRN* helicase and is characterized by early onset of age-associated pathologies such as cataracts and osteoporosis. Symptoms of WS start to appear in early 20s and result in death around 46-54 years. Tumours of WS patients are mainly of mesenchymal origin (e.g. sarcomas). Cells derived from WS patients show marks of genomic instability such as increased frequency of chromosomal rearrangements (Bernstein et al., 2010).

BLM helicase is mutated in Bloom syndrome (BS) that is characterized by dwarfism due to pre- and post-natal growth retardation. Beside this feature, patients with BS are light sensitive, show immunodeficiency, male infertility and predisposition to all types of

cancer. Cells derived from BS patients show increased level of spontaneous chromatid breaks/gaps, elevated rates of mutations, and most typically increased frequency of exchanges between homologous chromosomes and sister chromatids (SCEs) (Bernstein et al., 2010).

Mutations in *RECQL4* have been associated with Rothmund-Thompson syndrome type II, RAPADILINO syndrome and Baller-Gerold syndrome (Bernstein et al., 2010).

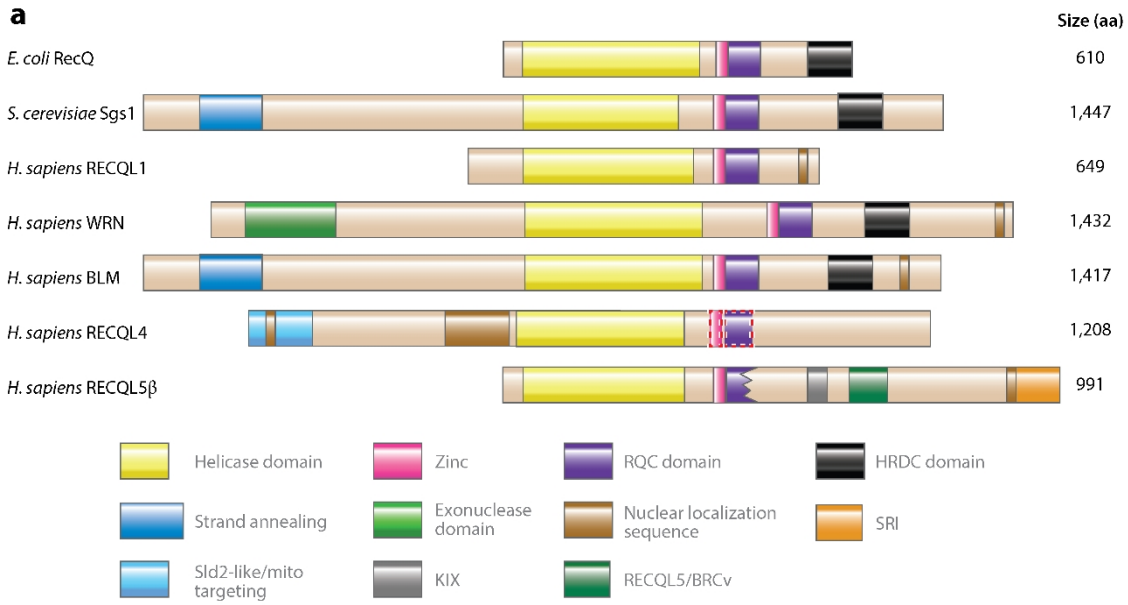

Figure 8. The domain structure of RecQ helicases from *E.coli, S.cerevisiae* and *H.sapiens*. Adapted from (Croteau et al., 2014).

RecQ helicases play role in replication, transcription, telomere maintenance and DNA damage repair and thus are important in maintenance of genome stability. During NHEJ, WRN and RECQL1 were shown to interact with KU heterodimer but their exact role in NHEJ are unknown (Cooper et al., 2000; Karmakar et al., 2002; Li and Comai, 2000; Parvathaneni et al., 2013). WRN interacts with Ligase III that is involved in MMEJ, however inhibition of WRN did not affect alt-NHEJ in I-SceI reporter system (Bothmer et al., 2013; Sallmyr et al., 2008). On the other hand efficiency of B cell class-switch recombination that requires alt-NHEJ was decreased by WRN inhibition or expression of hypomorphic allele of BLM (Bothmer et al., 2013).

There are many steps in which RecQ helicases play role during HR. Firstly Sgs1 was shown to interact with DNA2 during long-range resection mediating DNA duplex unwinding (Cejka et al., 2010a; Gravel et al., 2008; Mimitou and Symington, 2008; Nimonkar et al.,

2011). In human cells, it has been proposed that BLM is the ortholog that helps DNA2 in process of resection (Gravel et al., 2008; Nimonkar et al., 2011). On the other hand, WRN was found to function in DSB resection using extracts from *Xenopus laevis* (Liao et al., 2008; Toczylowski and Yan, 2006; Yan et al., 2005). Sgs1 as well as BLM and RECQL5 act as anti-recombinases during an early step of HR by disruption of RAD51 nucleofilament (Bugreev et al., 2007; Hu et al., 2007; Schwendener et al., 2010; Wu et al., 2001). In later steps of HR when dHJs are generated, BLM acts as a part of dissolution complex promoting non-crossover product formation (Wu and Hickson, 2003). As all RecQ helicases possess strand annealing activity, they all could play role in SDSA or SSA. Indeed, WRN and BLM were found to enhance strand annealing or stimulate SDSA, respectively (Baynton et al., 2003; Bugreev et al., 2007).

2 AIMS

1. Cells derived from Werner syndrome patients accumulate more 8-oxo-G lesions compared to cells with normal WRN expression. Molecular basis of this process is not known. **Therefore the first aim was to elucidate the role of WRN helicase in oxidative damage repair.**

2. Preferential use of SDSA sub-pathway during HR in interphase cells is important for maintenance of genomic stability as it leads to non-crossover products only. In yeast, there are two helicases that were found responsible for SDSA promotion, however their functional orthologs in mammalian cells were not described. Question to be addressed was: **Which helicase is responsible for SDSA sub-pathway promotion in human cells?**

3. Process of 5' to 3' DNA end resection during HR has been extensively studied in yeast but is not fully understood in mammalian cells. **Therefore, the goal of this part of the thesis was to explore this process in human cells.**

4. Mismatch repair recognition complexes as well as other proteins were found to be recruited to DSBs created by laser micro-irradiation. There is supportive evidence that they are somehow involved in double-strand break repair as deficient cells are more sensitive to agents causing DSBs. **The aim was to clarify the function of MSH2 complexes in the cellular response to DSBs.**

3 RESULTS

3.1 INVOLVEMENT OF WERNER SYNDROME PROTEIN IN MUTYH-MEDIATED REPAIR OF OXIDATIVE DNA DAMAGE

Reactive oxygen species are created as by-products of cell metabolism and attack other molecules in the cell including nucleic acid. Oxidized DNA bases are highly mutagenic due to mispairing during replication and thus compromise genomic stability. Cells derived from Werner syndrome patients show marks of increased genomic instability such as chromosomal aberrations and accumulate 8-oxo-G lesions. However, the mechanism underlying the accumulation of oxidative damage in these cells is not known. This prompted us to investigate the role of WRN in repair of 8-oxo-G lesions.

Firstly we analysed the recruitment of WRN to 8-oxo-G:A mispairs using *in vitro* system and found that indeed WRN protein is readily recruited to DNA containing 8-oxo-G:A mispair but not to paired control DNA. Moreover, we found that WRN recruitment was dependent on the presence of Polλ. To see if WRN also binds 8-oxo-G *in vivo* we treated cells with hydrogen peroxide to induce oxidative damage and using indirect immunofluorescence checked if WRN would colocalize with sites of damage. We found that after hydrogen peroxide treatment, WRN colocalized with Polλ and 8-oxo-G only in S-phase cells. Recruitment of WRN and Polλ was dependent on replication as aphidicolin treatment decreased number of cell containing damage induced foci. As expected from *in vitro* experiments, recruitment of WRN to 8-oxo-G sites was dependent on Polλ while Polλ recruitment was not affected in absence of WRN *in vivo*.

This finding propelled us to examine WRN - Polλ interaction *in vivo* and *in vitro*. We found that *in vivo* interaction of WRN with Polλ was stimulated upon oxidative damage and that this interaction is direct as purified recombinant proteins were also found to form complex *in vitro*. We mapped interaction sites of the WRN-Polλ complex to be in the Pol X domain of Polλ and in the helicase domain and C-terminal part of WRN protein.

Polλ knock-out cells were found to be sensitive to oxidative stress. To prove that WRN works in conjunction with Polλ during repair of oxidative damage we used cell viability and cell death assays to check sensitivity of cells depleted of these proteins. As expected, cells with depleted Polλ but also cells after WRN depletion were sensitive to increasing

concentrations of hydrogen peroxide. Moreover, depletion of both proteins did not further increase cell death or decreased cell viability suggesting that they act in the same pathway. To check if helicase or exonuclease function of WRN is needed during oxidative damage repair, we tested cell lines expressing WRN mutants that lack either helicase (K577M) or exonuclease (E84A) activity in cell viability assay. Neither the helicase nor the exonuclease activities of WRN were found to be employed in oxidative damage repair.

The first step in repair of 8-oxo-G:A mispairs is excision of mispaired A by MUTYH glycosylase that leads to single-strand break (SSB) creation. So we hypothesized that SSB creation could be the reason for increased sensitivity of cells to hydrogen peroxide. To test if depletion of MUTYH could rescue the hypersensitivity of WRN- and Polλ- depleted cells, we combined depletions of these proteins. Indeed, we found that co-depletion of MUTYH with WRN and/or Polλ decreased sensitivity of cells to hydrogen peroxide to control levels. Moreover, depletion of MUTYH dramatically impaired the formation of WRN and Polλ foci after oxidative damage.

To get insight into the molecular mechanism of WRN helicase in oxidative damage repair, we tested whether its presence would influence gap-filling activity of Polλ using substrate that already contains gap opposite to 8-oxo-G. WRN as well as its helicase and exonuclease dead mutants were found to stimulate gap-filling and strand displacement synthesis carried out by Polλ. In contrast, other helicases from RecQ family, namely BLM and RECQ5, were not able to stimulate Polλ activity. None of these RecQ helicases had effect on 8-oxo-G lesion bypass by Polβ. WRN was also able to bind to this gapped substrate containing 8-oxo-G in presence of Polλ. Finally, we investigated the influence of WRN on incorporation of dATP or dCTP opposite to 8-oxo-G by Polλ and found that WRN presence does not improve the fidelity of Polλ bypass.

Together these data suggest that WRN promotes long-patch BER during MUTYH-initiated repair of 8-oxo-G:A mispairs by stimulation of DNA repair synthesis by Polλ.

Published online 29 June 2012 *Nucleic Acids Research, 2012, Vol. 40, No. 17* ***8449–8459***
doi:10.1093/nar/gks648

Involvement of Werner syndrome protein in MUTYH-mediated repair of oxidative DNA damage

Radhakrishnan Kanagaraj[1], Prasanna Parasuraman[2], Boris Mihaljevic[1], Barbara van Loon[2], Kamila Burdova[3], Christiane König[1], Antonia Furrer[2], Vilhelm A. Bohr[4], Ulrich Hübscher[2,*] and Pavel Janscak[1,*]

[1]Institute of Molecular Cancer Research, [2]Institute of Veterinary Biochemistry and Molecular Biology, University of Zurich, Winterthurerstrasse 190, CH-8057 Zurich, Switzerland, [3]Institute of Molecular Genetics, Academy of Sciences of the Czech Republic, 14300 Prague, Czech Republic and [4]Laboratory of Molecular Gerontology, National Institute on Aging, NIH, Baltimore, MD 1224, USA

Received November 18, 2011; Revised June 6, 2012; Accepted June 10, 2012

ABSTRACT

Reactive oxygen species constantly generated as by-products of cellular metabolism readily attack genomic DNA creating mutagenic lesions such as 7,8-dihydro-8-oxo-guanine (8-oxo-G) that promote aging. 8-oxo-G:A mispairs arising during DNA replication are eliminated by base excision repair initiated by the MutY DNA glycosylase homologue (MUTYH). Here, by using formaldehyde crosslinking in mammalian cell extracts, we demonstrate that the WRN helicase/exonuclease defective in the premature aging disorder Werner syndrome (WS) is recruited to DNA duplex containing an 8-oxo-G:A mispair in a manner dependent on DNA polymerase λ (Polλ) that catalyzes accurate DNA synthesis over 8-oxo-G. Similarly, by immunofluorescence, we show that Polλ is required for accumulation of WRN at sites of 8-oxo-G lesions in human cells. Moreover, we show that nuclear focus formation of WRN and Polλ induced by oxidative stress is dependent on ongoing DNA replication and on the presence of MUTYH. Cell viability assays reveal that depletion of MUTYH suppresses the hypersensitivity of cells lacking WRN and/or Polλ to oxidative stress. Biochemical studies demonstrate that WRN binds to the catalytic domain of Polλ and specifically stimulates DNA gap filling by Polλ over 8-oxo-G followed by strand displacement synthesis. Our results suggest that WRN promotes long-patch DNA repair synthesis by Polλ during MUTYH-initiated repair of 8-oxo-G:A mispairs.

INTRODUCTION

Reactive oxygen species constantly produced in living organisms as byproducts of normal cellular metabolism or as a consequence of environmental exposure to various physical and chemical agents can generate a variety of oxidized DNA bases that are highly mutagenic and hence compromise genomic stability, promoting aging and carcinogenesis (1–4). One of the most frequent oxidative lesions is 7,8-dihydro-8-oxo-guanine (8-oxo-G) with a steady-state level of about 10^3 lesions per cell in normal tissue (5). Replication of genomic DNA containing 8-oxo-G lesions frequently leads to the formation of 8-oxo-G:A mispairs, giving rise to a G:C to T:A transversion mutations (6). Interestingly, these transversions are among the predominant somatic mutations found in lung, breast, ovarian, gastric and colorectal cancers, suggesting that a failure to eliminate 8-oxo-G lesions can initiate tumorigenesis and drive tumor progression (7).

Oxidized base lesions are primarily eliminated by the base excision repair (BER) system (8). In mammalian cells, the repair of 8-oxo-G:A mispairs is achieved via two BER events that occur sequentially on the two DNA strands (9). The first event is initiated by excision of the mispaired A residue by the MutY glycosylase homologue (MUTYH) in a reaction coordinated by proliferating cell nuclear antigen (PCNA) (10–12). This is followed by cleavage of the apurinic site (AP) by the AP endonuclease 1 (APE1), creating a DNA gap with a 3′-OH moiety (12,13). PCNA and replication protein A (RPA) then govern the bypass of the 8-oxo-G lesion by the DNA polymerase λ (Polλ), which in the presence of these two auxiliary factors preferentially incorporates dCTP opposite the lesion (12,14,15). Following lesion bypass, RPA dissociates and PCNA recruits flap

*To whom correspondence should be addressed. Tel: +41 446353470; Fax: +41 446353484; Email: pjanscak@imcr.uzh.ch
Correspondence may also be addressed to Ulrich Hübscher. Tel: +41 446355472; Fax: +41 446356840; Email: hubscher@vetbio.uzh.ch

The authors wish it to be known that, in their opinion, the first two authors should be regarded as joint First Authors.

endonuclease 1 (FEN1) to remove the 5′-single-stranded DNA (ssDNA) flap resulting from the limited strand displacement synthesis by Polλ (12). Finally, DNA ligase I interacts with PCNA loaded on the nick arising from FEN1 cleavage and seals it, creating the substrate for a second BER event, which leads to the elimination of the 8-oxo-G lesion (12). 8-oxo-G paired with C is predominantly excised by the OGG1 glycosylase in a short patch BER reaction in which Polβ fills the DNA gap and the DNA ligase III/XRCC1 complex restores the continuity of the damaged DNA strand (8).

Werner syndrome (WS) is an autosomal recessive disorder characterized by premature aging, cancer predisposition and genomic instability (16). It is caused by mutations in the *WRN* gene which encodes a multifunctional protein (WRN) possessing 3′–5′ DNA helicase and 3′–5′ exonuclease activities (16). Interestingly, WRN-deficient cells accumulate 8-oxo-G lesions at a much higher rate than WRN-proficient cells (17,18). However, the molecular basis of this phenomenon is not known. Here we present several lines of evidence suggesting that WRN cooperates with Polλ to carry out long-patch DNA repair synthesis during MUTYH-initiated repair of 8-oxo-G:A mispairs. Loss of such an activity might explain many cellular phenotypes associated with WS including accumulation of oxidative DNA lesions, accelerated telomere attrition and genomic instability.

MATERIALS AND METHODS

Antibodies and purified proteins

All primary antibodies used for immunofluorescence staining and immunoblotting are described in Supplementary Materials and Methods. Recombinant human Polλ protein was expressed and purified as previously described (19). His-tagged recombinant human Polλ fragments were purified on Ni-NTA agarose (Invitrogen) as recommended by the manufacturer. Recombinant human WRN protein and its mutants were produced and purified as previously described (20). These protein preparations had a purity of >95% (Supplementary Figure S1A) and did not contain any contaminating DNA polymerase activity (Supplementary Figure S1C). Purified wild-type WRN could unwind efficiently a forked DNA duplex (Supplementary Figure S1B). RECQ5 and BLM proteins were purified as previously described (21,22).

Cell culture experiments

All cell lines (HeLa, U2OS, HEK293, MEFs, MRC5) used in this study were maintained in DMEM (Gibco) supplemented with 10% fetal calf serum (Gibco) and streptomycin/penicillin (100 U/ml). Where required, H_2O_2 (Sigma) was added to cell cultures to a final concentration as indicated. Hydroxyurea (Sigma) was used at a concentration of 2 mM to synchronize cells at G1/S boundary. To arrest DNA replication, cells were treated with aphidicolin (Sigma) at a concentration of 1 μg/ml. Transfection of siRNA oligonucleotides was carried out using Lipofectamine RNAiMAX (Invitrogen) according to manufacturer's instructions. Cells were analyzed 72 h after siRNA transfection. The sequences of the siRNA oligonucleotides used in this study are indicated in Supplementary Materials and Methods.

Crosslinking assay

Formaldehyde crosslinking assays with cell extracts and hairpin oligonucleotide substrates attached to streptavidin magnetic beads (Invitrogen) were performed as described previously (12).

Chromatin-binding assay

Chromatin fractionation was done as previously described (23). Briefly, to obtain cytoplasmic fraction, HEK293T cells were resuspended in buffer A (10 mM HEPES pH 7.9, 10 mM KCl, 1.5 mM $MgCl_2$, 0.34 M sucrose, 10% glycerol, 1 mM DTT, 1 mg/ml digitonin, Roche complete protease inhibitor cocktail) and incubated on ice for 5 min. Nuclei were collected by centrifugation at 1500*g* for 4 min, washed once with buffer A, resuspended in buffer B (3 mM EDTA, 0.2 mM EGTA, 1 mM DTT, Roche complete protease inhibitor cocktail) and incubated on ice for 15 min. Chromatin was separated from nucleoplasmic fraction by low speed centrifugation at 2000*g* for 4 min, washed twice in buffer B, resuspended in SDS loading buffer and sonicated. Bound proteins were analyzed by western blotting.

Immunofluorescence assays

Cells cultured on glass coverslips were fixed with 3.7% formaldehyde for 10 min at room temperature (RT) and subsequently permeabilized by soaking in 0.2% (v/v) Triton X-100 for 5 min at RT. After blocking in PBS containing 5 mg/ml BSA for 30 min at RT, the fixed cells were incubated overnight at 4°C with appropriate primary antibodies. The slides were washed with PBS and incubated for 1.5 h at RT with secondary antibodies diluted in blocking solution: fluorescein isothiocyanate-(FITC) conjugated sheep anti-rabbit IgG (Sigma; 1:700) and Texas Red-conjugated donkey anti-mouse IgG (Jackson Immunoresearch, 1:200). After washing with PBS, coverslips were mounted on Vectashield (Vector Laboratories) and images were captured on an Olympus IX81 fluorescence microscope. At least 100 nuclei were analyzed in each of three independent experiments. For simultaneous detection of WRN and 8-oxo-G, cells were fixed and sequentially incubated with rabbit polyclonal anti-WRN antibody and anti-rabbit FITC-conjugated secondary antibody. Stained cells were then fixed with 100% cold methanol for 30 min at −20°C and immersed in 100% cold acetone for 30 s. After washing, the fixed cells were treated with 2M HCl for 30 min to denature the DNA and then neutralized with 0.1 M borate buffer (pH 8.5). After washing and blocking, cells were stained with mouse monoclonal anti-8-oxo-G (IgM) antibody (1:100) followed by Texas Red-conjugated donkey anti-mouse IgM secondary antibody (Jackson Immunoresearch, 1:150). After washing, coverslips were mounted and analyzed as described above. The same procedure was used for simultaneous detection of Polλ and 8-oxo-G lesion.

Immunoprecipitation assays

Total cell extract preparation and immunoprecipitation (IP) were carried out as described previously (24). For IP of purified recombinant proteins, a mixture of equal amounts of WRN (300 ng) and Polλ (300 ng) was incubated for 2 h at 4°C and then added to Protein A/G-agarose beads (20 µl) coated with rabbit polyclonal anti-WRN IgGs (2 µg). After incubation for 2 h at 4°C, the beads were washed and subjected to western blot analysis. All the IP reactions were conducted in the presence of DNase I (Roche) to exclude the possibility of protein–protein interaction mediated through DNA.

Gap-filling assay

Annealing of a 72-mer containing 8-oxo-G lesion (or a normal G) with the 5′-[^{32}P]-labeled 39-mer primer created a primer/template substrate with the lesion (or a normal G) at the +1 position relative to single-strand/double-strand junction. Annealing of a 32-mer oligonucleotide to the region 3′ of the lesion site in this structure yielded a duplex containing a one-nucleotide (1-nt) gap opposite 8-oxo-G (or normal G). The 32-mer oligonucleotide was phosphorylated by T4 polynucleotide kinase (NEB) prior to annealing. The reaction mixtures (10 µl) contained 50 mM Tris–HCl (pH 7.5), 2 mM DTT, 0.25 mg/ml BSA, 10 µM dNTP, 1 mM $MgCl_2$ and 10 fmol of the 5′-[^{32}P]-labeled DNA substrate. Concentrations of Polλ and WRN are indicated in figures and figure legends. Reactions were carried out at 37°C for 10 min. Reaction mixtures were separated on a denaturing urea-polyacrylamide gel and radiolabeled DNA species were visualized by phosphorimaging on a Typhoon 9400. Gel images were quantified using ImageQuant software.

Biotin pull-down assay

Pull-down assays using biotinylated gapped DNA duplexes with or without 8-oxo-G lesion were performed as described previously (15).

Cell viability assay

Cell viability assays were done as previously described (25). Briefly, HeLa cells were seeded at a confluency of 25% in cell culture plates containing complete medium (DMEM, 10% FCS and penicillin/streptomycin). After 24 h, cells were transfected with the appropriate siRNAs. 2 days after transfection, siRNA-treated cells were harvested and seeded in a 96-well plate at a density of 2500 cells/well in a volume of 100 µl of complete medium. After 24 h, cells were treated with different concentrations of H_2O_2 (Sigma) ranging from 0 to 640 µM. Experiments were carried out in hexaplicates for each H_2O_2 concentration. 2 h after H_2O_2 addition, cells were washed twice with PBS, and allowed to grow in complete medium. After 2 days, a mixture of resazurin and complete medium (ratio of 1:10; 100 µl) was added to individual wells. Cell viability was measured after 4 h of incubation using a SpectraMax reader M5 (Molecular Devices). The percentage of viable cells was calculated relative to mock treated cells and plotted using GraphPad Prism as mean ± SD. Data from at least two independent experiments were plotted.

RESULTS

WRN is involved in the processing of 8-oxo-G:A mispairs in mammalian cell extracts

To investigate whether WRN is involved in the repair of 8-oxo-G:A mispairs, we employed a previously established assay using formaldehyde crosslinking in human cell extracts to monitor the recruitment of BER proteins to damaged DNA (26). A 3′-biotinylated hairpin loop oligoduplex (27 bp) containing a single 8-oxo-G:A mispair was incubated with HeLa whole-cell extract in the presence of Mg^{2+} to initiate repair (12). As a control reaction, the corresponding lesion-free substrate was also tested. At different time points, the reactions were stopped by the addition of formaldehyde and cross-linked DNA–protein complexes, isolated using streptavidin magnetic beads, were analyzed by western blotting. We observed a rapid, damage-specific recruitment of WRN to the DNA substrate (Figure 1A). A robust damage-specific recruitment of Polλ was also detected as previously reported (12). To address whether the recruitment of WRN to the hairpin duplex containing 8-oxo-G:A mispair was dependent on Polλ, whole-cell extracts from Polλ$^{-/-}$ and Polλ$^{+/+}$

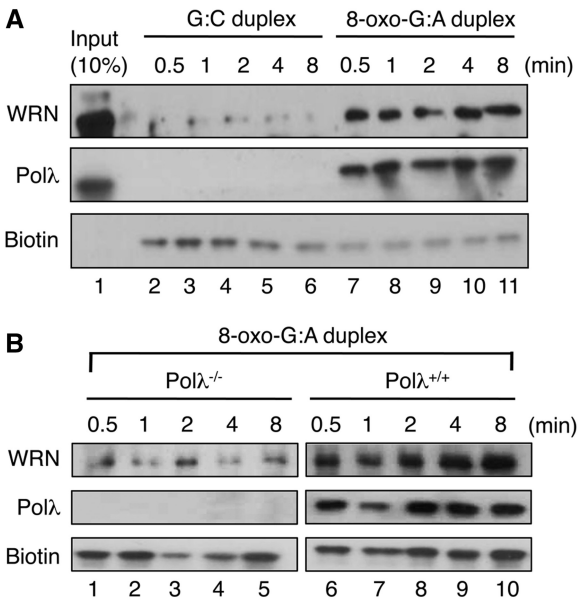

Figure 1. Polλ-dependent recruitment of WRN to sites of repair of 8-oxo-G:A mispairs in cell extracts. (**A**) Formaldehyde crosslinking assay using G:C (lanes 2–6) or 8-oxo-G:A (lanes 7–11) biotinylated hairpin DNA substrate and HeLa whole-cell extract. (**B**) Formaldehyde crosslinking assay using biotinylated 8-oxo-G:A hairpin substrate and whole-cell extracts from Polλ$^{-/-}$ (left panel, lanes 1–5) or Polλ$^{+/+}$ (right panel, lanes 6–10) MEFs. The experiments were performed under the conditions specified in the 'Materials and Methods' section. Blots were probed with antibodies against WRN and Polλ. Biotin was detected using HRP-conjugated Streptavidin. The indicated time points refer to the length of incubation of extracts with DNA before addition of the crosslinking agent. Note that western blot analysis of extracts from Polλ$^{+/+}$ and Polλ$^{-/-}$ MEFs is shown in Figure 4B (right panel).

mouse embryonic fibroblasts (MEFs) were prepared and subjected to formaldehyde crosslinking assay. We found that in the absence of Polλ, WRN was not cross-linked to the hairpin substrate, suggesting that Polλ mediates the recruitment of WRN to the sites of repair of 8-oxo-G:A mispairs (Figure 1B). This is further supported by the finding that complementation of Polλ$^{-/-}$ MEFs with human Polλ cDNA lead to a restoration of WRN recruitment to the hairpin duplex in formaldehyde crosslinking assay (Supplementary Figure S2). These results provide a strong evidence for the involvement of WRN in the repair of 8-oxo-G:A mispairs.

WRN accumulates at sites of 8-oxo-G lesions during S-phase in a manner dependent on DNA replication and the presence of Polλ

To investigate whether WRN is recruited to sites of oxidative DNA damage *in vivo*, we first performed sub-cellular fractionation to analyze chromatin binding of WRN in HEK293T cells prior to and after treatment with H_2O_2. We found that at 2.5 h after H_2O_2 addition, the amount of WRN bound to chromatin substantially increased as compared to non-treated cells (Figure 2). Likewise, we observed that H_2O_2 treatment promoted chromatin binding of Polλ (Figure 2).

Next, we used indirect immunofluorescence technique to monitor the spatial distribution of WRN and Polλ in U2OS cells after H_2O_2 treatment. In agreement with previous reports, WRN was observed to localize to the nucleolus in the majority of non-treated cells, whereas Polλ showed a dispersed nuclear staining (Figure 3A, top row). Upon treatment of cells with 500 μM H_2O_2 for 2 h, WRN and Polλ each formed ≥10 distinct foci per nucleus in 45 and 65% of cells, respectively. Approximately in 35% of these cells, more than 75% of WRN

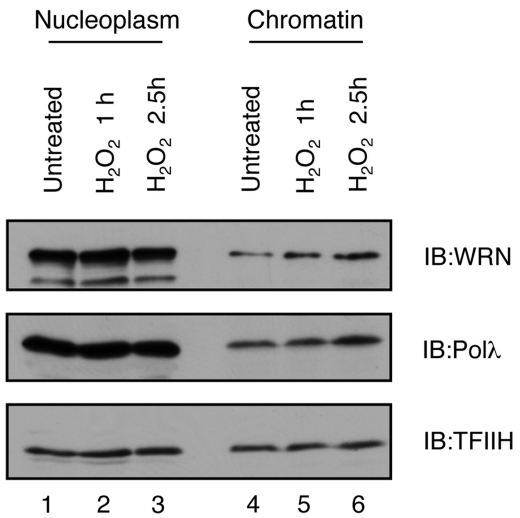

Figure 2. Accumulation of WRN and Polλ on chromatin after oxidative stress. HEK293 cells were treated with 500 μM H_2O_2 and fractionated under conditions specified in the 'Materials and Methods' section. Nucleoplasmic and chromatin fractions were analyzed by western blotting. Blots were probed with antibodies against WRN, Polλ and TFIIH.

foci co-localized with Polλ foci (Figure 3A, bottom row, and Supplementary Table S1). Notably, the frequency of nuclei with co-localizing foci of WRN and Polλ increased substantially when H_2O_2 was added to cells that had been released from G1/S blockade, suggesting that the re-localization of these proteins induced by oxidative stress is specific to S-phase cells (Figure 3B, Supplementary Figure S3). In accordance with this assumption, we found that after H_2O_2 treatment, WRN and Polλ formed foci only in cells expressing cyclin A (Supplementary Figure S4). To substantiate these findings, cells were treated with aphidicolin for 20 min prior to addition of H_2O_2 to inhibit DNA replication. We found that aphidicolin impaired the formation of WRN and Polλ foci after oxidative stress, suggesting that WRN and Polλ are recruited to site of oxidative DNA damage in a manner dependent on DNA replication that can give rise to 8-oxo-G:A mispairs (Figure 3C).

To prove that WRN and Polλ co-localized at sites of oxidative DNA damage, untreated and H_2O_2-treated cells were co-immunostained either for visualization of WRN and 8-oxo-G or for visualization of Polλ and 8-oxo-G. The results indicated that WRN and Polλ co-localized with sites of 8-oxo-G lesions in ~40 and ~50% of cells, respectively (Figure 4A, Supplementary Tables S2 and S3). To explore the mechanism underlying the recruitment of WRN to sites of 8-oxo-G lesions *in vivo*, we analyzed by immunofluorescence the spatial distribution of WRN in Polλ$^{+/+}$ and Polλ$^{-/-}$ MEFs prior to and after treatment with H_2O_2. The results demonstrated that genetic ablation of Polλ impaired the re-localization of WRN to sites of 8-oxo-G lesions (Figure 4B and Supplementary Figure S5), which is consistent with the data from the crosslinking experiments described above (Figure 1B). We also tested the effect of WRN depletion on the accumulation of Polλ at sites of 8-oxo-G lesions in U2OS cells. We found that lack of WRN did not abolish Polλ focus formation after oxidative stress (Figure 4C). Instead, a small increase in the frequency of cells with co-localizing foci of 8-oxo-G and Polλ was observed in WRN-deficient cells relative to WRN-proficient cells both in the presence and in the absence of H_2O_2 (Figure 4C). This is in agreement with the previous finding of elevated levels of spontaneous oxidative DNA damage in WRN-deficient cells (17).

Collectively, the results described above provide strong evidence that WRN is recruited to sites of 8-oxo-G lesions in a DNA replication- and Polλ-dependent manner.

WRN is required for repair of 8-oxo-G:A mispairs in human cells

Earlier studies revealed that Polλ$^{-/-}$ MEFs were more sensitive to oxidative stress than normal MEFs (27). To prove that WRN functions in repair of oxidative DNA damage in conjunction with Polλ, we employed resazurin-based cell viability assay to test the effect of single and combined depletions of WRN and Polλ on sensitivity of HeLa cells to H_2O_2 treatment. In agreement with the previous report, we found that Polλ-depleted cells displayed a higher sensitivity to H_2O_2 compared to mock-depleted cells (Figure 5A and E). WRN-depleted

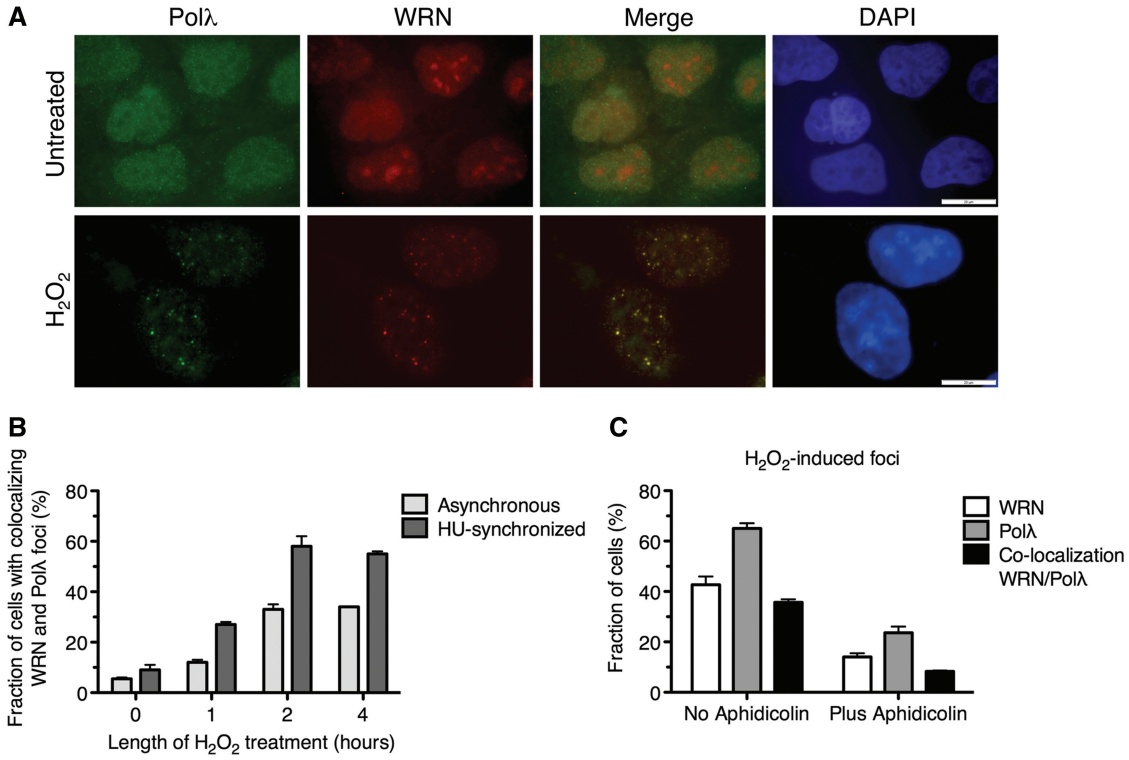

Figure 3. DNA replication-dependent co-localization of WRN and Polλ at nuclear foci in response to oxidative stress. (**A**) WRN co-localizes with Polλ after exposure of U2OS cells to oxidative stress. Cells grown on glass coverslips were either left untreated or treated with 500 μM H_2O_2 for 2 h. After treatment, cells were fixed and immunostained using antibodies against Polλ (green) and WRN (red). DAPI staining of the nucleus is shown in blue. Scale bar, 20 μm. (**B**) Frequency of the formation of co-localizing foci of WRN and Polλ in synchronized and non-synchronized populations of U2OS cells following H_2O_2 treatment. Prior to addition of H_2O_2, cells were synchronized at G1/S boundary by treatment with hydroxyurea (HU) for 16 h and then released to S phase by adding fresh medium without HU. (**C**) Effect of aphidicolin on the nuclear focus formation of WRN and Polλ in U2OS cells after H_2O_2 treatment. Aphidicolin was added to cells at a concentration of 1 μg/ml at 20 min prior to addition of H_2O_2 to arrest cellular DNA replication. The data points in (B) and (C) represent the mean of three independent experiments with at least 100 nuclei scored in each experiment.

cells exhibited a similar degree of sensitivity to H_2O_2 as Polλ-depleted cells (Figure 5A and E). Co-depletion of WRN and Polλ did not result in a further decrease in H_2O_2 sensitivity compared to singly-depleted cells, suggesting that WRN and Polλ act in the same pathway of oxidative DNA damage repair (Figure 5A and E).

To substantiate the above findings, we investigated whether depletion of WRN and Polλ caused cell death in response to oxidative stress. Using Annexin V-binding assay, we found that lack of either protein leads to a significant increase in the frequency of dead cells after H_2O_2 treatment as compared to mock-depleted cells (Supplementary Figure S6). Again, no additive effects on cell death were observed upon co-depletion of WRN and Polλ, confirming that these proteins act epistatically to protect cells against oxidative DNA damage (Supplementary Figure S6).

We reasoned that the hypersensitivity of cells deficient for WRN and Polλ to H_2O_2 was a consequence of accumulation of ssDNA breaks resulting from MUTYH-mediated processing of 8-oxo-G:A mispairs. Therefore, we tested whether the defect conferred by WRN/Polλ deficiency could be rescued by the elimination of MUTYH. Indeed, we found that depletion of MUTYH from HeLa cells lacking WRN and/or Polλ restored the cellular sensitivity to H_2O_2 to control levels (Figure 5B–E and Supplementary Figure S6). Depletion of MUTYH alone did not significantly alter H_2O_2 sensitivity of cells proficient for WRN and Polλ (Figure 5, compare panels B–D with panel A). Together, these data provide strong evidence that WRN and Polλ are required for repair of 8-oxo-G:A mispairs initiated by the MUTYH DNA glycosylase.

To obtain further evidence for the above statement, we tested the effect of MUTYH depletion on the re-localization of WRN and Polλ to nuclear foci in response to oxidative stress. We found that lack of MUTYH dramatically impaired the nuclear focus formation of both WRN and Polλ in U2OS cells after H_2O_2 treatment, suggesting that these foci represent sites of repair of 8-oxo-G:A mispairs (Figure 5F).

WRN physically interacts with Polλ

To investigate whether WRN and Polλ interact physically, an extract of HEK293 cells was subjected to IP with anti-WRN antibody. We found that Polλ co-immunoprecipitated with WRN, while it was not present in an immunoprecipitate obtained with control IgG, suggesting that these proteins formed a stable complex *in vivo* (Figure 6A). Interestingly, the level of WRN–Polλ

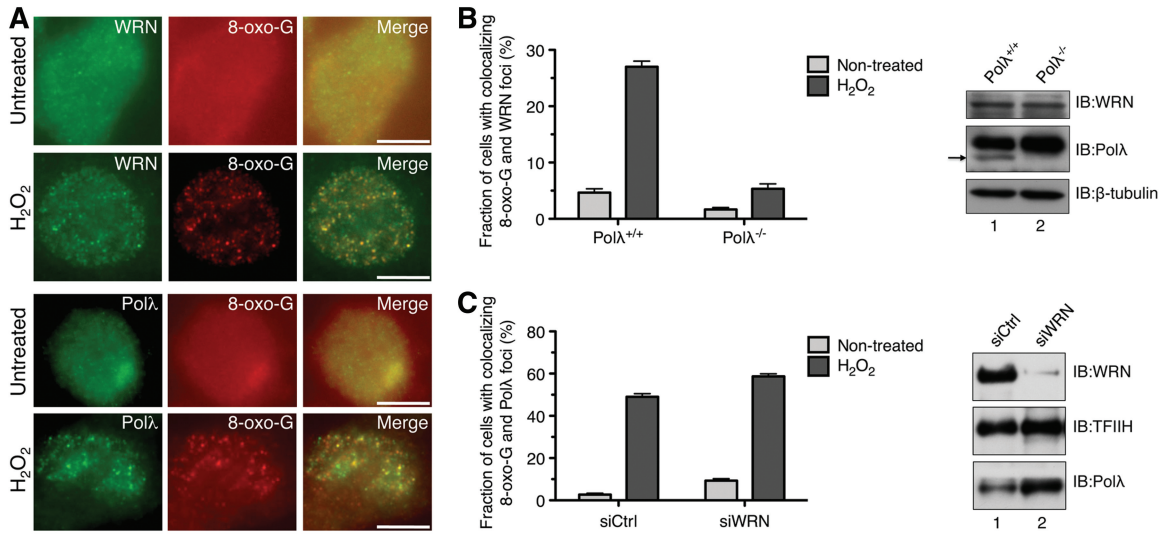

Figure 4. WRN localizes to sites of 8-oxo-G lesions *in vivo* in a manner dependent on Polλ. (**A**) WRN and Polλ accumulate at sites of 8-oxo-G lesions. U2OS cells were left either non-treated (top panels) or treated with 500 μM H_2O_2 for 2 h (lower panels), fixed and co-stained either with antibodies against WRN (green) and anti-8-oxo-G (red) or with antibodies against Polλ (green) and 8-oxo-G (red) under conditions described in the 'Materials and Methods' section. Images were captured on an Olympus IX81 fluorescence microscope. Scale bar, 20 μm. (**B**) Graph showing the proportion of $Polλ^{+/+}$ and $Polλ^{-/-}$ MEFs positive for co-localization of WRN and 8-oxo-G foci after mock- or H_2O_2-treatment, respectively. H_2O_2 was present at a concentration of 100 μM for 2 h. After treatment, cells were fixed and stained for WRN and 8-oxo-G. (Right panel) Western blot analysis of extracts from $Polλ^{+/+}$ and $Polλ^{-/-}$ MEFs. Blots were probed with antibodies against WRN, Polλ and β-tubulin (loading control). The arrowhead indicates the band corresponding to mouse Polλ. (**C**) Graph showing the proportion of siCtrl- and siWRN-treated cells positive for co-localization between Polλ and 8-oxo-G foci after mock- or H_2O_2-treatment. Cells were treated with 500 μM H_2O_2 (or mock-treated) for 2 h, fixed and immunostained to visualize Polλ and 8-oxo-G. Treatment was carried out 72 h after siRNA transfection (right panel). Western blot analysis of extracts of U2OS cells transfected with WRN siRNA (siWRN) and control siRNA (siCtrl), respectively. Cells were harvested 72 h post-transfection. Blots were probed with antibodies against WRN, Polλ and TFIIH (loading control). The data points in (B) and (C) represent the mean of three independent experiments with at least 100 nuclei counted in each experiment.

complex in the extract from cells treated with H_2O_2 was notably higher compared to that in the extract from non-treated cells, suggesting that the formation of WRN–Polλ complex in cells might be stimulated by oxidative DNA damage (Figure 6A, compare lanes 3 and 4). We also performed co-IP experiments with a mixture of purified recombinant proteins and found that WRN and Polλ co-precipitated with anti-WRN antibody, but not with control IgG, indicating that WRN and Polλ interact directly (Figure 6B).

To map the WRN-binding site on Polλ, co-IP experiments were performed with different deletion variants of Polλ (Figure 6C). A stable interaction of WRN with $Polλ_{244–575}$, but not with $Polλ_{1–244}$ and $Polλ_{133–244}$ was observed, suggesting that WRN binds to the catalytic core domain of Polλ (Figure 6C). We also used GST pull-down assay to map the region of WRN that binds to Polλ. We found that Polλ bound well to GST–$WRN_{949–1432}$ and GST–$WRN_{500–946}$, but not to GST–$WRN_{51–499}$ or to GST alone (Supplementary Figure S7). These results indicated that Polλ interacted with the helicase domain of WRN (amino acids 500–946) as well as with the C-terminal region of WRN, which contains winged-helix domain, a binding site of a number of other proteins shown to interact with WRN (28).

WRN specifically stimulates the bypass of 8-oxo-G by Polλ on gapped DNA duplex

In order to gain insight into the role of WRN in the repair of 8-oxo-G:A mispairs, we tested its effect on the gap-filling activity of Polλ using a synthetic DNA duplex containing a centrally located 1-nt gap opposite to 8-oxo-G (Figure 7A). We found that WRN significantly stimulated Polλ to fill the gap opposite the 8-oxo-G lesion and to carry out strand displacement synthesis (Figure 7A, lanes 11–14). Quantification of gel images from these experiments indicated that WRN increased the extent of Polλ reaction about 3-fold (Figure 7B). In contrast, WRN did not stimulate the gap-filling activity of Polλ on DNA substrate containing a normal G opposite the gap (Figure 7A, lanes 3–6). Moreover, stimulation of Polλ was not observed with other RecQ helicases such as BLM and RECQ5, and WRN did not enhance 8-oxo-G bypass by Polβ on gapped DNA duplex (Figure 7A, lanes 11, 15 and 16, and Supplementary Figure S8). These data indicate that WRN stimulates specifically Polλ-mediated bypass of 8-oxo-G on gapped DNA duplex.

We also tested the effect of WRN on 8-oxo-G bypass by Polλ following MUTYH/APE1-mediated processing of an 8-oxo-G:A mispair in a 100-bp DNA duplex (12). We found that WRN significantly enhanced the trans-lesion synthesis mediated by Polλ in this system (~1.7-fold), providing evidence that WRN promotes lesion bypass by Polλ during MUTYH-initiated repair of 8-oxo-G:A mispairs (Supplementary Figure S9).

To substantiate these findings, we tested binding of WRN to the 8-oxo-G-containing and lesion-free gapped DNA substrates in the presence and in the absence of Polλ. Reactions also contained dCTP to allow Polλ to

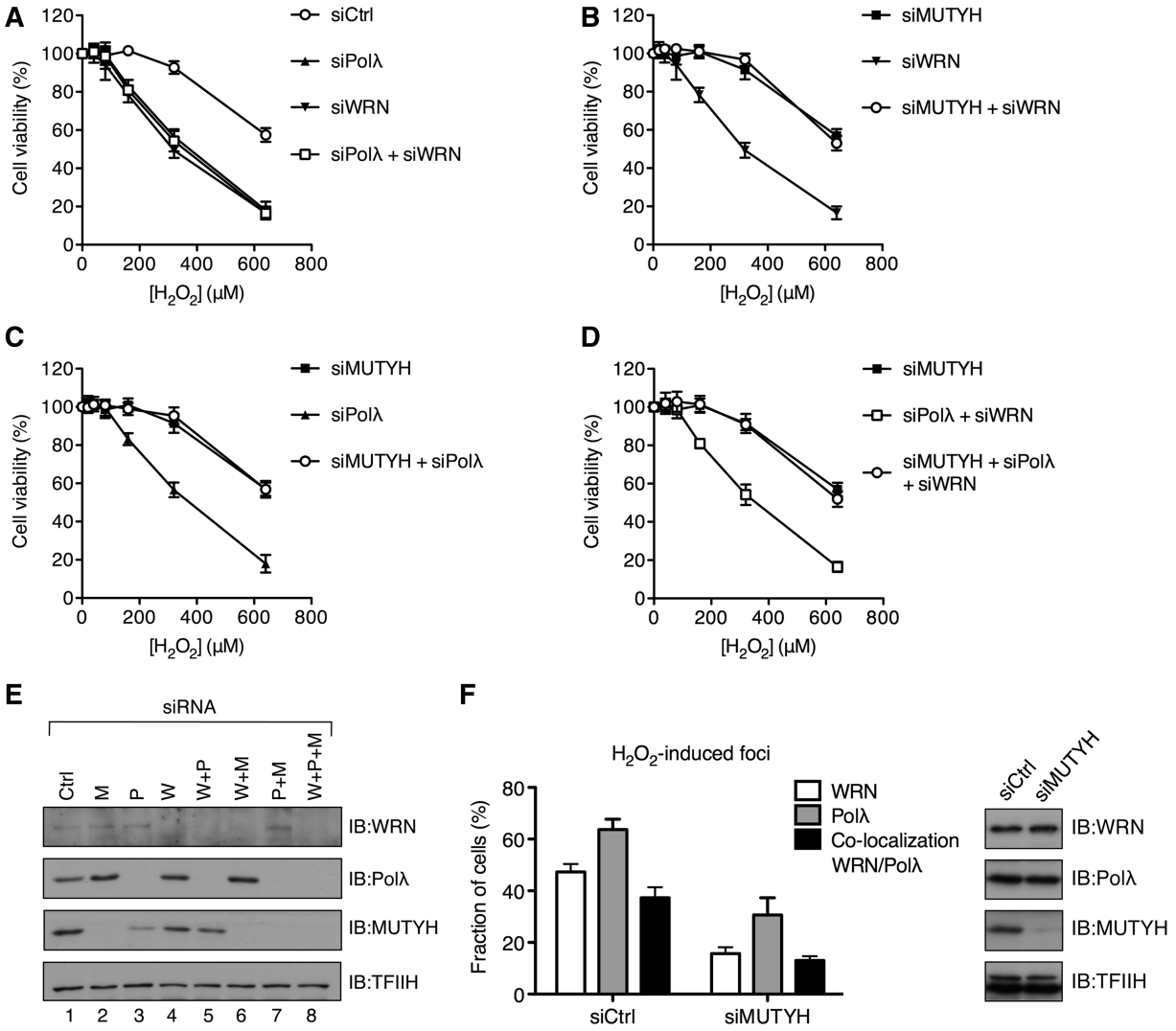

Figure 5. Depletion of MUTYH confers oxidative stress tolerance to WRN- and Polλ-deficient cells and impairs the recruitment of WRN and Polλ to sites of oxidative DNA damage. (**A–D**) Graphs showing sensitivity of siRNA-depleted HeLa cells to indicated concentrations of H_2O_2. siCtrl, siMUTYH, siWRN and siPolλ represent siRNA against luciferase, MUTYH, WRN and Polλ, respectively. Cell viability assays were performed as described in the 'Materials and Methods' section. Each data point represents mean ± SD (n = 12). (**E**) Western blot analysis of extracts of HeLa cells transfected with different siRNAs as indicated. W, P and M stand for WRN, Polλ and MUTYH, respectively. Cells were harvested 72 hours after transfection. Blots were probed with antibodies against MUTYH, WRN, Polλ and TFIIH (loading control). IB, immunoblotting. (**F**) Effect of MUTYH depletion on nuclear focus formation of WRN and Polλ in U2OS cells after oxidative stress. Cells were treated with 500 μM H_2O_2 for 2 h, fixed and immunostained as in Figure 3A. H_2O_2-treatment was carried out 72 h after siRNA transfection. The data points represent the mean of three independent experiments with at least 100 nuclei scored in each experiment. (Right panel) Western blot analysis of extracts of U2OS cells transfected with siCtrl and siMUTYH, respectively. Cells were harvested 72 h post-transfection. Blots were probed with antibodies against WRN, Polλ, MUTYH and TFIIH (loading control).

incorporate 2 nt. We found that Polλ was bound to both DNA substrates irrespective of the presence or absence of WRN, showing a higher affinity for the 8-oxo-G substrate (Figure 7C, compare lanes 4, 5, 8 and 9). Importantly, WRN did not bind to the gapped duplex containing normal G opposite the gap even in the presence of Polλ, while it did bind efficiently to the 8-oxo-G-containing gapped duplex providing that Polλ was present (Figure 7C, lanes 3, 5, 7 and 9).

To address whether the enzymatic activities of WRN were required for its stimulatory effect on DNA synthesis by Polλ, we used previously established mutants of WRN defective either in the exonuclease (E84A) or in the helicase (K577M) activity (29,30). We found that both mutants stimulated translesion synthesis by Polλ on the 8-oxo-G-containing gapped duplex to a similar degree as wild-type WRN (Figure 7D). In agreement with this result, we found that expression of either WRN mutant in WS fibroblasts restored oxidative stress tolerance to the wild-type level, suggesting that WRN might act non-catalytically in repair of oxidative DNA damage *in vivo* (Supplementary Figure S10).

RPA and PCNA were shown to promote accurate bypass of 8-oxo-G by Polλ, by repressing the formation

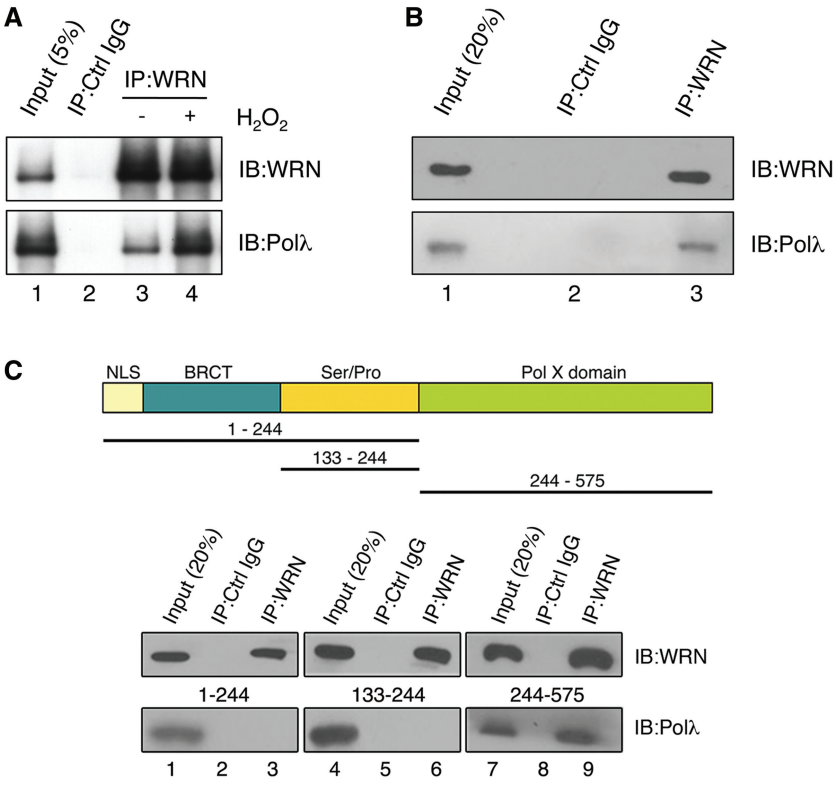

Figure 6. Physical interaction between WRN and Polλ. (**A**) Co-immunoprecipitation of Polλ with WRN from extracts of non-treated and H_2O_2-treated HEK293 cells. Cells were treated with 500 μM H_2O_2 for 2 h or mock-treated. WRN was immunoprecipitated using rabbit polyclonal anti-WRN antibody as described under the 'Materials and Methods' section. Blots were probed with anti-Polλ and anti-WRN antibodies. Lane 2, control immunoprecipitate obtained with preimmune rabbit IgGs. (**B**) Co-immunoprecipitation of Polλ with WRN from a mixture of purified proteins (300 ng of each protein) pre-incubated on ice for 2 h. Blots were probed as in (A). (**C**) Mapping of WRN-interacting domain on Polλ. (Top panel) Domain organization of Polλ. NLS, nuclear localization sequence; BRCT, BRCA1 C-terminal domain; Ser/Pro, serine/proline rich domain; PolX domain, catalytic domain conserved in the X family DNA polymerases. Black lines indicate fragments used for mapping. (Bottom panel) Co-immunoprecipitation assay. Purified $(His)_6$-tagged Polλ fragments were incubated with full-length WRN followed by immunoprecipitation with rabbit polyclonal antibody against WRN or with control (Ctrl) IgG. Immunoprecipitates were analyzed by western blotting as in (A).

of 8-oxo-G:A mispair and stimulating the formation of 8-oxo-G:C base pair (12). Therefore, we finally investigated the effect of WRN on incorporation by Polλ of individual nucleotides opposite 8-oxo-G. We found that WRN stimulated the incorporation of both dCTP and dATP opposite 8-oxo-G on gapped DNA duplex, indicating that WRN does not improve the fidelity of 8-oxo-G bypass by Polλ *per se* (Supplementary Figure S11).

DISCUSSION

The WRN protein has been implicated in a number of cellular processes including telomere maintenance, homologous recombination, replication fork recovery and repair of alkylation DNA damage (31–35). There are also reports suggesting a role for WRN in repair of oxidative DNA damage, but the underlying mechanism is not clear (17,18). Here we provide several lines of evidence suggesting that WRN is required for the correction of 8-oxo-G:A mispairs, which is mediated by the long patch BER pathway initiated by the MUTYH DNA glycosylase (12). Firstly, we found that WRN accumulated at sites of 8-oxo-G lesions in a manner dependent on Polλ, an X-family DNA polymerase that mediates translesion synthesis during MUTYH-initiated repair of 8-oxo-G:A mispairs (12). Nuclear focus formation of WRN and Polλ after exposure of cells to oxidative stress was found to be dependent on DNA replication and on the presence of MUTYH, strongly suggesting that WRN and Polλ accumulated at sites of 8-oxo-G:A mispairs.

Secondly, we found that depletion of WRN from human cells increased their sensitivity to H_2O_2 to a level similar to that displayed by cells lacking Polλ. Together with the finding that co-depletion of WRN and Polλ did not have an additive effect on the cellular sensitivity to oxidative stress, these data demonstrate that WRN and Polλ act in the same DNA repair pathway. Most importantly, the hypersensitivity of WRN- and Polλ-deficient cells to H_2O_2 was completely suppressed by depletion of MUTYH, strongly suggesting that WRN and Polλ are involved in the repair of 8-oxo-G:A mispairs initiated by the MUTYH DNA glycosylase. One can imagine a scenario where in absence of Polλ and/or WRN, ssDNA breaks resulting from the processing of 8-oxo-G:A mispairs by MUTYH and APE1 are converted to DNA double-strand breaks in the next round of DNA replication, leading to cell cycle arrest followed either by DNA repair or by cell death (Supplementary Figure S12).

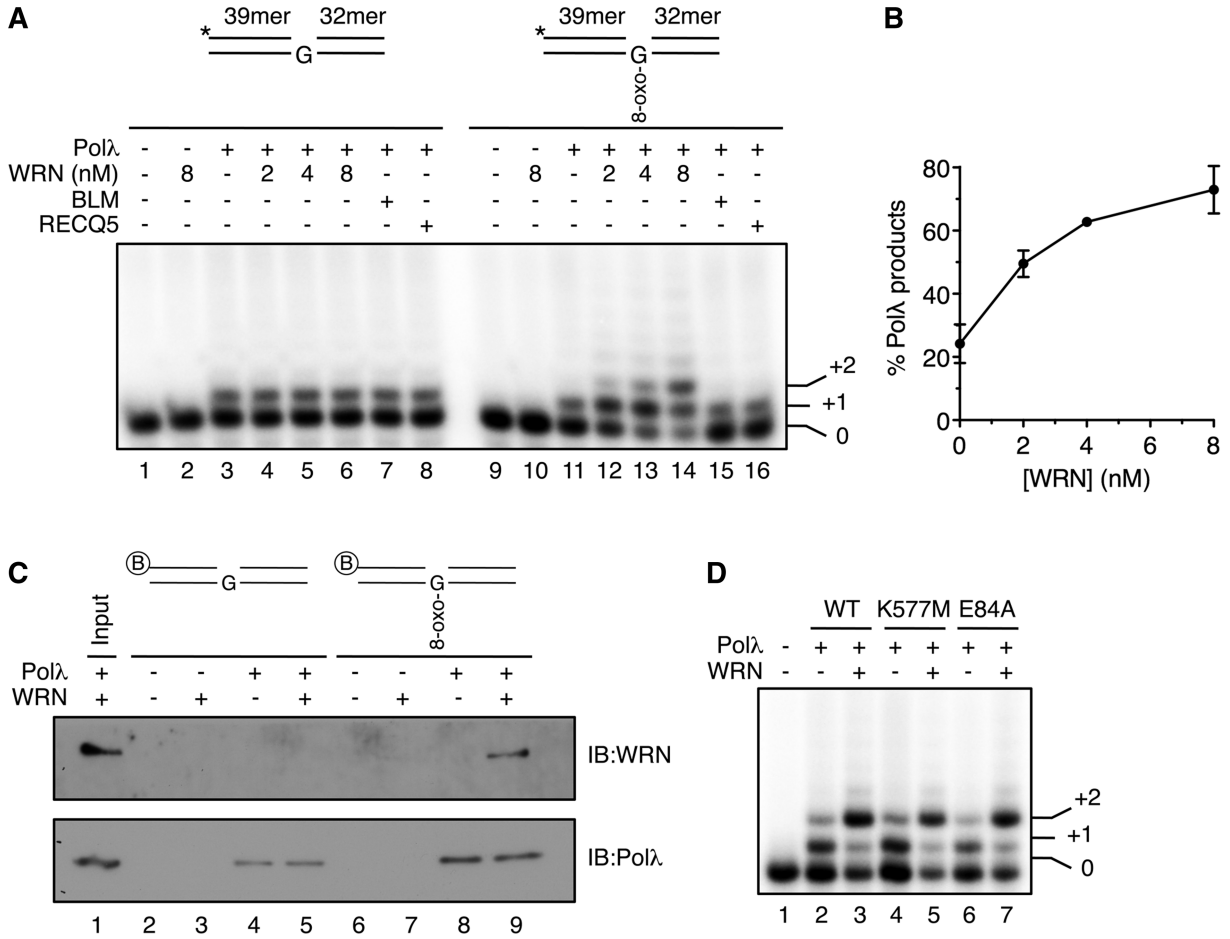

Figure 7. WRN promotes bypass of 8-oxo-G by Polλ on gapped DNA duplex. (**A**) Effect of WRN, BLM and RECQ5 on primer extension by Polλ across a 1-nt DNA gap opposite either a normal G or an 8-oxo-G. Reaction mixtures contained 1 nM DNA substrate, 5 nM Polλ, 10 μM dNTPs and indicated concentrations of WRN. BLM and RECQ5 were present at concentrations of 20 nM and 80 nM, respectively. Schemes of the DNA substrate are shown above the gels. Asterisks indicate radioactive label on the 5′-end of the primer. Reactions were analyzed as specified under the 'Materials and Methods' section. (**B**) Quantification of Polλ activity on gapped DNA duplex containing 8-oxo-G in the presence of increasing amounts of WRN as shown in (A). Relative concentration of Polλ products is plotted. Data points represent the mean of values from three independent experiments. (**C**) Binding of WRN and Polλ to 1-nt gap DNA duplexes with or without 8-oxo-G lesion. 20 nM Polλ and 20 nM WRN were incubated alone or in combination with 100 nM 5′-biotinylated gapped DNA duplexes in the presence of 1 μM dCTP. Bound proteins were isolated using streptavidin beads and analyzed by immunoblotting (IB). Lane 1 contains 100% of input material. (**D**) Incorporation of dCTP by Polλ on 8-oxo-G-containing gapped DNA substrate in the presence of helicase-deficient (K557M) and exonuclease-deficient (E84A) mutants of WRN. Reactions were carried out as in (A). Wild type (WT) and mutant forms of WRN were present at a concentration of 8 nM.

Finally, we show that WRN forms a stable complex with Polλ *in vivo* and *in vitro* and stimulates specifically the bypass of 8-oxo-G by Polλ on a gapped DNA duplex resembling the DNA intermediate generated during MUTYH-initiated repair of 8-oxo-G:A mispairs. Moreover, we show that WRN stimulates 8-oxo-G bypass by Polλ following MUTYH/APEI-mediated processing of 8-oxo-G:A mispairs *in vitro*. WRN stimulated not only DNA gap filling by Polλ opposite 8-oxo-G, but it also enhanced the subsequent strand displacement synthesis by Polλ. Therefore, it appears that the role of WRN in MUTYH-initiated repair of 8-oxo-G:A mispair is to promote this pathway in direction of long-patch BER. It is known that DNA ligase I is not able to efficiently ligate a DNA substrate containing a nick in the vicinity of 8-oxo-G:C pair, but is able to seal a nick located 1 nt downstream of the correctly incorporated C (12). Thus stimulation of Polλ-mediated strand displacement synthesis would enable more efficient completion of accurate MUTYH-initiated BER. Interestingly, previous studies have shown that WRN physically interacts with FEN1 and strongly stimulates FEN1-catalyzed cleavage of 5′-flap substrates (36). Such an activity is essential to generate a ligateable 5′-P end following strand displacement synthesis by Polλ during the MUTYH-initiated repair of 8-oxo-G:A mispairs. Thus, it is possible that, in addition to stimulation of Polλ-mediated long-patch DNA repair synthesis, WRN promotes the endonucleolytic cleavage by FEN1 in this BER pathway.

Our study has shown that the helicase and exonuclease activities of WRN are dispensable for Polλ stimulation by WRN. Similarly, the functional interaction of WRN with FEN1 was independent of the WRN catalytic functions (36). These findings suggested that the stimulatory effect of WRN on these enzymes stems from direct protein–protein interaction. It is possible that physical interaction

between WRN and Polλ triggers a conformational change in the polymerase, which alters its catalytic properties. Of note, WRN was shown to stimulate DNA synthesis by the Y-family translesion polymerases η, ι and κ by increasing the reaction rate (37).

We have also obtained evidence suggesting that the catalytic activities of WRN are not essential for repair of oxidative DNA damage in the cell. This notion is consistent with the fact that there are no case reports of WS patients carrying loss-of-function mutations in the exonuclease or in the helicase domains of WRN. All WS-causing mutations reported thus far result either in the elimination of the nuclear localization signal located at the C-terminus of WRN or lead to an unstable protein (38).

Importantly, WRN stimulated DNA gap filling and strand displacement synthesis by Polλ only if the DNA substrate contained an 8-oxo-G lesion opposite the gap. Accordingly, although Polλ could bind to both lesion-free and 8-oxo-G-containing substrates, WRN was bound only to the latter substrate in a manner dependent on Polλ. Thus, it is possible that binding of Polλ to the lesion generates a particular structure either on the DNA or in Polλ itself, allowing Polλ-WRN interaction. Our finding of direct interaction of WRN with the catalytic domain of Polλ suggest that a lesion-induced structural change in Polλ leading to the exposure of the WRN interaction site is the more likely scenario. In the complex of Polλ with lesion-free gapped duplex, the WRN interaction site on Polλ might be hindered by DNA. Future structural studies will be needed to shed more light on this issue.

Cells derived from individuals suffering from WS show premature senescence and accelerated telomere shortening, which explains the early onset of aging manifested in these patients and suggest that WRN plays a role in telomere metabolism (16). Evidence indicates that genomic instability in WS cells depends directly on telomere dysfunction, suggesting that the primary cause of high cancer incidence in WS is a breakdown in telomere integrity (39). It is well known that oxidative stress accelerates telomere shortening and shortens replicative lifespan of cultured human primary fibroblasts (40). A recent study has revealed that disruption of the mouse Ogg1 gene is associated with accumulation of oxidative guanine lesions in telomeres and increased telomere attrition upon oxidative stress, suggesting that oxidative stress compromises telomere integrity through induction of oxidative base damage (41). Thus, based on the earlier finding that WRN deficiency leads to accumulation of 8-oxo-G lesions in the genomic DNA (17,18) and our data implicating WRN in the repair of 8-oxo-G:A mispairs, it is tempting to speculate that WS phenotypes arise from a defect in repair of oxidative DNA base damage in telomeres. CO-FISH analysis of telomeric repeats revealed that the oxidative stress-induced telomere shortening in Ogg1$^{-/-}$ primary MEFs most frequently arises from single-strand breaks in the G-strand, which compromise telomere lagging strand synthesis (41). Interestingly, preferential telomere lagging strand loss was also demonstrated in cells lacking WRN or FEN1 (31,42). Thus, it is possible that the accelerated telomere shortening observed in these cells stems from persistence of 8-oxo-G lesions within the telomeric G-strand due to defective repair of 8-oxo-G:A mispairs. Therefore, it will be interesting to evaluate the role of the other enzymes acting in this BER pathway, such as MUTYH or Polλ, in promoting telomere integrity upon oxidative stress. Such studies will shed more light on how oxidative stress contributes to aging and cancer development.

SUPPLEMENTARY DATA

Supplementary Data are available at NAR Online: Supplementary Tables 1–3, Supplementary Figures 1–12, Supplementary Materials and Methods and Supplementary References [12,22,24,43–45].

ACKNOWLEDGMENTS

We thank S.H. Wilson for Polλ$^{+/+}$ and Polλ$^{-/-}$ MEFs, L. Blanco for antibody against mouse Polλ, K. Surendranath for help with Annexin V-binding assay and A. Franchitto for WS fibroblasts stably expressing WRN-E84A and WRN-K577M, respectively. We are also grateful to J. Jiricny and G. Maga for fruitful discussions.

FUNDING

Swiss National Science Foundation [31003A-129747/1 to P.J.]; [3100-109312/2 to U.H., P.P. and B.V.L.]; UBS AG to P.J. and R.K.; Oncosuisse [KLS-02344-02-2009 to P.J.]; Stiftung zur Krebsbekämpfung (to P.J.); University of Zurich (to U.H., B.V.L. and P.J.). National Institutes of Health Intramural Program of the National Institute on Aging [Z01-AG000726-17, in part]. Funding for open access charge: Swiss National Science Foundation.

Conflict of interest statement. None declared.

REFERENCES

1. Valko,M., Izakovic,M., Mazur,M., Rhodes,C.J. and Telser,J. (2004) Role of oxygen radicals in DNA damage and cancer incidence. *Mol. Cell. Biochem.*, **266**, 37–56.
2. Klaunig,J.E. and Kamendulis,L.M. (2004) The role of oxidative stress in carcinogenesis. *Annu. Rev. Pharmacol. Toxicol.*, **44**, 239–267.
3. Klaunig,J.E., Kamendulis,L.M. and Hocevar,B.A. (2010) Oxidative stress and oxidative damage in carcinogenesis. *Toxicol. Pathol.*, **38**, 96–109.
4. Maynard,S., Schurman,S.H., Harboe,C., de Souza-Pinto,N.C. and Bohr,V.A. (2009) Base excision repair of oxidative DNA damage and association with cancer and aging. *Carcinogenesis*, **30**, 2–10.
5. Friedberg,E.C., Walker,G.C., Siede,W., Wood,R.D., Schultz,R.A. and Ellenberger,T. (2006) *DNA Repair and Mutagenesis*, 2nd edn. ASM Press, Washington, DC, p. 16.
6. Avkin,S. and Livneh,Z. (2002) Efficiency, specificity and DNA polymerase-dependence of translesion replication across the oxidative DNA lesion 8-oxoguanine in human cells. *Mutat. Res.*, **510**, 81–90.
7. Greenman,C., Stephens,P., Smith,R., Dalgliesh,G.L., Hunter,C., Bignell,G., Davies,H., Teague,J., Butler,A., Stevens,C. *et al.* (2007) Patterns of somatic mutation in human cancer genomes. *Nature*, **446**, 153–158.

8. Hazra,T.K., Das,A., Das,S., Choudhury,S., Kow,Y.W. and Roy,R. (2007) Oxidative DNA damage repair in mammalian cells: a new perspective. *DNA Repair (Amst.)*, **6**, 470–480.
9. van Loon,B., Markkanen,E. and Hubscher,U. (2010) Oxygen as a friend and enemy: how to combat the mutational potential of 8-oxo-guanine. *DNA Repair (Amst.)*, **9**, 604–616.
10. Takao,M., Zhang,Q.M., Yonei,S. and Yasui,A. (1999) Differential subcellular localization of human MutY homolog (hMYH) and the functional activity of adenine:8-oxoguanine DzNA glycosylase. *Nucleic Acids Res.*, **27**, 3638–3644.
11. Hayashi,H., Tominaga,Y., Hirano,S., McKenna,A.E., Nakabeppu,Y. and Matsumoto,Y. (2002) Replication-associated repair of adenine:8-oxoguanine mispairs by MYH. *Curr. Biol.*, **12**, 335–339.
12. van Loon,B. and Hubscher,U. (2009) An 8-oxo-guanine repair pathway coordinated by MUTYH glycosylase and DNA polymerase lambda. *Proc. Natl Acad. Sci. USA*, **106**, 18201–18206.
13. Yang,H., Clendenin,W.M., Wong,D., Demple,B., Slupska,M.M., Chiang,J.H. and Miller,J.H. (2001) Enhanced activity of adenine-DNA glycosylase (Myh) by apurinic/apyrimidinic endonuclease (Ape1) in mammalian base excision repair of an A/GO mismatch. *Nucleic Acids Res.*, **29**, 743–752.
14. Maga,G., Villani,G., Crespan,E., Wimmer,U., Ferrari,E., Bertocci,B. and Hubscher,U. (2007) 8-oxo-guanine bypass by human DNA polymerases in the presence of auxiliary proteins. *Nature*, **447**, 606–608.
15. Maga,G., Crespan,E., Wimmer,U., van Loon,B., Amoroso,A., Mondello,C., Belgiovine,C., Ferrari,E., Locatelli,G., Villani,G. *et al.* (2008) Replication protein A and proliferating cell nuclear antigen coordinate DNA polymerase selection in 8-oxo-guanine repair. *Proc. Natl Acad. Sci. USA*, **105**, 20689–20694.
16. Rossi,M.L., Ghosh,A.K. and Bohr,V.A. (2010) Roles of Werner syndrome protein in protection of genome integrity. *DNA Repair (Amst.)*, **9**, 331–344.
17. Von Kobbe,C., May,A., Grandori,C. and Bohr,V.A. (2004) Werner syndrome cells escape hydrogen peroxide-induced cell proliferation arrest. *FASEB J.*, **18**, 1970–1972.
18. Das,A., Boldogh,I., Lee,J.W., Harrigan,J.A., Hegde,M.L., Piotrowski,J., de Souza Pinto,N., Ramos,W., Greenberg,M.M., Hazra,T.K. *et al.* (2007) The human Werner syndrome protein stimulates repair of oxidative DNA base damage by the DNA glycosylase NEIL1. *J. Biol. Chem.*, **282**, 26591–26602.
19. Ramadan,K., Maga,G., Shevelev,I.V., Villani,G., Blanco,L. and Hubscher,U. (2003) Human DNA polymerase lambda possesses terminal deoxyribonucleotidyl transferase activity and can elongate RNA primers: implications for novel functions. *J. Mol. Biol.*, **328**, 63–72.
20. Orren,D.K., Brosh,R.M. Jr, Nehlin,J.O., Machwe,A., Gray,M.D. and Bohr,V.A. (1999) Enzymatic and DNA binding properties of purified WRN protein: high affinity binding to single-stranded DNA but not to DNA damage induced by 4NQO. *Nucleic Acids Res.*, **27**, 3557–3566.
21. Garcia,P.L., Liu,Y., Jiricny,J., West,S.C. and Janscak,P. (2004) Human RECQ5β, a protein with DNA helicase and strand-annealing activities in a single polypeptide. *EMBO J.*, **23**, 2882–2891.
22. Kanagaraj,R., Saydam,N., Garcia,P.L., Zheng,L. and Janscak,P. (2006) Human RECQ5β helicase promotes strand exchange on synthetic DNA structures resembling a stalled replication fork. *Nucleic Acids Res.*, **34**, 5217–5231.
23. Xu,X. and Stern,D.F. (2003) NFBD1/KIAA0170 is a chromatin-associated protein involved in DNA damage signaling pathways. *J. Biol. Chem.*, **278**, 8795–8803.
24. Saydam,N., Kanagaraj,R., Dietschy,T., Garcia,P.L., Pena-Diaz,J., Shevelev,I., Stagljar,I. and Janscak,P. (2007) Physical and functional interactions between Werner syndrome helicase and mismatch repair initiation factors. *Nucleic Acids Res.*, **35**, 5706–5716.
25. Kanagaraj,R., Huehn,D., Mackellar,A., Menigatti,M., Zheng,L., Urban,V., Shevelev,I., Greenleaf,A.L. and Janscak,P. (2010) RECQ5 helicase associates with the C-terminal repeat domain of RNA polymerase II during productive elongation phase of transcription. *Nucleic Acids Res.*, **38**, 8131–8140.
26. Parsons,J.L. and Dianov,G.L. (2004) Monitoring base excision repair proteins on damaged DNA using human cell extracts. *Biochem. Soc. Trans.*, **32**, 962–963.
27. Braithwaite,E.K., Kedar,P.S., Stumpo,D.J., Bertocci,B., Freedman,J.H., Samson,L.D. and Wilson,S.H. (2010) DNA polymerases beta and lambda mediate overlapping and independent roles in base excision repair in mouse embryonic fibroblasts. *PLoS One*, **5**, e12229.
28. Lee,J.W., Harrigan,J., Opresko,P.L. and Bohr,V.A. (2005) Pathways and functions of the Werner syndrome protein. *Mech. Ageing Dev.*, **126**, 79–86.
29. Huang,S., Li,B., Gray,M.D., Oshima,J., Mian,I.S. and Campisi,J. (1998) The premature ageing syndrome protein, WRN, is a 3′–>5′ exonuclease. *Nat. Genet.*, **20**, 114–116.
30. Gray,M.D., Shen,J.C., Kamath-Loeb,A.S., Blank,A., Sopher,B.L., Martin,G.M., Oshima,J. and Loeb,L.A. (1997) The Werner syndrome protein is a DNA helicase. *Nat. Genet.*, **17**, 100–103.
31. Crabbe,L., Verdun,R.E., Haggblom,C.I. and Karlseder,J. (2004) Defective telomere lagging strand synthesis in cells lacking WRN helicase activity. *Science*, **306**, 1951–1953.
32. Saintigny,Y., Makienko,K., Swanson,C., Emond,M.J. and Monnat,R.J. Jr (2002) Homologous recombination resolution defect in Werner syndrome. *Mol. Cell. Biol.*, **22**, 6971–6978.
33. Franchitto,A., Pirzio,L.M., Prosperi,E., Sapora,O., Bignami,M. and Pichierri,P. (2008) Replication fork stalling in WRN-deficient cells is overcome by prompt activation of a MUS81-dependent pathway. *J. Cell Biol.*, **183**, 241–252.
34. Ammazzalorso,F., Pirzio,L.M., Bignami,M., Franchitto,A. and Pichierri,P. (2010) ATR and ATM differently regulate WRN to prevent DSBs at stalled replication forks and promote replication fork recovery. *EMBO J.*, **29**, 3156–3169.
35. Harrigan,J.A., Wilson,D.M. III, Prasad,R., Opresko,P.L., Beck,G., May,A., Wilson,S.H. and Bohr,V.A. (2006) The Werner syndrome protein operates in base excision repair and cooperates with DNA polymerase beta. *Nucleic Acids Res.*, **34**, 745–754.
36. Brosh,R.M. Jr, von Kobbe,C., Sommers,J.A., Karmakar,P., Opresko,P.L., Piotrowski,J., Dianova,I., Dianov,G.L. and Bohr,V.A. (2001) Werner syndrome protein interacts with human flap endonuclease 1 and stimulates its cleavage activity. *EMBO J.*, **20**, 5791–5801.
37. Kamath-Loeb,A.S., Lan,L., Nakajima,S., Yasui,A. and Loeb,L.A. (2007) Werner syndrome protein interacts functionally with translesion DNA polymerases. *Proc. Natl Acad. Sci. USA*, **104**, 10394–10399.
38. Huang,S., Lee,L., Hanson,N.B., Lenaerts,C., Hoehn,H., Poot,M., Rubin,C.D., Chen,D.F., Yang,C.C., Juch,H. *et al.* (2006) The spectrum of WRN mutations in Werner syndrome patients. *Hum. Mutat.*, **27**, 558–567.
39. Crabbe,L., Jauch,A., Naeger,C.M., Holtgreve-Grez,H. and Karlseder,J. (2007) Telomere dysfunction as a cause of genomic instability in Werner syndrome. *Proc. Natl Acad. Sci. USA*, **104**, 2205–2210.
40. von Zglinicki,T. (2002) Oxidative stress shortens telomeres. *Trends Biochem. Sci.*, **27**, 339–344.
41. Wang,Z., Rhee,D.B., Lu,J., Bohr,C.T., Zhou,F., Vallabhaneni,H., de Souza-Pinto,N.C. and Liu,Y. (2010) Characterization of oxidative guanine damage and repair in mammalian telomeres. *PLoS Genet.*, **6**, e1000951.
42. Saharia,A., Guittat,L., Crocker,S., Lim,A., Steffen,M., Kulkarni,S. and Stewart,S.A. (2008) Flap endonuclease 1 contributes to telomere stability. *Curr. Biol.*, **18**, 496–500.
43. Braithwaite,E.K., Prasad,R., Shock,D.D., Hou,E.W., Beard,W.A. and Wilson,S.H. (2005) DNA polymerase lambda mediates a back-up base excision repair activity in extracts of mouse embryonic fibroblasts. *J. Biol. Chem.*, **280**, 18469–18475.
44. Wimmer,U., Ferrari,E., Hunziker,P. and Hubscher,U. (2008) Control of DNA polymerase lambda stability by phosphorylation and ubiquitination during the cell cycle. *EMBO Rep.*, **9**, 1027–1033.
45. Pirzio,L.M., Pichierri,P., Bignami,M. and Franchitto,A. (2008) Werner syndrome helicase activity is essential in maintaining fragile site stability. *J. Cell Biol.*, **180**, 305–314.

Supplementary Information

Involvement of Werner syndrome protein in MUTYH-mediated repair of oxidative DNA damage

Radhakrishnan Kanagaraj, Prasanna Parasuraman, Boris Mihaljevic, Barbara van Loon, Kamila Burdova, Christiane König, Antonia Furrer, Vilhelm A. Bohr, Ulrich Hübscher and Pavel Janscak

Supplementary Materials and Methods

DNA substrates and siRNA

Oligonucleotides used for gap-filling and primer extension assays were purchased from Purimix and purified by denaturing PAGE. The sequences are:
72-mer template:
3′-ATGTTGGTTCTCGTATGCTGCCGGTCACGGCTTAAGTGT**X**GCGGCCGCG GGTTGGAGGGCTTATAGATTATG-5′; the bold letter X denotes G or 8-oxo-G. The underlined sequences correspond to the primer-annealing site.
39-mer primer:
5′-TACAACCAAGAGCATACGACGGCCAGTGCCGAATTCACA-3′
32-mer oligonucleotide:
5′-CGCCGGCGCCCAACCTCCCGAATATCTAATAC-3′

The 39-mer primer was 5′-end labeled with T4 polynucleotide kinase (NEB) and γ[^{32}P]ATP (GE Healthcare) mixed with appropriate template oligonucleotide at 1:1 (M/M) ratio in the presence of 20 mM Tris-HCl (pH 7.4) and 150 mM NaCl, heated at 95°C for 10 minutes and then slowly cooled down to room temperature. To generate gapped substrates, annealing mixtures also contained the equimolar amount of the 32-mer oligonucleotide phosphorylated at the 5′-end by T4 polynucleotide kinase (NEB) prior to annealing.

A 5′-end biotinylated version of the above 39-mer oligonucleotide was purchased from MWG-Biotech AG.

All siRNA oligoduplexes used in this study were purchased from Microsynth. The sequences of the sense strands of these duplexes are shown below:
siWRN: 5′-UAGAGGGAAACUUGGCAAAdTdT-3′
siPolλ: 5′-CAAAAGUACUUGCAAAGAUdTdT-3′
siMUTYH: 5′-UCACAUCAAGCUGACAUAUCAAGUAdTdT-3′
siCtrl: 5′-CGUACGCGGAAUACUUCGAdTdT-3′

Antibodies

Affinity purified rabbit polyclonal antibodies against human Polλ (used for immunofluorescence staining at a 1:500 dilution) and WRN (used for immunofluorescence staining at a 1:500 dilution) were described previously (1,2). Rabbit polyclonal antibody against human Polλ used for immunoblotting was purchased from Bethyl Laboratories (IHC-00325). Rabbit polyclonal antibody against mouse Polλ was a kind gift from Dr. L. Blanco. Rabbit polyclonal antibody against human WRN used for

immunoprecipitation was purchased from Abcam (ab17988). Goat polyclonal antibody against human WRN used for immunoblotting was purchased from Santa Cruz (sc-1956). Mouse monoclonal anti-WRN antibodies were purchased from BD Biosciences (611169; used for immunoblotting) and Abcam (ab 66601; used for immunofluorescence staining at a 1:50 dilution). Mouse monoclonal antibodies against MUTYH and 8-oxo-G were purchased from Abcam (ab55551) and Millipore (MAB3560, clone 483.15), respectively. Antibodies against TFIIH (rabbit polyclonal), β-tubulin (mouse monoclonal) and cyclin-A (mouse monoclonal) were from Santa Cruz.

Cell lines

Immortalized Polλ$^{+/+}$ and Polλ$^{-/-}$ mouse embryonic fibroblasts (MEFs) were obtained from Dr. S.H. Wilson (3). Polλ$^{-/-}$ MEFs stably transduced with a retroviral vector encoding human Polλ-myc were described previously (4). SV-40 immortalized WS fibroblasts (AG11395) stably expressing WRN-E84A and WRN-K577M, respectively, were maintained as previously described (5).

BrdU incorporation analysis

BrdU was added to media to a final concentration 10 μM at 30 minutes before harvesting the cells. Staining with FITC-conjugated anti-BrdU antibody was done according to manufacturer protocol (BD Biosciences). Flow cytometry analysis was performed using FACSCalibur (BD Biosciences) and FlowJo software.

GST pull-down assay

Binding of Polλ to GST-tagged fragments of WRN was tested as previously described (2). Briefly, bacterially expressed GST-WRN fusion proteins were bound to glutathione-Sepharose beads (20 μl; GE Healthcare) and incubated with 0.5 μg of recombinant human Polλ for 2 hours at 4°C. Bound proteins were analyzed by Western blotting. Glutathione beads coated with GST-protein only were used as control.

Annexin V-binding assay

Cell death was monitored using Annexin V-Cy3 apoptosis detection kit (APOAC; Sigma) according to the manufacturer's instructions. Briefly, cells were either left untreated or treated with 500 μM H_2O_2 for 2 hours, and subsequently released into fresh DMEM medium. After 48 hours, cells were harvested and spotted on a glass slide. Live and dead cells were detected by labeling with 6-carboxyfluorescein (green fluorescence) and Annexin V (red fluorescence), respectively. Cells were immediately observed by fluorescence microscope. The percentage of dead cells was calculated relative to total number of cells and plotted using GraphPad Prism as mean ± SD. Data from at least two independent experiments were plotted.

MUTYH-initiated repair assay

5′-labeled 100-mer DNA duplex containing a 8-oxo-G:A mispair was prepared as previously described (1). Reaction mixtures (10 μl) contained 50 mM Tris-HCl (pH 7.5), 20 mM KCl, 2 mM DTT and 5 μM dNTPs. Concentrations of MUTYH, APE1 and Polλ were 50, 0.6 and 2 nM, respectively. WRN was present at concentrations ranging from 0 to 32 nM as indicated. Reaction mixtures containing MUTYH and DNA substrate were treated as follows: (i) incubation for 5 minutes at 30°C, (ii) addition of APE1 and 0.5 mM Mg^{2+}, (iii) incubation for 10 minutes at 30°C, (iv) addition of dNTPs, WRN and Polλ, (v) incubation 15 minutes at 37°C. All reactions were stopped by addition of standard denaturing gel loading buffer (95% formamide, 10 mM EDTA, xylene cyanol and bromophenol blue), heated at 95°C for 3 minutes and loaded on a 7M urea/15% polyacrylamide gel. Gels were scanned using Typhoon 9400 phosphorimager and quantified using ImageQuant software.

Biotin pull-down assay

Gapped DNA duplexes containing the biotinylated version of the 39-mer oligonucleotide were prepared as described above. Before annealing, the 32-mer oligonucleotide was phosphorylated at the 5′-end using T4 polynucleotide kinase (NEB). Binding reactions (50 μl) were carried out at 37 °C for 5 minutes in a buffer containing 50 mM Tris-HCl (pH 7.0), 0.25 mg/ml BSA, 1 mM DTT, 1 mM $MgCl_2$ and 1 μM dCTP. Polλ and WRN were present at a concentration of 20 nM and DNA substrates (with or without 8-oxo-G lesion) at a concentration of 100 nM. DNA-protein complexes were isolated using Streptavidin agarose beads (20 μl; Invitrogen). After incubation on ice for 10 minutes, beads were washed thrice with PBS and bound proteins were analyzed by Western blotting using antibodies against WRN and Polλ.

Supplementary References

1. van Loon,B. and Hubscher,U. (2009) An 8-oxo-guanine repair pathway coordinated by MUTYH glycosylase and DNA polymerase lambda. *Proc. Natl. Acad. Sci. USA*, **106**, 18201-18206.
2. Saydam,N., Kanagaraj,R., Dietschy,T., Garcia,P.L., Pena-Diaz,J., Shevelev,I., Stagljar,I. and Janscak,P. (2007) Physical and functional interactions between Werner syndrome helicase and mismatch-repair initiation factors. *Nucleic Acids Res.*, **35**, 5706-5716.
3. Braithwaite,E.K., Prasad,R., Shock,D.D., Hou,E.W., Beard,W.A. and Wilson,S.H. (2005) DNA polymerase lambda mediates a back-up base excision repair activity in extracts of mouse embryonic fibroblasts. *J. Biol. Chem.*, **280**, 18469-18475.
4. Wimmer,U., Ferrari,E., Hunziker,P. and Hubscher,U. (2008) Control of DNA polymerase lambda stability by phosphorylation and ubiquitination during the cell cycle. *EMBO Rep.*, **9**, 1027-1033.
5. Pirzio, L.M., Pichierri, P., Bignami, M. and Franchitto, A. (2008) Werner syndrome helicase activity is essential in maintaining fragile site stability. *J Cell Biol*, **180**, 305-314.

Supplementary Table 1. Quantitative analysis of immunofluorescence images of U2OS cells stained for WRN and Polλ prior to and after H_2O_2 treatment

	Nuclei scored as foci positive[a] (%)			Nuclei with co-localizing foci[b] (%)
	WRN	Polλ	WRN and Polλ	
Untreated	6	7.5	4.5	4
H_2O_2	45	65	41	34.5

Representative images are shown in Figure 3A.

At least 300 nuclei from three independent experiments were analyzed.

[a]Foci positive nuclei: if nuclei contained at least ten distinct foci.

[b]Co-localization positive nuclei: if $\geq$ 75% of WRN foci overlapped with Polλ foci.

Supplementary Table 2. Quantitative analysis of immunofluorescence images of U2OS cells stained for WRN and 8-oxo-G prior to and after H_2O_2 treatment

	Nuclei scored as foci positive[a] (%)			Nuclei with co-localizing foci[b] (%)
	WRN	8-oxo-G	WRN and 8-oxo-G	
Untreated	4	3	3	2
H_2O_2	47.4	51	45.5	42

Representative images are shown in Figure 4A (*first two rows*).

At least 300 nuclei from three independent experiments were analyzed.

[a]Foci positive nuclei: if nuclei contained at least six distinct foci.

[b]Co-localization positive nuclei: if ≥75% of 8-oxo-G foci overlapped with WRN foci.

Supplementary Table 3. Quantitative analysis of immunofluorescence images of U2OS cells stained for Polλ and 8-oxo-G prior to and after H_2O_2 treatment

	Nuclei scored as foci positive[a] (%)			Nuclei with co-localizing foci[b] (%)
	Polλ	8-oxo-G	Polλ and 8-oxo-G	
Untreated	5.5	4	2	2
H_2O_2	61.5	54	52.5	50.5

Representative images are shown in Figure 4A (*last two rows*).

At least 300 nuclei from three independent experiments were analyzed.

[a]Foci positive nuclei: if nuclei contained at least six distinct foci.

[b]Co-localization positive nuclei: if ≥75% of 8-oxo-G foci overlapped with Polλ foci.

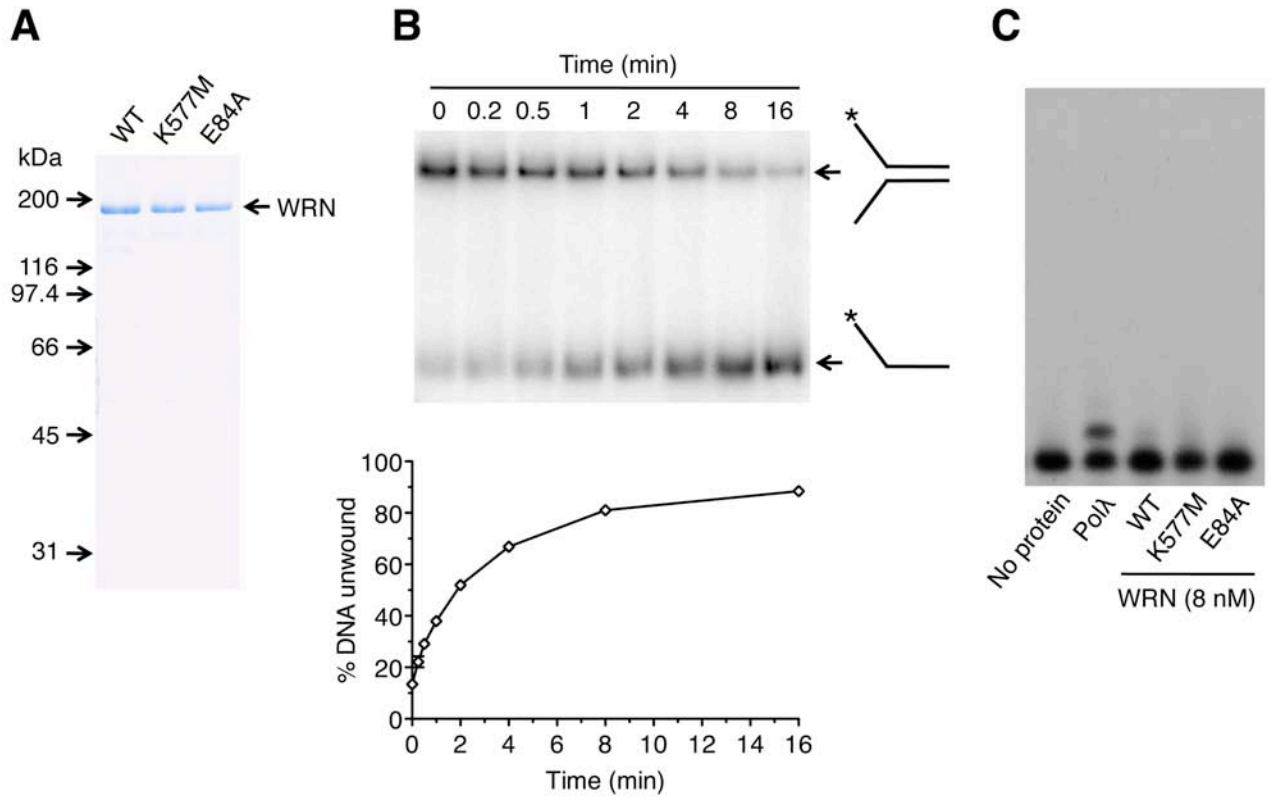

Figure S1. Characterization of purified wild-type and mutant forms of WRN protein used in this study. (A) SDS PAGE analysis. Gel was stained with Coomassie Brilliant Blue R-250. The molecular masses of protein standards are indicated on the left. (B) Kinetics of WRN-mediated unwinding of 30-bp forked DNA duplex. Reaction contained 1 nM [^{32}P]DNA. (*Top panel*) Reaction aliquots at indicated time points were analyzed by native PAGE followed by phosphorimaging. Schemes of the substrate and the reaction products are also shown. The position of the radioactive label (5′-end) is indicated by asterisks. (*Bottom panel*) Gel image was quantified using ImageQuant software. Relative concentration of unwound products calculated as a percentage of total DNA is plotted. (C) Preparations of WRN and its mutants do not contain a contaminating DNA polymerase activity. The primer extension assay was carried out as described in Experimental Procedures using the lesion-free template. WRN and its mutants were present at a concentration of 8 nM and Polλ at a concentration of 6 nM.

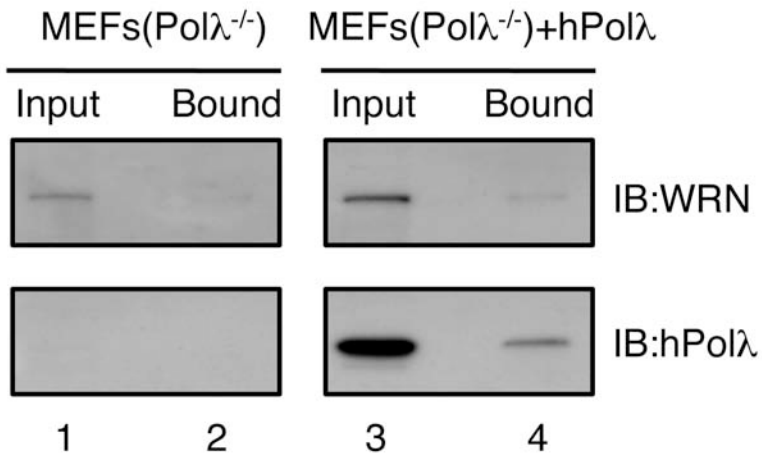

Figure S2. Protein recruitment assay using biotinylated 8-oxo-G:A hairpin substrate and whole cell extract from Polλ$^{-/-}$ MEFs (*left panel*) or Polλ$^{-/-}$ MEFs complemented with human Polλ (hPolλ) cDNA (*right panel*). Polλ$^{-/-}$ MEFs were stably transduced with a retroviral vector expressing Myc-tagged hPolλ. Cell extracts were incubated with the DNA substrate for 8 minutes before formaldehyde crosslinking. Bound proteins were analyzed by western blotting. Blots were probed with antibodies against WRN and Polλ. 10% of input material was loaded.

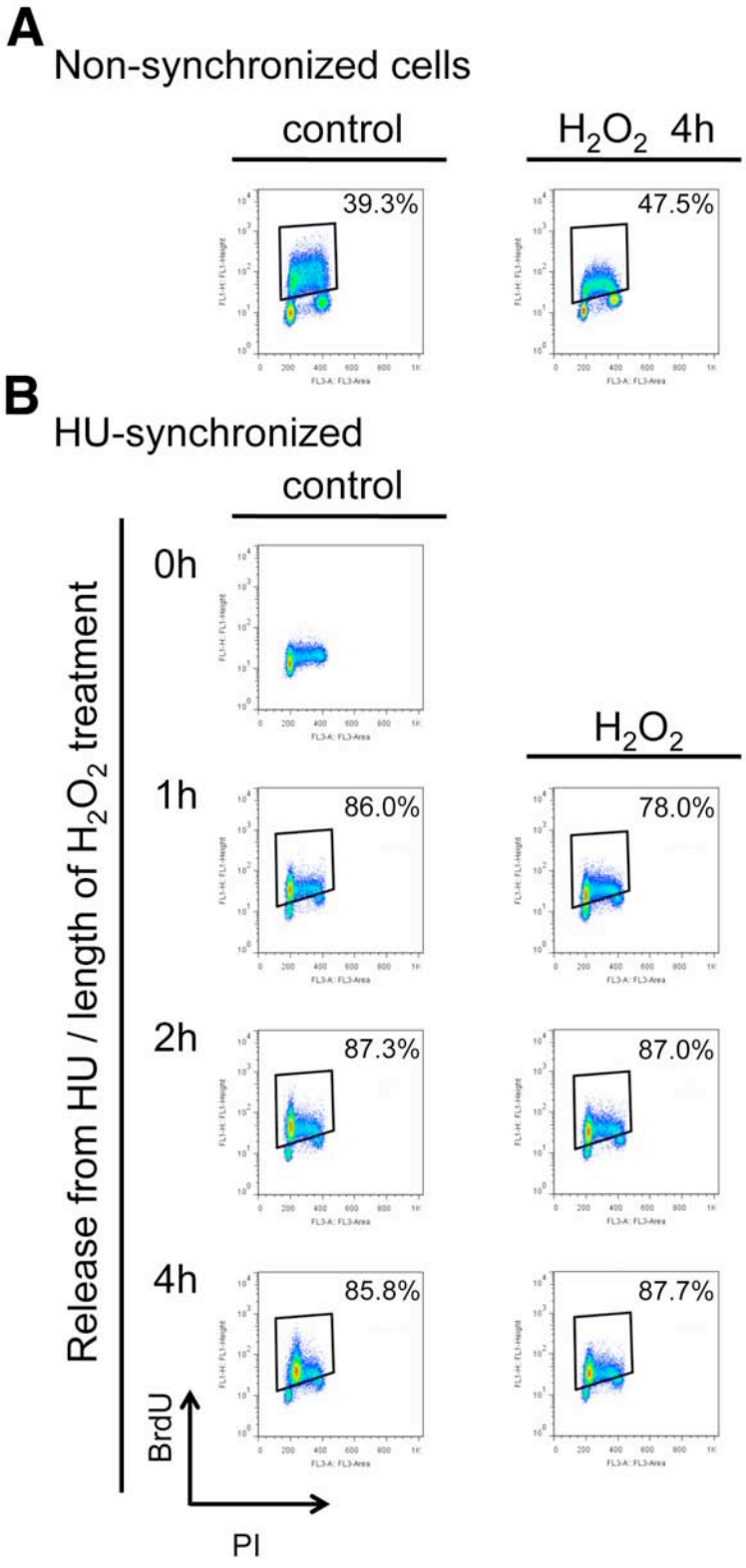

Figure S3. Flow cytometry analysis of BrdU incorporation in asynchronous U2OS cells (A) and hydroxyurea (HU)-synchronized U2OS cells (B) prior to and after treatment with hydrogen peroxide (500 μM). BrdU incorporation (FITC) (*y* axis) was measured against DNA content (propidium iodide, PI) (*x* axis). BrdU was added 30 minutes before harvesting the cells. The percentage of cell incorporating BrdU is indicated.

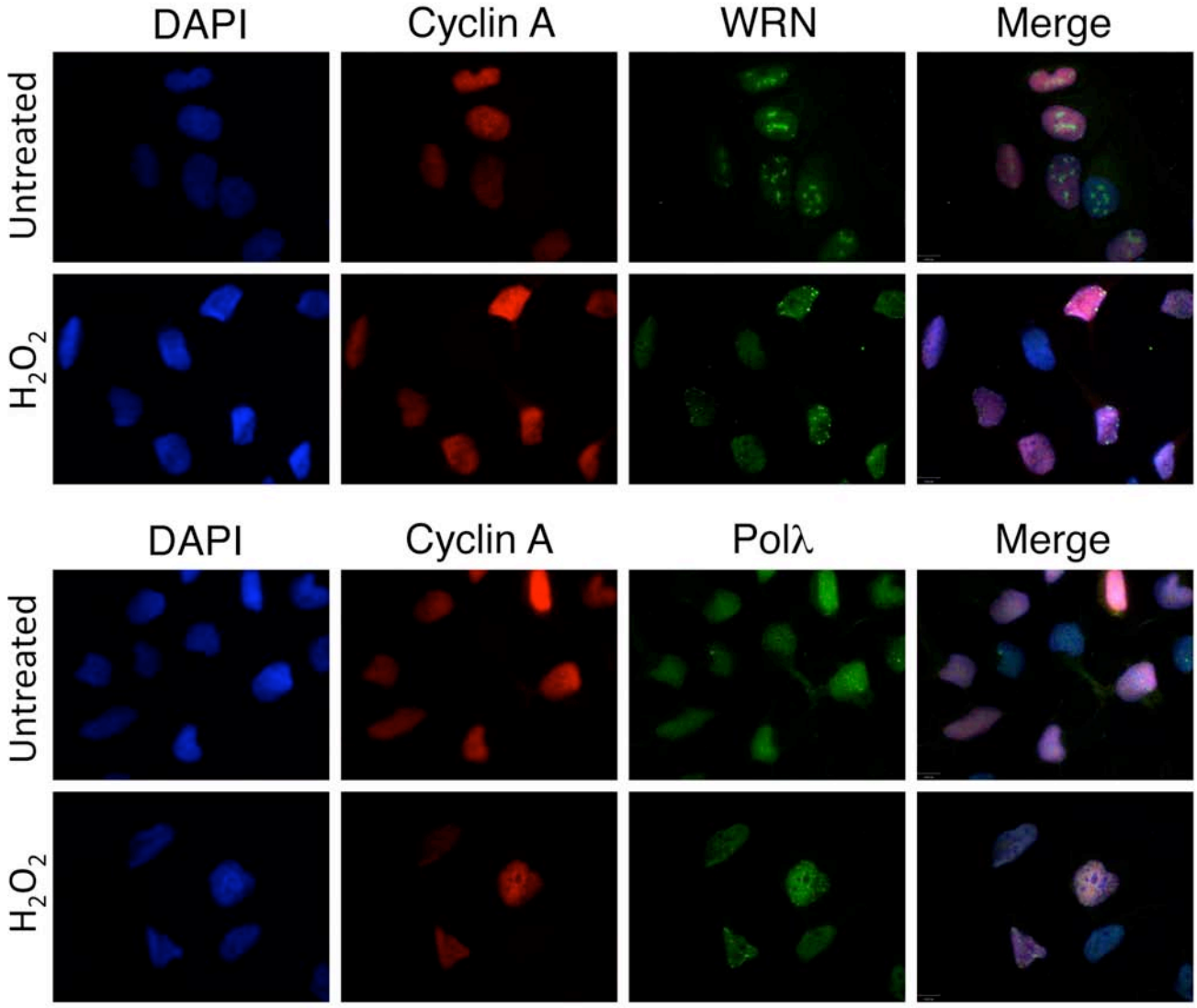

Figure S4. S/G2 phase-specific formation of WRN and Polλ foci in response to oxidative stress. Cells grown on glass coverslips were either left untreated or treated with 500 μM H_2O_2 for 2 hours. After treatment, cells were fixed and immunostained using antibodies against WRN (green) and cyclin A (red) (*top panel*) or against Polλ (green) and cyclin A (red) (*bottom panel*). DAPI staining of the nucleus is shown in blue. Cells positive for cyclin A (dispersed nuclear staining) are in S/G2, whereas cells lacking cyclin A are in G1.

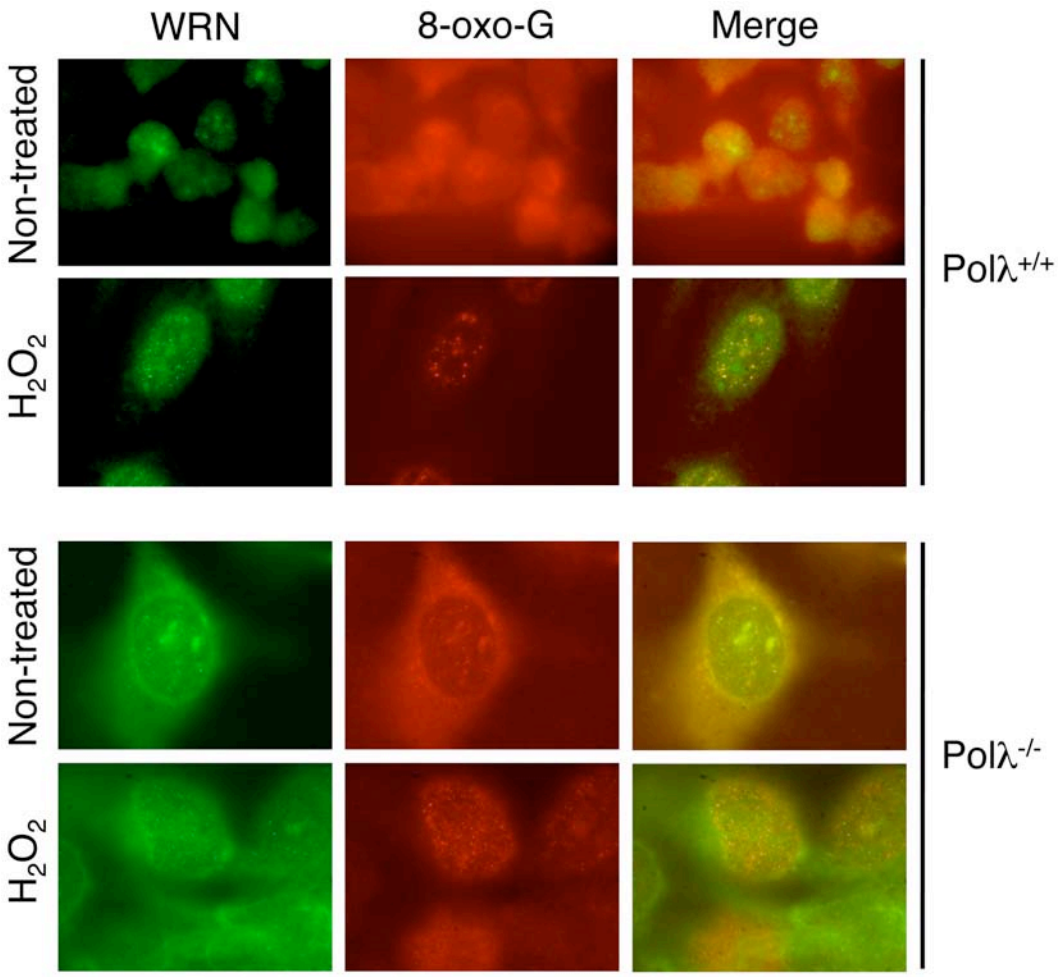

Figure S5. Polλ is required for the recruitment of WRN to sites of 8-oxo-G lesions. Polλ$^{+/+}$ (*top panel*) and Polλ$^{-/-}$ (*bottom panel*) mouse embryonic fibroblasts were treated with 100 μM H_2O_2 (or left untreated) for 2 hours. Cells were fixed and immunostained to visualize WRN (green) and 8-oxo-G (red). Representative images are shown.

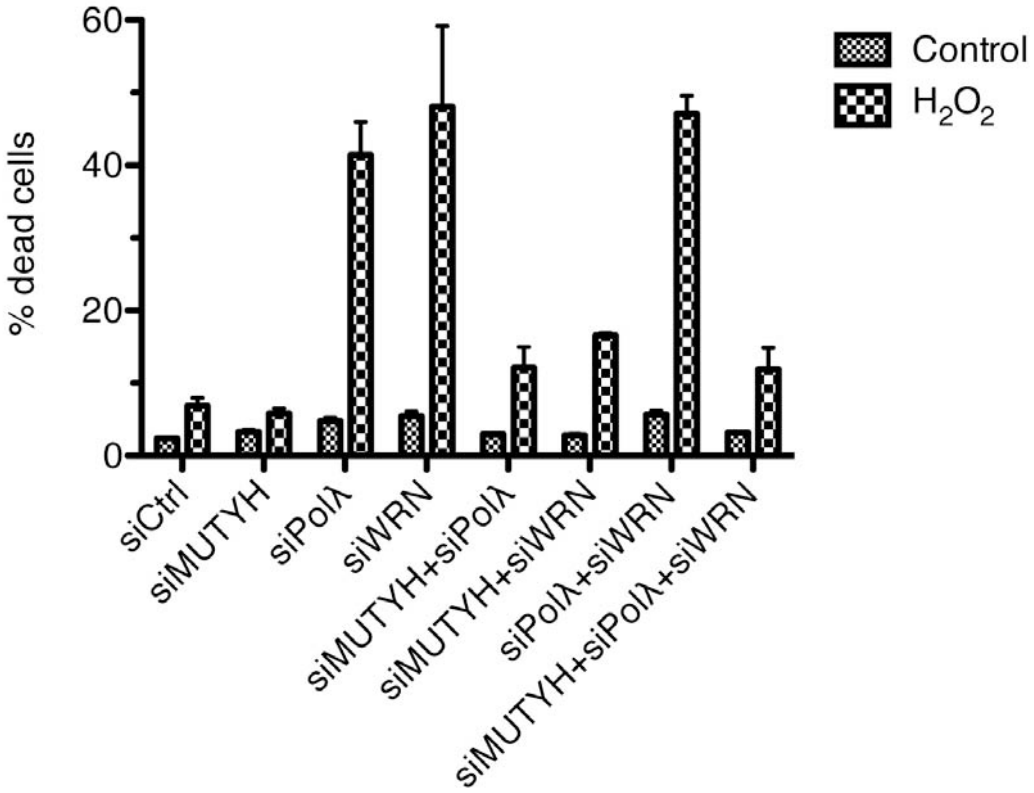

Figure S6. Depletion of MUTYH suppresses cell death caused by WRN- or Polλ-deficiency under conditions of oxidative stress. HeLa cells transfected with indicated siRNAs were treated with 500 μM H_2O_2 for 2 hours or mock-treated. 48 hours post-treatment, percentage of dead cells was determined using Annexin V-binding assay as described in Supplementary Materials and Methods. The data points represent the mean of two independent experiments with at least 1000 cells scored in each experiment. siCtrl, siMUTYH, siWRN and siPolλ represent siRNA against luciferase, MUTYH, WRN and Polλ, respectively.

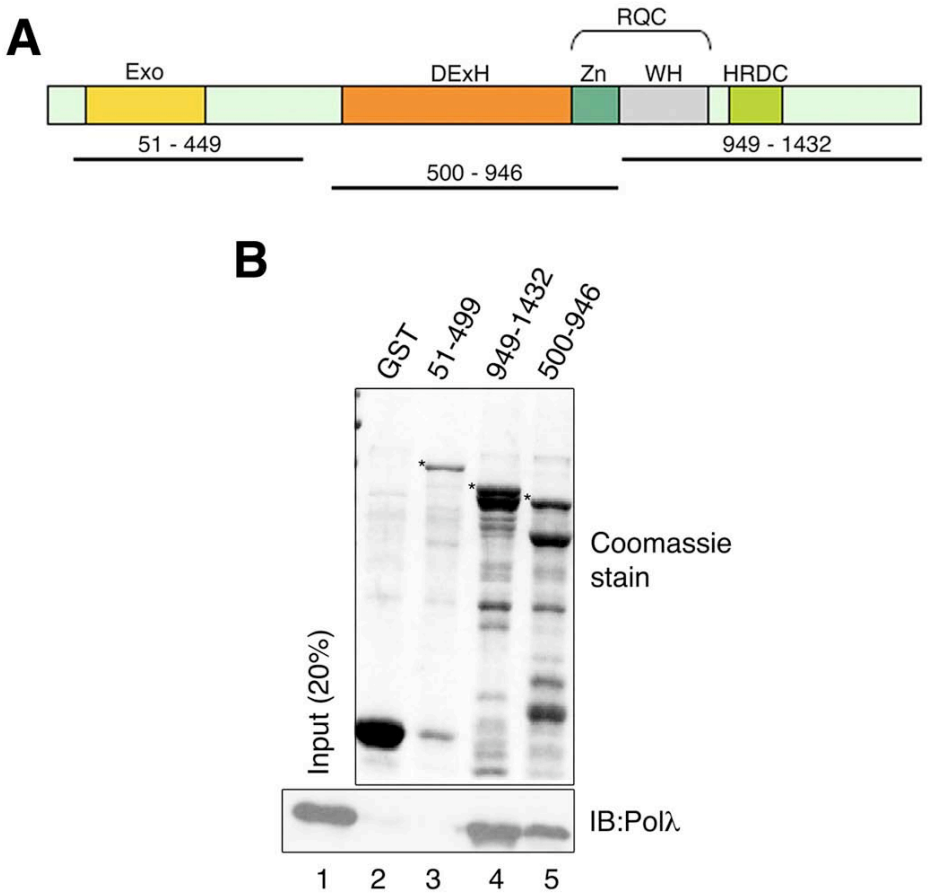

Figure S7. Mapping of Polλ-interacting domain of WRN. (A) Domain organization of WRN. Exo, Exonuclease domain; DExH, helicase domain conserved in the DExH family of helicases; RQC, RecQ C-terminal domain composed of Zn-binding (Zn) and winged-helix (WH) subdomains; HRDC, helicase and RNase D C-terminal domain. The black lines indicate WRN fragments used. (B) GST pull-down assay. The indicated WRN fragments were produced as fusions with GST and immobilized on glutathione beads. Binding of purified recombinant Polλ to the beads was analyzed by Western blotting. The Coomassie Brilliant Blue-stained gel from SDS-PAGE analysis of the GST-WRN fragments isolated on glutathione beads is also shown. Asterisks indicate the GST-WRN fragments. The additional protein bands correspond to proteolytic degradation products as determined by immunoblotting using an anti-GST antibody (data not shown). Lane 1, 20% of input of Polλ. IB, immunoblotting.

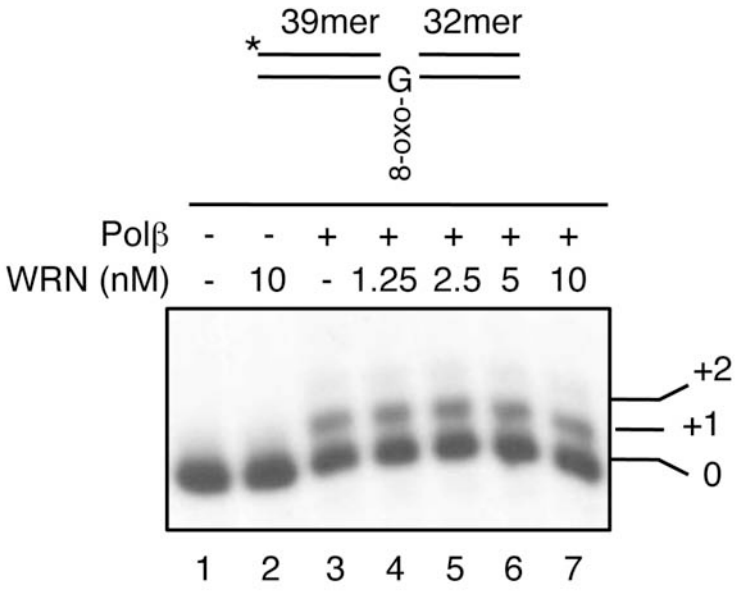

Figure S8. WRN does not promote DNA gap filling by Polβ opposite 8-oxo-G. Reaction mixtures contained 1 nM DNA substrate, 3 nM Polβ, 10 μM dNTPs and indicated concentrations of WRN. Scheme of the DNA substrate is shown. Asterisks indicate radioactive label on the 5′-end of 39-mer primer. Reactions were analyzed as specified under Materials and Methods.

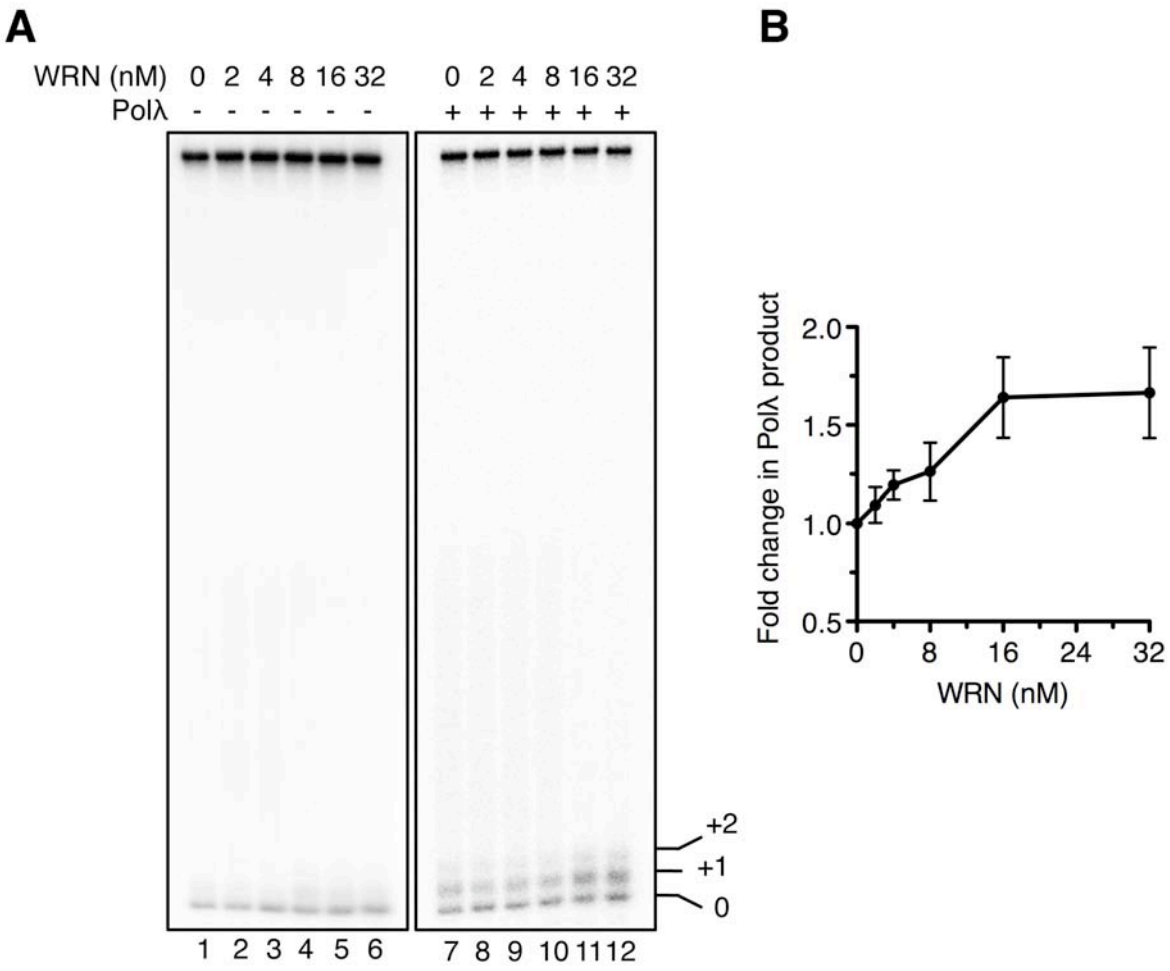

Figure S9. WRN promotes MUTYH/Polλ-mediated repair of 8-oxo-G:A mispairs. (A, *left panel*) Effect of WRN on the removal of A mispaired to 8-oxo-G mediated by MUTYH and APE1. Reaction mixtures contained 1 nM DNA substrate, 50 nM MUTYH, 0.6 nM APE1, 5μM dNTPs and indicated concentrations of WRN. Reactions were analyzed as specified under Supplemental Experimental Procedures. (A, *right panel*) Effect of WRN on Polλ-mediated bypass of 8-oxo-G following the removal of mispaired A by MUTYH and APE1. Reaction mixtures contain 1 nM DNA substrate, 50 nM MUTYH, 0.6 nM APE1, 2 nM Polλ and 5μM dNTPs. Reactions were analyzed as in (A). The positions of MUTYH/APE1 cleavage product (0) and Polλ extension products (+1, +2) are indicated. (B) Quantification of Polλ activity in the presence of MUTYH, APE1 and increasing amounts of WRN from three different experiments as the one documented in (A); error bars, ± SD values.

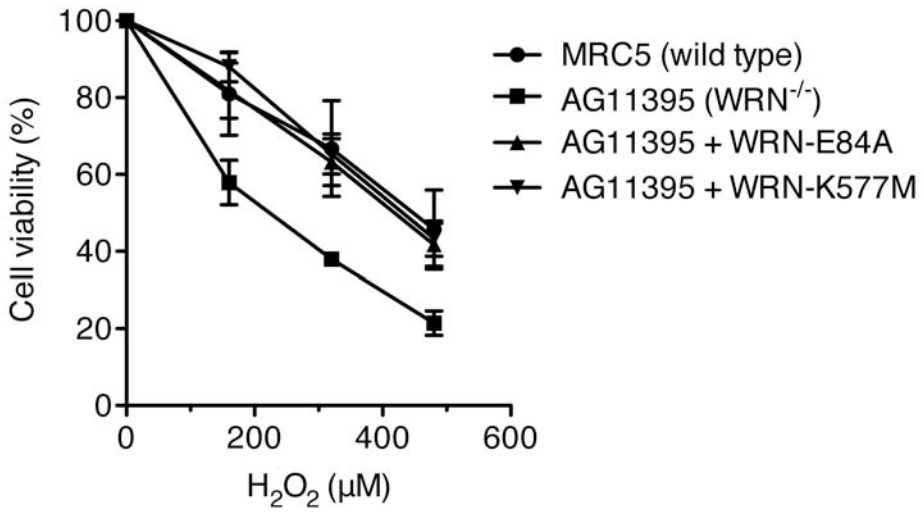

Figure S10. Catalytically inactive mutants of WRN restore tolerance to oxidative stress in Werner syndrome cells. Indicated cell lines were treated with different concentrations of H_2O_2 for 2 hours. Cell viability assay was performed as described in Materials and Methods. Data points represent the mean of three independent experiments ± SD. WRN-E84A, exonuclease-dead mutant of WRN; WRN-K577M, helicase-dead mutant of WRN.

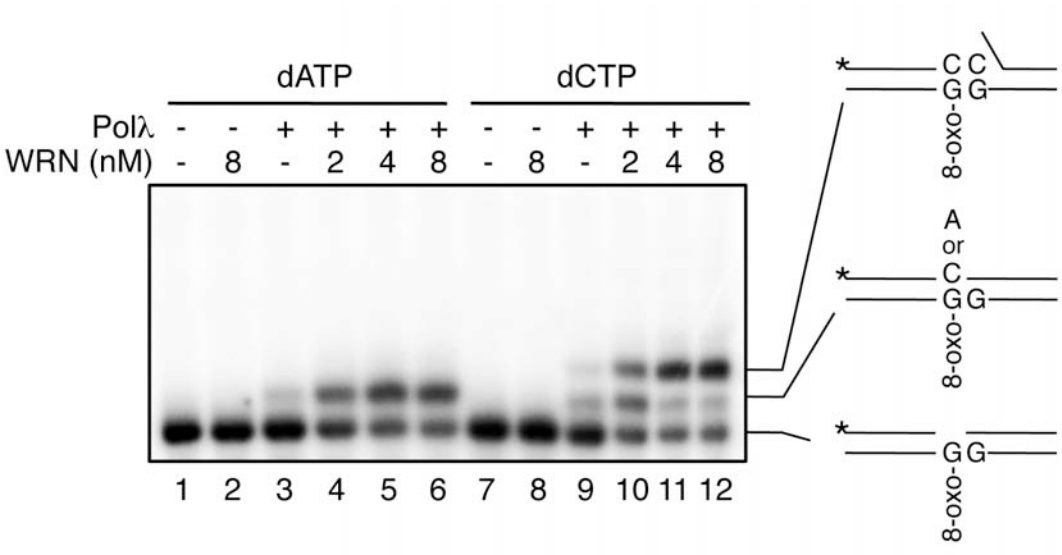

Figure S11. Effect of WRN on bypass of 8-oxo-G by Polλ on gapped DNA duplex as measured by single nucleotide incorporation assay. Reactions were carried out in the presence of either 10 μM dATP or 10 μM dCTP as described under Materials and methods and as documented in Figure 7A.

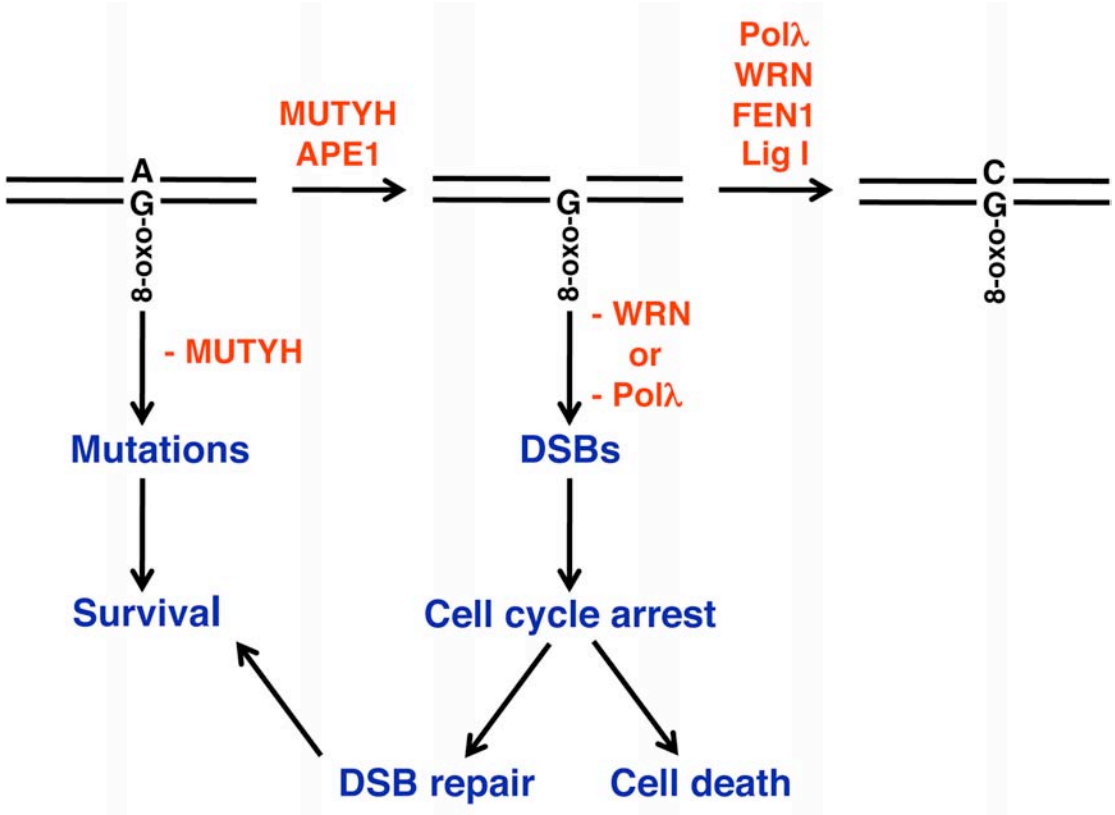

Figure S12. MUTYH-initiated repair of 8-oxo-G:A mispair. WRN promotes 8-oxo-G bypass by DNA polymerase λ (Polλ). Proposed phenotypic consequences of defects in different steps of repair of 8-oxo-G:A mispairs are also shown. Mutations (G:C to T:A transversions) or DNA double-strand breaks (DSBs) are generated during the next round of DNA replication.

3.2 Human RECQ5 Helicase Promotes Repair of DNA Double-Strand Breaks by Synthesis-Dependent Strand Annealing

The majority of HR events proceed through the SDSA subpathway. There are known DNA helicases that promote SDSA subpathway during HR in yeast, namely Mph1 and Srs2. However, the human functional ortholog of Srs2 has not yet been identified. Two candidates for Srs2 ortholog were proposed, namely FBH1 and RECQ5. The aim of this study was to define the roles of FBH1 and RECQ5 in HR-mediated repair of DSBs in human cells.

In the first step, we took the advantage of using established U2OS/HEK293-DR-GFP reporter cell lines that monitor only non-crossover events in HR to elucidate the role of FBH1 and RECQ5 in SDSA. As a control, we firstly depleted cells of RAD51 or BRCA2 using RNA interference and found that their depletion led to dramatic decrease in HR repair efficiency. Also depletion of RAD52 that has been shown to play role in SDSA in yeast led to significant decrease in HR repair efficiency. Next we tested effect of depletion of BLM as it has two proposed opposing roles in HR. Firstly, BLM was found to be able to disrupt RAD51 nucleofilaments and thus acts as anti-recombinase. On the other hand, BLM togehter with TopIIIα-RMI1-RMI2 complex can dissolve dHJ formed during DSBR. Interestingly, depletion of BLM by two independent siRNAs increased HR repair efficiency in HEK293 cells, suggesting that BLM indeed acts as anti-recombinase in human cells. When we tested FBH1 and RECQ5 we found that only RECQ5 depletion led to decrease in HR repair efficiency while FBH1 depletion increased HR repair efficiency. Moreover, RECQ5 depletion was able to rescue the increase in HR repair efficiency caused by BLM depletion.

To study SDSA subpathway, we used another reporter cell line to monitor SSA (U2OS/HEK293-SA-GFP) as this process resembles the post-synaptic phase of SDSA. As expected RAD51 and BRCA2 depletion led to increase in SSA repair efficiency while RAD52 depletion led to significant decrease. RECQ5 depletion resulted in decrease in SSA repair efficiency that was dependent on RAD51 and BRCA2. To get more insight into the underlying mechanism, we tested the phenotypes of helicase-dead mutant of RECQ5 (K58R) and RECQ5 with mutation that interferes with binding of RAD51 (F666A). Overexpression of wild-type RECQ5 resulted in increased repair efficiency by SSA while overexpression of K58R mutant decreased the efficiency of SSA and F666A mutant had no

effect on SSA repair efficiency. These data suggest that RECQ5 enhances the efficiency of SSA by disruption of RAD51 nucleofilaments. This hypothesis is supported by the finding that there is increased occupancy of DNA flanking DSB by RAD51 after depletion of RECQ5 *in vivo*. Moreover, cells depleted for RECQ5 show increased number of sister chromatid exchanges after camptothecin treatment and number of SCE was further increased after co-depletion of BLM.

To biochemically prove above the hypothesis we investigated the effect of RECQ5 on the inhibition of RAD52-mediated DNA annealing activity by RAD51. For this purpose we used ATP-hydrolysis deficient mutant of RAD51 (K133R) that forms stable nucleofilaments *in vitro* in the presence of ATP. As described previously, binding of RAD51 inhibited RAD52-mediated DNA annealing in presence of RPA. When RECQ5 was added to reaction, wild-type protein but not helicase dead mutant was able to rescue the inhibitory effect of RAD51.

To mimic the postsynaptic phase of SDSA we added blunt-ended homologous double-stranded DNA to the reaction and still RAD52-mediated DNA annealing activity could be seen in absence of RAD51. As expected RAD51 had inhibitory effect on RAD52-mediated DNA annealing activity that was opposed by addition of wild-type but not mutant RECQ5. Together these data suggest that RAD51 can promote reformation of D-loop during SDSA and that this process is opposed by RECQ5.

2380–2390 Nucleic Acids Research, 2014, Vol. 42, No. 4 Published online 6 December 2013
doi:10.1093/nar/gkt1263

Human RECQ5 helicase promotes repair of DNA double-strand breaks by synthesis-dependent strand annealing

Shreya Paliwal[1], Radhakrishnan Kanagaraj[1], Andreas Sturzenegger[1], Kamila Burdova[2] and Pavel Janscak[1,2,*]

[1]Institute of Molecular Cancer Research, University of Zurich, CH-8057 Zurich, Switzerland and [2]Institute of Molecular Genetics, Academy of Sciences of the Czech Republic, 14300 Prague, Czech Republic

Received August 21, 2013; Revised November 9, 2013; Accepted November 12, 2013

ABSTRACT

Most mitotic homologous recombination (HR) events proceed via a synthesis-dependent strand annealing mechanism to avoid crossing over, which may give rise to chromosomal rearrangements and loss of heterozygosity. The molecular mechanisms controlling HR sub-pathway choice are poorly understood. Here, we show that human RECQ5, a DNA helicase that can disrupt RAD51 nucleoprotein filaments, promotes formation of non-crossover products during DNA double-strand break-induced HR and counteracts the inhibitory effect of RAD51 on RAD52-mediated DNA annealing *in vitro* and *in vivo*. Moreover, we demonstrate that RECQ5 deficiency is associated with an increased occupancy of RAD51 at a double-strand break site, and it also causes an elevation of sister chromatid exchanges on inactivation of the Holliday junction dissolution pathway or on induction of a high load of DNA damage in the cell. Collectively, our findings suggest that RECQ5 acts during the post-synaptic phase of synthesis-dependent strand annealing to prevent formation of aberrant RAD51 filaments on the extended invading strand, thus limiting its channeling into potentially hazardous crossover pathway of HR.

INTRODUCTION

DNA double-strand break (DSB) is the most dangerous type of DNA damage because its inaccurate repair can lead to chromosomal rearrangements, a hallmark of tumorigenesis and tumor progression. In eukaryotic cells, two mechanistically distinct pathways are known to efficiently repair DNA DSBs: non-homologous end joining and homologous recombination (HR). HR is mainly restricted to S phase, peaking in mid-S, and requires an intact homologous sequence to be used as a repair template (1–3). It is initiated by nuclease-mediated resection of the DNA ends to generate 3′-single-stranded (ss) DNA tails that are coated by the ssDNA-binding protein RPA (4). In the next step, the RAD51 recombinase replaces RPA on these ssDNA tails with the help of mediators such as BRCA2 to form a nucleoprotein filament that catalyzes the invasion of the donor chromatid, giving rise to a three-stranded structure called the displacement (D)-loop (1). After DNA synthesis primed by the invading strand, repair can proceed *via* two main sub-pathways referred to as the canonical DSB repair (DSBR) and synthesis-dependent strand annealing (SDSA) (1,2). In DSBR pathway, the second DNA end is captured by the D-loop to form an intermediate with two Holliday junctions, referred to as double Holliday junction (dHJ). This joint DNA molecule can be either resolved by specialized endonucleases into crossover (CO) or non-crossover (NCO) products or dissolved by the BLM-TOPOIIIα-RMI1/2 (BTR) complex, which gives rise exclusively to NCO products (5–7). In the SDSA pathway, the extended D-loop is disrupted by a DNA helicase, and the newly synthesized DNA is annealed to the ssDNA tail of the other part of the broken chromosome, which is followed by gap-filling DNA synthesis and ligation. As a result, SDSA yields exclusively NCO products (8).

The HR sub-pathways are under strict regulation to select the most appropriate outcome in a given state of the cell (2,9). Although formation of COs is favored during meiosis to ensure genetic diversity and accurate chromosome segregation, it is suppressed in mitotic cells to prevent loss of heterozygosity and chromosomal translocations (10,11). Recent studies in yeast and mammalian cells suggest that HJ resolvases are active only during

*To whom correspondence should be addressed. Tel: +41 446353470; Fax: +41 446353484; Email: pjanscak@imcr.uzh.ch
Present address:
Radhakrishnan Kanagaraj, London Research Institute, Cancer Research UK, Clare Hall Laboratories, South Mimms, Herts EN6 3LD, UK.

mitosis, biasing the outcome of recombination toward NCO products while also ensuring the elimination of any persistent joint DNA molecules (11). Most NCOs arising during HR-mediated DSBR are produced by SDSA rather than by the canonical DSBR pathway (12). Moreover, the resolution of HJs is highly constrained to generate CO products (12). Thus, it appears that the SDSA mechanism is preferred over DSBR in mitotic cells.

In budding yeast, the Mph1 DNA helicase suppresses COs by acting in a pathway distinct from dHJ dissolution (13). Mph1 influences outcome rather than the efficiency of recombinational repair events, suggesting that it acts by shunting a DNA repair intermediate into the SDSA pathway (13). In support of this notion, biochemical evidence indicates that Mph1 is capable of disrupting Rad51-made D-loops (13). Another suppressor of COs in yeast proposed to act via promotion of SDSA is Srs2, an UvrD-type DNA helicase that has the capacity to displace Rad51 from ssDNA (14,15). The mechanism of CO suppression by Srs2 appears to differ from that of Mph1. Cells lacking Srs2 display a failure to complete ectopic gene conversion with NCO outcome, which reduces the overall repair efficiency, and therefore increases the proportion of CO products among completed recombination events (14). Although Srs2 can unwind DNA duplexes covered by Rad51, it fails to unwind Rad51-made D-loops (13,16). Instead, the anti-recombinase activity of Srs2 *in vivo* is dependent on its ability to bind RAD51, suggesting that Srs2 might promote SDSA by regulating Rad51 filament stability (17).

The closest sequence homolog of Srs2 in mammals and other vertebrates is FBH1, which is also found in fission yeast but not in budding yeast. Several lines of *in vivo* evidence suggest that this UvrD-type helicase regulates HR at the stage of RAD51 filament assembly, but its role in SDSA is yet to be assessed (18). Another potential ortholog of Srs2 in mammals is RECQ5, which belongs to RecQ family of DNA helicases (19). Biochemical studies have shown that RECQ5 binds directly to RAD51 and possesses the ability to disrupt the ATP-bound form of RAD51-ssDNA filament in a manner dependent on its ssDNA-translocase activity and interaction with RAD51 (20,21). In accordance with this finding, phenotypic analysis of chicken and mouse knockout cells have revealed that RECQ5 regulates HR to suppress the formation of COs (20,22,23). Moreover, a recent study using chicken DT40 cells has demonstrated that RECQ5 suppresses COs in a manner dependent on its interaction with RAD51 (24). Here we provide several lines of evidence suggesting that RECQ5 promotes SDSA by disrupting aberrant RAD51-ssDNA filaments formed during the post-synaptic stage of HR.

MATERIALS AND METHODS

Antibodies and siRNAs

All antibodies and siRNAs used in this study are described in Supplementary Materials and Methods.

HR and SSA reporter assays

Maintenance of reporter cell lines (HEK293/DR-GFP, U2OS/DR-GFP, HEK293/SA-GFP or U2OS/SA-GFP), culture conditions and FACS analysis were done as described previously (25,26). Cells were seeded in a poly-lysine-coated 6-well plate at a density of 0.6×10^6 cells per well and transfected 24 h later with appropriate siRNA (40 nM). After 24 h, 0.2×10^6 cells for each siRNA tested were seeded in a 12-well plate, and a day later transfected with 0.6 μg of the I-SceI-expressing plasmid pCBASce (27) or empty vector (pcDNA3.1) using JETprime (Polyplus) for HEK293 cells or Lipofectamine 2000 (Invitrogen) for U2OS cells according to the manufacturer's instructions. After 6 h, cells were again transfected with appropriate siRNA (15 nM), and 48–72 h later, GFP-positive cells were quantified by flow cytometry on a Cyan ADP (Dako) using Summit software (Beckman Coulter). For overexpression of RECQ5 in U2OS/SA-GFP cells, a pcDNA3.1/HisC-based vector expressing the wild-type or mutant forms of RECQ5 (0.6 μg) was co-transfected with pCBASce (0.6 μg) using Lipofectamine 2000 (21). Cells were subjected to FACS analysis 72 h after transfection.

Strand-annealing assays

Proteins used for strand-annealing assays were purified as described in Supplementary Materials and Methods. All reactions were carried out at 30°C in buffer R [20 mM Tris-acetate (pH 7.9), 50 mM potassium acetate, 10 mM magnesium acetate and 1 mM DTT] supplemented with ATP-regenerating system (10 U/ml creatine phosphokinase and 12 mM phosphocreatine). The 5 nM 5′-^{32}P-labeled f9 oligonucleotide (59-mer) was pre-incubated for 3 min with or without 200 nM RAD51^{K133R} in a final volume of 20 μl (reaction A). In a separate tube, 5 nM f7 oligonucleotide (30-mer), complementary to 5′ end of f9, was mixed with 120 nM RAD52 and 40 nM RPA in a final volume of 20 μl (reaction B). Where required, the latter reaction mixture also contained 5 nM 59-bp DNA duplex prepared by annealing of unlabeled f9 and f9-C oligonucleotides. The reactions A and B were mixed together, and where required RECQ5, RECQ5^{K58R}, RECQ5$^{\Delta 652-674}$, WRN or FBH1 were added to a final concentration of either 80 or 40 nM. In all, 5 μl aliquots were removed at the indicated time points and mixed with 2.5 μl of stop solution [125 nM f9 (unlabeled), 33% (v/v) glycerol, 1% (w/v) SDS, 0.15 M EDTA, 0.5 mg/ml proteinase K and 0.1% (w/v) Bromophenol Blue] followed by a 5 min incubation at 30°C. Samples were subjected to electrophoresis in a 10% non-denaturing PAGE run at 100 V for 2 h in 1× TBE buffer. Radiolabeled DNA species were visualized by phosphorimaging and quantified using ImageQuant TL software.

Chromatin immunoprecipitation assay

Chromatin immunoprecipitation (ChIP) experiments were done with the ChIP-IT® Express kit (Active Motif) as described previously (28). Briefly, U2OS/DR-GFP cells were seeded in a 10-cm plate and transfections of siRNA

and I-SceI plasmid were performed as described for DR-GFP reporter assays. Two days after I-SceI plasmid transfection, cells were cross-linked with formaldehyde [1% (v/v)] at room temperature for 10 min, followed by addition of glycine (125 mM) to quench the cross-linking reaction. Chromatin fragments used in immunoprecipitation reactions were prepared by shearing of cross-linked chromatin using a bioruptor sonication device (Diagenode). One tenth of the sonicated chromatin was stored at −70°C to be used as an input sample. For each ChIP reaction, sonicated chromatin (8 μg) was immunoprecipitated overnight at 4°C with either anti-RAD51 antibody or control IgG (4 μg each) and protein G-coated magnetic beads (Active Motif). After washing, immunocomplexes were eluted from the beads and de-cross-linked according to the manufacturer's instructions (Active Motif). ChIPed and input samples were purified with the QIAquick PCR Purification Kit (Qiagen), and DNA was eluted with 50 μl of water. At least two independent experiments were performed for each ChIP reaction. In each case, eluted DNA sample (2–3 μl) was subjected to quantitative real-time PCR (qPCR) analysis in hexaplicate on a Roche LightCycler 480 Real-time PCR system with the use of Roche LightCycler 480 DNA SYBR Green I master. Data were analyzed using the Pfaffl's method (29). Fold enrichment of RAD51 binding on each target region was calculated as a ratio of the amount of DNA estimated for the RAD51-specific antibody versus the amount of DNA estimated for the control IgG. Primers used in ChIP-qPCR assays are described in Supplementary Materials and Methods.

Sister chromatid exchange assay

Sister chromatid exchange (SCE) assay was done as described previously (30). Details are provided in Supplementary Materials and Methods.

RESULTS

RECQ5 promotes formation of non-crossover products during DSB-induced HR in human cells

To gain deeper insight into the molecular mechanism of SDSA in mammalian cells, we investigated the role of two potential human orthologs of Srs2, namely, FBH1 and RECQ5, in the formation of NCO products during repair of endonuclease-induced DSBs. To selectively detect NCO events, we used the established reporter cell lines HEK293/DR-GFP and U2OS/DR-GFP (25,26,31). The DR-GFP reporter consists of a direct repeat of two mutated GFP alleles: a full length GFP interrupted by a recognition site for the I-SceI endonuclease and an internal GFP fragment that serves as a donor for HR-mediated repair of a DSB created by I-SceI in the proximal GFP allele (Figure 1A). HR-mediated repair of this DSB *via* an NCO event gives rise to a functional GFP allele, whereas repair by crossing over yields a C-terminally truncated GFP allele that does not encode for a fluorescent protein. Thus, quantification of GFP-positive cells by flow cytometry provides a measure of NCO repair efficiency. Proteins of interest were depleted from the DR-GFP reporter cell line by transfection of small interfering RNAs (siRNAs) (Figure 1B and Supplementary Figure S1). Cells were subsequently transfected with an I-SceI expression vector to induce a DSB in the reporter cassette, and the percentage of GFP positive cells arising upon DSBR was measured 2–3 days after plasmid transfection. As expected, formation of a functional GFP allele was impaired in cells depleted for the RAD51 recombinase or its loader BRCA2 (Figure 1C and D). Repair efficiency also significantly decreased on depletion of RAD52 that mediates DNA strand annealing in a reaction stimulated by RPA and is required for SDSA in budding yeast (Figure 1C) (32,33). Interestingly, depletion of BLM, the key component of the BTR complex, led to a significant increase in repair efficiency relative to control, indicating that dHJ dissolution has no role in formation of NCO repair products in the DR-GFP system (Supplementary Figure S2). This is consistent with the proposal that limited regions of homology, as is the case during ectopic recombination, decrease the possibility of forming a dHJ structure due to impediment of strand exchange by DNA end resection beyond the homologous region (34). This would imply that SDSA accounts for the majority of NCO repair events induced by I-SceI in cells harboring the DR-GFP cassette. BLM helicase probably disrupts joint DNA molecules formed during the repair process.

As for the putative Srs2 orthologs tested, only depletion of RECQ5 led to a marked reduction of repair efficiency both in HEK293 and U2OS cells, without any significant changes in cell cycle distribution (Figure 1C and D and Supplementary Figure S3). RECQ5 depletion also dramatically reduced the elevated NCO repair efficiency in HEK293/DR-GFP cells lacking BLM (Supplementary Figure S2). On the contrary, depletion of FBH1 led to a significant elevation of repair efficiency particularly in U2OS cells (Figure 1C and D). Thus, our results suggest that RECQ5 might promote DNA DSBR by the SDSA pathway of HR, whereas FBH1 might act as an SDSA suppressor.

RECQ5 counteracts the inhibitory effect of RAD51 on DSBR by SSA in human cells

It is possible that RECQ5 promotes SDSA by catalyzing disruption of an aberrant RAD51 filament that might form on the newly synthesized DNA strand after unwinding of the extended D-loop. This filament would inhibit the ssDNA-annealing step of SDSA and could promote reformation of the D-loop, shifting the balance between the HR sub-pathways in favor of DSBR. To explore this possibility, we used a GFP-based reporter for DSBR by single-strand annealing (SSA), which mechanistically resembles the post-synaptic phase of SDSA (25,31). The reporter cassette, termed SA-GFP, contains two directly oriented GFP gene fragments, 5′GFP and Sce3′GFP, forming a 280-bp repeat (Figure 2A). SSA-mediated recombination between the repeated sequences triggered by an I-SceI-generated DSB in the distal GFP fragment results in the formation of a functional GFP gene. Using HEK293-based SA-GFP reporter system (HEK293/SA-GFP), we found that

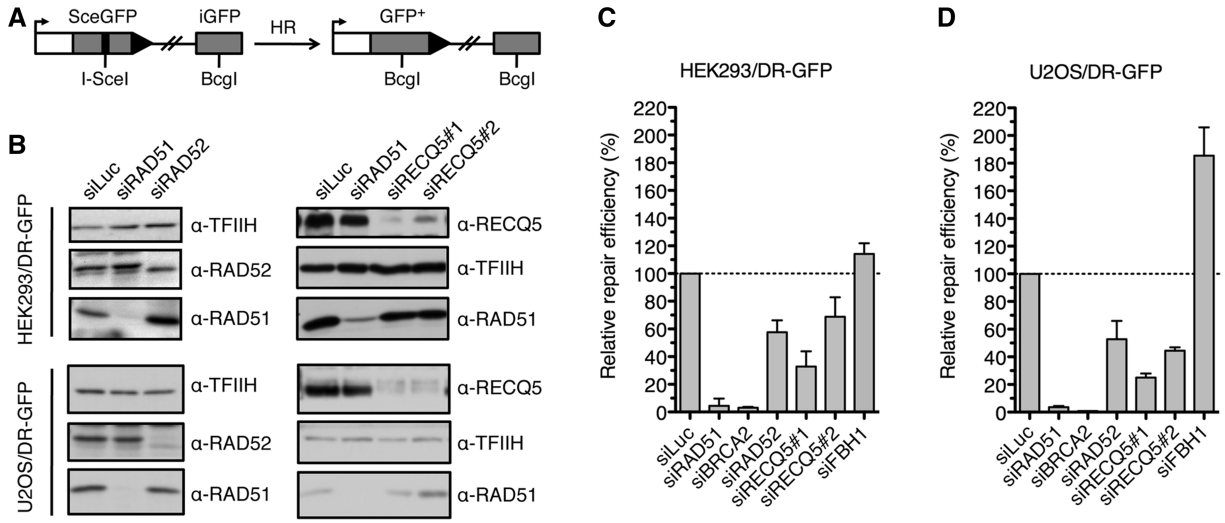

Figure 1. RECQ5 promotes homologous recombination with non-crossover outcome. (**A**) Scheme of the DR-GFP reporter cassette. The site-specific DSB in the reporter cassette is generated by I-SceI endonuclease. Only NCO events give rise to a functional GFP allele. (**B**) Western blot analysis of extracts from HEK293/DR-GFP and U2OS/DR-GFP cells transfected with indicated siRNAs. Blots were probed with indicated antibodies. (**C**) Efficiency of HR-mediated repair of I-SceI-induced DSB in HEK293/DR-GFP cells treated with indicated siRNAs. Cells were transfected with appropriate siRNA (40 nM) two days before transfection of I-SceI-expressing plasmid. Percentage of GFP-positive cells was measured by flow cytometry 2 days after DSB induction and taken as a measure of DSBR efficiency. Values plotted represent relative repair efficiency calculated as a percentage of repair efficiency measured in cells transfected with control siRNA (siLuc; 100%). All data points represent an average of at least three replicates with error bars indicating standard deviation. (**D**) Efficiency of HR-mediated repair of I-SceI-induced DSB in U2OS/DR-GFP cells treated with indicated siRNAs as compared with cells transfected with control siRNA. Experiments were performed as in (C) except that the flow cytometry analysis was performed 3 days after I-SceI transfection. HR, homologous recombination; DSB, double-strand break; NCO, non-crossover; and GFP, green fluorescent protein.

depletion of RAD51 or its loader BRCA2 resulted in a marked increase (2- to 4- fold) in SSA repair efficiency compared with control, providing evidence that formation of RAD51 filaments on resected DNA ends inhibits DSBR by SSA in human cells (Figure 2B and C and Supplementary Figure S4). On the contrary, depletion of RAD52 protein resulted in a dramatic decrease in the frequency of SSA repair events, which is consistent with the proposed role for RAD52 in promoting DNA annealing during SSA (Figure 2B and C) (31). We repeated our experiments with U2OS/SA-GFP cells, and we found that knockdown of RAD51 resulted in lethality. However, cells depleted for BRCA2 were viable and showed a dramatic increase in SSA repair efficiency compared with control cells, further supporting the aforementioned proposal (Figure 2D). As shown with the HEK293/SA-GFP cells, knockdown of RAD52 in U2OS/SA-GFP cells dramatically impaired SSA repair efficiency (Figure 2D).

Depletion of RECQ5 caused a significant reduction in SSA repair efficiency, but only if the cells contained RAD51 (HEK293/SA-GFP cells) and BRCA2 (HEK293/SA-GFP and U2OS/SA-GFP cells) (Figure 2 and Supplementary Figure S4). HEK293/SA-GFP cells depleted for both RECQ5 and RAD51 displayed a SSA repair capacity that was similar to that of cells depleted for RAD51 alone (Figure 2B and C). Similarly, the SSA defect caused by lack of RECQ5 was rescued by co-depletion of BRCA2 (Figure 2D and Supplementary Figure S4). Thus, these data suggest that RECQ5 counteracts the inhibitory effect of RAD51 on DSBR by SSA, most likely by catalyzing disruption of RAD51 filaments formed on ssDNA generated by DNA-end resection.

To verify this hypothesis, we compared the effects of overexpression of wild-type and mutant forms of RECQ5 on the efficiency of SSA-mediated repair of I-SceI-induced DSBs in U2OS/SA-GFP cells. The following RECQ5 mutants were tested: (i) mutant containing a K58R substitution in the ATP-binding site of RECQ5, which abolishes the ATPase and helicase activities of the enzyme; and (ii) mutant containing an F666A substitution in the RAD51-binding domain of RECQ5, which impairs RECQ5-RAD51 complex formation (21,35). Both mutants are defective in catalyzing RAD51 filament disruption (20,21). In line with the proposed model, we found that overexpression of wild-type RECQ5 in U2OS/SA-GFP cells resulted in a marked increase in SSA repair efficiency as compared with cells harboring control vector (Figure 2E and F). In contrast, the K58R mutant of RECQ5, which is proficient in binding to RAD51, exhibited a significant trans-dominant negative effect on the repair efficiency, possibly by preventing the access of the endogenous RECQ5 protein to RAD51 filaments formed on resected DNA ends (Figure 2E and F). For the F666A mutant of RECQ5, we found that its overexpression had no effect on SSA-mediated DSBR in U2OS/SA-GFP cells, which is consistent with the inability of this mutant to interact with RAD51 filaments (Figure 2E and F). Thus, our data strongly suggest that RECQ5 enhances the efficiency of SSA-mediated DSBR by disrupting RAD51-ssDNA filaments formed at resected DNA ends.

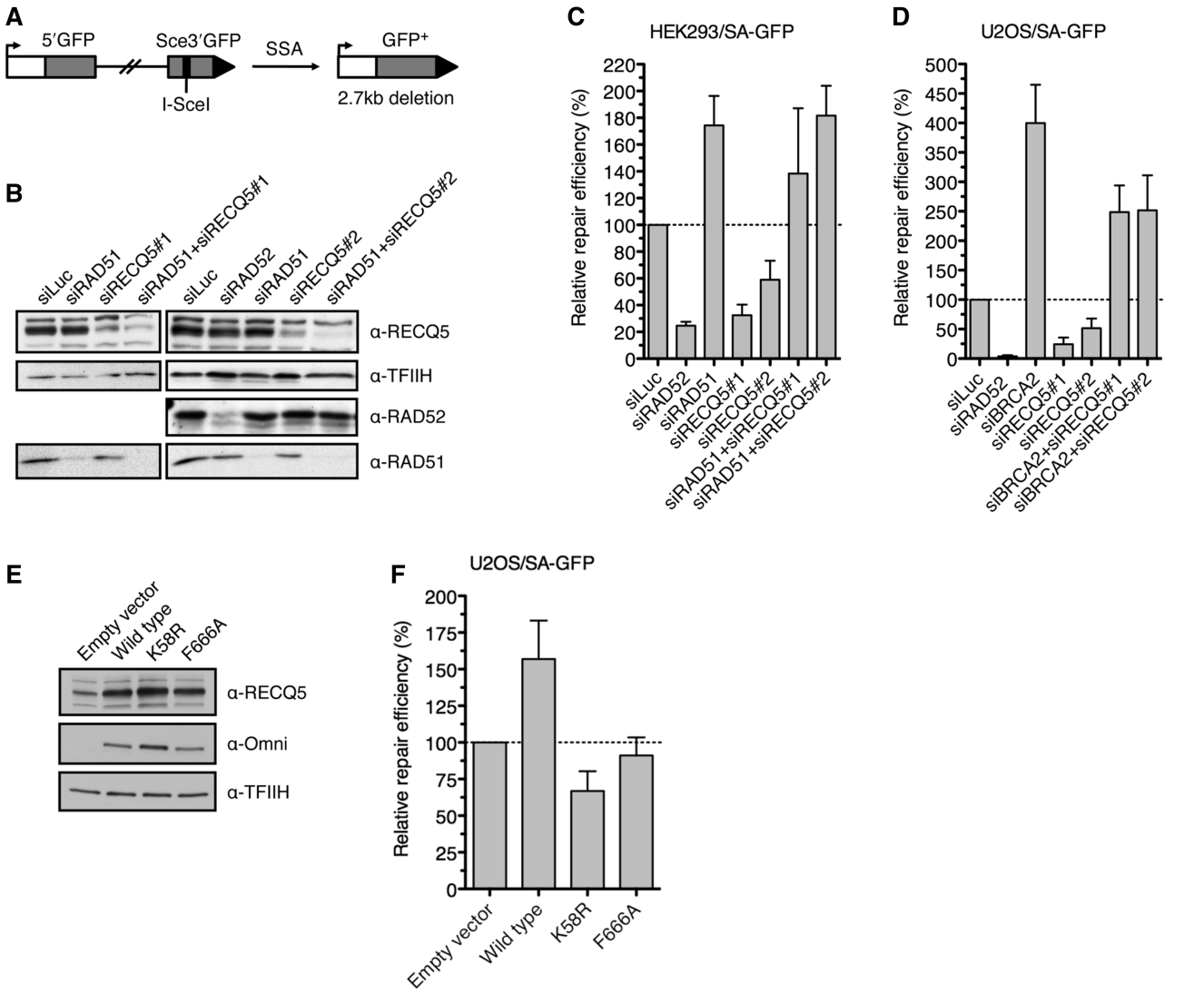

Figure 2. RECQ5 suppresses inhibitory effect of RAD51 on DNA DSBR by SSA. (**A**) Scheme of the SA-GFP reporter cassette. SSA-mediated repair of I-SceI-generated DSB results in the formation of a functional GFP allele. (**B**) Western blot analysis of extracts from HEK293/SA-GFP cells transfected with indicated siRNAs. The blots were probed with indicated antibodies. (**C**) Efficiency of SSA-mediated repair of I-SceI-induced DSB in HEK293/SA-GFP cells transfected with indicated siRNAs. Cells were transfected with appropriate siRNA (40 nM) 2 days before transfection of I-SceI-expressing plasmid. Percentage of GFP-positive cells was determined by flow cytometry 2 days after DSB induction and taken as a measure of repair efficiency. Values plotted represent relative repair efficiency calculated as a percentage of repair efficiency measured in cells transfected with control siRNA (siLuc; 100%). All data points represent an average of at least three replicates with error bars indicating standard deviation. (**D**) Efficiency of SSA-mediated repair of I-SceI-induced DSB in U2OS/SA-GFP cells transfected with indicated siRNAs. Experiments were performed as in (C) except that the percentage of GFP-positive cells was determined 3 days after DSB induction. (**E**) Western blot analysis of extracts from U2OS/SA-GFP cells transfected with pcDNA3.1/HisC-based vectors expressing wild-type RECQ5 or its mutants, K58R and F666A, respectively, as fusions with an Omni-tag. The blots were probed with indicated antibodies. (**F**) Effect of overexpression of the wild-type and mutant forms of RECQ5 on the efficiency of SSA-mediated repair of I-SceI-induced DSB in U2OS/SA-GFP. Cells were transfected with appropriate RECQ5 expression vector in combination with the plasmid expressing I-SceI. Percentage of GFP-positive cells was determined 3 days after plasmid transfection. Values plotted represent relative repair efficiency calculated as a percentage of repair efficiency measured in cells transfected with empty vector. All data points represent an average of at least three replicates with error bars indicating standard deviation. SSA, single-strand annealing; DSB, double-strand break; and GFP, green fluorescent protein.

RECQ5 counteracts the inhibitory effect of RAD51 on RAD52-mediated DNA annealing *in vitro*

Next, we performed biochemical experiments addressing the effect of RAD51 on RAD52-mediated annealing of two complementary oligonucleotides either in the absence or in the presence of RECQ5. In these assays, we used an ATP hydrolysis-deficient mutant of RAD51, $RAD51^{K133R}$, which can form a stable nucleoprotein filament in the presence of ATP, mimicking the *in vivo* ATP-bound form of the filament that is capable of catalyzing DNA strand exchange (20). Before annealing reactions, a 30-mer oligonucleotide was pre-incubated with RPA to form an ssDNA-RPA complex, whereas the other oligonucleotide (59-mer, radioactively labeled at its 5′ end) was pre-incubated either with $RAD51^{K133R}$

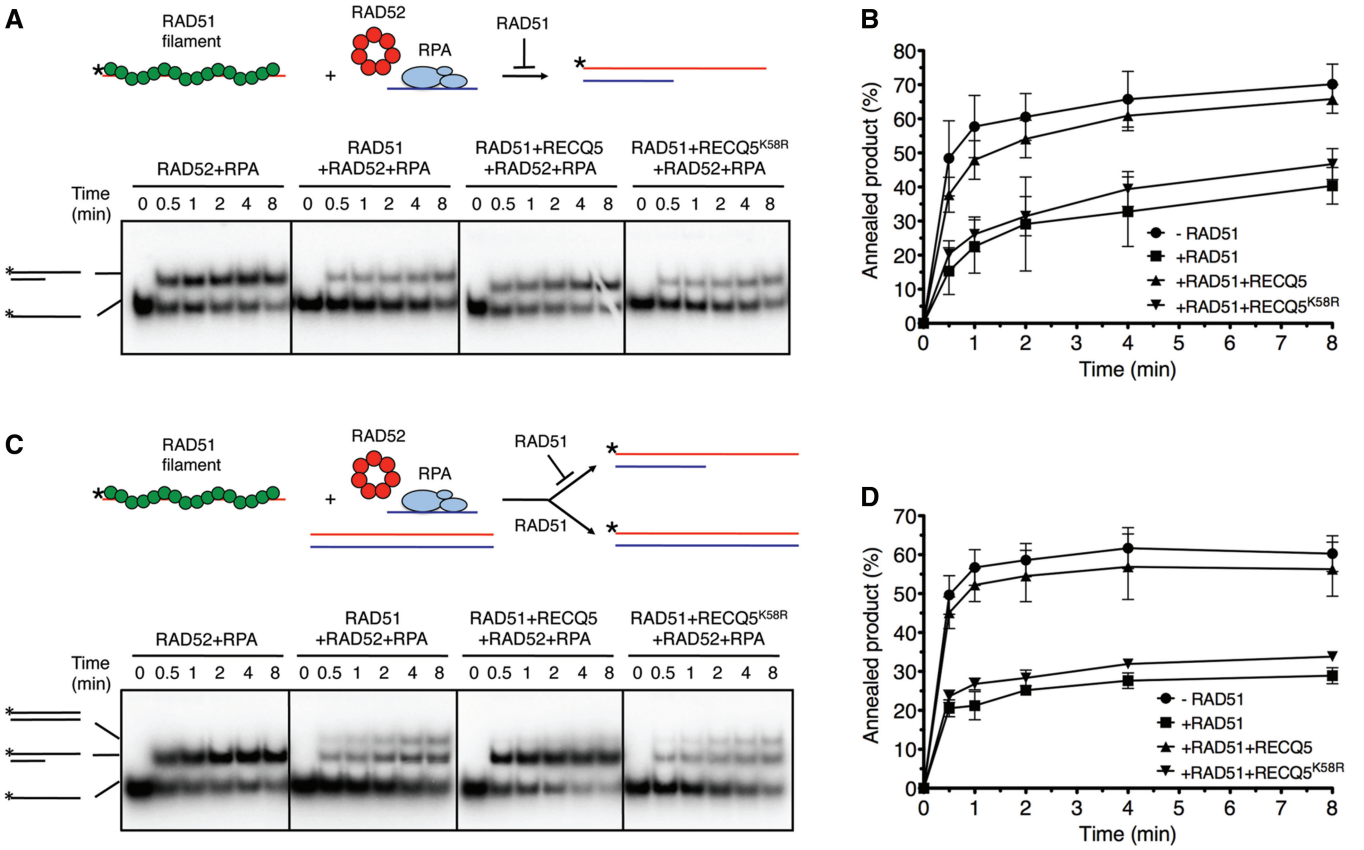

Figure 3. RECQ5 helicase counteracts the inhibitory effect of RAD51 on RAD52-mediated ssDNA annealing *in vitro*. (**A**) Upper panel: reaction scheme depicting the effect of RAD51 (green circles) on annealing of two complementary oligonucleotides (59-mer and 30-mer represented by red and blue lines, respectively) in presence of RAD52 and RPA. RAD52 is depicted as a heptameric ring structure (red circles). The 30-mer oligonucleotide can accommodate binding of one RPA heterotrimer (light blue ovals). Lower panel: all reactions were carried out at 30°C in buffer R supplemented with ATP-regenerating system. Reactions contained 5′ end radiolabeled 59-mer oligonucleotide (2.5 nM), either free or pre-coated with $RAD51^{K133R}$ (100 nM), a 30-mer oligonucleotide (2.5 nM) complementary to the 5′-half of the 59-mer, RAD52 (60 nM) and RPA (30 nM). Where indicated, RECQ5 or $RECQ5^{K58R}$ were present at a concentration of 80 nM. Reaction aliquots at indicated time points were subjected to PAGE followed by phosphorimaging as described in 'Materials and Methods'. (**B**) Quantification of data shown in (A). Each data point represents the mean of three independent experiments. Error bars represent standard deviation. (**C**) Upper panel: reaction scheme depicting the effect of RAD51 on annealing of two complementary oligonucleotides in presence of a homologous duplex, RAD52 and RPA. RAD51 filament formed on the radiolabeled oligonucleotide (red line with asterisk) inhibits RAD52/RPA-mediated annealing and promotes strand exchange with the homologous duplex. Lower panel: reactions were carried out and analyzed as in (B). Homologous 59-mer duplex was present at a concentration of 2.5 nM. Schemes of radiolabeled DNA species are shown on left. Radioactive label at the 5′ end is depicted by asterisks. (**D**) Quantification of data shown in (C). Each data point represents the mean of three independent experiments. Error bars represent standard deviation.

to form a nucleoprotein filament or with the reaction buffer alone. We found that addition of RPA-coated 30-mer oligonucleotide to free 59-mer oligonucleotide in presence of RAD52 resulted in rapid formation of partial DNA duplex structure with a 3′-tail (Figure 3A, *first panel from the left*, and Supplementary Figure S5). However, this RAD52-mediated ssDNA annealing was impaired if the 59-mer oligonucleotide was pre-coated with $RAD51^{K133R}$ before its addition to the annealing reaction, demonstrating that formation of RAD51-ssDNA filaments inhibits ssDNA annealing by RAD52 (Figure 3A and B). Similar results were obtained with wild-type RAD51, although the observed inhibitory effect was less pronounced than that of $RAD51^{K133R}$ (Supplementary Figure S6). Remarkably, the inhibitory effect of $RAD51^{K133R}$ on RAD52-mediated ssDNA annealing was almost completely lost on addition of RECQ5 to the reaction (Figure 3A and B). On the contrary, the helicase-deficient mutant of RECQ5 ($RECQ5^{K58R}$) or a RECQ5 mutant lacking the RAD51-interacting domain ($RECQ5^{\Delta 652-674}$) did not alleviate this inhibitory effect, suggesting that RECQ5 stimulated the ssDNA-annealing reaction by disrupting $RAD51^{K133R}$-ssDNA filaments (Figure 3A and B and Supplementary Figure S7). In addition, we found that the inhibition of RAD52-mediated ssDNA annealing by $RAD51^{K133R}$ was not relieved if RECQ5 was substituted by WRN RecQ helicase or by FBH1, indicating that this reaction is specific for RECQ5 (Supplementary Figure S7).

To substantiate the aforementioned findings, ssDNA annealing reactions were also carried out in presence of a homologous DNA duplex (59-mer), conditions resembling the post-synaptic phase of SDSA. We found that this DNA duplex had no effect on RAD52-mediated annealing of the two complementary oligonucleotides (Figure 3C and D). However, if the 59-mer

oligonucleotide was pre-coated with RAD51^{K133R}, we again observed a strong inhibition of RAD52-mediated ssDNA annealing with concomitant appearance of radioactively labeled 59-mer oligoduplex, an indicative of strand exchange reaction (Figure 3C and D). On addition of RECQ5, RAD51^{K133R}-catalyzed strand exchange was inhibited, and RAD52-mediated ssDNA annealing was restored to a level detected in absence of RAD51^{K133R} (Figure 3C and D). Again this effect was not seen with the K58R mutant of RECQ5 (Figure 3C and D). These data suggest that RAD51 can promote reformation of D-loop during the post-synaptic phase of SDSA and that RECQ5 can counteract this reverse reaction by removing RAD51 from the invading strand.

RECQ5 deficiency is associated with increased occupancy of RAD51 on DNA sequences flanking a DSB

To prove that the lack of RECQ5 is associated with persistence of RAD51 filaments on resected DNA ends during HR, we used ChIP to evaluate the effect of RECQ5 knockdown on RAD51 occupancy at chromatin flanking the I-SceI site in U2OS/DR-GFP cells two days after I-SceI plasmid transfection. Immunoprecipitated DNA fragments were subjected to quantitative real-time PCR analysis using primers amplifying the regions located downstream of I-SceI recognition sequence: P1, +181 to +325 and P2, +1037 to +1172 (Figure 4A). We found that RECQ5 knockdown in U2OS/DR-GFP cells was accompanied by a marked increase in the abundance of RAD51 localized near the I-SceI cutting site as compared with mock-depleted cells (Figure 4B). No significant binding of RAD51 to chromatin flanking the I-SceI site was detected in absence of I-SceI expression with both RECQ5-proficient and RECQ5-deficient cells. Thus, these data provide direct evidence that RECQ5 regulates RAD51 filament formation at DNA DSB sites.

RECQ5 acts as CO suppressor in human cells

To assess the role of RECQ5 in suppression of mitotic COs, we investigated the effect of siRNA-mediated depletion of RECQ5 and BLM on the frequency of SCEs in U2OS cells before and after induction of DNA DSBs by camptothecin (CPT). We observed that RECQ5 depletion in untreated cells had no significant effect on the SCE frequency, whereas depletion of BLM increased the SCE frequency by almost 3-fold compared with control cells (Figure 5A and C). Cells depleted for RECQ5 and BLM showed a much higher SCE frequency than cells depleted for BLM alone (Figure 5A and C), which is consistent with the studies in chicken and mouse cells (22,23). Importantly, on CPT treatment, a marked elevation of SCE frequency was observed not only in BLM-deficient cells but also in RECQ5-deficient cells, suggesting that RECQ5 has a role in CO suppression even in the presence of BLM if the load of DNA damage exceeds a certain threshold (Figure 5B). Again cells depleted for both RECQ5 and BLM exhibited a much higher frequency of CPT-induced SCEs than cells depleted for either of these proteins (Figure 5B). Thus, these data indicate that RECQ5 and BLM act in two different

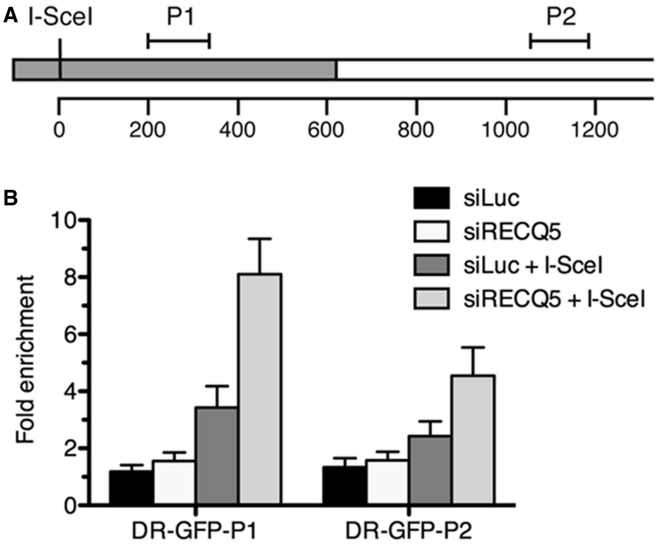

Figure 4. Effect of RECQ5 deficiency on RAD51 occupancy at chromatin flanking the I-SceI-induced DSB in U2OS/DR-GFP cells. (**A**) A schematic diagram of a part of the DR-GFP reporter cassette showing the locations of the regions amplified in ChIP-qPCR assays (P1 and P2). The GFP open reading frame with a single I-SceI recognition site is shown as gray box. The numbers correspond to base pairs. (**B**) Plot of ChIP-qPCR data. Mock-depleted (siLuc) and RECQ5-depleted (siRECQ5#1) cells were transfected with either I-SceI expression vector (+I-SceI) or empty vector, respectively. Chromatin for ChIP analysis was prepared 2 days after I-SceI transfection. Fold enrichment was calculated as a ratio of RAD51 antibody signal versus control IgG. ChIP, chromatin immunoprecipitation; and qPCR, quantitative real-time PCR.

pathways to suppress CO formation during HR and support our hypothesis that RECQ5 promotes SDSA. It is conceivable that at low levels of DSBs in the cell, all dHJs formed as a consequence of SDSA failure (e.g. due to RECQ5 deficiency) are dissolved by the BTR complex to yield NCO products. However, at high load of DSBs, the level of dHJs formed in SDSA-deficient cells is likely to exceed the repair capacity of the BTR complex, favoring resolution to CO products. This is consistent with our finding that RECQ5-deficient cells exhibited a marked increase in SCE frequency only on exposure to CPT (Figure 5B).

DISCUSSION

Here we provide several lines of evidence suggesting that the human RECQ5 helicase promotes DNA DSBR by the SDSA pathway of HR. We show that (i) RECQ5 promotes the formation of NCO products during DSB-induced HR and counteracts the inhibitory effect of RAD51 filaments on DSBR by SSA; (ii) RECQ5 helicase alleviates the inhibitory effect of RAD51-ssDNA filament on RAD52-mediated DNA annealing *in vitro*; (iii) RECQ5 depletion in human cells leads to increased occupancy of RAD51 at chromatin flanking a DSB; and (iv) RECQ5 depletion is associated with increased frequency of SCEs in cells lacking the dHJ dissolvasome or in normal cells on induction of a high load of DNA damage. These data suggest that RECQ5

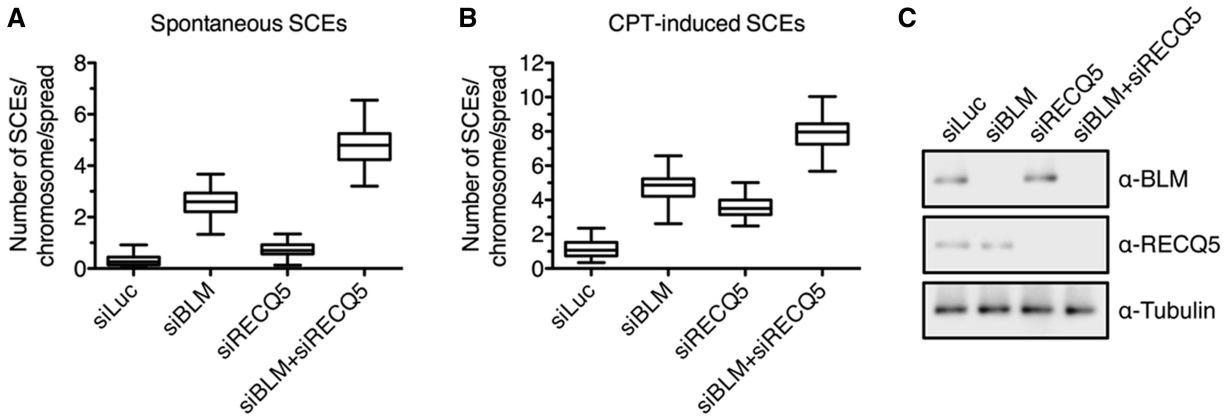

Figure 5. RECQ5 and BLM act in different pathways to suppress crossovers in human cells. (**A**) Frequency of spontaneous SCEs in U2OS cells transfected with indicated siRNAs. (**B**) Frequency of CPT-induced SCEs in U2OS cells transfected with indicated siRNA. Cells were treated with 40-nM CPT for 20 h where indicated. SCE assay and analysis was conducted as described in 'Materials and Methods'. Each data point represents number of SCEs per chromosome in a single metaphase spread. The 50 metaphase spreads were analyzed from each condition. (**C**) Western blot analysis of extracts from U2OS cells transfected with indicated siRNAs. Blots were probed with indicated antibodies. SCE, sister chromatid exchange; and CPT, camptothecin.

might act as a RAD51 filament disruptase during the post-synaptic phase of SDSA to prevent reformation of the D-loop, which would favor the classical DSBR pathway and hence increase the risk of COs (Figure 6). Futile cycles of D-loop disruption and reformation could also lead to cell death due to persistence of recombination intermediates. Consistent with our hypothesis, it has been shown that genetic ablation of RECQ5 in mouse cells is associated with persistence of RAD51 foci and increased lethality after exposure of cells to CPT, which induces DSBs during replication (20,36). Moreover, ablation of the interaction between RECQ5 and RAD51 leads to an elevation of SCEs in chicken DT40 cells lacking BLM (24). Our hypothesis is also supported by the finding that overexpression of human RAD51 has a dominant negative effect on DSB-induced gene conversion in CHO and human cells (37). RAD51 overexpression can also stimulate SCEs and the formation of interchromosomal COs (38,39). Thus, our study establishes RECQ5 as a factor that controls HR sub-pathway choice.

Counteracting Rad51 filament formation during post-synaptic phase of SDSA could as well be the underlying mechanism for the anti-recombinase function of Srs2 in budding yeast. Consistent with this proposal, it has been shown that overexpression of Rad51 in Δ*srs2* mutant cells reduces cell survival on DSB induction and nearly eliminates the NCO pathway without affecting the formation of COs, providing evidence that Rad51 inhibits the post-synaptic stage of SDSA (14,40). In addition, like RECQ5, Srs2 counteracts the inhibitory effect of Rad51 on DSBR by SSA (14,41–43). Moreover, it has been shown that overexpression of Srs2 suppresses the high level of COs in Δ*sgs1* cells, suggesting that Srs2 can shift the balance between DSBR and SDSA pathways in favor of the latter (14). This is further supported by the observation that Δ*srs2* cells show increased frequency of CO events during allelic recombination (14). Finally, yeast Rad51 was shown to inhibit Rad52-mediated DNA annealing *in vitro* (44).

It remains to be determined as to how the anti-recombinase activity of RECQ5 is regulated to prevent disassembly of the legitimate RAD51 filaments. One possibility that deserves further investigation is that the action of this helicase on RAD51 filaments might be counteracted by RAD51 mediators such as BRCA2, which facilitates filament assembly by stabilizing RAD51 binding to ssDNA (45,46). In support of this notion, it has been demonstrated that the inhibitory effect of Srs2 on Rad51 focus formation in yeast cells is antagonized by Rad52, which promotes Rad51 filament assembly by a mechanism similar to that of BRCA2 (47). Moreover, yeast Rad52 has been shown to inhibit Srs2-catalyzed Rad51-ssDNA filament disruption *in vitro* (47). It is also interesting to note that it has recently been shown that RECQ5 and BRCA2 interact with the same region on RAD51, suggesting that they exert their effect on RAD51 in a mutually competitive manner (24). In addition, overexpression of RECQ5 has been shown to impair HR-mediated repair of I-SceI-induced DSB in the HEK293/DR-GFP cells, suggesting that high levels of RECQ5 inhibit HR at the step of presynaptic RAD51 filament assembly by outcompeting the action of RAD51 mediators (21).

A previous study has shown that deletion of the mouse RECQ5 gene results in an increased frequency of I-SceI-induced HR events in cells carrying an *SCneo* reporter cassette (20). However, it has been reported that in addition to NCO-associated gene conversion, a functional *Neo* gene in this reporter system is generated by a CO recombination event, which might increase in frequency in absence of RECQ5 (48). Similarly, the frequency of I-SceI-induced HR repair within an integrated *SCneo* substrate was significantly elevate on depletion of RTEL1, which is proposed to promote SDSA by catalyzing D-loop disruption (49,50).

Disruption of the RECQ5 gene in mice leads to elevated levels of chromosomal rearrangements and cancer susceptibility (20). Moreover, a recent study has shown that

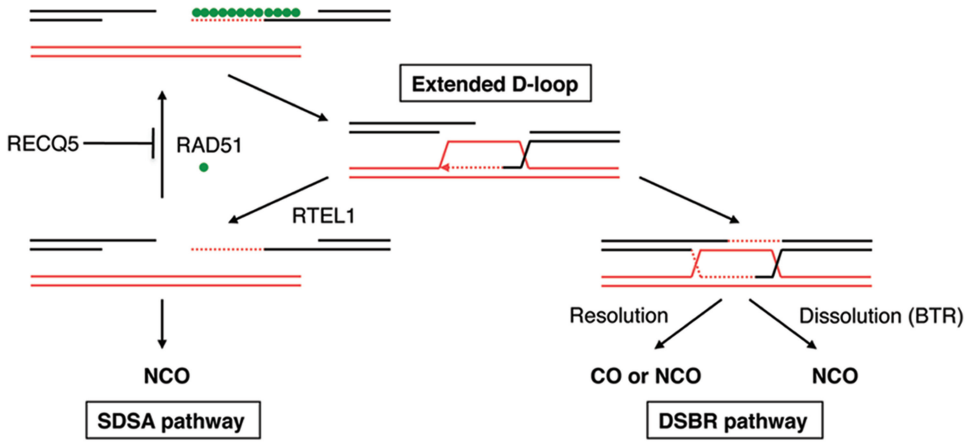

Figure 6. Model for the roles of RECQ5 and BLM in suppression of COs during DSBR by HR. RECQ5 promotes SDSA by disrupting aberrant RAD51-filaments formed after unwinding of the extended D-loop. BLM acts as a part of the BTR (BLM-TOPOIIIα-RMI1/2) complex to mediate dissolution of dHJs. RAD51 filaments formed during the post-synaptic phase of SDSA can promote re-invasion of the homologous duplex followed by formation of a dHJ structutre, increasing the risk of COs. RTEL1 promotes SDSA by catalyzing D-loop disruption. SDSA, synthesis-dependent strand annealing; dHJ, double Holliday junction; and DSBR, double-strand break repair.

RECQ5 expression levels are significantly reduced in primary colorectal cancer cells (51). Our findings suggest that these phenotypes may be a consequence of deregulation of RAD51 filament assembly, which may alter recombination pathways, leading to genomic instability. Interestingly, increased expression of the RAD51 protein has been reported in immortalized and tumor cells and its link to the genomic instability observed in these cells has been established (39,52). Thus, our study provides further insight into the molecular mechanisms underlying the build up of genomic instability associated with tumor progression.

SUPPLEMENTARY DATA

Supplementary Data are available at NAR Online, including [21,30,35,51–59].

ACKNOWLEDGEMENTS

The authors thank Jeremy Stark for DR-GFP and SA-GFP reporter cell lines, Stephen West for providing the BL21 pLysS strain overexpressing human RAD52 protein and Kasper Fugger for performing western blot analysis of FBH1 expression levels.

FUNDING

Swiss National Science Foundation [31003A-129747 and 31003A_146206], Promedica Stiftung, Czech Science Foundation [GA204/09/0565 and GAP305/10/0281]; Stiftung zur Krebsbekämpfung and Theodor und Ida Herzog-Egli Stiftung. Postdoctoral fellowship from UBS AG (to R.K.). Funding for open access charge: Promedica Stiftung.

Conflict of interest statement. None declared.

REFERENCES

1. San Filippo,J., Sung,P. and Klein,H. (2008) Mechanism of eukaryotic homologous recombination. *Annu. Rev. Biochem.*, **77**, 229–257.
2. Heyer,W.D., Ehmsen,K.T. and Liu,J. (2010) Regulation of homologous recombination in eukaryotes. *Annu. Rev. Genet.*, **44**, 113–139.
3. Karanam,K., Kafri,R., Loewer,A. and Lahav,G. (2012) Quantitative live cell imaging reveals a gradual shift between DNA repair mechanisms and a maximal use of HR in Mid S Phase. *Mol. Cell*, **47**, 320–329.
4. Symington,L.S. and Gautier,J. (2011) Double-strand break end resection and repair pathway choice. *Annu. Rev. Genet.*, **45**, 247–271.
5. Wechsler,T., Newman,S. and West,S.C. (2011) Aberrant chromosome morphology in human cells defective for Holliday junction resolution. *Nature*, **471**, 642–646.
6. Wu,L. and Hickson,I.D. (2003) The Bloom's syndrome helicase suppresses crossing over during homologous recombination. *Nature*, **426**, 870–874.
7. Xu,D., Guo,R., Sobeck,A., Bachrati,C.Z., Yang,J., Enomoto,T., Brown,G.W., Hoatlin,M.E., Hickson,I.D. and Wang,W. (2008) RMI, a new OB-fold complex essential for Bloom syndrome protein to maintain genome stability. *Genes Dev.*, **22**, 2843–2855.
8. Nassif,N., Penney,J., Pal,S., Engels,W.R. and Gloor,G.B. (1994) Efficient copying of nonhomologous sequences from ectopic sites via P-element-induced gap repair. *Mol. Cell. Biol.*, **14**, 1613–1625.
9. Chapman,J.R., Taylor,M.R. and Boulton,S.J. (2012) Playing the end game: DNA double-strand break repair pathway choice. *Mol. Cell*, **47**, 497–510.
10. Youds,J.L. and Boulton,S.J. (2011) The choice in meiosis—defining the factors that influence crossover or non-crossover formation. *J. Cell Sci.*, **124**, 501–513.
11. Matos,J., Blanco,M.G., Maslen,S., Skehel,J.M. and West,S.C. (2011) Regulatory control of the resolution of DNA recombination intermediates during meiosis and mitosis. *Cell*, **147**, 158–172.
12. Mitchel,K., Zhang,H., Welz-Voegele,C. and Jinks-Robertson,S. (2010) Molecular structures of crossover and noncrossover intermediates during gap repair in yeast: implications for recombination. *Mol. Cell*, **38**, 211–222.
13. Prakash,R., Satory,D., Dray,E., Papusha,A., Scheller,J., Kramer,W., Krejci,L., Klein,H., Haber,J.E., Sung,P. *et al.* (2009) Yeast Mph1 helicase dissociates Rad51-made D-loops: implications for crossover control in mitotic recombination. *Genes Dev.*, **23**, 67–79.

14. Ira,G., Malkova,A., Liberi,G., Foiani,M. and Haber,J.E. (2003) Srs2 and Sgs1-Top3 suppress crossovers during double-strand break repair in yeast. *Cell*, **115**, 401–411.
15. Krejci,L., Van Komen,S., Li,Y., Villemain,J., Reddy,M.S., Klein,H., Ellenberger,T. and Sung,P. (2003) DNA helicase Srs2 disrupts the Rad51 presynaptic filament. *Nature*, **423**, 305–309.
16. Dupaigne,P., Le Breton,C., Fabre,F., Gangloff,S., Le Cam,E. and Veaute,X. (2008) The Srs2 helicase activity is stimulated by Rad51 filaments on dsDNA: implications for crossover incidence during mitotic recombination. *Mol. Cell*, **29**, 243–254.
17. Colavito,S., Macris-Kiss,M., Seong,C., Gleeson,O., Greene,E.C., Klein,H.L., Krejci,L. and Sung,P. (2009) Functional significance of the Rad51-Srs2 complex in Rad51 presynaptic filament disruption. *Nucleic Acids Res.*, **37**, 6754–6764.
18. Fugger,K., Mistrik,M., Danielsen,J.R., Dinant,C., Falck,J., Bartek,J., Lukas,J. and Mailand,N. (2009) Human Fbh1 helicase contributes to genome maintenance via pro- and anti-recombinase activities. *J. Cell Biol.*, **186**, 655–663.
19. Bernstein,K.A., Gangloff,S. and Rothstein,R. (2010) The RecQ DNA helicases in DNA repair. *Annu. Rev. Genet.*, **44**, 393–417.
20. Hu,Y., Raynard,S., Sehorn,M.G., Lu,X., Bussen,W., Zheng,L., Stark,J.M., Barnes,E.L., Chi,P., Janscak,P. *et al.* (2007) RECQL5/Recql5 helicase regulates homologous recombination and suppresses tumor formation via disruption of Rad51 presynaptic filaments. *Genes Dev.*, **21**, 3073–3084.
21. Schwendener,S., Raynard,S., Paliwal,S., Cheng,A., Kanagaraj,R., Shevelev,I., Stark,J.M., Sung,P. and Janscak,P. (2010) Physical interaction of RECQ5 helicase with RAD51 facilitates its anti-recombinase activity. *J. Biol. Chem.*, **285**, 15739–15745.
22. Wang,W., Seki,M., Narita,Y., Nakagawa,T., Yoshimura,A., Otsuki,M., Kawabe,Y., Tada,S., Yagi,H., Ishii,Y. *et al.* (2003) Functional relation among RecQ family helicases RecQL1, RecQL5, and BLM in cell growth and sister chromatid exchange formation. *Mol. Cell. Biol.*, **23**, 3527–3535.
23. Hu,Y., Lu,X., Barnes,E., Yan,M., Lou,H. and Luo,G. (2005) Recql5 and Blm RecQ DNA helicases have nonredundant roles in suppressing crossovers. *Mol. Cell. Biol.*, **25**, 3431–3442.
24. Islam,M.N., Paquet,N., Fox,D. III, Dray,E., Zheng,X.F., Klein,H., Sung,P. and Wang,W. (2012) A variant of the breast cancer type 2 susceptibility protein (BRC) repeat is essential for the RECQL5 helicase to interact with RAD51 recombinase for genome stabilization. *J. Biol. Chem.*, **287**, 23808–23818.
25. Bennardo,N., Cheng,A., Huang,N. and Stark,J.M. (2008) Alternative-NHEJ is a mechanistically distinct pathway of mammalian chromosome break repair. *PLoS Genet.*, **4**, e1000110.
26. Gunn,A. and Stark,J.M. (2012) I-SceI-based assays to examine distinct repair outcomes of mammalian chromosomal double strand breaks. *Methods Mol. Biol.*, **920**, 379–391.
27. Richardson,C., Moynahan,M.E. and Jasin,M. (1998) Double-strand break repair by interchromosomal recombination: suppression of chromosomal translocations. *Genes Dev.*, **12**, 3831–3842.
28. Kanagaraj,R., Huehn,D., MacKellar,A., Menigatti,M., Zheng,L., Urban,V., Shevelev,I., Greenleaf,A.L. and Janscak,P. (2010) RECQ5 helicase associates with the C-terminal repeat domain of RNA polymerase II during productive elongation phase of transcription. *Nucleic Acids Res.*, **38**, 8131–8140.
29. Pfaffl,M.W. (2001) A new mathematical model for relative quantification in real-time RT-PCR. *Nucleic Acids Res.*, **29**, e45.
30. Bayani,J. and Squire,J.A. (2005) Sister chromatid exchange. *Curr. Protoc. Cell Biol.*, Chapter 22, Unit 22.27.
31. Stark,J.M., Pierce,A.J., Oh,J., Pastink,A. and Jasin,M. (2004) Genetic steps of mammalian homologous repair with distinct mutagenic consequences. *Mol. Cell. Biol.*, **24**, 9305–9316.
32. Sugiyama,T., New,J.H. and Kowalczykowski,S.C. (1998) DNA annealing by RAD52 protein is stimulated by specific interaction with the complex of replication protein A and single-stranded DNA. *Proc. Natl Acad. Sci. USA*, **95**, 6049–6054.
33. Paques,F. and Haber,J.E. (1999) Multiple pathways of recombination induced by double-strand breaks in Saccharomyces cerevisiae. *Microbiol. Mol. Biol. Rev.*, **63**, 349–404.
34. Prado,F. and Aguilera,A. (2003) Control of cross-over by single-strand DNA resection. *Trends Genet.*, **19**, 428–431.
35. Garcia,P.L., Liu,Y., Jiricny,J., West,S.C. and Janscak,P. (2004) Human RECQ5beta, a protein with DNA helicase and strand-annealing activities in a single polypeptide. *EMBO J.*, **23**, 2882–2891.
36. Hu,Y., Lu,X., Zhou,G., Barnes,E.L. and Luo,G. (2009) Recql5 plays an important role in DNA replication and cell survival after camptothecin treatment. *Mol. Biol. Cell*, **20**, 114–123.
37. Kim,P.M., Allen,C., Wagener,B.M., Shen,Z. and Nickoloff,J.A. (2001) Overexpression of human RAD51 and RAD52 reduces double-strand break-induced homologous recombination in mammalian cells. *Nucleic Acids Res.*, **29**, 4352–4360.
38. Arnaudeau,C., Helleday,T. and Jenssen,D. (1999) The RAD51 protein supports homologous recombination by an exchange mechanism in mammalian cells. *J. Mol. Biol.*, **289**, 1231–1238.
39. Richardson,C., Stark,J.M., Ommundsen,M. and Jasin,M. (2004) Rad51 overexpression promotes alternative double-strand break repair pathways and genome instability. *Oncogene*, **23**, 546–553.
40. Paffett,K.S., Clikeman,J.A., Palmer,S. and Nickoloff,J.A. (2005) Overexpression of Rad51 inhibits double-strand break-induced homologous recombination but does not affect gene conversion tract lengths. *DNA Repair (Amst)*, **4**, 687–698.
41. Sugawara,N., Ira,G. and Haber,J.E. (2000) DNA length dependence of the single-strand annealing pathway and the role of Saccharomyces cerevisiae RAD59 in double-strand break repair. *Mol. Cell. Biol.*, **20**, 5300–5309.
42. Vaze,M.B., Pellicioli,A., Lee,S.E., Ira,G., Liberi,G., Arbel-Eden,A., Foiani,M. and Haber,J.E. (2002) Recovery from checkpoint-mediated arrest after repair of a double-strand break requires Srs2 helicase. *Mol. Cell*, **10**, 373–385.
43. Carter,S.D., Vigasova,D., Chen,J., Chovanec,M. and Astrom,S.U. (2009) Nej1 recruits the Srs2 helicase to DNA double-strand breaks and supports repair by a single-strand annealing-like mechanism. *Proc. Natl Acad. Sci. USA*, **106**, 12037–12042.
44. Wu,Y., Kantake,N., Sugiyama,T. and Kowalczykowski,S.C. (2008) Rad51 protein controls Rad52-mediated DNA annealing. *J. Biol. Chem.*, **283**, 14883–14892.
45. Thorslund,T., McIlwraith,M.J., Compton,S.A., Lekomtsev,S., Petronczki,M., Griffith,J.D. and West,S.C. (2010) The breast cancer tumor suppressor BRCA2 promotes the specific targeting of RAD51 to single-stranded DNA. *Nat. Struct. Mol. Biol.*, **17**, 1263–1265.
46. Jensen,R.B., Carreira,A. and Kowalczykowski,S.C. (2010) Purified human BRCA2 stimulates RAD51-mediated recombination. *Nature*, **467**, 678–683.
47. Burgess,R.C., Lisby,M., Altmannova,V., Krejci,L., Sung,P. and Rothstein,R. (2009) Localization of recombination proteins and Srs2 reveals anti-recombinase function in vivo. *J. Cell Biol.*, **185**, 969–981.
48. Johnson,R.D., Liu,N. and Jasin,M. (1999) Mammalian XRCC2 promotes the repair of DNA double-strand breaks by homologous recombination. *Nature*, **401**, 397–399.
49. Barber,L.J., Youds,J.L., Ward,J.D., McIlwraith,M.J., O'Neil,N.J., Petalcorin,M.I., Martin,J.S., Collis,S.J., Cantor,S.B., Auclair,M. *et al.* (2008) RTEL1 maintains genomic stability by suppressing homologous recombination. *Cell*, **135**, 261–271.
50. Uringa,E.J., Youds,J.L., Lisaingo,K., Lansdorp,P.M. and Boulton,S.J. (2011) RTEL1: an essential helicase for telomere maintenance and the regulation of homologous recombination. *Nucleic Acids Res.*, **39**, 1647–1655.
51. Lao,V.V., Welcsh,P., Luo,Y., Carter,K.T., Dzieciatkowski,S., Dintzis,S., Meza,J., Sarvetnick,N.E., Monnat,R.J. Jr, Loeb,L.A. *et al.* (2013) Altered RECQ helicase expression in sporadic primary colorectal cancers. *Transl Oncol.*, **6**, 458–469.
52. Klein,H.L. (2008) The consequences of Rad51 overexpression for normal and tumor cells. *DNA Repair (Amst)*, **7**, 686–693.
53. Sigurdsson,S., Van Komen,S., Petukhova,G. and Sung,P. (2002) Homologous DNA pairing by human recombination factors Rad51 and Rad54. *J. Biol. Chem.*, **277**, 42790–42794.
54. Henricksen,L.A., Umbricht,C.B. and Wold,M.S. (1994) Recombinant replication protein A: expression, complex formation, and functional characterization. *J. Biol. Chem.*, **269**, 11121–11132.

55. Benson,F.E., Baumann,P. and West,S.C. (1998) Synergistic actions of Rad51 and Rad52 in recombination and DNA repair. *Nature*, **391**, 401–404.
56. Orren,D.K., Brosh,R.M. Jr, Nehlin,J.O., Machwe,A., Gray,M.D. and Bohr,V.A. (1999) Enzymatic and DNA binding properties of purified WRN protein: high affinity binding to single-stranded DNA but not to DNA damage induced by 4NQO. *Nucleic Acids Res.*, **27**, 3557–3566.
57. Simandlova,J., Zagelbaum,J., Payne,M.J., Chu,W.K., Shevelev,I., Hanada,K., Chatterjee,S., Reid,D.A., Liu,Y., Janscak,P. *et al.* (2013) FBH1 disrupts RAD51 filaments *in vitro* and modulates homologous recombination in mammalian cells. *J. Biol. Chem.*, **288**, 34168–34180.
58. Fugger,K., Chu,W.K., Haahr,P., Nedergaard Kousholt,A., Beck,H., Payne,M.J., Hanada,K., Hickson,I.D. and Storgaard Sorensen,C. (2013) FBH1 co-operates with MUS81 in inducing DNA double-strand breaks and cell death following replication stress. *Nat. Commun.*, **4**, 1423.
59. Kanagaraj,R., Saydam,N., Garcia,P.L., Zheng,L. and Janscak,P. (2006) Human RECQ5beta helicase promotes strand exchange on synthetic DNA structures resembling a stalled replication fork. *Nucleic Acids Res.*, **34**, 5217–5231.

Supplementary Information

Supplementary Materials and Methods

Antibodies and chemicals

Rabbit polyclonal anti-RECQ5 and anti-RAD51 antibodies used for Western blotting were made in the laboratory. Control IgG used for ChIP was purified from a rabbit preimmune serum. The following commercial antibodies were used in this study: rabbit polyclonal anti-BLM antibody was purchased from Abcam; rabbit polyclonal anti-TFIIH, anti-RAD51 (used for ChIP) and anti-RAD52 antibodies, goat polyclonal Omni-probe antibody and mouse monoclonal anti-β-tubulin were purchased from Santa Cruz. Chemicals used were purchased either from Sigma-Aldrich or Roche.

DNA oligonucleotides

DNA oligonucleotides used for strand-annealing assays were purchased PAGE-purified from Microsynth. The sequences of oligonucleotides used were the following:
f9 (59-mer):
5′ACTATCATTCAGTCATGTAACCTAGTCAATCTGCGAGCTCGAATTCACTGGAGTGACCT-3′
f7 (30-mer, complementary to the 5′-half of f9):
5′-ATTGACTAGGTTACATGACTGAATGATAGT-3′
f9-C (59-mer, fully complementary to f9):
5′-AGGTCACTCCAGTGAATTCGAGCTCGCAGATTGACTAGGTTACATGACTGAATGATAG-3′.
Primers used in ChIP-qPCR assays were the following:
DR-GFP-P1
Forward: 5′-TCTTCTTCAAGGACGACGGCAACT-3′
Reverse: 5′-TTGTAGTTGTACTCCAGCTTGTGC-3′
DR-GFP-P2
Forward: 5′-ACGAGAGATCTATAGATCTATAGATCATGA-3′
Reverse: 5′-CTCTTTACTGAAGGCTCTTTA-3′

Protein purification

Human RECQ5, RECQ5K58R, RECQ5$^{\Delta 652\text{-}674}$, RAD51, RAD51^{K133R} and RPA were over-produced in bacteria and purified as described previously (1-4). Human RAD52 was over-produced in *E. coli* BL21 (DE3) pLysS as a fusion with a hexahistidine (6xHis) tag, and purified to homogeneity as described previously with minor modifications (5). Briefly, harvested cells were resuspended in 40 ml of buffer N [20 mM Tris-HCl (pH 8.0), 0.5 M NaCl, 10% (v/v) glycerol, 0.02% (v/v) Triton X-100] containing 5 mM imidazole and lysed by sonication. After high-speed centrifugation, the lysate was loaded on a 5-ml Ni^{2+}-charged HiTrap Chelating HP column (GE Healthcare) equilibrated with buffer N containing 10mM imidazole. After washing with 50 mM imidazole in buffer N, 6xHis-RAD52 was eluted with a 50-500 mM imidazole gradient in buffer N. Peak fractions were pooled, diluted five times with buffer H [20 mM Tris-HCl (pH 8.0), 1 mM EDTA, 0.5 mM DTT, 10% (v/v) glycerol) and loaded onto a 5-ml HiTrap Heparin HP column (GE Healthcare) equilibrated with buffer H containing 100 mM KCl. After

washing with equilibration buffer, 6xHis-RAD52 was eluted with a 0.1-1.0 M KCl gradient in buffer H. Peak fractions were diluted twice with buffer H and aliquots were stored at -70 °C. WRN-6xHis and GST-FBH1-6xHis were produced in Sf9 insect cells and purified as previously described (6,7).

Cell culture

All cells lines used in this study were cultured in Dulbecco's modified Eagle medium (DMEM, Gibco) supplemented with 10% fetal calf serum (FCS, Gibco) and 100 U/ml penicillin/streptomycin.

Cell Cycle Analysis

For cell cycle analysis, cells were collected, washed with PBS and fixed with 70% ethanol. Next, cells were washed with PBS, treated with 0.5 mg/ml RNaseA for 30 min at RT and stained with 50 μg/ml propidium iodide. The distribution of cell cycle phases with different DNA content was determined using LSRII (BD Biosciences) and FlowJo software.

siRNA transfection

Unless indicated otherwise, all the siRNAs used in the study were purchased from Microsynth. Transfection of siRNA was carried out using Lipofectamine RNAimax (Invitrogen) according to manufacturer's instructions. The sense strand sequences of all siRNAs used are indicated below:
siLuc: 5′-CGU ACG CGG AAU ACU UCG A dTdT-3′
siRAD51: 5′-AAG GGA AUU AGU GAA GCC AAA dTdT-3′
siBRCA2: 5′-CAGGACACAAUUACAACUAAAdTdT-3′
siRAD52: 5′-AAG GAU GGU UCA UAU CAU GAA dTdT-3′
siRECQ5#1: 5′-CAG GAG GCU GAU AAA GGG UUA dTdT-3′
siRECQ5#2: 5′-GGA GAG UGC GAC CAU GGC U dTdT-3′
siFBH1: 5′-GGG AUG UUC UUU UGA UAA AdTdT-3′ (8)
siBLM#1: 5′-CCG AAU CUC AAU GUA CAU AGA dTdT-3′
siBLM#2: a smartpool siRNA from Dharmacon (a kind gift from Dr. Pietro Pichierri).

Western blotting

Whole-cell extracts were prepared as described previously with minor modifications (9). Briefly, cells were extracted using buffer W [50 mM Tris-HCl (pH 7.5), 120 mM NaCl, 0.5% (v/v) NP-40, 20 mM NaF, 15 mM sodium pyrophosphate, 1 mM EDTA, 6 mM EGTA] supplemented with 0.1 mM PMSF and protease inhibitor cocktail (cOmplete, EDTA-free; Roche). After incubation on ice for 10 min, the lysate was sonicated and clarified by centrifugation. Total protein concentration was estimated by Bradford method. For Western blotting, whole cell extracts (50 μg) were separated on either 8% or 12% SDS-polyacrylamide gel. Proteins were transferred to PVDF membrane (Hybond, GE Healthcare), probed with appropriate antibodies and immune complexes were visualized using ECL system (Pierce).

Sister chromatid exchange assay

SCE assay was done as described previously with minor modifications (10). Briefly, cells were seeded in a 6-cm plate, and two rounds of transfection with appropriate siRNAs were performed at 24 h and 48 h post seeding. Cells were then grown for 40 h in the presence of 100 μM 5-bromo-2'-deoxyuridine (BrdU), and further incubated for 2 h with 0.2 μg/ml colcemid. Camptothecin (CPT; 40 nM) was added 20 h prior to cell harvest where indicated. Metaphase cells were harvested by mitotic shake-off, swollen in 75 mM KCl for 15 min, fixed with Carnoy's buffer (3:1 methanol and glacial acetic acid), spread on a clean glass slide and air-dried. The slides were then stained with Hoechst 33258 (50 μg/ml) for 30 min, rinsed with PBS, UV (254 nm, Stratalinker) exposed for 10 min and incubated in 2x SSC for 60 min. The slides were finally stained with 7% Giemsa solution for 15 min, washed twice with water and examined under light microscope. All quantifications were carried out blind and 50 metaphases were analyzed from each condition. Data were plotted using Prism 6 software as mean with SD.

Supplementary References

1. Garcia, P.L., Liu, Y., Jiricny, J., West, S.C. and Janscak, P. (2004) Human RECQ5beta, a protein with DNA helicase and strand-annealing activities in a single polypeptide. *EMBO J*, 23, 2882-2891.
2. Schwendener, S., Raynard, S., Paliwal, S., Cheng, A., Kanagaraj, R., Shevelev, I., Stark, J.M., Sung, P. and Janscak, P. (2010) Physical interaction of RECQ5 helicase with RAD51 facilitates its anti-recombinase activity. *J Biol Chem*, 285, 15739-15745.
3. Sigurdsson, S., Van Komen, S., Petukhova, G. and Sung, P. (2002) Homologous DNA pairing by human recombination factors Rad51 and Rad54. *J Biol Chem*, 277, 42790-42794.
4. Henricksen, L.A., Umbricht, C.B. and Wold, M.S. (1994) Recombinant replication protein A: expression, complex formation, and functional characterization. *J Biol Chem*, 269, 11121-11132.
5. Benson, F.E., Baumann, P. and West, S.C. (1998) Synergistic actions of Rad51 and Rad52 in recombination and DNA repair. *Nature*, 391, 401-404.
6. Orren, D.K., Brosh, R.M., Jr., Nehlin, J.O., Machwe, A., Gray, M.D. and Bohr, V.A. (1999) Enzymatic and DNA binding properties of purified WRN protein: high affinity binding to single-stranded DNA but not to DNA damage induced by 4NQO. *Nucleic Acids Res*, 27, 3557-3566.
7. Simandlova, J., Zagelbaum, J., Payne, M.J., Chu, W.K., Shevelev, I., Hanada, K., Chatterjee, S., Reid, D.A., Liu, Y., Janscak, P. *et al.* (2013) FBH1 disrupts RAD51 filaments in vitro and modulates homologous recombination in mammalian cells. *J Biol Chem*, *in press*.
8. Fugger, K., Chu, W.K., Haahr, P., Nedergaard Kousholt, A., Beck, H., Payne, M.J., Hanada, K., Hickson, I.D. and Storgaard Sorensen, C. (2013) FBH1 co-operates with MUS81 in inducing DNA double-strand breaks and cell death following replication stress. *Nat Commun*, 4, 1423.
9. Kanagaraj, R., Saydam, N., Garcia, P.L., Zheng, L. and Janscak, P. (2006) Human RECQ5beta helicase promotes strand exchange on synthetic DNA structures resembling a stalled replication fork. *Nucleic Acids Res*, 34, 5217-5231.
10. Bayani, J. and Squire, J.A. (2005) Sister chromatid exchange. *Curr Protoc Cell Biol*, Chapter 22, Unit 22 27.

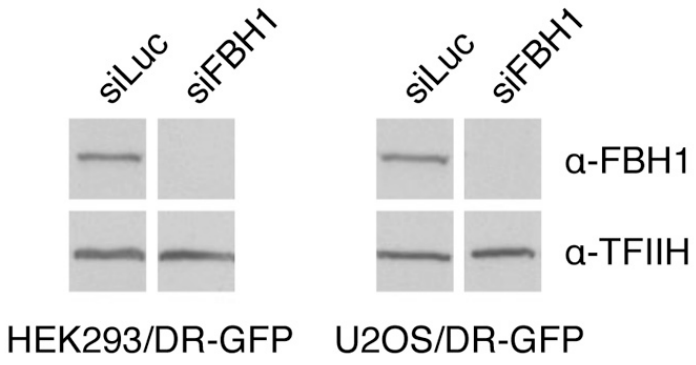

Figure S1. Confirmation of FBH1 knockdown. HEK293/DR-GFP and U2OS/DR-GFP cells were treated with indicated siRNAs. Cell extracts were subjected to Western blot analysis. Blots were probed with indicated antibodies.

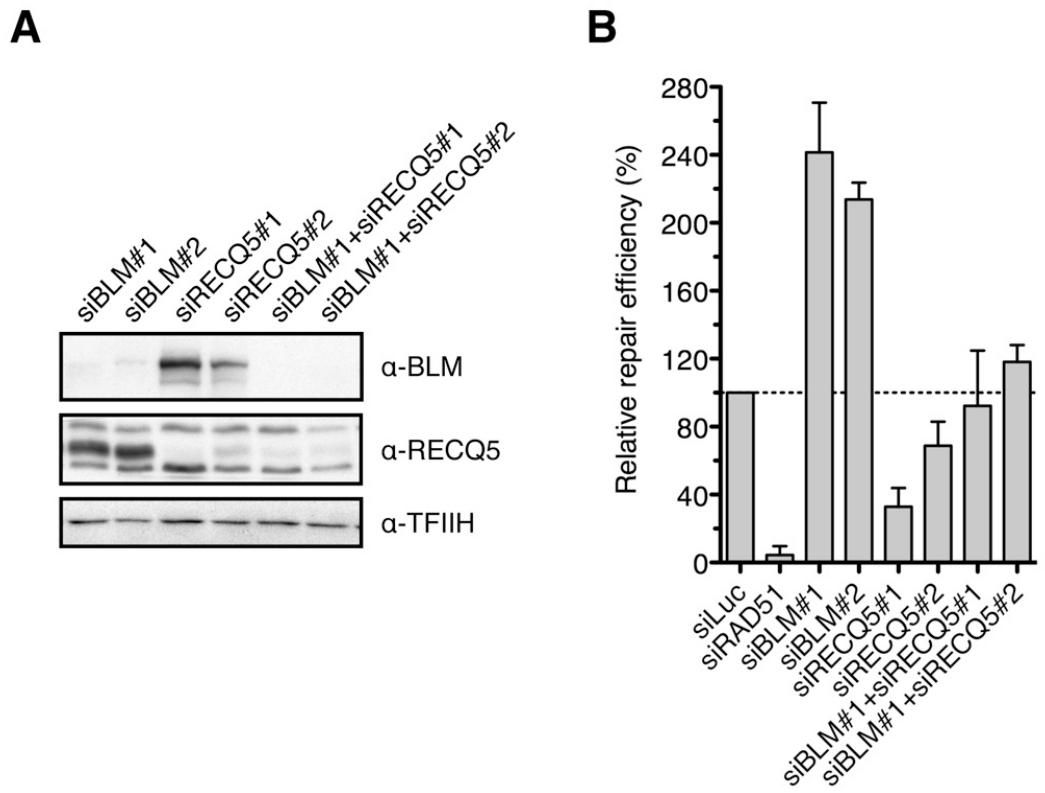

Figure S2. (A) Western blot analysis of extracts from HEK293/DR-GFP transfected with indicated siRNAs. Blots were probed with indicated antibodies. **(B)** Efficiency of HR-mediated repair of I-SceI-induced DSB in HEK293/DR-GFP cells treated with indicated siRNAs. Cells were transfected with appropriate siRNA (40 nM) two days prior to transfection of I-SceI-expressing plasmid. Percentage of GFP positive cells was measured by flow cytometry two days after DSB induction and taken as a measure of DSB repair efficiency. Values plotted represent relative repair efficiency calculated as a percentage of repair efficiency measured in cells transfected with control siRNA (siLuc; 100%). All data points represent an average of at least three replicates with error bars indicating standard deviation.

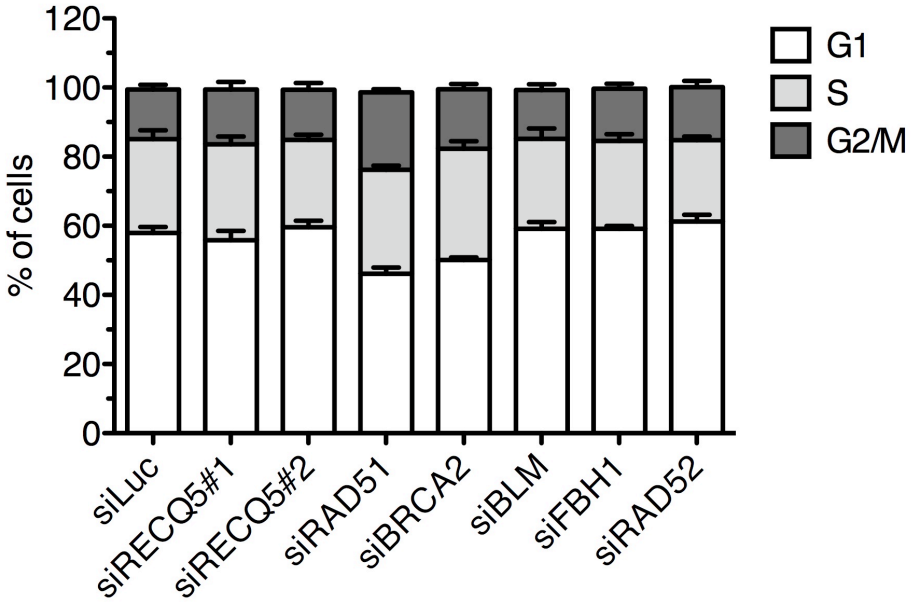

Figure S3. Cell cycle distribution of HEK293/DR-GFP cells transfected with indicated siRNAs. siRNA transfections and flow cytometry analysis were carried out as described under Materials and Methods. All data points represent an average of three replicates with error bars indicating standard deviation.

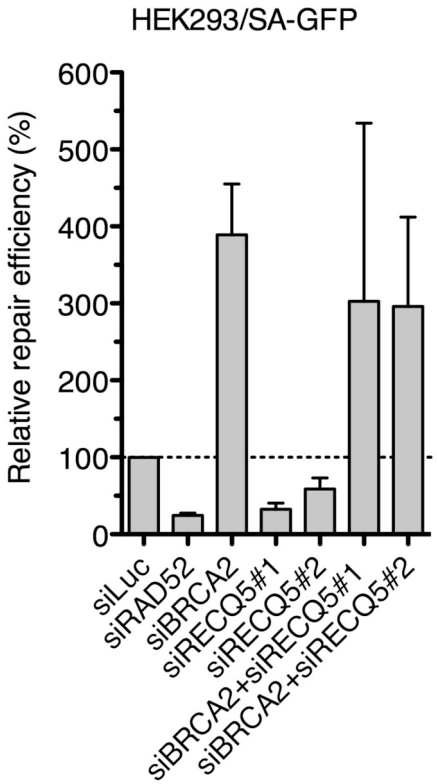

Figure S4. SSA defect of RECQ5-deficient cells is rescued by BRCA2 depletion. **(A)** Efficiency of SSA-mediated repair of I-SceI-induced DSB in HEK293/SA-GFP cells transfected with indicated siRNAs. SSA reporter assays were performed as described under Materials and Methods.

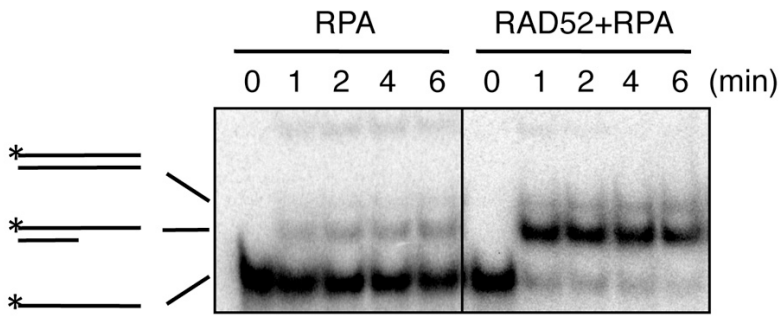

Figure S5. RAD52-mediated DNA annealing. Two complementary oligonucleotides, 5′-end radiolabeled 59mer (f9) and 30mer (f7), at a concentration of 2.5 nM, were incubated for 5 minutes in presence of RPA (30 nM) and a homologous 59mer duplex (2.5 nM). This was followed by addition of RAD52 (60 nM) where indicated. Reaction aliquots were collected at indicated time points and analyzed as in Figure 3.

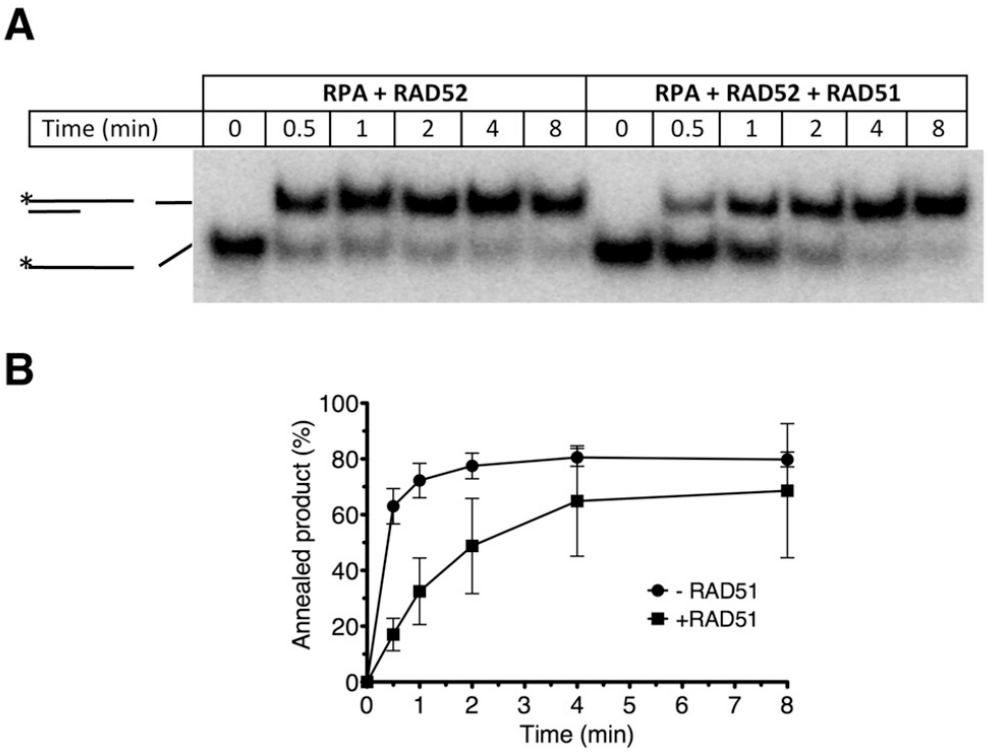

Figure S6. RAD51 inhibits RAD52-mediated ssDNA annealing *in vitro*. **(A)** Annealing reactions were carried out at 30˚C in buffer R supplemented with ATP-regenerating system. Reactions contained 5′-end radiolabeled 59-mer oligonucleotide (2.5 nM), either free or pre-coated with wild-type RAD51 (300 nM), a 30-mer oligonucleotide (2.5 nM) complementary to the 5′-half of the 59-mer, RAD52 (60 nM) and RPA (30 nM). Reaction aliquots at indicated time points were subjected to PAGE followed by phosphorimaging as described in Materials and Methods. (**B**) Quantification of data shown in (A). Each data point represents the mean of three independent experiments. Error bars represent standard deviation.

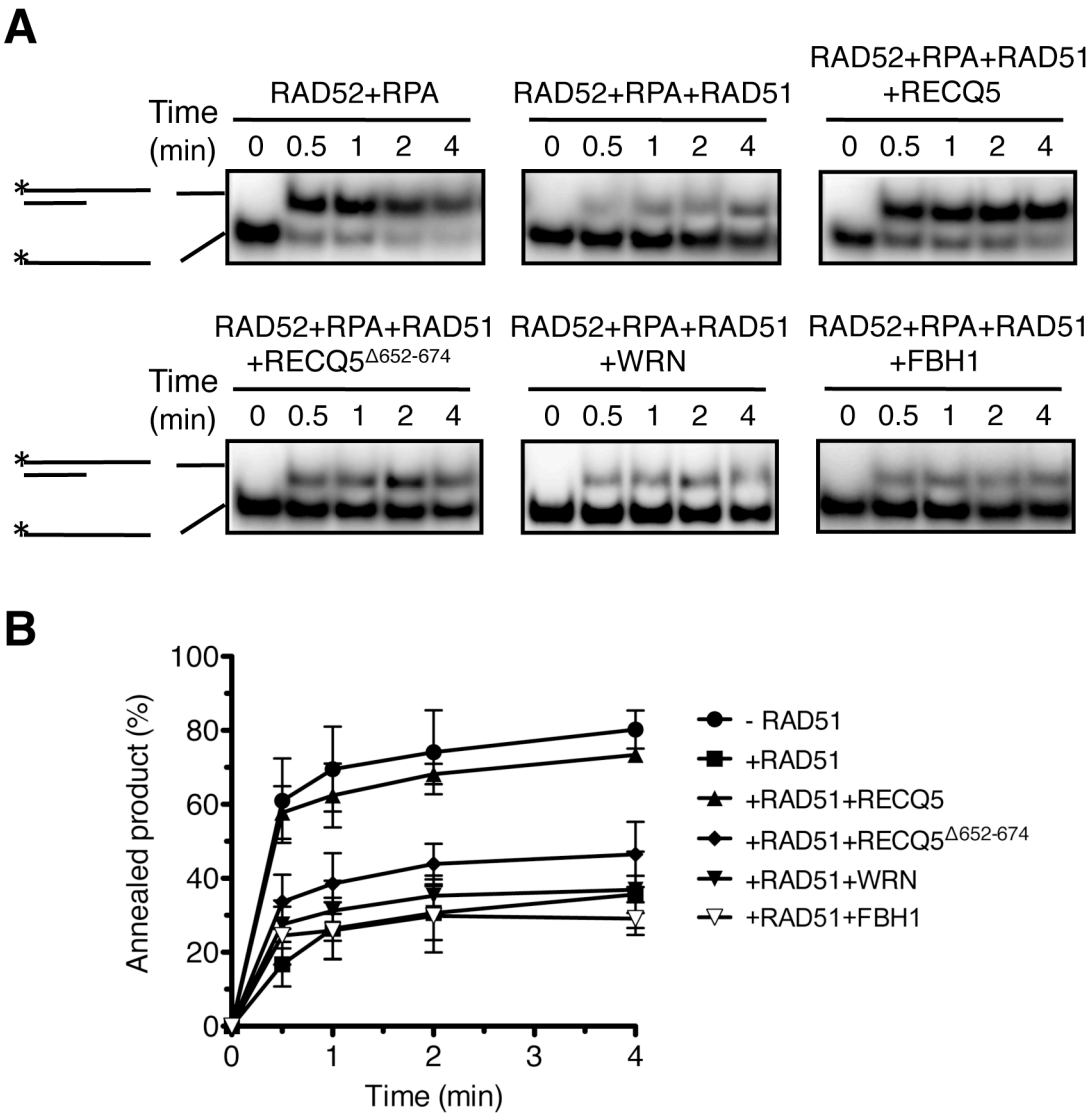

Figure S7. RECQ5, but not WRN or FBH1, alleviates the inhibitory effect of RAD51^{K133R} on RAD52-mediated ssDNA annealing. (**A**) Reactions were carried out at 30˚C in buffer R supplemented with ATP-regenerating system. Reactions contained 5′-end radiolabeled 59-mer oligonucleotide (2.5 nM), either free or pre-coated with RAD51^{K133R} (100 nM), a 30-mer oligonucleotide (2.5 nM) complementary to the 5′-half of the 59-mer, RAD52 (60 nM) and RPA (30 nM). Where indicated, RECQ5, RECQ5$^{\Delta 652-674}$, WRN and FBH1 were present at a concentration of 40 nM. Reaction aliquots at indicated time points were subjected to PAGE followed by phosphorimaging as described in Materials and Methods. (**B**) Quantification of data shown in (A). Each data point represents the mean of two independent experiments. Error bars represent standard deviation.

3.3 DNA2 Cooperates with the WRN and BLM RecQ Helicases to Mediate Long-Range DNA-End Resection in Human Cells.

DNA end resection of DSBs is process consisting of two-steps: short-range and long-range resection. During short-range resection, DNA ends are trimmed and resected up to 100 bases by MRN/X complex in conjunction with CtIP/Sae2. In the second step, DNA is further resected by Exo1 or Sgs1 in conjunction with Dna2. This process is well studied in yeast but there is missing reliable evidence for Sgs1 orthologs that function in human cells during long-range resection. This urged us to investigate the role of proposed functional orthologs of Sgs1 helicase in human cells.

We took advantage of recently described assay to monitor DNA resection *in vitro* using annealing of short radioactively labelled oligonucleotides after resection reaction is stopped. As BLM has been shown and WRN was proposed not to be able to cooperate with DNA2 during DNA resection, we firstly tested WRN helicase together with DNA2 and indeed we saw that WRN is capable of DNA end resection in conjunction with DNA2. As both WRN and DNA2 contain helicase and exo/endonuclease domains we tested which of these are involved in DNA resection and found that only helicase activity of WRN and endonuclease activity of DNA2 are necessary for this process.

Next we checked if WRN and DNA2 interact physically. We could show that WRN and DNA2 form complex in cells as well as in mixture of purified proteins, indicating a direct interaction. We mapped the interaction between WRN and DNA2 to be in the helicase domain and C-terminal part of WRN. We also compared the strength of WRN-DNA2 interaction with previously published BLM-DNA2 interaction and found them to be about the same intensity. When we compared the ability of these complexes to resect DNA *in vitro*, we observed much higher rate of resection when WRN-DNA2 complex was used.

Yeast Sgs1 helicase has been shown to be a part of a complex with Top3 and Rmi1. Helicase activity of Sgs1 is stimulated in this complex also in the process of DNA end resection. In human cells, BLM exists in complex with TopIIIα-RMI1-RMI2 (TRR) but its influence on BLM during DNA end resection has not been evaluated. To this end, we used *in vitro* resection assay and found that indeed helicase activity of BLM is mildly stimulated by the presence of TRR complex.

We also wanted to evaluate the role of WRN and BLM *in vivo*. For this purpose we employed HEK293/U2OS-SA-GFP reporter cell lines to monitor resection as there is need to resect 2.7kb in order restore functional GFP upon DSB creation during SSA process. We depleted all proteins of our interest and checked for SSA repair efficiency first in HEK293-SA-GFP cell line. As expected, depletion of MRE11 and CtIP as well as EXO1 dramatically decreased SSA repair efficiency. Interestingly, while WRN and DNA2 depletion led to reduction of SSA repair efficiency, BLM depletion increased efficiency of repair by SSA in HEK293 cells. Depletion of both WRN and DNA2 did not show any additional decrease suggesting that they work together in the same pathway. Moreover, when we depleted them together with EXO1 we saw additional reduction in SSA repair efficiency showing that also in human cells there are two active subpathways of long-range resection depending on EXO1 and WRN-DNA2.

To substantiate the results from HEK293 cells we employed another cell line – U2OS cells. As expected, depletion of MRE11, CtIP and EXO1 as well as WRN and DNA2 led to decrease in SSA repair efficiency also in U2OS-SA-GFP cell line. However, BLM depletion decreased SSA repair efficiency in U2OS cells in contrast to HEK293. Moreover, we could still see additional effect of combined depletion of EXO1 with DNA2, WRN or BLM. These data suggest that in contrast to HEK293 cells, EXO1 and DNA2-WRN or DNA2-BLM represent two subpathways of long-range resection in U2OS cell line. To test the role of TRR complex in DNA resection *in vivo* we depleted RMI1 alone or in combination with BLM or DNA2 and while RMI1 depletion caused decrease in SSA repair efficiency, there was no additional decrease when RMI1 was depleted together with BLM or DNA2.

To appraise the result from U2OS reporter cell line we employed quantification of RPA foci formed after DNA damage induction in U2OS cells using indirect immunofluorescence. Interestingly, cells depleted of either WRN or BLM displayed mild decrease in RPA foci number. On the other hand, depletion of CtIP and DNA2 as well as combined depletion of BLM and WRN had much stronger effect. Together these results support the hypothesis that DNA2 can cooperate with either BLM or WRN in long-range resection of DNA ends in U2OS cells.

THE JOURNAL OF BIOLOGICAL CHEMISTRY VOL. 289, NO. 39, pp. 27314–27326, September 26, 2014

DNA2 Cooperates with the WRN and BLM RecQ Helicases to Mediate Long-range DNA End Resection in Human Cells*

Received for publication, May 3, 2014, and in revised form, August 12, 2014 Published, JBC Papers in Press, August 13, 2014, DOI 10.1074/jbc.M114.578823

Andreas Sturzenegger[‡1], Kamila Burdova[§1], Radhakrishnan Kanagaraj[‡2], Maryna Levikova[‡], Cosimo Pinto[‡], Petr Cejka[‡], and Pavel Janscak[‡§3]

From the [‡]Institute of Molecular Cancer Research, University of Zurich, 8057 Zurich, Switzerland and the [§]Institute of Molecular Genetics, Academy of Sciences of the Czech Republic, 14300 Prague, Czech Republic

Background: DNA end resection is a critical step in the homology-directed repair of DNA double strand breaks (DSBs).
Results: Human WRN helicase stimulates the DNA2-catalyzed resection of DNA ends and acts in concert with DNA2 to promote DSB repair by single strand annealing.
Conclusion: DNA2 cooperates with WRN or BLM to mediate the resection of DSBs in mammalian cells.
Significance: Defects in DNA end resection might, in part, account for the genomic instability phenotype of Werner syndrome.

The 5′-3′ resection of DNA ends is a prerequisite for the repair of DNA double strand breaks by homologous recombination, microhomology-mediated end joining, and single strand annealing. Recent studies in yeast have shown that, following initial DNA end processing by the Mre11-Rad50-Xrs2 complex and Sae2, the extension of resection tracts is mediated either by exonuclease 1 or by combined activities of the RecQ family DNA helicase Sgs1 and the helicase/endonuclease Dna2. Although human DNA2 has been shown to cooperate with the BLM helicase to catalyze the resection of DNA ends, it remains a matter of debate whether another human RecQ helicase, WRN, can substitute for BLM in DNA2-catalyzed resection. Here we present evidence that WRN and BLM act epistatically with DNA2 to promote the long-range resection of double strand break ends in human cells. Our biochemical experiments show that WRN and DNA2 interact physically and coordinate their enzymatic activities to mediate 5′-3′ DNA end resection in a reaction dependent on RPA. In addition, we present *in vitro* and *in vivo* data suggesting that BLM promotes DNA end resection as part of the BLM-TOPOIIIα-RMI1-RMI2 complex. Our study provides new mechanistic insights into the process of DNA end resection in mammalian cells.

DNA double strand breaks (DSBs)[4] are a very dangerous form of DNA damage because they can cause cell death or chromosomal rearrangements, a hallmark of cancer (1). DSBs can occur accidentally during normal cellular metabolism or upon exposure of cells to exogenous agents such as ionizing radiation and radiomimetic drugs (2). There are also programmed DSBs that drive recombination events essential for physiological processes, such as meiosis and lymphocyte development (3, 4). In eukaryotic cells, DSBs are repaired by one of two major pathways: non-homologous end joining (NHEJ) and homologous recombination (HR). NHEJ involves religation of the broken DNA ends and is frequently associated with a short deletion or insertion of DNA at the break site (5). In contrast, HR restores the DNA integrity accurately because it uses sister chromatids or homologous chromosomes as a template for repair (6, 7). HR is initiated by resection of the broken DNA ends to generate 3′ single-stranded (ss) DNA tails that are utilized by the RAD51 recombinase for a homology search on the donor DNA molecule (6, 7). Genetic and biochemical studies in budding yeast have shown that broken DNA ends are resected in a two-step process (8–10). DNA end resection in yeast is initiated by the Mre11-Rad50-Xrs2 complex in conjunction with Sae2 (8, 9, 11). These proteins may initiate resection of the 5′ strand of the broken DNA to remove a stretch of about 100–200 nucleotides from the DNA end (8, 9, 11). The Mre11-Rad50-Xrs2 complex also recruits the components of the long-range resection pathways Exo1 or Dna2-Sgs1 (8–10, 12, 13). Exo1 is a dsDNA-dependent 5′-3′ exonuclease that preferentially degrades DNA substrates with a 3′ ssDNA tail in a reaction stimulated by the ssDNA-binding protein RPA (13). Dna2 is a ssDNA-specific nuclease and a DNA helicase that functions in conjunction with the RecQ family DNA helicase Sgs1 and RPA to catalyze long-range DNA end resection (10, 14). In this reaction, RPA stimulates DNA unwinding by Sgs1 and promotes degradation of the 5′-terminated strand by Dna2 while protecting the growing 3′ ssDNA tail (10). DNA end resection is also the initial step in two other DSB repair pathways, single strand annealing (SSA) and microhomology-mediated end joining (8, 15).

The molecular machinery of DNA end resection appears to be largely conserved between yeast and man (15–19). However, it remains a matter of debate which DNA helicase mediates DNA2-catalyzed resection in mammalian cells. Mammals pos-

* This work was supported by Swiss National Science Foundation Grants 31003A-129747 and 31003A_146206, by Czech Science Foundation Grant GAP305/10/0281, and by the Stiftung zur Krebsbekämpfung. This work was also supported by Swiss National Science Foundation Grant PP00P3 133636 (to P.C.) and by Forschungskredit of the University of Zurich Grant FK-13-098 (to A. S.).
[1] Both authors contributed equally to this work.
[2] Present address: London Research Institute, Cancer Research UK, Clare Hall Laboratories, South Mimms, Herts, EN6 3LD, UK.
[3] To whom correspondence should be addressed: Institute of Molecular Cancer Research, University of Zurich, Winterthurerstr. 190, 8057 Zurich, Switzerland. Tel.: 41-44-6353470; Fax: 41-44-6353484; E-mail: pjanscak@imcr.uzh.ch.
[4] The abbreviations used are: DSB, double strand break; NHEJ, non-homologous end joining; HR, homologous recombination; ssDNA, single-stranded DNA; SSA, single strand annealing; BTRR, BLM-TOPOIIIα-RMI1-RMI2; nt, nucleotide(s); CPT, camptothecin.

sess five RecQ homologues: RECQ1, BLM, WRN, RECQ4, and RECQ5 (20). Biochemical studies have shown that human DNA2 can act in conjunction with the BLM helicase and RPA to mediate 5′-3′ resection of DNA ends *in vitro* (17). In agreement with these findings, it has been observed that cells depleted of both BLM and EXO1 show a reduction in the formation of RPA foci in response to DSBs and are defective in DSB repair by HR (16, 19). However, studies using *Xenopus* egg extracts and purified proteins have shown that Dna2 mediates DNA end resection together with WRN rather than BLM (21–23). This discrepancy prompted us to investigate the role of WRN in DNA end resection in human cells. Here we demonstrate that WRN helicase is capable of acting in concert with DNA2 and RPA to resect 5′-recessed DNA ends *in vitro* with a catalytic efficiency even higher than that of BLM. Moreover, our results show that human cells may employ either BLM or WRN to assist DNA2 in long-range DNA end resection. Finally, we present data suggesting that BLM acts in DNA end resection as part of the BLM-TOPOIIIα-RMI1-RMI2 (BTRR) complex.

EXPERIMENTAL PROCEDURES

Antibodies and siRNA—Primary antibodies used for immunoblotting were as follows: mouse monoclonal anti-WRN (BD Biosciences, catalog no. 611169), rabbit polyclonal anti-DNA2 (Abcam, catalog no. ab96488), rabbit polyclonal anti-BLM (Abcam, catalog no. ab476), rabbit polyclonal anti-TFIIH (Santa Cruz Biotechnology, catalog no. sc293), mouse monoclonal anti-FLAG (Sigma, catalog no. F1804), and rabbit polyclonal anti-RMI1 (Proteintech, catalog no. 14630-1-AP). Anti-FLAG M2 magnetic beads (Sigma) were used for immunoprecipitation. Primary antibodies used for immunofluorescence staining were as follows: mouse monoclonal anti-RPA2 (Abcam, catalog no. ab2175) and rabbit monoclonal anti-γ-H2AX (Cell Signaling Technology, catalog no. 9718S). Rabbit polyclonal anti-WRN antibody used for immunoprecipitation has been described previously (24).

All siRNA oligoduplexes used in this study were purchased from Microsynth. The sequences of the sense strands of these duplexes were as follows: siLuc, 5′-CGUACGCGGAAUACUUCGAdTdT-3′; siWRN, 5′-UAGAGGGAAACUUGGCAAAdTdT-3′; siBLM, 5′-CCGAAUCUCAAUGUACAUAGAdTdT-3′; siDNA2, 5′-UACCGCUUAAAUCUAAGUCAAdTdT-3′; siEXO1, 5′-CAGCCAUUCUUACUACGCUAAdTdT-3′; siMRE11, 5′-GAGCAUAACUCCAUAAGUAdTdT-3′ (25); siCtIP, 5′-UCCACAACAUAAUCCUAAUdTdT-3′ (26); and siRMI1, 5′-AGCCUUCACGAAUGUUGAUdTdT-3′ (27).

Plasmid Constructions—The human DNA2 (hDNA2) ORF was amplified by PCR without the initiation and stop codons to generate a fragment including ggatcc-hDNA2-ctcgag. After digestion with BamHI and XhoI, the hDNA2 fragment was cloned into pFLAG-CMV2 (Sigma) digested with BglII/SalI (pFLAG-CMV2-hDNA2). The human WRN (hWRN) ORF was inserted into pcDNA3.1/Hygro(−) (Invitrogen) via the NheI and DraI sites (pcDNA3.1-hWRN). The siRNA-resistant form of this construct was generated by changing four nucleotides in the siWRN-targeting region (T270C, A273G, G276C, and A279G) using the QuikChange site-directed mutagenesis kit (Stratagene).

Protein Purifications—Wild-type and mutant forms of WRN, BLM, EXO1, and RPA were produced and purified as described previously (28–31). The TOPOIIIα-RMI1-RMI2 (TRR) complex was a gift from Drs. Kata Sarlos and Ian Hickson (University of Copenhagen, Denmark). DNA2 was produced as a fusion with a His_6 tag (N terminus) and a FLAG tag (C terminus) in Sf9 cells using the Bac-to-Bac baculovirus expression system (Invitrogen). The transfer vector for bacmid preparation was a gift from Dr. Judith L. Campbell (32). The transfer vectors for nuclease-deficient (D227A) and helicase-deficient (K654R) mutants of DNA2 were generated using the QuikChange site-directed mutagenesis kit (Stratagene). Sf9 cells expressing DNA2 fusion proteins were harvested 52 h after infection (typically a 800-ml culture) and washed with PBS. All subsequent steps were carried out at 4 °C. Pelleted cells were resuspended in lysis buffer (25 mM Tris-HCl (pH 7.5), 2 mM β-mercaptoethanol, 1× complete EDTA-free protease inhibitor (Roche), 1 mM phenylmethylsulfonyl fluoride, 30 μg/ml leupeptin, and 15 mM imidazole) and incubated for 20 min under continuous stirring. Subsequently, glycerol and 5 M NaCl were added slowly to final concentrations of 15% (v/v) and 300 mM, respectively, while mixing the sample. The cell suspension was then incubated for an additional 30 min under continuous stirring. The cell lysate was centrifuged at 55,000 × *g* for 30 min to obtain soluble extract, which was then incubated with 5 ml of nickel-nitrilotriacetic acid-agarose beads (Qiagen) for 1 h batchwise. The resin was washed extensively with lysis buffer containing 10% (v/v) glycerol and 1 M NaCl. The protein was eluted with lysis buffer supplemented with 10% (v/v) glycerol, 100 mM NaCl, and 250 mM imidazole. Fractions containing detectable amounts of protein, as measured by Bradford assay, were pooled, diluted 1:1 with TBS buffer (50 mM Tris-HCl (pH 7.5) and 150 mM NaCl) and incubated batchwise with 1 ml of anti-FLAG M2 affinity resin (Sigma) for 30 min. The resin was then transferred to a gravity flow column and washed with TBS-PI buffer (TBS buffer containing 1 mM β-mercaptoethanol and 5 μg/ml leupeptin). Elution of the protein was achieved by adding TBS-PI buffer supplemented with 200 μg/ml 3× FLAG peptide (Sigma). Fractions containing DNA2 were pooled, diluted with 0.5 volumes of water and 1 volume of AQ buffer (25 mM Tris-HCl (pH 7.5), 100 mM NaCl, 10% (v/v) glycerol, and 5 mM β-mercaptoethanol) and loaded onto a 1-ml HiTrap Q column (GE Healthcare) pre-equilibrated with AQ buffer. The column was washed with AQ buffer and DNA2 was eluted by AQ buffer supplemented with 600 mM NaCl. Fractions containing DNA2 were identified by SDS-PAGE, pooled, and stored at −80 °C. The activity of purified recombinant DNA2 proteins was tested using a Y structure oligonucleotide duplex with single-stranded arms (10). In agreement with previous reports, wild-type DNA2 was found to be capable of degrading both ssDNA arms of this structure (data not shown) (10, 17). In the presence of RPA, the cleavage of the 3′ ssDNA arm by DNA2 was inhibited, and DNA2 degraded preferentially the 5′ ssDNA arm (data not shown) (10, 17). The DNA2-D227A mutant did not contain any nuclease activity, which indicated that the nuclease activity of our wild-type DNA2 preparation was inherent to DNA2 (data not shown).

Nuclease and Helicase Assays—To test the activity of purified DNA2, we used a 31-bp forked duplex with 19-nt ssDNA arms, as described previously (10). The helicase activity of WRN and BLM was tested using a 29-bp forked duplex generated by annealing of the following oligonucleotides: f-9 (5′-ACTATCATTC AGTCATGTAA CCTAGTCAAT CTGCGAGCTC GAATTCACTG GAGTGACCT-3′) and f-10 (5′-GAGGTCACTC CAGTGAATTC GAGCTCGCAG TCAATGTCGA CATACCTAGT ACTTTACTCC-3′). Both DNA substrates were radiolabeled at the end of the 5′ ssDNA arm.

Nuclease and helicase assays were performed in buffer containing 25 mM Tris acetate (pH 7.5), 2 mM magnesium acetate, 1 mM dithiothreitol, 0.1 mg/ml BSA, 10.7 mM phosphocreatine, and 0.02 mg/ml creatine phosphokinase. Reactions (15 μl) contained 1 nM ^{32}P-labeled forked DNA substrate and the indicated concentrations of DNA2 or WRN/BLM. Where indicated, RPA was present at a concentration of 6 nM. Reactions were assembled on ice and started by addition of ATP to a concentration of 1 mM. Reactions were incubated for 30 min at 37 °C. Termination of the reactions was achieved by adding 1/3 volume of stop solution (150 mM EDTA, 2% (w/v) SDS, 30% (v/v) glycerol, and 0.1% (w/v) bromphenol blue) and 1/15 volume of Proteinase K (10 mg/ml), followed by incubation at 37 °C for 15 min. The reaction products were separated by electrophoresis in a 10% Tris borate-EDTA polyacrylamide gel. Gels were dried on Whatman MM3 paper and analyzed by phosphorimaging using a Typhoon 9400 scanner (GE Healthcare). Images were quantified using ImageQuantTL software.

Construction of DNA Substrates for Resection Assays—The DNA substrates used in resection assays were derived from the plasmid pUC19 (2686 bp). The self-complementary oligonucleotide, 5′-AGCT GCTGAGG GCTGAGG GCTGAGG GCTGAGG AGGCCT CCTCAGC CCTCAGC CCTCAGC CCTCAGC-3′, was annealed to form a duplex that was cloned into the HindIII site of pUC19. This destroyed the HindIII site and inserted a single recognition sequence for StuI (AGGCCT) flanked on each side by four recognition sequences for the nickase Nt.BbvCI (CC*TCAGC; the cleavage position is indicated by the asterisk) that are oriented as an inverted repeat with respect to the StuI site. The resulting pOH-S plasmid allowed us to prepare a linear DNA substrate with 3′ overhangs of 26 nucleotides (nt) in length. A blunt-ended substrate was generated by digestion of pOH-S with StuI (New England Biolabs), followed by DNA purification using a Macherey Nagel NucleoSpin® gel and PCR cleanup kit. The substrate with 26-nt 3′ overhangs was generated as follows. After digestion of pOH-S with StuI and its heat inactivation, Nt.BbvCI (New England Biolabs) was added, and the reaction was incubated further for 2 h at 37 °C. Subsequently, the reaction mixture was diluted six times with water and incubated at 85 °C for 15 min. DNA purification was performed as described above. DNA concentration was determined using a NanoDrop ND-1000 spectrophotometer (Witec AG).

DNA End Resection Assays—DNA end resection reactions were carried out in a buffer containing 25 mM Tris acetate (pH 7.5), 2 mM magnesium acetate, 1 mM dithiothreitol, 0.1 mg/ml BSA, 10.7 mM phosphocreatine, 0.02 mg/ml creatine phosphokinase, and 1 mM ATP. Reactions contained 2 nM DNA substrate (molecules), 8 nM DNA2, 350 nM RPA (100% DNA strand coverage, assuming all DNA was single-stranded), and various concentrations of WRN or BLM as indicated. EXO1 was present at a concentration of 20 nM. The reactions were assembled on ice and initiated by the addition of ATP. Reaction mixtures (15 μl) were incubated at 37 °C for 60 min in the case of protein titration experiments. In time course experiments, 15-μl reaction aliquots were withdrawn at defined time points as indicated. Reactions were terminated as described for the helicase assays. The samples were subjected to electrophoresis in a 1% agarose gel run in 1× TAE buffer. Gels were post-stained with SYBR Gold (Invitrogen) and analyzed using MultiImage Light Cabinet (Alpha Innotech). To monitor resection by hybridization of radiolabeled oligonucleotide probes, terminated reactions (21 μl) were divided equally into two tubes. 5′ end-labeled oligonucleotide probes were then added to a final concentration of 5 nM. This mixture was heated in an oven to 75 °C for 5 min and then slowly cooled down to room temperature over 2.5 h. Reaction products were separated by electrophoresis in a 1% agarose gel. Gels were dried on DE81 anion exchange paper (Whatman) and subjected to phosphorimaging analysis using a Typhoon 9400 scanner (GE Healthcare). Images were quantified using ImageQuantTL software. The relative concentration of the resection products generated in WRN-DNA2 or BLM-DNA2 reactions was calculated as a percentage of the product generated in a reaction containing 20 nM EXO1 at the 2-min time point, which led to 100% resection within the region probed with radiolabeled oligonucleotides. Usually, the EXO1 reaction was loaded on each gel in triplicates. The following oligonucleotides were used for the preparation of the hybridization probes: oligo#224, 5′-GGCCGTCGTTTTACAACGTCGT-3′ (it anneals to the 3′-terminated strand; annealing position, 112–133 nt upstream of the StuI cleavage site; the complementary sequence is underlined); oligo#227, 5′-GGCATAGTTAAGCCAGCCCCGA-3′ (it anneals to the 3′-terminated strand; annealing position, 353–374 nt upstream of the StuI cleavage site); and oligo#237, 5′-GGTCGGGGCTGGCTTAACTATG-3′ (it anneals to the 5′-terminated strand; annealing position, 122–133 nt upstream of the StuI cleavage site). Oligonucleotides were 5′ end-labeled using [γ-^{32}P]ATP and T4 polynucleotide kinase (New England Biolabs). The two noncomplementary dG residues at the 5′ end of the oligonucleotides were added to ensure equal labeling efficiency.

Cell Culture and Transfection—U2OS and HEK293 cells were grown in DMEM (Sigma) supplemented with 10% fetal calf serum (Invitrogen) and streptomycin/penicillin (100 units/ml). Plasmid DNA was transfected using standard linear polyethyleneimine method. Lipofectamine RNAiMAX (Invitrogen) was used for siRNA transfection. To generate HEK293 clones stably expressing FLAG-DNA2, cells were cotransfected with pFLAG-CMV2-hDNA2 and pBABE-puro (Addgene) and subjected to puromycin 1 (μg/ml) selection. Puromycin-resistant clones were tested for expression of FLAG-DNA2 by Western blotting.

Immunoprecipitation—HEK293 cells were transfected with the pcDNA3.1-hWRN and/or pFLAG-CMV2-hDNA2 vectors. Cells were harvested to lysis buffer (50 mM Tris-HCl (pH 8.0), 120 mM NaCl, 20 mM NaF, 15 mM sodium pyrophosphate, and

0.5% (v/v) Nonidet P-40) supplemented before use with protease (Complete EDTA-free, Roche) and phosphatase (PhosSTOP, Roche) inhibitors, 2 mM $MgCl_2$ and benzonase (50 units/ml). Cells were sonicated briefly, and lysates were clarified by centrifugation at 16,000 × *g* for 30 min. Cell extracts (1 mg of protein) were subjected to immunoprecipitation using anti-FLAG M2 magnetic beads (10 μl) or Protein A/G Plus UltraLink Resin (10 μl, Thermo Scientific) coated with rabbit polyclonal anti-WRN antibody (10 μg), which was carried out overnight at 4 °C. Immunoprecipitates were washed four times with lysis buffer. Bound proteins were eluted by Laemmli sample buffer and analyzed by SDS-PAGE and Western blotting. To test the interaction between purified WRN and DNA2 proteins, 500 ng of each protein was mixed in 200 μl of NET-N100 buffer (10 mM Tris-HCl (pH 8.0), 1 mM EDTA, 100 mM NaCl, and 0.5% (v/v) Nonidet P-40) and incubated at 4 °C for 4 h. As a control, DNA2 was incubated in the absence of WRN. The protein mixtures were subsequently subjected to immunoprecipitation using anti-WRN antibody (4 μg), which was carried out at 4 °C for 2 h. Immunoprecipitates were washed four times with NET-N100 buffer. Bound proteins were eluted by Laemmli sample buffer and analyzed by SDS-PAGE and Western blotting.

GST Pulldown Assay—GST-tagged fragments of WRN were produced in the *Escherichia coli* BL21-CodonPlus(DE3)-RIL strain (Stratagene) and bound to GSH Sepharose 4B (GE Healthcare) as described previously (24). As a control, beads were coated with GST protein only. The beads were incubated with 500 ng of purified His_6-DNA2-FLAG protein in 400 μl of NET-N100 buffer at 4 °C for 2 h. After extensive washing with NET-N100 buffer, proteins bound to the beads were analyzed by Western blotting. Blots were first stained in Ponceau S solution (0.1% (w/v) Ponceau S and 5% (v/v) acetic acid) to visualize WRN fragments and subsequently probed with anti-FLAG antibody.

Reverse Transcription and Quantitative Real-time PCR—Total RNA was isolated from cells using the RNeasy mini kit (Qiagen). 200 ng of RNA was used for cDNA synthesis using a high-capacity cDNA reverse transcription kit (Applied Biosystems). The target gene expression level was determined by quantitative real-time PCR that was performed on a ABI Prism 7300 (Applied Biosystems) using SYBR Select Master Mix (Applied Biosystems). The following primer pairs were used to determine EXO1 mRNA levels: 5′-ACCTCTAAGG AACAAGGTTC-3′ (forward) and 5′-AGGAGGAAGC TTTTC-AGAATC-3′ (reverse). The housekeeping gene RPLPO, used as a control, was amplified with the following primers: 5′-CCAG-TCTGGA GAAACTGCTG-3′ (forward) and 5′-CAGCAG-CTGG CACCTTATTGG-3′ (reverse). The Pfaffl equation was used for normalization and calculation of relative EXO1 expression levels in comparison with the control gene (33).

SA-GFP Reporter Assay—SA-GFP reporter assays were performed as described previously (34, 35). HEK293/SA-GFP cells were seeded in poly-L-lysine-coated 6-well plates at a density of 0.5 million cells/well. U2OS/SA-GFP cells were seeded in 6-well plates at a density of 0.25 million cells/well. The next day, cells were transfected with appropriate siRNA (40 nM) using Lipofectamine RNAiMAX (Invitrogen). After 24 h, siRNA-transfected cells were transferred into a 12-well plate, with 200,000 cells/well for HEK293/SA-GFP and 100,000 cells/well for U2OS/SA-GFP. 44 h after siRNA transfection, cells were transfected with 0.6 μg of the I-SceI expression vector pCBASce (36) using linear polyethyleneimine and, 6 h later, with appropriate siRNA (20 nM) using the standard calcium phosphate method. 52 h after I-SceI transfection, cells were harvested and subjected to flow cytometry analysis using LSRII (BD Biosciences) and FlowJo software to determine the percentage of GFP-positive cells. The mean values obtained with control siRNA (siLuc) samples were 0.9% for HEK293/SA-GFP cells and 2.0% for U2OS/SA-GFP cells. To test the effect of ectopic expression of WRN on SSA repair efficiency of WRN-depleted HEK293/SA-GFP cells, the mutant form of the pcDNA3.1-hWRN construct harboring silent mutations in the siWRN-targeting region (0.6 μg) was cotransfected with pCBASce (0.6 μg). The plasmid pcDNA3.1 was used as a control vector in these experiments. Cells were subjected to flow cytometry analysis at 52 h after plasmid transfection.

Immunofluorescence Assays—U2OS cells transfected with the indicated siRNAs were cultured on glass coverslips. 48 h after siRNA transfection, cells were treated with 1 μM camptothecin (CPT) for 1 h. After pre-extraction for 5 min on ice in 25 mM HEPES (pH 7.4) buffer containing 0.5% (v/v) Triton X-100, 50 mM NaCl, 1 mM EDTA, 3 mM $MgCl_2$ and 0.3 M sucrose, cells were fixed with 4% (v/v) formaldehyde for 15 min at room temperature. Subsequently, cells were permeabilized by soaking in 0.2% (v/v) Triton X-100 for 5 min at room temperature. After blocking in PBS containing 10 mg/ml BSA for 30 min at room temperature, fixed cells were incubated for 2 h at room temperature with the indicated primary antibodies. The slides were washed with PBS and incubated for 1 h at room temperature with secondary antibodies diluted in blocking solution (Alexa Fluor 568-conjugated goat anti-rabbit IgG and Alexa Fluor 488-conjugated goat anti-mouse IgG (Invitrogen)). After washing with PBS, coverslips were mounted using Vectashield containing DAPI (Vector Laboratories). Automated image acquisition was performed using an Olympus IX70 microscope equipped with the Scan^R imaging platform. A ×40/1.3 numerical aperture objective was used. 10 z stacks at a spacing of 0.3 μm were taken, and 100 images were acquired for each sample. Analysis was performed using Scan^R analysis software. Nuclei were identified on the basis of the DAPI signal, and RPA foci were identified on the basis of edge-based subobject counts. At least 1000 cells were analyzed for each condition.

RESULTS

DNA2 Can Mediate DNA End Resection in Conjunction with WRN Helicase—To test whether the human WRN helicase can mediate resection of broken DNA ends in concert with DNA2, we purified these proteins to homogeneity and analyzed their activities *in vitro* (Fig. 1*A*). WRN and BLM unwind DNA in the 3′-5′ direction and require a 3′ ssDNA tail for loading onto the DNA substrate (37, 38). Therefore, we generated a derivative of the pUC19 plasmid in which a StuI site was flanked on each side by four recognition sites for the nicking endonuclease Nt. BbvCI. Cleavage of this pUC19 derivative with StuI and Nt.BbvCI resulted in a 2.7-kb-long linear DNA molecule ending with 3′

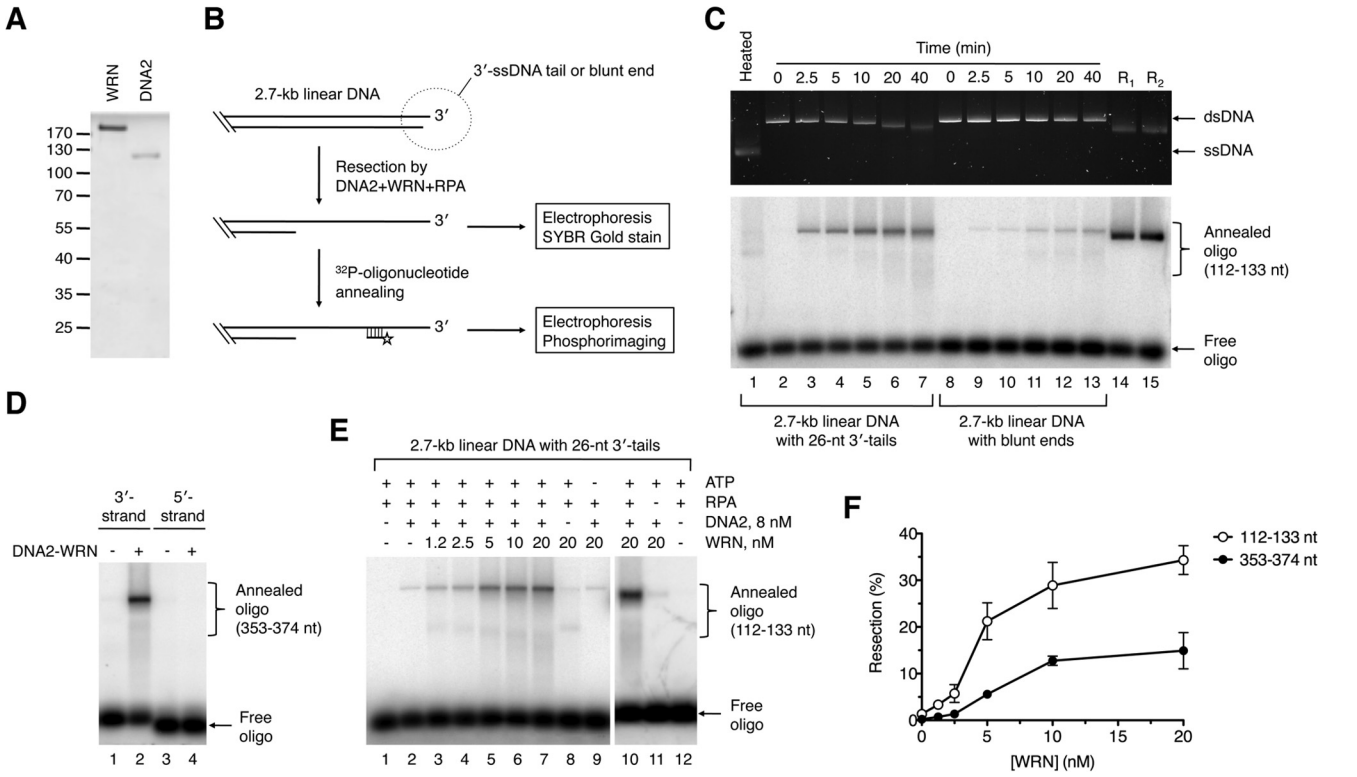

FIGURE 1. **DNA end resection by DNA2 and WRN.** *A*, SDS-PAGE analysis of purified WRN (0.7 μg) and DNA2 (0.4 μg) proteins. Gel was stained with Coomassie Brilliant Blue R-250. The molecular weights of protein standards are indicated on the *left*. *B*, schematic of the DNA end resection assay. The resection products were either left untreated or hybridized with synthetic ^{32}P-labeled oligonucleotides complementary to the 3′-terminated strand. DNA species were separated by electrophoresis in a 1% agarose gel and visualized by SYBR gold staining and phosphorimaging, respectively. Probes complementary to the regions spanning nt positions 112–133 and 353–374 (relative to the 3′ end) were used in this study. Only a part of the DNA substrate is shown. *C*, time course of resection of 3′-tailed (26 nt) and blunt-ended DNA substrates by DNA2 and WRN. Reactions were carried out at 37 °C and contained 2 nM DNA, 350 nM RPA, 10 nM WRN, and 8 nM DNA2. Reaction products at the indicated time points were analyzed as outlined in *B*. The 112- to 133-nt probe was used in this analysis. *Lane 1*, heat-denatured substrate; *lane 14*, 3′-tailed substrate incubated with 20 nM EXO1 and 350 nM RPA for 2 min (R1); *lane 15*, blunt-ended substrate incubated with 20 nM EXO1 and 350 nM RPA for 2 min (R2). *D*, directionality of DNA end resection by WRN-DNA2. Reactions were carried out at 37 °C for 60 min and contained 2 nM 3′-tailed DNA substrate, 350 nM RPA, 8 nM DNA2, and 10 nM WRN. Resection products were annealed with radiolabeled oligonucleotide probes complementary to either 3′-terminated (position 353–374 nt relative to the 3′ end) or 5′-terminated (position 353–374 nt relative to 3′ end) strand and analyzed as in *C*. *E*, 5′ end resection of 3′-tailed DNA substrate by WRN-DNA2 is dependent on WRN concentration and the presence of ATP and RPA. Reactions were carried out at 37 °C for 60 min and contained, as indicated, 2 nM DNA, 350 nM RPA, 1 mM ATP, 8 nM DNA2, and different WRN concentrations. Resection products were detected using the 112–133-nt probe. *F*, dependence of WRN-DNA2-catalyzed resection of 3′-tailed substrate on WRN concentration. Resection at the positions of 112–133 nt and 353–374 nt from the 3′ end of the DNA substrate was monitored. Reactions were carried out as in *E*. Relative concentration of the resection product generated by WRN-DNA2 at each WRN concentration was calculated as a percentage of the product generated by 20 nM EXO1 after 2 min. Data are mean ± S.D. ($n = 3$).

overhangs of 26 nt in length, whereas its cleavage by StuI alone gave rise to a linear DNA molecule with blunt ends. Processing of the DNA substrates was monitored by agarose gel electrophoresis followed by SYBR gold staining (Fig. 1*B*). In addition, ^{32}P-labeled synthetic oligonucleotides complementary to the 3′-terminated strand were used as hybridization probes to detect ssDNA generated by resection at specific positions (Fig. 1*B*) (10). We found that WRN, together with DNA2 and RPA, could catalyze efficient 5′ end resection on the 3′-tailed substrate but not the blunt-ended substrate (Fig. 1*C*). As expected, no reaction products were detected with an oligonucleotide probe complementary to the 5′-terminated strand, indicating that the observed DNA resection activity is limited to the 5′ strand (Fig. 1*D*). Of note, the end product of the resection reaction on the 3′-tailed DNA substrate appeared as a discrete band on SYBR gold-stained gel that was clearly shifted with respect to the unprocessed dsDNA substrate, indicating extensive resection (Fig. 1*C*, *top panel*, compare *lanes 2* and *7*). In contrast, no gradual shift in the electrophoretic mobility of the resection product was apparent after annealing of the radioactive probes. This is most likely due to the fact that DNA2 nuclease generates short oligonucleotides that can reanneal to the resected DNA along with the radioactive probe, leading to a DNA molecule with an electrophoretic mobility similar to that of the DNA substrate. Together, these results clearly demonstrate that DNA2, in conjunction with WRN and RPA, can catalyze extensive 5′ end resection, providing that the DNA substrate contains a 3′ ssDNA overhang.

To further characterize the DNA end resection reaction mediated by WRN-DNA2, reactions with the 3′-tailed substrate were carried out at various WRN concentrations, whereas DNA2 was kept at a concentration of 8 nM. We observed that the amount of resection product increased gradually with WRN concentration, reaching a plateau at about 10 nM (Fig. 1*E*, *lanes 2–7*, and Fig. 1*F*). Quantitative analysis of gel images revealed that about 35% of the DNA substrate was resected to the position of 133 nt from the 3′ end and that about 15% of the DNA substrate was resected to the position of 374 nt

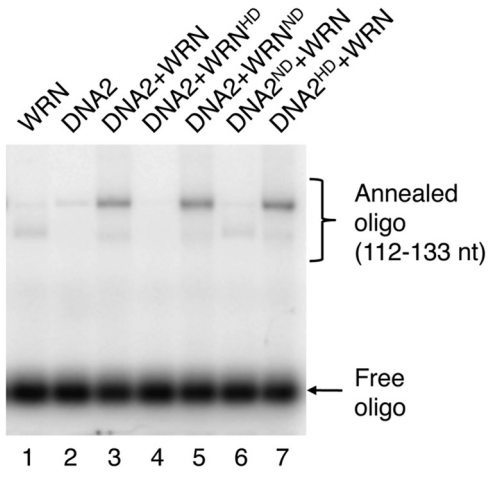

FIGURE 2. **5′ end resection of 3′-tailed DNA substrate by WRN-DNA2 depends on the helicase activity of WRN and the nuclease activity of DNA2.** Reactions were carried out at 37 °C for 60 min and contained 2 nM DNA, 350 nM RPA, 1 mM ATP, 8 nM DNA2, and 10 nM WRN. Resection products were detected using the 112–133 nt probe. *WRN^{HD}*, helicase-deficient mutant of WRN (K567M); *WRNND*, nuclease-deficient mutant of WRN (E84A); *DNA2^{HD}*, helicase-deficient mutant of DNA2 (K654R); *DNA2ND*, nuclease-deficient mutant of DNA2 (D277A).

within 1 h of incubation (Fig. 1*F*). Interestingly, a small amount of resected product (1–2%) could also be detected in the absence of WRN, suggesting that DNA2 itself could slowly resect dsDNA ends, likely following RPA-mediated stabilization of ssDNA ends generated by thermal fraying (Fig. 1*E*, *lane 2*). In the absence of DNA2, WRN was only capable of DNA unwinding, as evident from the appearance of a fast-migrating band (Fig. 1*E*, *lane 8*). The resection process catalyzed by WRN and DNA2 was found to be dependent on the presence of ATP and RPA, as expected for a helicase-driven reaction (Fig. 1*E*, compare *lanes 9–12*).

WRN acts not only as a 3′-5′ DNA helicase, but it also possesses a dsDNA-dependent 3′-5′ exonuclease activity residing in a separate domain located in the N-terminal portion of the protein (39, 40). DNA2 functions as a 5′-3′ helicase and a ssDNA-specific endonuclease (32, 41). To define the functions of the enzymatic activities of WRN and DNA2 in DNA end resection, we carried out a set of resection reactions with the 3′-tailed pUC19 substrate where either WRN or DNA2 were substituted with catalytically inactive mutants. We found that the helicase-deficient mutant of WRN (K567M) failed to stimulate DNA resection by DNA2, whereas the nuclease-deficient mutant of WRN (E84A) behaved similarly as the wild-type WRN in this reaction (Fig. 2, *lanes 2–4*). Substitution of DNA2 with its nuclease-deficient mutant (D277A) completely abolished resection and stimulated unwinding of the plasmid substrate (Fig. 2, *lane 6*). In contrast, the helicase-deficient mutant of DNA2 (K654E) could resect the DNA substrate to the same degree as the wild-type protein (Fig. 2, compare *lanes 3* and *7*). These results indicate that DNA end resection mediated by DNA2, WRN, and RPA is dependent on the helicase activity of WRN and the endonuclease activity of DNA2.

DNA2 and WRN Interact Physically—Yeast Dna2 has been shown to interact physically with Sgs1 (10). Likewise, BLM forms a complex with human DNA2 (17). Therefore, we investigated whether human DNA2 interacts physically with WRN. To this end, HEK293 cells were transfected with plasmids expressing WRN and FLAG-tagged DNA2, respectively, and complex formation between these proteins was tested by immunoprecipitation using beads conjugated with anti-FLAG M2 antibody. We found that WRN coimmunoprecipitated with FLAG-DNA2, indicating that these proteins form a complex *in vivo* (Fig. 3*A*, *lane 3*). This interaction was specific because anti-FLAG beads did not immunoprecipitate WRN from an extract lacking FLAG-DNA2 (Fig. 3*A*, *lane 1*). To further investigate complex formation between WRN and DNA2, we generated a stable HEK293 cell line expressing FLAG-DNA2. By immunoprecipitation using anti-FLAG M2 beads or anti-WRN antibody, we found that FLAG-DNA2 formed a complex with endogenous WRN in these cells (Fig. 3, *B* and *C*). Western blot analysis indicated that the level of FLAG-DNA2 in these cells was only slightly higher than that of endogenous DNA2, suggesting that WRN and DNA2 form a complex under physiological conditions (Fig. 3*B*, *top panel*). Interaction between FLAG-DNA2 and endogenous BLM was also detected as expected (Fig. 3*B*) (17). The cellular concentration of these protein complexes was not altered when cells were subjected to treatment with CPT, which causes breakage of DNA replication forks (Fig. 3*B*, *lanes 2–5*) (42). This suggests that the interaction of DNA2 with WRN and BLM in the cell is not dependent on DNA damage.

To test whether WRN and DNA2 interact directly, purified proteins were mixed and incubated at 4 °C for 4 h. Complex formation between WRN and DNA2 was tested by immunoprecipitation using anti-WRN antibody. We found that DNA2 coimmunoprecipitated with WRN. DNA2 was not present in the immunoprecipitated material whether WRN was omitted, confirming a direct protein-protein interaction (Fig. 3*D*). To map the interaction site of DNA2 on WRN, we tested binding of purified His_6-DNA2-FLAG protein to various WRN fragments covering the entire WRN polypeptide (Fig. 3*E*). The WRN fragments were produced in *E. coli* as fusions with a GST tag and isolated on GSH-Sepharose beads. Using a GST pulldown assay, we found that DNA2 bound specifically to a WRN fragment including the core helicase domain (helicase/Zn^{2+}-binding domains) and the winged helix domain (Fig. 3*F*, compare *lanes 1* and *4*) a binding site of a number of other proteins shown to interact with WRN (43, 44). DNA2 was also bound to a fragment containing only the helicase core or to the C-terminal portion of WRN starting at the beginning of the winged helix domain (Fig. 3*F*, compare *lanes 1*, *3*, *4*, and *5*). In contrast, DNA2 did not bind the N-terminal portion of WRN containing the exonuclease domain (Fig. 3*F*, *lane 2*). Collectively, these results suggest that there are at least two DNA2-interaction sites on WRN: one located in the central helicase domain and the other in the C-terminal region of WRN.

WRN-DNA2 Resects DNA Ends More Efficiently Than BLM-DNA2—Next, we set out to compare WRN and BLM with respect to their abilities to resect DNA ends in concert with DNA2 and RPA *in vitro*. Using a Y structure oligonucleotide duplex (29 bp) with single-stranded arms (30 nt each), we found that our preparations of WRN and BLM exhibited similar levels of specific helicase activity (Fig. 4*A*). For resection reactions, we used the 3′-tailed DNA substrate that was readily processed by

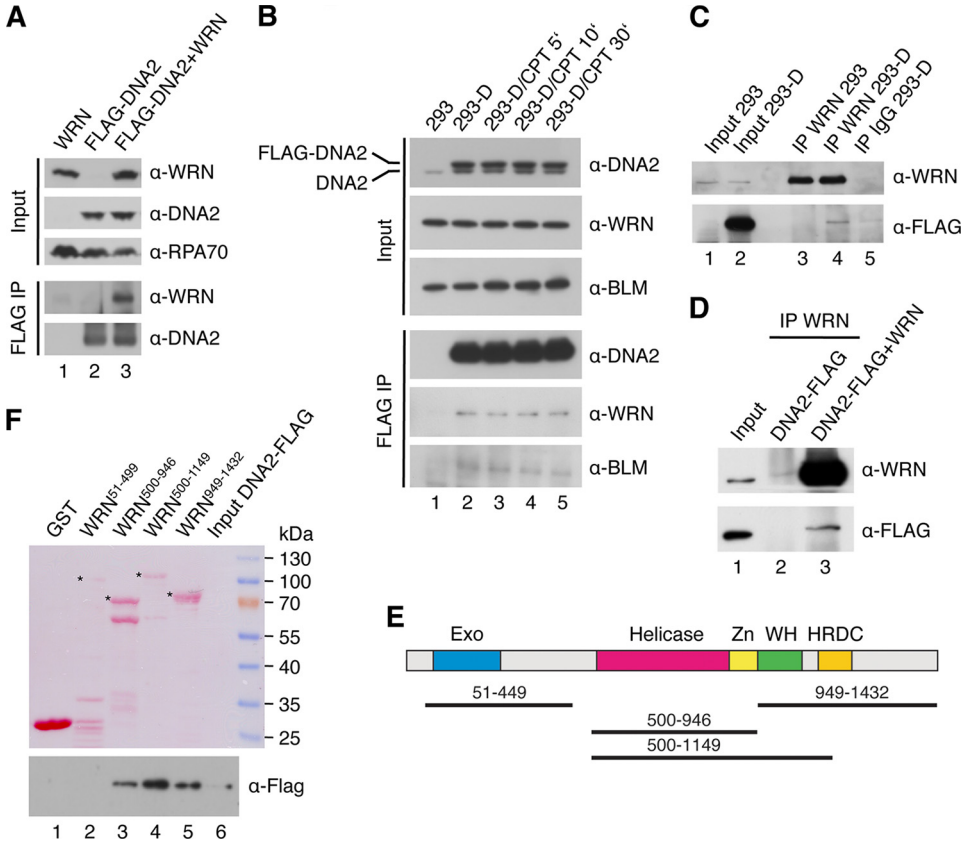

FIGURE 3. **Physical interaction between DNA2 and WRN *in vitro* and *in vivo*.** *A*, coimmunoprecipitation of WRN with DNA2 from human cells. HEK293 cells were transfected with vectors expressing FLAG-DNA2 and WRN as indicated. Cell extracts were immunoprecipitated (*IP*) with anti-FLAG antibody as described under "Experimental Procedures." Blots were probed with the indicated antibodies. 5% of input material was loaded. *B*, effect of DNA damage on the formation of DNA2-WRN and DNA2-BLM complexes in human cells. HEK293 cells stably transfected with the FLAG-DNA2 construct (*HEK293-D*) were treated with 1 μM CPT. At the indicated time points, complex formation between FLAG-DNA2 and endogenous WRN and BLM, respectively, was tested by immunoprecipitation using anti-FLAG antibody. *C*, coimmunoprecipitation of DNA2 with WRN from human cells. Extracts from HEK293-D cells were subjected to immunoprecipitation with anti-WRN antibody or control IgG. The immunoprecipitates were tested for the presence of FLAG-DNA2 and WRN by Western blotting. As a control, a WRN immunoprecipitate from HEK293 cells was also analyzed (*lane 3*). *D*, coimmunoprecipitation of DNA2 with WRN from a mixture of purified proteins. DNA2 (500 ng) was incubated with or without WRN (500 ng) at 4 °C for 4 h. The mixtures were subjected to immunoprecipitation with anti-WRN antibody. *E*, domain organization of WRN. *Exo*, exonuclease domain; *Zn*, zinc-binding domain; *WH*, winged-helix domain; *HRDC*, helicase and RNaseD C-terminal domain. *Black lines* indicate WRN fragments used for mapping the DNA2-interaction site on WRN. *F*, GST pulldown assay. Glutathione beads coated with the indicated GST-tagged fragments of WRN were incubated with purified His_6-DNA2-FLAG protein at 4 °C for 2 h, and bound proteins were analyzed by Western blotting as described under "Experimental Procedures." 1% of input was loaded in *B* and *C*, whereas 10% of input was loaded in *D* and *F*.

WRN-DNA2 in the presence of RPA (Fig. 1*C*). The extent of DNA resection at various reaction time points was monitored by annealing of radiolabeled oligonucleotide probes. These experiments clearly showed that WRN-DNA2 resected the DNA substrate at a much higher rate compared with BLM-DNA2 (Fig. 4, *B* and *C*). Notably, WRN-DNA2-catalyzed resection to the position of 374 nt away from the 3′ end was faster than BLM-DNA2-catalyzed resection to the position of 133 nt (Fig. 4, *B* and *C*). We also compared the activities of WRN-DNA2 and BLM-DNA2 on blunt-ended DNA substrate in the presence of RPA. We found that this DNA substrate was largely refractory not only to processing by WRN-DNA2 but also to processing by BLM-DNA2 (Fig. 4*D*, compare *lanes 4* and *5* to *lanes 10* and *11*). Taken together, we show that WRN-DNA2 resects DNA ends more efficiently than BLM-DNA2 *in vitro*.

Dissection of Pathways Involved in DNA End Resection in Human Cells—To assess whether WRN is involved in DNA end resection *in vivo*, we investigated the effect of its depletion on the efficiency of SSA-mediated repair of endonuclease-induced DSBs in cells that were either proficient or deficient for EXO1 and DNA2, respectively. For this epistasis analysis, we initially used the human embryonic kidney cell line HEK293 stably transfected with the SA-GFP reporter cassette consisting of two truncated *GFP* gene alleles (*5′GFP* and *Sce3′GFP*) that form a direct sequence repeat (280 bp) separated by a region of about 2.4 kb (Fig. 5*A*) (34, 45). SSA-mediated recombination between these homologous sequences triggered by a DSB generated in the distal GFP allele by the I-SceI endonuclease results in the formation of a functional *GFP* gene (Fig. 5*A*). This requires extensive DNA end resection to expose the complementary ssDNA regions for annealing. The proteins of interest were depleted from HEK293/SA-GFP cells by RNA interference. Cells were subsequently transfected with an I-SceI expression vector to create a DSB in the reporter cassette, and the percentage of GFP positive cells arising upon SSA-mediated repair was determined by flow cytometry 2 days after plasmid transfection. We found that cells depleted of either EXO1, WRN, or DNA2 exhibited a marked reduction in the frequency of SSA repair events (55, 65, and 75%, respectively) compared with mock-depleted cells (Fig. 5, *B* and *C*). In contrast, knockdown of

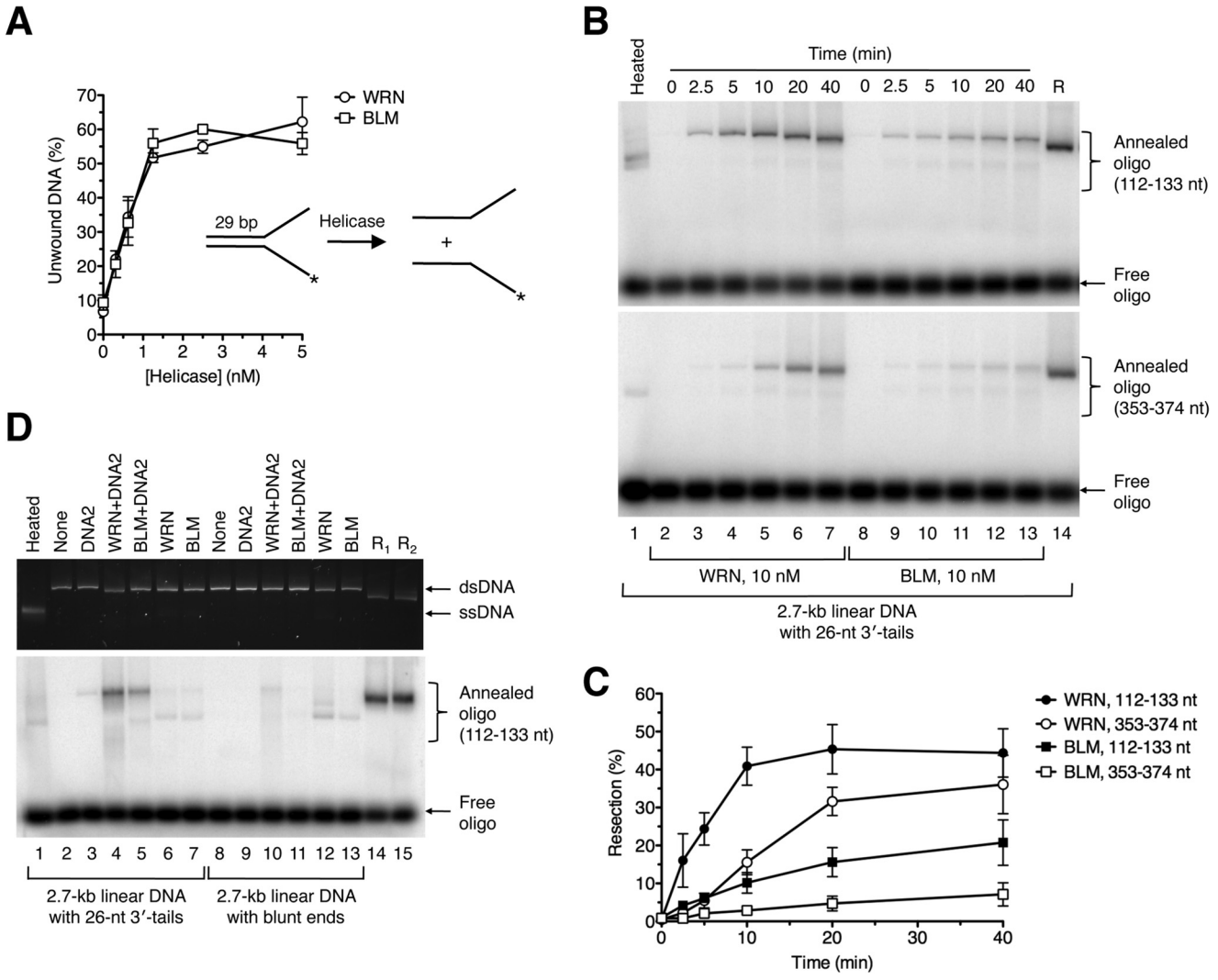

FIGURE 4. **Comparison of DNA end resection activities of WRN-DNA2 and BLM-DNA2.** *A*, comparison of helicase activities of WRN and BLM. Reactions contained 1 nM ^{32}P-labeled forked DNA duplex (*inset*) and different concentrations of WRN or BLM. Reactions were incubated at 37 °C for 30 min, and reaction products were quantified as described under "Experimental Procedures." Data are mean ± S.D. ($n = 3$). *B*, time course of resection of 3′-tailed DNA substrate catalyzed by WRN-DNA2 and BLM-DNA2, respectively. Reactions contained 2 nM DNA, 350 nM RPA, 8 nM DNA2, and 10 nM WRN/BLM. Reaction aliquots withdrawn at the indicated time points were subjected to electrophoresis on a 1% agarose gel after hybridization of radiolabeled probes complementary to 3′-terminated strand at the indicated positions. Radiolabeled DNA species were visualized by phosphorimaging. *C*, quantification of the reactions in *B*. Relative concentration of resection products generated at each time point was calculated as a percentage of the product generated by 20 nM EXO1 after 2 min. Data are mean ± S.D. ($n = 3$). *D*, processing of 3′-tailed (26 nt) and blunt-ended DNA substrates in reactions with indicated composition. Reactions were carried out at 37 °C for 60 min and contained 2 nM DNA, 350 nM RPA, and, where indicated, 8 nM DNA2, 20 nM WRN, and 20 nM BLM. Reaction products were analyzed as in Fig. 1*C*. *Lane 1*, heat-denatured substrate; *lane 14*, 3′-tailed substrate incubated with 20 nM EXO1 for 2 min (R1); *lane 15*, blunt-ended substrate incubated with 20 nM EXO1 for 2 min (R2).

BLM was found to be associated with a significant increase in SSA repair efficiency (140%) compared with control cells (Fig. 5, *B* and *C*). Of note, the SSA repair defect of WRN-depleted cells could be rescued by ectopic expression of the siRNA-resistant form of WRN, excluding an off-target effect of the WRN siRNA used in this study (Fig. 5*D*). Combined depletion of EXO1 and WRN or EXO1 and DNA2 further decreased the repair efficiency compared with the respective single depletions, whereas codepletion of DNA2 and WRN did not (Fig. 5, *B* and *C*). In addition, combined depletion of EXO1 and BLM had nearly the same effect on the SSA repair efficiency as EXO1 depletion (Fig. 5, *B* and *C*). Therefore, these findings suggest that HEK293 cells have at least two pathways for long-range resection of DSB ends: one mediated by EXO1 and the other dependent upon DNA2 and WRN.

To substantiate these findings, we performed a similar set of experiments using U2OS/SA-GFP cells (35). This analysis indicated that combined depletion of EXO1 and DNA2 almost completely abolished (reduced by 91%) SSA-mediated DSB repair in U2OS/SA-GFP cells, as did depletion of MRE11 (by 89%) or CtIP (by 82%), suggesting that long-range DNA end resection in U2OS cells is largely dependent on EXO1 and DNA2 (Fig. 5, *E*–*G*). However, in contrast to the results obtained with HEK293/SA-GFP cells, we observed a significant reduction in SSA repair efficiency not only after depletion of WRN (by 57%) but also after depletion of BLM (by 59%) (Fig. 5, *E* and *F*). Codepletion of BLM and WRN further decreased the repair efficiency to a level comparable with that in DNA2-depleted (by 73%) cells (Fig. 5, *E* and *F*). Moreover, combined depletion of DNA2 with either BLM or WRN had nearly the

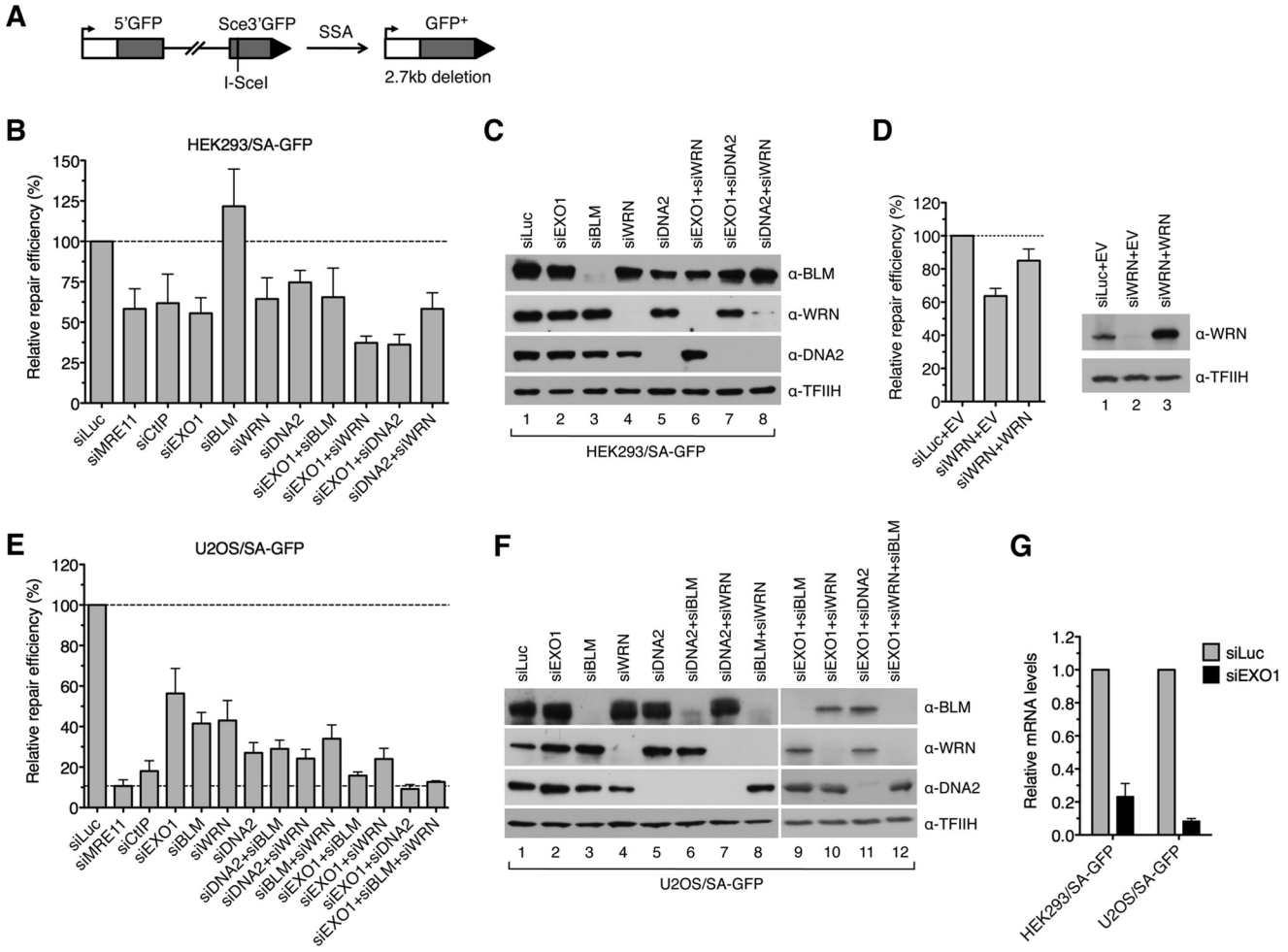

FIGURE 5. **WRN and BLM interact epistatically with DNA2 to promote DSB repair by SSA in human cells.** *A*, schematic of the SA-GFP reporter cassette. SSA-mediated repair of a DSB at the I-SceI-cutting site results in the formation of a functional GFP allele. *B*, efficiency of SSA-mediated repair of I-SceI-induced DSB in HEK293/SA-GFP cells treated with the indicated siRNAs. Cells were transfected with the appropriate siRNAs (40 nM) 2 days prior to transfection of the I-SceI-expressing plasmid. The percentage of GFP-positive cells in each sample was measured by flow cytometry 2 days after I-SceI plasmid transfection and taken as a measure of DSB repair efficiency. The plotted values represent the relative repair efficiency calculated as a percentage of repair efficiency measured in cells transfected with control siRNA (*siLuc*, 100%). Data are mean ± S.D. ($n \geq 3$). *C*, Western blot analysis of extracts from HEK293/SA-GFP cells transfected with indicated siRNAs under the same conditions as for SA-GFP reporter assays. Blots were probed with the indicated antibodies. *D*, rescue of the SSA-repair defect of WRN-depleted HEK293/SA-GFP cells by expression of the siRNA-resistant variant of WRN. An SA-GFP reporter assay was performed as in *B*. The WRN plasmid (*WRN*) or empty vector (*EV*) were cotransfected with the I-SceI plasmid. *E*, efficiency of SSA-mediated repair of I-SceI-induced DSB in U2OS/SA-GFP cells treated with the indicated siRNAs. Experiments were performed as in *B*. *F*, Western blot analysis of extracts from U2OS/SA-GFP cells transfected with the indicated siRNAs. Blots were probed with the indicated antibodies. *G*, quantitative real-time PCR showing that EXO1 mRNA levels are down-regulated by specific siRNA. Data are mean ± S.D. ($n = 3$).

same inhibitory effect on SSA repair as DNA2 depletion (Fig. 5, *E* and *F*). On the contrary, codepletion of EXO1 with either WRN or BLM caused a much higher reduction in repair efficiency than depletion of DNA2 alone, and triple depletion of EXO1, BLM, and WRN brought repair efficiency down to the level measured in cells depleted of EXO1 and DNA2 (Fig. 5, *E* and *F*). Collectively, these data suggest that, in U2OS cells, both WRN and BLM assist DNA2 to mediate long-range resection of broken DNA ends.

To bolster our conclusion that DNA2, WRN, and BLM have an epistatic relationship in DSB end resection, we extended our analysis to measurement of RPA focus formation in U2OS cells treated with CPT. As expected, 1 h after addition of CPT, RPA formed numerous foci in γ-H2AX-positive cells, which were dependent on the presence of CtIP (Fig. 6). Depletion of DNA2 resulted in a marked reduction in the number of RPA foci per cell compared with mock-depleted cells (Fig. 6). Cells depleted of BLM or WRN displayed a mild decrease in RPA focus frequency compared with mock-depleted cells (Fig. 6). In contrast, combined depletion of BLM and WRN caused approximately the same reduction in RPA focus frequency as depletion of DNA2 alone. Moreover, cells depleted of DNA2 and BLM or DNA2 and WRN displayed an RPA foci frequency comparable with that of DNA2-depleted cells (Fig. 6). These data further support the conclusion that DNA2, WRN, and BLM operate in the same DNA end resection pathway.

Role of the BLM-TOPOIIIα-RMI1-RMI2 Complex in DNA End Resection—In human cells, BLM exists in a complex with TOPOIIIα, RMI1, and RMI2, which is known to catalyze double Holliday junction dissolution during HR (46–49). Studies in yeast have shown that Top3α and Rmi1 are also required for DNA-end resection *in vivo* and stimulate DNA end resection by

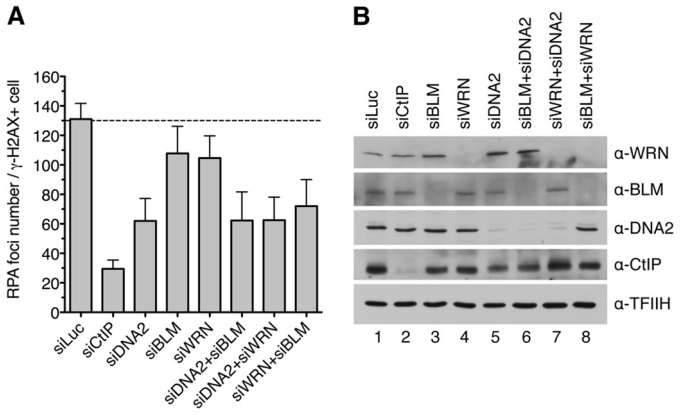

FIGURE 6. **DNA2, WRN, and BLM act in the same pathway of DSB end resection.** *A*, frequency of camptothecin-induced RPA foci in nuclei of U2OS cells depleted of the indicated proteins. Cells were transfected with appropriate siRNAs and, 48 h later, treated with 1 μM camptothecin for 1 h. Cells were then detergent-extracted and fixed with formaldehyde. RPA and γ-H2AX (a marker of DNA damage) were visualized by indirect immunofluorescence. DAPI was used to stain nuclei. The average number of RPA foci per γ-H2AX-positive cell was determined for each sample using an Olympus Scan^R screening station. The data points are mean ± S.D. ($n = 3$). *B*, Western blot analysis of extracts from U2OS cells transfected with indicated siRNAs. Blots were probed with the antibodies indicated on the *right*.

Sgs1-Dna2 *in vitro* by promoting the helicase activity of Sgs1 (9, 10, 14). Our study revealed that BLM-DNA2 resects DNA ends less efficiently than WRN-DNA2 *in vitro*, whereas *in vivo*, at least in U2OS cells, BLM and WRN appeared to contribute equally to promote DNA end resection (Fig. 5*E*). Therefore, we investigated whether BLM requires TOPOIIIα, RMI1, and RMI2 (TRR) to efficiently support DNA end resection by DNA2. To this end, we first investigated the effect of a purified TRR complex on DNA end resection by BLM-DNA2 *in vitro* (Fig. 7*A*). We found that TRR enhanced resection of the 3′-tailed pUC19 substrate by BLM-DNA2 (Fig. 7, *B* and *C*, *lanes 3–6*). On the contrary, the TRR complex had no effect on DNA end resection by WRN-DNA2 (data not shown). Moreover, it could not enhance DNA end resection by DNA2 in the absence of BLM (Fig. 7, *B* and *C*, compare *lanes 2* and *7*).

Next we tested the effect of depletion of RMI1 on the efficiency of SSA-mediated repair of I-SceI-induced DSBs in U2OS/SA-GFP cells. We found that RMI1 depletion reduced the repair efficiency to the level displayed by BLM- or DNA2-depleted cells (Fig. 7, *D* and *E*). Importantly, codepletion of RMI1 with BLM or DNA2 did not further reduce the repair efficiency compared with single depletions of these proteins, suggesting that RMI1, BLM, and DNA2 act in the same pathway (Fig. 7, *D* and *E*). Collectively, these results suggest that, in human cells, BLM promotes long-range DNA end resection as part of the BTRR complex.

DISCUSSION

Here we present evidence suggesting that human DNA2 acts in conjunction with either WRN or BLM to mediate long-range resection of broken DNA ends *in vivo*. Moreover, we show that WRN helicase can cooperate with DNA2 and RPA to catalyze resection of DNA ends *in vitro*, generating long 3′-terminated ssDNA tails. Our study also reveals that both WRN-DNA2 and BLM-DNA2 require a 3′ ssDNA overhang to efficiently initiate DNA end resection *in vitro*, which is in agreement with the "two-step" resection model in which the initial 5′ end trimming is carried out by the MRE11-RAD50-NBS1/Xrs2 complex in conjunction with CtIP/Sae2 (8, 9, 11, 19). In addition, we present evidence that BLM and DNA2 interact epistatically with RMI1 to mediate DNA end resection *in vivo*. Moreover, we show that the TRR complex stimulates DNA end resection by BLM-DNA2 *in vitro*. These data suggest that, in cells, BLM mediates DNA end resection as part of the BTRR complex.

Our discovery of the involvement of WRN in DNA end resection is consistent with the findings that WRN interacts physically with the MRN complex and accumulates at sites of DSBs in human cells (50, 51). Moreover, it has been demonstrated that WRN depletion leads to a marked reduction in the frequency of RPA and BrdU/ssDNA foci formed in response to ionizing radiation, indicative of a resection defect (52). A similar phenotype has been observed in DNA2-depleted cells (18). Although the previous studies did not address the relationship between WRN and DNA2, they demonstrated that these enzymes act synergistically with EXO1 to promote DNA end resection in human cells (18, 52). A role for WRN as a critical DNA end resection factor is also consistent with the cellular phenotype of Werner syndrome, a severe premature aging disorder caused by inherited mutations in the *WRN* gene (53). Cells derived from Werner syndrome patients are characterized by non-homologous chromosome exchanges, termed variegated translocation mosaicism, and large chromosomal deletions that may result from aberrant DSB repair by NHEJ as a consequence of a defect in DNA end resection (54–56). Indeed, it is becoming clear that NHEJ accounts for most chromosomal translocations in humans (57). Moreover, a role for DNA end resection as the critical determinant of DSB repair pathway choice is well established (58). Accumulating evidence suggests that defects in homology-directed repair pathways, which are dependent on DNA end resection, result in overuse of NHEJ for repair, leading to accumulation of chromosomal rearrangements (57). However, it should be noted that WRN is also known to promote DSB repair by the classical Ku-dependent NHEJ (C-NHEJ) pathway to suppress microhomology-mediated end joining (59, 60). This alternative end joining pathway is capable of producing chromosomal translocations, particularly when Ku-dependent NHEJ is deficient (57). Moreover, WRN has been shown to be involved in the resolution HR intermediates (61, 62). Therefore, it seems that the genomic instability in Werner syndrome is a consequence of multiple defects in DNA repair pathways.

Our finding that the TRR complex stimulates DNA end resection by BLM-DNA2 *in vitro* is consistent with previous reports showing that the association of BLM with TOPOIIIα and RMI1 enhances its DNA unwinding activity, which drives the BLM-DNA2-catalyzed resection reaction (17, 63). Similarly, RMI1 and RMI2 have been shown to enhance the efficiency of the BLM-TOPOIIIα-mediated double Holliday junction dissolution reaction (48, 49, 64). It has also been shown that RMI1 forms a complex with RPA and that this interaction is essential for the stimulatory effect of RPA on double Holliday junction dissolution by the BTRR complex (65). Therefore, it is possible that a physical interaction between RMI1 and RPA

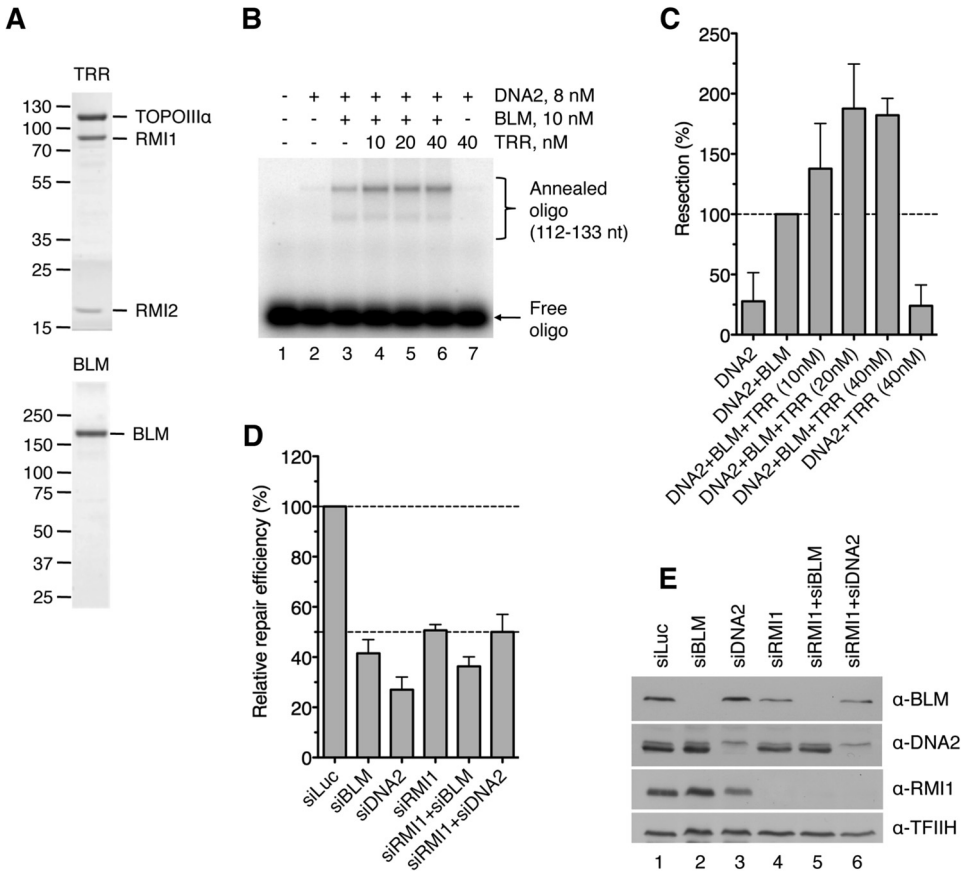

FIGURE 7. **Involvement of TOPOIIIα, RMI1, and RMI2 in DNA end resection.** *A*, SDS-PAGE analysis of purified TRR complex (1.5 μg) and BLM (0.5 μg). The gel was stained with Coomassie Brilliant Blue R-250. The molecular weights of protein standards are indicated on the *left*. *B*, stimulation of BLM-DNA2-catalyzed DNA end resection by the TRR complex. Reactions contained 2 nM 3′-tailed pUC19 substrate, 8 nM DNA2, 10 nM BLM, 350 nM RPA, and varying concentrations of TRR. BLM and TRR were preincubated for 5 min on ice prior to addition to the reaction. Reaction products were analyzed as in Fig. 1*C* using the 112–133-nt probe. *C*, quantification of the product of reactions in *B*. Data are mean ± S.D. ($n = 3$). The data are normalized to the amount of product in the reaction containing only BLM and DNA2 (100%). *D*, RMI1 acts epistatically with BLM and DNA2 to promote DSB repair by SSA in human cells. Efficiency of SSA-mediated repair of I-SceI-induced DSB in U2OS/SA-GFP cells transfected with indicated siRNAs was measured as in Fig. 5*E*. *E*, Western blot analysis of extracts from U2OS/SA-GFP cells transfected with indicated siRNAs under the same conditions as for SA-GFP reporter assays. Blots were probed with the indicated antibodies.

loaded on the 3′-terminated DNA strand during DNA2-catalyzed resection might enhance the DNA unwinding processivity of the BTRR complex and, hence, increase the efficiency of the resection reaction. However, it should be noted that the stimulatory effect of the TRR complex on DNA end resection by BLM-DNA2 *in vitro* was rather modest under our experimental conditions. On the contrary, RMI1 depletion in U2OS/SA-GFP cells reduced the efficiency of SSA-mediated DSB repair to levels displayed by BLM- or DNA2-deficient cells, suggesting that BLM requires RMI1 to promote DNA end resection *in vivo*. Of note, it has been shown that silencing of RMI1 or RMI2 expression by RNA interference destabilizes both BLM and TOPOIIIα (47, 49). Therefore, it is evident that, in addition to being important for the functional attributes of the BTRR complex, RMI1 and RMI2 are indispensable for the structural integrity of its components *in vivo*.

Although BLM depletion compromised SSA-mediated DSB repair in U2OS/SA-GFP cells, it had an opposite effect on SSA in HEK293/SA-GFP cells. Similarly, the efficiency of SSA-mediated DSB repair in HEK293/SA-GFP cells was elevated significantly upon depletion of RMI1 (data not shown). These findings suggest that, in HEK293 cells, the BTRR complex might act as an SSA suppressor, most likely through unwinding of the annealed intermediate formed following DNA end resection. Strikingly, we found that BLM concentration in HEK293 cells was much higher than in U2OS cells (data not shown). Therefore, it appears that the BTRR complex exerts an inhibitory effect on SSA when its concentration in the cell exceeds certain threshold.

Acknowledgments—We thank Kata Sarlos and Ian D. Hickson for the purified TRR complex, Judith L. Campbell for the transfer vector for preparation of the bacmid expressing His_6-hDNA2-FLAG, Jeremy M. Stark for the HEK293/SA-GFP and U2OS/SA-GFP cell lines, Stefano Ferrari and Stephanie Bregenhorn for help with protein purification, and Christiane Koenig for technical assistance.

REFERENCES

1. Jackson, S. P., and Bartek, J. (2009) The DNA-damage response in human biology and disease. *Nature* **461,** 1071–1078
2. Khanna, K. K., and Jackson, S. P. (2001) DNA double-strand breaks: signaling, repair and the cancer connection. *Nat. Genet.* **27,** 247–254
3. Longhese, M. P., Bonetti, D., Guerini, I., Manfrini, N., and Clerici, M. (2009) DNA double-strand breaks in meiosis: checking their formation,

processing and repair. *DNA Repair* **8,** 1127–1138
4. Soulas-Sprauel, P., Rivera-Munoz, P., Malivert, L., Le Guyader, G., Abramowski, V., Revy, P., and de Villartay, J. P. (2007) V(D)J and immunoglobulin class switch recombinations: a paradigm to study the regulation of DNA end-joining. *Oncogene* **26,** 7780–7791
5. Lieber, M. R. (2010) The mechanism of double-strand DNA break repair by the nonhomologous DNA end-joining pathway. *Annu. Rev. Biochem.* **79,** 181–211
6. San Filippo, J., Sung, P., and Klein, H. (2008) Mechanism of eukaryotic homologous recombination. *Annu. Rev. Biochem.* **77,** 229–257
7. Heyer, W. D., Ehmsen, K. T., and Liu, J. (2010) Regulation of homologous recombination in eukaryotes. *Annu. Rev. Genet.* **44,** 113–139
8. Mimitou, E. P., and Symington, L. S. (2008) Sae2, Exo1 and Sgs1 collaborate in DNA double-strand break processing. *Nature* **455,** 770–774
9. Zhu, Z., Chung, W. H., Shim, E. Y., Lee, S. E., and Ira, G. (2008) Sgs1 helicase and two nucleases Dna2 and Exo1 resect DNA double-strand break ends. *Cell* **134,** 981–994
10. Cejka, P., Cannavo, E., Polaczek, P., Masuda-Sasa, T., Pokharel, S., Campbell, J. L., and Kowalczykowski, S. C. (2010) DNA end resection by Dna2-Sgs1-RPA and its stimulation by Top3-Rmi1 and Mre11-Rad50-Xrs2. *Nature* **467,** 112–116
11. Nicolette, M. L., Lee, K., Guo, Z., Rani, M., Chow, J. M., Lee, S. E., and Paull, T. T. (2010) Mre11-Rad50-Xrs2 and Sae2 promote 5′ strand resection of DNA double-strand breaks. *Nat. Struct. Mol. Biol.* **17,** 1478–1485
12. Shim, E. Y., Chung, W. H., Nicolette, M. L., Zhang, Y., Davis, M., Zhu, Z., Paull, T. T., Ira, G., and Lee, S. E. (2010) *Saccharomyces cerevisiae* Mre11/Rad50/Xrs2 and Ku proteins regulate association of Exo1 and Dna2 with DNA breaks. *EMBO J.* **29,** 3370–3380
13. Cannavo, E., Cejka, P., and Kowalczykowski, S. C. (2013) Relationship of DNA degradation by *Saccharomyces cerevisiae* exonuclease 1 and its stimulation by RPA and Mre11-Rad50-Xrs2 to DNA end resection. *Proc. Natl. Acad. Sci. U.S.A.* **110,** E1661–E1668
14. Niu, H., Chung, W. H., Zhu, Z., Kwon, Y., Zhao, W., Chi, P., Prakash, R., Seong, C., Liu, D., Lu, L., Ira, G., and Sung, P. (2010) Mechanism of the ATP-dependent DNA end-resection machinery from *Saccharomyces cerevisiae*. *Nature* **467,** 108–111
15. Truong, L. N., Li, Y., Shi, L. Z., Hwang, P. Y., He, J., Wang, H., Razavian, N., Berns, M. W., and Wu, X. (2013) Microhomology-mediated end joining and homologous recombination share the initial end resection step to repair DNA double-strand breaks in mammalian cells. *Proc. Natl. Acad. Sci. U.S.A.* **110,** 7720–7725
16. Gravel, S., Chapman, J. R., Magill, C., and Jackson, S. P. (2008) DNA helicases Sgs1 and BLM promote DNA double-strand break resection. *Genes Dev.* **22,** 2767–2772
17. Nimonkar, A. V., Genschel, J., Kinoshita, E., Polaczek, P., Campbell, J. L., Wyman, C., Modrich, P., and Kowalczykowski, S. C. (2011) BLM-DNA2-RPA-MRN and EXO1-BLM-RPA-MRN constitute two DNA end resection machineries for human DNA break repair. *Genes Dev.* **25,** 350–362
18. Karanja, K. K., Cox, S. W., Duxin, J. P., Stewart, S. A., and Campbell, J. L. (2012) DNA2 and EXO1 in replication-coupled, homology-directed repair and in the interplay between HDR and the FA/BRCA network. *Cell Cycle* **11,** 3983–3996
19. Shibata, A., Moiani, D., Arvai, A. S., Perry, J., Harding, S. M., Genois, M. M., Maity, R., van Rossum-Fikkert, S., Kertokalio, A., Romoli, F., Ismail, A., Ismalaj, E., Petricci, E., Neale, M. J., Bristow, R. G., Masson, J. Y., Wyman, C., Jeggo, P. A., and Tainer, J. A. (2014) DNA double-strand break repair pathway choice is directed by distinct MRE11 nuclease activities. *Mol. Cell* **53,** 7–18
20. Bernstein, K. A., Gangloff, S., and Rothstein, R. (2010) The RecQ DNA helicases in DNA repair. *Annu. Rev. Genet.* **44,** 393–417
21. Yan, H., McCane, J., Toczylowski, T., and Chen, C. (2005) Analysis of the *Xenopus* Werner syndrome protein in DNA double-strand break repair. *J. Cell Biol.* **171,** 217–227
22. Liao, S., Toczylowski, T., and Yan, H. (2008) Identification of the Xenopus DNA2 protein as a major nuclease for the 5′→3′ strand-specific processing of DNA ends. *Nucleic Acids Res.* **36,** 6091–6100
23. Liao, S., Guay, C., Toczylowski, T., and Yan, H. (2012) Analysis of MRE11's function in the 5′→3′ processing of DNA double-strand breaks. *Nucleic Acids Res.* **40,** 4496–4506
24. Saydam, N., Kanagaraj, R., Dietschy, T., Garcia, P. L., Peña-Diaz, J., Shevelev, I., Stagljar, I., and Janscak, P. (2007) Physical and functional interactions between Werner syndrome helicase and mismatch-repair initiation factors. *Nucleic Acids Res.* **35,** 5706–5716
25. Adams, K. E., Medhurst, A. L., Dart, D. A., and Lakin, N. D. (2006) Recruitment of ATR to sites of ionising radiation-induced DNA damage requires ATM and components of the MRN protein complex. *Oncogene* **25,** 3894–3904
26. Sartori, A. A., Lukas, C., Coates, J., Mistrik, M., Fu, S., Bartek, J., Baer, R., Lukas, J., and Jackson, S. P. (2007) Human CtIP promotes DNA end resection. *Nature* **450,** 509–514
27. Yang, J., O'Donnell, L., Durocher, D., and Brown, G. W. (2012) RMI1 promotes DNA replication fork progression and recovery from replication fork stress. *Mol. Cell Biol.* **32,** 3054–3064
28. Orren, D. K., Brosh, R. M., Jr., Nehlin, J. O., Machwe, A., Gray, M. D., and Bohr, V. A. (1999) Enzymatic and DNA binding properties of purified WRN protein: high affinity binding to single-stranded DNA but not to DNA damage induced by 4NQO. *Nucleic Acids Res.* **27,** 3557–3566
29. Kanagaraj, R., Saydam, N., Garcia, P. L., Zheng, L., and Janscak, P. (2006) Human RECQ5β helicase promotes strand exchange on synthetic DNA structures resembling a stalled replication fork. *Nucleic Acids Res.* **34,** 5217–5231
30. El-Shemerly, M., Janscak, P., Hess, D., Jiricny, J., and Ferrari, S. (2005) Degradation of human exonuclease 1b upon DNA synthesis inhibition. *Cancer Res.* **65,** 3604–3609
31. Henricksen, L. A., Umbricht, C. B., and Wold, M. S. (1994) Recombinant replication protein A: expression, complex formation, and functional characterization. *J. Biol. Chem.* **269,** 11121–11132
32. Masuda-Sasa, T., Imamura, O., and Campbell, J. L. (2006) Biochemical analysis of human Dna2. *Nucleic Acids Res.* **34,** 1865–1875
33. Pfaffl, M. W. (2001) A new mathematical model for relative quantification in real-time RT-PCR. *Nucleic Acids Res.* **29,** e45
34. Bennardo, N., Cheng, A., Huang, N., and Stark, J. M. (2008) Alternative-NHEJ is a mechanistically distinct pathway of mammalian chromosome break repair. *PLoS Genet.* **4,** e1000110
35. Gunn, A., and Stark, J. M. (2012) I-SceI-based assays to examine distinct repair outcomes of mammalian chromosomal double strand breaks. *Methods Mol. Biol.* **920,** 379–391
36. Richardson, C., Moynahan, M. E., and Jasin, M. (1998) Double-strand break repair by interchromosomal recombination: suppression of chromosomal translocations. *Genes Dev.* **12,** 3831–3842
37. Karow, J. K., Chakraverty, R. K., and Hickson, I. D. (1997) The Bloom's syndrome gene product is a 3′-5′ DNA helicase. *J. Biol. Chem.* **272,** 30611–30614
38. Brosh, R. M., Jr., Waheed, J., and Sommers, J. A. (2002) Biochemical characterization of the DNA substrate specificity of Werner syndrome helicase. *J. Biol. Chem.* **277,** 23236–23245
39. Shen, J. C., Gray, M. D., Oshima, J., Kamath-Loeb, A. S., Fry, M., and Loeb, L. A. (1998) Werner syndrome protein: I: DNA helicase and DNA exonuclease reside on the same polypeptide. *J. Biol. Chem.* **273,** 34139–34144
40. Kamath-Loeb, A. S., Shen, J. C., Loeb, L. A., and Fry, M. (1998) Werner syndrome protein: II: characterization of the integral 3′ → 5′ DNA exonuclease. *J. Biol. Chem.* **273,** 34145–34150
41. Kim, J. H., Kim, H. D., Ryu, G. H., Kim, D. H., Hurwitz, J., and Seo, Y. S. (2006) Isolation of human DNA2 endonuclease and characterization of its enzymatic properties. *Nucleic Acids Res.* **34,** 1854–1864
42. Avemann, K., Knippers, R., Koller, T., and Sogo, J. M. (1988) Camptothecin, a specific inhibitor of type I DNA topoisomerase, induces DNA breakage at replication forks. *Mol. Cell Biol.* **8,** 3026–3034
43. Lee, J. W., Harrigan, J., Opresko, P. L., and Bohr, V. A. (2005) Pathways and functions of the Werner syndrome protein. *Mech. Ageing Dev.* **126,** 79–86
44. Kanagaraj, R., Parasuraman, P., Mihaljevic, B., van Loon, B., Burdova, K., König, C., Furrer, A., Bohr, V. A., Hübscher, U., and Janscak, P. (2012) Involvement of Werner syndrome protein in MUTYH-mediated repair of oxidative DNA damage. *Nucleic Acids Res.* **40,** 8449–8459
45. Stark, J. M., Pierce, A. J., Oh, J., Pastink, A., and Jasin, M. (2004) Genetic steps of mammalian homologous repair with distinct mutagenic conse-

quences. *Mol. Cell Biol.* **24,** 9305–9316
46. Wu, L., and Hickson, I. D. (2003) The Bloom's syndrome helicase suppresses crossing over during homologous recombination. *Nature* **426,** 870–874
47. Yin, J., Sobeck, A., Xu, C., Meetei, A. R., Hoatlin, M., Li, L., and Wang, W. (2005) BLAP75, an essential component of Bloom's syndrome protein complexes that maintain genome integrity. *EMBO J.* **24,** 1465–1476
48. Wu, L., Bachrati, C. Z., Ou, J., Xu, C., Yin, J., Chang, M., Wang, W., Li, L., Brown, G. W., and Hickson, I. D. (2006) BLAP75/RMI1 promotes the BLM-dependent dissolution of homologous recombination intermediates. *Proc. Natl. Acad. Sci. U.S.A.* **103,** 4068–4073
49. Xu, D., Guo, R., Sobeck, A., Bachrati, C. Z., Yang, J., Enomoto, T., Brown, G. W., Hoatlin, M. E., Hickson, I. D., and Wang, W. (2008) RMI, a new OB-fold complex essential for Bloom syndrome protein to maintain genome stability. *Genes Dev.* **22,** 2843–2855
50. Cheng, W. H., von Kobbe, C., Opresko, P. L., Arthur, L. M., Komatsu, K., Seidman, M. M., Carney, J. P., and Bohr, V. A. (2004) Linkage between Werner syndrome protein and the Mre11 complex via Nbs1. *J. Biol. Chem.* **279,** 21169–21176
51. Lan, L., Nakajima, S., Komatsu, K., Nussenzweig, A., Shimamoto, A., Oshima, J., and Yasui, A. (2005) Accumulation of Werner protein at DNA double-strand breaks in human cells. *J. Cell Sci.* **118,** 4153–4162
52. Tomimatsu, N., Mukherjee, B., Deland, K., Kurimasa, A., Bolderson, E., Khanna, K. K., and Burma, S. (2012) Exo1 plays a major role in DNA end resection in humans and influences double-strand break repair and damage signaling decisions. *DNA Repair* **11,** 441–448
53. Yu, C. E., Oshima, J., Fu, Y. H., Wijsman, E. M., Hisama, F., Alisch, R., Matthews, S., Nakura, J., Miki, T., Ouais, S., Martin, G. M., Mulligan, J., and Schellenberg, G. D. (1996) Positional cloning of the Werner's syndrome gene. *Science* **272,** 258–262
54. Salk, D., Au, K., Hoehn, H., and Martin, G. M. (1981) Cytogenetics of Werner's syndrome cultured skin fibroblasts: variegated translocation mosaicism. *Cytogenet. Cell Genet.* **30,** 92–107
55. Fukuchi, K., Martin, G. M., and Monnat, R. J., Jr. (1989) Mutator phenotype of Werner syndrome is characterized by extensive deletions. *Proc. Natl. Acad. Sci. U.S.A.* **86,** 5893–5897
56. Melcher, R., von Golitschek, R., Steinlein, C., Schindler, D., Neitzel, H., Kainer, K., Schmid, M., and Hoehn, H. (2000) Spectral karyotyping of Werner syndrome fibroblast cultures. *Cytogenet. Cell Genet.* **91,** 180–185
57. Bunting, S. F., and Nussenzweig, A. (2013) End-joining, translocations and cancer. *Nat. Rev. Cancer* **13,** 443–454
58. Symington, L. S., and Gautier, J. (2011) Double-strand break end resection and repair pathway choice. *Annu. Rev. Genet.* **45,** 247–271
59. Chen, L., Huang, S., Lee, L., Davalos, A., Schiestl, R. H., Campisi, J., and Oshima, J. (2003) WRN, the protein deficient in Werner syndrome, plays a critical structural role in optimizing DNA repair. *Aging Cell* **2,** 191–199
60. Perry, J. J., Yannone, S. M., Holden, L. G., Hitomi, C., Asaithamby, A., Han, S., Cooper, P. K., Chen, D. J., and Tainer, J. A. (2006) WRN exonuclease structure and molecular mechanism imply an editing role in DNA end processing. *Nat. Struct. Mol. Biol.* **13,** 414–422
61. Saintigny, Y., Makienko, K., Swanson, C., Emond, M. J., and Monnat, R. J., Jr. (2002) Homologous recombination resolution defect in Werner syndrome. *Mol. Cell Biol.* **22,** 6971–6978
62. Swanson, C., Saintigny, Y., Emond, M. J., and Monnat, R. J., Jr. (2004) The Werner syndrome protein has separable recombination and survival functions. *DNA Repair* **3,** 475–482
63. Bussen, W., Raynard, S., Busygina, V., Singh, A. K., and Sung, P. (2007) Holliday junction processing activity of the BLM-Topo IIIα-BLAP75 complex. *J. Biol. Chem.* **282,** 31484–31492
64. Raynard, S., Bussen, W., and Sung, P. (2006) A double Holliday junction dissolvasome comprising BLM, topoisomerase IIIα, and BLAP75. *J. Biol. Chem.* **281,** 13861–13864
65. Xue, X., Raynard, S., Busygina, V., Singh, A. K., and Sung, P. (2013) Role of replication protein A in double Holliday junction dissolution mediated by the BLM-Topo IIIα-RMI1-RMI2 protein complex. *J. Biol. Chem.* **288,** 14221–14227

3.4 A ROLE FOR THE MISMATCH-BINDING FACTOR MUTSβ AS A MEDIATOR OF ATR ACTIVATION IN RESPONSE TO DNA DOUBLE-STRAND BREAKS.

Mismatch repair proteins were shown to accumulate at sites of DSBs created by laser micro-irradiation. However, the molecular mechanism underlying their function at sites of DSBs has not been described. Studies in mouse cells proposed the role of Msh2 in DSB repair by HR although which Msh2 complex is involved in this process has not been revealed.

We used laser micro-irradiation to test in which step of HR is MSH2 recruited to site of DNA damage and found that the factors needed for MSH2 recruitment are MRN complex and CtIP, but not RAD51, suggesting that MSH2 is recruited in presynaptic phase of HR.

To test the role of mismatch repair complexes in homologous recombination, we employed established cell-based reporter system. Using RNA interference we depleted U2OS and HEK293-DR-GFP cells of MSH2, MSH3 and MSH6 proteins and saw that there is defect in HR only in cells after depletion of MSH2 and MSH3, but not MSH6.

Knowing that MSH2 comes to sites of DNA damage after initial short-range resection and that it promotes HR in complex with MSH3, we next tested if MSH2-MSH3 complex influences long-range resection. For this purpose we used RPA foci quantification after DNA damage induction in U2OS cells. We saw no defect in RPA foci formation after depletion of MSH2, MSH3 or MSH6.

To test if there would be defect in signalling pathways triggered by DNA damage we used phosphospecific antibodies to detect modified forms of proteins involved in DNA damage response. Interestingly, we saw a decreased level of RPA2 phosphorylation at serine 4/8 and serine 33 after DNA damage in cells with MSH2 and MSH3 depletion although there is no defect in p53 phosphorylation at serine 15 and γ-H2AX formation. As phosphorylation of RPA2 at serine 33 occurs before phosphorylation at serine 4/8 and this site is phosphorylated specifically by ATR kinase, we also tested other substrates of this kinase. Among these CHK1 phosphorylation at serine 317 and serine 345 is one of the first and of most importance leading to cell cycle arrest. Again we depleted cells using RNA interference to knock down MSH3 or MSH6 and saw decreased phosphorylation of CHK1 after MSH3 depletion specifically. Moreover, we tested if purified MSH2-MSH3 complex

could stimulate phosphorylation of ATR targets in nuclear extracts from HCT116 cells that lack MSH3 protein. Indeed we saw that addition of MSH2-MSH3 but not MSH2-MSH6 to kinase reaction stimulated phosphorylation of RPA2 and CHK1 but not p53 or CHK2. This led us to conclusion that ATR activation after DNA damage is somehow regulated by MSH2-MSH3 complex.

As it has been already published that MSH2 interacts with ATR-ATRIP complex, we tested whether MSH3 is also present in this complex. Using immunoprecipitation, we could detect interaction of MSH2-MSH3 complex with ATR-ATRIP complex. Moreover, we found defect in ATRIP foci formation after DNA damage in cells depleted of MSH2 and MSH3.

These results led us to hypothesis that MSH2-MSH3 complex could interact with ssDNA coated by RPA that was created by short-range resection. We employed *in vitro* pull down assay and detected that only MSH2-MSH3 but not MSH2-MSH6 was capable of binding to RPA-coated ssDNA but not to RPA itself. We also tested stability of binding of MSH2-MSH3 to RPA-coated ssDNA upon addition of ATP as in canonical mismatch repair it has been shown that these complexes dissociates from DNA upon ATP binding. We found that binding of ATP caused dissociation of MSH2-MSH3 also from RPA-coated ssDNA.

To determine if presence of MSH2-MSH3 could stimulate recruitment of ATR-ATRIP to RPA-coated ssDNA we utilized *in vitro* pull down assay using cell extracts. In this assay, binding of MSH2-MSH3 to RPA-coated ssDNA stimulated recruitment of ATR-ATRIP complex although ATP present in the cell extract caused dissociation of MSH2-MSH3.

ssDNA oligomer used in our study has random sequence thus contains secondary structures. We were wondering if oligomers of the same length with other secondary structure or without any secondary structure would work in the same way. We used poly(dT) oligomer and other random sequence ssDNA oligomers, coated them with RPA and determined the binding of MSH2-MSH3 to these structures. Interestingly, MSH2-MSH3 was only capable of binding to oligomers containing secondary structures.

From these results we hypothesized that MSH2-MSH3 complex mediates binding of the ATR-ATRIP complex to RPA-coated ssDNA by binding to secondary structures in RPA-ssDNA at sites of DNA damage to promote ATR activation and DNA repair.

A role for the mismatch-binding factor MutSβ as a mediator of ATR activation in response to DNA double-strand breaks

Kamila Burdova[1], Boris Mihaljevic[2] and Pavel Janscak[1,2,*]

[1]Institute of Molecular Genetics, Academy of Sciences of the Czech Republic, 143 00 Prague, Czech Republic, [2]Institute of Molecular Cancer Research, University of Zurich, CH-8057 Zurich, Switzerland

[*]Correspondence: pjanscak@imcr.uzh.ch

Running title: MutSβ mediates ATR activation

SUMMARY

Ataxia telangiectasia and Rad3-related (ATR) protein kinase, a master regulator of DNA damage response, is activated by RPA-coated single-stranded DNA (ssDNA) generated at stalled replication forks or DNA double-strand breaks (DSBs). Here we identify the mismatch-binding protein MutSβ, a heterodimer of MSH2 and MSH3, as a key component of the ATR signaling cascade. MutSβ accumulates at sites of DSBs in a manner dependent on DNA-end resection and promotes DSB repair by homologous recombination. MSH2 and MSH3 form a complex with ATR and its regulatory partner ATRIP, and their depletion compromises the formation of ATRIP foci and the phosphorylation of ATR substrates in cells responding to replication-associated DSBs. Purified MutSβ heterodimer binds to DNA secondary structures persisting in RPA-ssDNA complexes and promotes ATRIP recruitment. These results suggest that MutSβ mediates binding of the ATR-ATRIP complex to RPA-coated ssDNA at sites of DNA damage to promote ATR activation and DNA repair.

INTRODUCTION

Cells are constantly challenged by various types of DNA damage that can induce genomic instability, a hallmark of tumorigenesis and cancer progression (Ciccia and Elledge, 2010; Jackson and Bartek, 2009). The most dangerous DNA lesion in the cell is DNA double-strand break (DSB) because it can give rise to chromosomal rearrangements (Jackson and Bartek, 2009). DSBs can be generated by agents such as ionizing radiation and radiomimetic drugs, or can result as a consequence of replication fork collapse (Jackson and Bartek, 2009). Eukaryotic cells respond to DSBs by activating a complex network of pathways that lead to cell cycle arrest, DNA repair, and, in the case of excessive damage, to apoptosis or senescence (Ciccia and Elledge, 2010; Jackson and Bartek, 2009). Cells evolved two

mechanistically-distinct pathways to repair DSBs: non-homologous end joining (NHEJ) and homologous recombination (HR). NHEJ involves religation of the broken DNA ends and is frequently associated with a short deletion or insertion of DNA at the break site (van Gent and van der Burg, 2007). On the contrary, HR provides an accurate means of DSB repair, because it is directed by an intact homologous DNA sequence (San Filippo et al., 2008). This process is largely restricted to S/G2 phases of the cell cycle to ensure that the undamaged sister chromatid is used as a repair template, a mechanism preventing chromosomal rearrangements (San Filippo et al., 2008; Symington and Gautier, 2011).

The HR process is initiated by nuclease-mediated resection of broken DNA ends to generate 3'-single-stranded (ss) DNA tails that are immediately coated by the heterotrimeric ssDNA-binding protein RPA (Symington and Gautier, 2011). This nucleoprotein structure serves as a platform for the recruitment and activation of the *Ataxia telangiectasia*-mutated and Rad3-related (ATR) kinase, a master DNA damage response regulator which phosphorylates the checkpoint kinase 1 (CHK1) and other proteins such as SMC1 and RPA to promote cell-cycle arrest and DNA repair (Cimprich and Cortez, 2008). ATR is targeted to RPA-coated ssDNA via its interacting partner ATRIP (Zou and Elledge, 2003). Activation of the ATR kinase depends on its interaction with TOPBP1 that is recruited to the DNA damage site and associates with the RAD9-RAD1-HUS1 (9-1-1) complex loaded on dsDNA at the ssDNA/dsDNA junction by the RAD17-RFC clamp loader (Delacroix et al., 2007; Duursma et al., 2013; Kumagai et al., 2006; Lee et al., 2007; Mordes et al., 2008; Zou et al., 2002). ATR can be also activated in a 9-1-1/RAD17-independent manner through targeting of TOPBP1 to RPA-coated ssDNA via the MRE11-RAD50-NBS1 (MRN) complex (Shiotani et al., 2013). In addition, there is evidence that TOPBP1 can be recruited to RPA-ssDNA through its interaction with ATRIP and can activate ATR in the absence of other factors (Choi et al., 2010; Hashimoto et al., 2006; Kumagai et al., 2006).

The mismatch repair (MMR) system corrects DNA mismatches arrising during DNA replication and genetic recombination (Jiricny, 2006; Kunkel and Erie, 2005). Germline mutations in the genes responsible for MMR are the major cause of hereditary non-polyposis colon cancer, a dominantly-inherited disorder with high penetrance (Peltomaki, 2001). The key proteins involved in the initiation of MMR reaction are highly conserved in evolution. In eukaryotic cells, mispaired bases are recognized by two heterodimeric complexes, MSH2-MSH6 (MutSα) and MSH2-MSH3 (MutSβ), that have different, but overlapping, DNA substrate specificity. The MutSα complex recognizes base-base mismatches and single- and double-base insertions, while the MutSβ complex binds to loops of 1-14 extrahelical nucleotides (Habraken et al., 1996; Palombo et al., 1996). In addition to mismatch-binding functionality, both MutSα and MutSβ contain two Walker-type ATP-binding sites, one in each subunit, and display ATPase activity, which is essential for the MMR reaction (Kunkel and Erie, 2005). Binding of MutSα or MutSβ to a mismatch brings about an exchange of ADP for ATP in the ATP-binding sites of the enzyme and converts it into a sliding DNA clamp that, in a complex with MutLα (heterodimer of MLH1 and PMS1), triggers EXO1-mediated excision of the error-containing strand followed by DNA resynthesis (Gradia et al., 1999; Jiricny, 2006; Wilson et al., 1999).

Interestingly, a number of studies have demonstrated that the proteins required for the initiation of MMR are also involved in the cellular response to DSBs. It has been shown that the human MMR proteins MSH2, MSH3, MSH6 and MLH1 accumulate rapidly at sites of DSBs generated by laser microirradiation, with MLH1 recruitment being dependent on MSH2 as in the case of canonical MMR reaction (Hong et al., 2008). Studies in mouse cells have revealed that Msh2 is required for efficient repair of DSBs by HR and conferes resistance to DSB-inducing agents (Bennardo et al., 2009; Franchitto et al., 2003; Pichierri et al., 2001). In response to ionizing radiation, G2/M checkpoint activation in $Msh2^{-/-}$ cells is

inefficient, such that the cells arrest only transiently before progressing into mitosis (Franchitto et al., 2003). More recently, it has been shown that Msh2$^{-/-}$ and Msh3$^{-/-}$, but not Msh6$^{-/-}$, mouse emryonic fibroblasts display a significant increase in chromatid breaks compared to wild type cells, indicating a defect in DSB repair due to loss of MutSβ function (van Oers et al., 2013). However, the role of MutSβ in the cellular response to DSBs remains largely uncharacterized. Here, we present several lines of evidence suggesting that MutSβ mediates ATRIP recruitment to RPA-coated ssDNA at sites of replication-associated DSBs to promote ATR activation and HR-mediated DSB repair.

RESULTS

MSH2 and MSH3, but not MSH6, are required for efficient repair of DSBs by HR

A previous study in mouse embryonic stem cells using GFP-based chromosomal reporters for different DSB repair pathways showed that MSH2 was required for efficient repair of DSBs via HR, whereas it was dispensable for DSB repair via NHEJ and single-strand annealing (Bennardo et al., 2009). In order to determine which of the two heterodimeric complexes of MSH2, MutSα and MutSβ, is involved in HR-mediated DSB repair, we tested the effect of siRNA-mediated depletion of MSH2, MSH3 and MSH6 on the HR repair activity of the established reporter cell lines HEK293/DR-GFP and U2OS/DR-GFP (Bennardo et al., 2009; Gunn and Stark, 2012). In these cells, a single HR event triggered by a DSB created by the I-SceI endonuclease gives rise to a functional GFP allele, which can be scored by flow cytometry (Bennardo et al., 2009; Gunn and Stark, 2012). We found that cells depleted of MSH2 or MSH3 showed a markedly reduced frequency of I-SceI-induced HR repair events as compared to mock-depleted cells (Figure 1A). In contrast, lack of MSH6 did not significantly affect HR repair efficiency in either reporter cell line (Figure 1A). Thus, these results provide evidence that MSH2 promotes HR-mediated DSB repair as part of the

MutSβ heterodimer.

MSH2 accumulates at DSB sites during the presynaptic phase of HR

To gain insight into the role of human MutSβ in DSB repair by HR, we asked which HR factors are required for the recruitment of MSH2 to sites of laser-induced DSBs in U2OS cells. Since MMR proteins are known to act on the heteroduplex DNA intermediates formed during HR in order to inhibit recombination between divergent sequences, we tested whether MSH2 accumulation at DSB sites is dependent on the presence of RAD51 recombinase (Chen and Jinks-Robertson, 1998). We found that RAD51 depletion in U2OS cells did not significantly affect MSH2 recruitment to laser-induced DSB stripes revealed by staining for the phosphorylated form of histone H2AX (γ-H2AX), suggesting that during DSB repair by HR, MSH2 is recruited prior to the formation of joint DNA molecules (Figure 2A and B). Interestingly, MSH2 accumulated at laser-induced DSB stripes in both cyclin A-positive (S/G2) and cyclin A-negative (G1) cells, indicating that it is recruited to DSBs throughout interphase (Figure 2A).

Next, we asked whether MSH2 recruitment to sites of DSBs is dependent on DNA-end resection. Resection of broken DNA ends relies on CtIP that acts in conjunction with the MRN complex to initiate the resection process and is also involved in the extension of resection tracts (Peterson et al., 2013; Sartori et al., 2007). We found that CtIP depletion significantly abrogated the recruitment of MSH2 to laser-induced DSB stripes both in G1 and S/G2 cells (Figure 2A and B). In addition, using ATLD1 cells that carry a hypomorphic mutation in the *MRE11* gene, we found that the trafficking of MSH2 to DSB sites was dependent on the MRN complex (Figure 2C and D). Together, these results suggest that MSH2 is recruited to sites of DSBs during the presynaptic phase of HR.

MutSβ promotes ATR activation in response to DSBs

Having obtained evidence that MMR proteins operate at sites of DSBs prior to the formation of recombination intermediates, we sought to assess whether they have a role in DNA-end resection. First, we evaluated the effect of MSH2 depletion on the accumulation of RPA at laser-induced DSB stripes in U2OS cells. We found that in cells lacking MSH2, RPA recruitment to laser-induced DSBs was not significantly affected, whereas it was impaired in cells lacking CtIP or in cells depleted of EXO1 and BLM to block long-range resection (Supplemental Figure S1A-E) (Gravel et al., 2008). Next we investigated the role of MMR proteins in the formation of RPA foci in response to camptothecin (CPT). This DNA topoisomerase I inhibitor induces DSBs only in replicating S-phase cells (Avemann et al., 1988). We found that siRNA-mediated depletion of MSH2, as well as of MSH3, MSH6 or MLH1, had no significant effect on the formation of RPA foci in CPT-treated U2OS cells (Figure 3A, and Supplemental Figure S1C and D). In contrast, the formation of CPT-induced RPA foci was severely compromised by depletion of CtIP (Figure 3A, and Supplemental Figure S1C and D). Thus, these data indicate that neither MutSα nor MutSβ are involved in the resection of broken DNA ends during S-phase.

In response to CPT, the N-terminal domain of the middle subunit of RPA, RPA2, is sequentially phosphorylated at multiple sites including Ser4, Ser8, Thr21 and Ser33, a process required for DSB repair (Anantha et al., 2007; Sartori et al., 2007; Shiotani et al., 2013). We therefore asked whether MMR proteins play a role in CPT-induced phosphorylation of RPA in U2OS cells. Using phospho-specific antibodies, we found that depletion of MSH2 or MSH3, but not MSH6 or MLH1, abrogated RPA2 phosphorylation at Ser4/8 (Figure 3B-D, and Supplemental Figure S2A and B), which is mediated by DNA-PKcs or ATM following RPA2 Ser33 phosphorylation by ATR (Anantha et al., 2007; Shiotani et al., 2013). We also found that depletion of MSH2 or MSH3 significantly reduced

the phosphorylation of RPA2 Ser33 as compared to mock-depleted cells (Supplemental Figure S2B). Notably, the fold of reduction of RPA2 Ser33 phosphorylation caused by lack the MutSβ subunits was comparable to that observed upon depletion of CtIP (Supplemental Figure S2B). The defect in CPT-induced RPA phosphorylation of cells lacking MSH2 or MSH3 was also apparent from disappearance of the RPA2 band with a reduced electrophoretic mobility, which corresponds to hyper-phosphorylated form of RPA2 (Figure 3B and Supplemental Figure S2B). Depletion of MMR proteins did not cause a reduction in BrdU incorporation in U2OS cells, excluding the possibility that the observed impairment of CPT-induced phosphorylation of RPA2 in MSH2- and MSH3-depleted cells was due to a defect in DNA replication that is required for the induction of DSBs by CPT (Supplemental Figure S2C). Moreover, depletion of MMR proteins affected neither p53 phosphorylation at Ser15 nor the formation of γ-H2AX foci after CPT treatment, further confirming that CPT-induced DSBs arise normally in these cells (Figure 3B, and data not shown).

Phosphorylation of RPA2 on Ser33 is characteristic of ATR activation (Shiotani et al., 2013). Thus, the finding that MSH2- and MSH3-deficient cells have a defect in RPA2 Ser33 phosphorylation in response to CPT treatment prompted us to further explore a possible role of MutSβ in the activation of ATR by DSBs. In response to CPT, ATR rapidly phosphorylates the checkpoint effector kinase CHK1 at several sites including Ser317 and Ser345 (Shiotani et al., 2013) (Figure 3D, Supplemental Figure S3A). Hence we asked whether depletion of MutSβ affected this critical event in the ATR-mediated DNA damage checkpoint pathway (Bartek and Lukas, 2003). We found that depletion of MSH3, but not MSH6, largely abolished CHK1 Ser317 and Ser345 phosphorylation in U2OS cells treated with CPT, suggesting that MutSβ indeed promotes ATR activation (Figure 3D). On the contrary, the CPT-induced CHK2 phosphorylation at Thr68 was not affected in cells lacking

MSH3, indicating that MutSβ has no role in the activation of ATM (Figure 3D) (Bartek and Lukas, 2003).

ATR-dependent phosphorylation of RPA2 can be induced in HeLa cell nuclear extracts by addition of ssDNA (Shiotani et al., 2013). In order to substantiate the above findings, we measured the levels of RPA2 phospho-Ser4/8, RPA2 phospho-Ser33 and CHK1 phospho-Ser317 in nuclear extracts of the MSH3-deficient colorectal cancer cell line HCT116 that were supplemented with increasing concentrations of purified recombinant MutSβ (or MutSα) together with a 90-mer ssDNA oligonucleotide. We found that MutSβ, but not MutSα, stimulated phosphorylation of both RPA2 and CHK1 in a dose-dependent manner, whereas it had no effect on CHK2 phosphorylation at Thr68 under these conditions (Figure 3E). Similar results were obtained with HeLa cell nuclear extracts (Supplemental Figure S2D).

Together, these results provide strong evidence that MutSβ promotes ATR activation in response to DSBs.

MutSβ forms a complex with ATR and ATRIP and mediates ATRIP recruitment to sites of DSBs in human cells

MSH2 has been shown to form a complex with ATR and ATRIP in human cells (Wang and Qin, 2003). This suggests that MutSβ might mediate ATR activation by recruiting ATR-ATRIP to resected DNA ends. To explore this possibility, we first investigated whether the cellular complex formed between MSH2, ATR and ATRIP contains MSH3. To do so, HEK293 cells were transfected with vectors expressing Flag-ATR and HA-ATRIP, respectively, and complex formation between the above proteins was investigated by immunoprecipitation using beads conjugated with an anti-Flag antibody. We found that the Flag-ATR immunoprecipitate from these cells contained ATRIP, RPA1, MSH2 and MSH3

(Figure 4A). None of those proteins was present in a control immunoprecipitate from cells transfected with the empty vector (Figure 4A). Thus, these data demonstrate that in human cells, MSH2 interacts with the ATR-ATRIP complex as part of the MutSβ heterodimer.

To determine whether MutSβ promotes the recruitment of ATR-ATRIP to sites of DSBs, we evaluated the effect of depletion of MSH2 or MSH3 on the formation of ATRIP foci in U2OS cells treated with CPT. We found that, one hour after addition of CPT, nearly 90% of γ-H2AX-positive cells contained ATRIP foci (Figure 4B, and Supplemental Figure S4). However, if cells were depleted of MSH2 or MSH3, the formation of ATRIP foci in response to CPT was markedly attenuated, with only 45% of γ-H2AX-positive cells displaying ATRIP foci under these conditions (Figure 4C and D, and Supplemental Figure S4). A comparable reduction in the frequency of ATRIP foci was observed with cells depleted of CtIP (Figure 4C and D, and Supplemental Figure S4). Thus, these data provide strong evidence for a role of MutSβ in the recruitment of ATR-ATRIP complex to sites of DSBs.

MutSβ binds to DNA secondary structures persisting in RPA-coated ssDNA and promotes ATRIP recruitment

Finally, we asked how MutSβ might mediate ATRIP recruitment to sites of DNA damage. The ATR-ATRIP complex is recruited to DNA damage sites by RPA-coated ssDNA (Zou and Elledge, 2003). We therefore tested whether MutSβ binds to RPA, both free and in complex with ssDNA. In these experiments, we used a recombinant MutSβ heterodimer carrying a His_6-tag on the MSH3 subunit and a 90-mer oligonucleotide biotinylated at the 5'-end (b90). Where necessary, the ssDNA substrate was pre-incubated with over-stoichiometric amounts of RPA to ensure full DNA coverage. A 90-mer oligonucleotide is expected to accommodate three RPA molecules assuming that the RPA trimer occupies a

region spanning about 30 nucleotides (Fan and Pavletich, 2012). By a pull-down assay with Ni-NTA beads, we found that MutSβ was bound to RPA-ssDNA complexes, whereas it did not show any detectable binding to free RPA (Figure 5A). MutSα (His_6-tag on MSH6), that was also included in this analysis, failed to bind both free RPA and RPA-ssDNA (Figure 5A). By pull-down assays with streptavidin-coated magnetic beads, we then compared binding of MutSα and MutSβ to free- and RPA-coated ssDNA (b90). We found that although both proteins were bound to free ssDNA, RPA-ssDNA associated efficiently only with MutSβ (Figure 5B). Interestingly, binding of MutSβ to RPA-ssDNA was completely inhibited by ATP (Figure 5C, lanes 2 and 3). Full inhibition of MutSβ binding to RPA-ssDNA was also observed upon addition of the poorly-hydrolysable analog of ATP, ATPγS, but not ADP, suggesting that ATP binding by MutSβ rather than its hydrolysis triggers its dissociation from RPA-ssDNA (Figure 5C, lane 4, and Supplemental Figure S5A). This is further supported by the observation that ATP-induced dissociation of MutSβ from RPA-ssDNA was blocked by EDTA that sequesters the ATPase cofactor Mg^{2+}, which is required for both ATP binding and hydrolysis (Supplemental Figure S5B). Of note, in the presence of ATP or ATPγS, MutSβ also failed to stably bind free ssDNA (Figure 5C, lanes 5-7).

Next, we tested whether MutSβ enhances binding of ATRIP to RPA-ssDNA complexes *in vitro*. To this end, the b90 oligonucleotide coated with RPA was pre-incubated with or without recombinant MutSβ protein followed by addition of an extract of HEK293 cells over-producing HA-tagged ATRIP. At different time points after addition of the cell extract, protein-DNA complexes were isolated using streptavidin magnetic beads and analyzed by western blotting. We found that, in the presence of MutSβ, HA-ATRIP was bound to RPA-ssDNA more efficiently than in its absence (Figure 5D and E). Of note, MutSβ gradually dissociated from RPA-ssDNA after addition of the cell extract, which is most likely caused by ATP from the extract. In support of this notion, MutSβ dissociation

was inhibited if the extract was supplemented with EDTA (Supplemental Figure S5B). Conversely, dissociation of MutSβ from RPA-ssDNA was dramatically accelerated if the extract was supplemented with an ATP-regenerating system (Supplemental S5C).

As MutSβ was not bound to free RPA, it is possible that its interaction with RPA-coated ssDNA is mediated by DNA-hairpin structures that persist in ssDNA in the presence of RPA. In fact, the 90-mer oligonucleotide b90 used in our study can form a strong hairpin loop at its 3' terminus (Supplementary Figure S6A). We therefore repeated our experiments using a 90-mer oligonucleotide containing only dT residues (b90dT), which cannot form secondary structures. We found that MutSβ failed to bind b90dT oligonucleotide if it was pre-coated with RPA (Figure 5F). In absence of RPA, MutSβ to was bound to b90dT, but much less efficiently compared to its binding to b90 (Supplemental Figure S6B, compare lanes 1 and 2). To substantiate our findings, we tested binding of MutSβ to five other oligonucleotides that can form various hairpin loop structures (Supplementary Figure S6B). We found that MutSβ was bound efficiently to all these oligonucleotides irrespective of the presence of RPA (Figure 5F and Supplementary Figure S6B). Thus it appears that MutSβ associates with RPA-coated ssDNA through binding to DNA secondary structures that are not eliminated by RPA binding.

Together, our results suggest that MutSβ targets ATR-ATRIP complex to RPA-coated ssDNA for ATR activation.

DISCUSSION

The MSH2-MSH3 heterodimer, termed MutSβ, binds to insertion/deletion loops in DNA generated by DNA polymerase slippage during DNA replication and activates the MMR machinery (Habraken et al., 1996; Jiricny, 2006; Kunkel and Erie, 2005; Palombo et al., 1996). Recent studies have shown that, in addition to its role in MMR, MutSβ promotes

repair of DNA DSBs, which might in part underlie its tumor suppression effect in $p53^{-/-}$ mice (van Oers et al., 2013). However, the molecular basis of this genome maintenance function of MutSβ has not been elucidated. Here we provide several lines of evidence suggesting that MutSβ promotes HR-mediated DSB repair by acting as a key component of the ATR signaling pathway, which is essential for the execution of HR (Wang et al., 2004) (Supplementary Figure 4B). First, we demonstrate that depletion of either of the two MutSβ subunits compromises phosphorylation of the ATR targets CHK1 and RPA in response to replication-associated DSBs, which are preferentially repaired by HR (Britton et al., 2013). Second, we show that MSH2 accumulates at DSBs prior to the formation of RAD51 filaments in a manner dependent on DNA-end resection, suggesting that MutSβ is recruited to DSBs by RPA-coated ssDNA. Third, we provide evidence that MutSβ binds to DNA-hairpin loop structures persisting in RPA-ssDNA complexes. Fourth, we show that both subunits of MutSβ exist is a complex with ATR, ATRIP and RPA in human cells and are required for the formation of ATRIP foci in response to replication-associated DSBs. Finally, we establish that MutSβ enhances the binding of ATRIP to RPA-ssDNA complexes *in vitro*. Based on these findings, we propose that MutSβ mediates ATR-ATRIP recruitment to RPA-coated ssDNA formed upon resection of broken chromosome ends and hence promotes ATR activation and homology-directed repair. It is likely that MutSβ also promotes ATR activation by ssDNA generated upon replication arrest or by processing of other types of DNA damage (Cimprich and Cortez, 2008). In support of this notion, it has been demonstrated that MSH2 is required for the formation of ATR/ATRIP foci in response to cisplatin that induces replisome stalling by forming intra- and inter-strand DNA crosslinks (Pabla et al., 2011). This study has also revealed that MSH2-deficient cells are resistant to cisplatin-induced apoptosis, which indicates a defect in ATR-mediated checkpoint signaling (Pabla et al., 2011).

A recent study has shown that the ATR-CHK1 pathway is also activated in G1 cells to maintain genomic integrity upon ionizing radiation-induced DNA damage (Gamper et al., 2013). This could explain our observation that MSH2 was recruited to sites of laser-induced DSBs not only in S/G2 cells, but also in G1 cells. Although multiple mechanisms exist to force DNA-end resection to occur only in S/G2 cells, there is accumulating evidence that DSBs arising in G1 cells are subjected to limited resection, yielding sufficient amounts of RPA-coated ssDNA for ATR activation (Balogun et al., 2013; Barlow et al., 2008; Gamper et al., 2013; Helmink et al., 2011; Yun and Hiom, 2009). Of note, we found that MSH2 recruitment to DSBs in G1 cells was dependent on the key resection factor CtIP, as was also the case for S/G2 cells (Figure 2A). Thus, it appears that MutSβ promotes ATR activation throughout the interphase.

The current model of ATR activation has been challenged by the finding that ATR phosphorylates CHK1 even when the binding of ATRIP to RPA-ssDNA is impaired by mutations in ATRIP, suggesting that ATRIP-RPA-ssDNA interaction is not absolutely essential for ATR activation (Ball et al., 2005). Our finding that MutSβ binds to RPA-ssDNA complexes *via* DNA secondary structures and promotes ATRIP recruitment helps resolve this discrepancy. We propose that MutSβ initially mediates binding of the ATR-ATRIP complex to RPA-coated ssDNA at sites of DNA damage and hence facilitates ATR activation by TOPBP1 towards phosphorylation of CHK1 and other ATR substrates (Figure 6). After ATR activation, the ATR-ATRIP complex could switch to a direct mode of binding to RPA-ssDNA involving the N-terminal region of ATRIP, which constitutes a major RPA-ssDNA-interacting domain of ATRIP (Ball et al., 2005; Namiki and Zou, 2006). In support of this notion, it has been shown that the direct interaction of ATRIP with RPA-ssDNA via this domain is required for accumulation of ATRIP at sites of DNA DSBs or stalled replication forks (Ball et al., 2005). It is possible that this switch in the mode of association

of ATR-ATRIP complex with RPA-coated ssDNA is regulated by the ATPase domains of MutSβ, as we found that, following ATRIP recruitment, MutSβ dissociated from RPA-ssDNA in an ATP-dependent manner, while ATRIP remained bound to it (Figure 5D and Supplemental Figure S5B and C). Moreover, we obtained evidence that the ATP-induced dissociation of MutSβ from RPA-ssDNA is dependent of ATP binding rather than hydrolysis (Figure 5C). Thus, we propose that a nucleotide-free form of MutSβ binds to DNA hairpin-loops persisting in RPA-coated ssDNA and as such promotes ATR-ATRIP recruitment (Figure 6). Subsequently, ATP binding by MutSβ triggers its dissociation from RPA-ssDNA reminiscent of the ATP-driven dissociation of MutSβ from the mismatch site, which is thought to be triggered by conformational changes in MutSβ subunits induced by ATP binding (Figure 6) (Wilson et al., 1999). However, we cannot rule out the possibility that ATR activation occurs after the switch to the direct mode of interaction between ATRIP and RPA-ssDNA (Figure 6). Of note, ATRIP contains two additional RPA-ssDNA-interacting domains that could play a role in such a case, especially in the absence of the N-terminal domain (Namiki and Zou, 2006). .

A recent study has identified the PRP19 ubiquitin ligase as a new component of the ATR signaling pathway (Marechal et al., 2014). PRP19 binds to RPA-ssDNA and facilitates accumulation of ATRIP at DNA damage sites by catalyzing the formation of K63-linked ubiquitin chains on RPA to which ATRIP directly binds (Marechal et al., 2014). Interestingly, the interaction of PRP19 with RPA at DNA damage sites is enhanced by ATR, suggesting that ATR-ATRIP and PRP19 constitute a mutually reinforcing forward loop to enhance the recruitment and/or retention of each other on RPA-ssDNA (Marechal et al., 2014). Based on our findings, we propose that MutSβ participates in this loop by mediating ATR-ATRIP recruitment to RPA-ssDNA. However, it is likely that a subset of ATR activation events in the cells is mediated via a direct, MutSβ-independent, recruitment of

ATR-ATRIP to RPA-ssDNA, as we have found that depletion of the MutSβ subunits did not completely abolish ATR-mediated phosphorylation of CHK1 and RPA in response to CPT. In support of this notion, purified ATR-ATRIP complex could efficiently phosphorylate CHK1 in a reconstituted system containing only RPA-ssDNA and TOPBP1 (Choi et al., 2010).

It should be noted that the S_N1-type alkylating agents producing O^6-methyl-G DNA adducts induce ATR-mediated checkpoint response in a manner requiring the MMR proteins MutSα and MutLα (Wang and Qin, 2003; Yoshioka et al., 2006). Interestingly, studies addressing the underlying mechanism provided evidence for a mode of ATR activation that does not include DNA processing to form RPA-coated ssDNA (Yoshioka et al., 2006). It has been shown that MutSα along with MutLα bind to O^6-methyl-G/T mismatches generated by replication O^6-methyl-G-containg DNA and serve as a scaffold for the recruitment of ATR-ATRIP and TOPBP1 to trigger ATR activation (Liu et al., 2009; Yoshioka et al., 2006). Direct interactions of MutSα with ATR and TOPBP1 and of MutLα with TOPBP1 have been demonstrated with purified proteins (Liu et al., 2009). Thus, these finding along with our data highlight a role for the MMR proteins in ATR targeting to sites of DNA damage *via* recognition of DNA structures that are similar to those these proteins recognize in the canonical MMR reaction. One key mechanistic difference between the ATR activation processes mediated by MutSα and MutSβ, respectively, is that the latter is independent of MutLα as we found that MLH1 was not required for ATR-dependent phosphorylation of RPA in response to CPT (Figure 3B and C). In the process of ATR activation by O^6-methyl-G/T mismatches, MutLα is likely to mediate the recruitment of TOPBP1 (Liu et al., 2009). Obviously, this activity is not needed in case of ATR activation on RPA-coated ssDNA where TOPBP1 can be loaded by the 9-1-1 or MRN complexes (Delacroix et al., 2007; Lee et al., 2007; Shiotani et al., 2013).

In conclusion, our study identifies the MMR factor MutSβ as a critical component of the ATR signaling cascade and provides new insights into the molecular mechanism underlying ATR activation by RPA-coated ssDNA. The recent discovery of synthetic lethal interaction between ATR and the ATM-p53 tumor suppressor pathway in cells exposed to DNA-damaging agents or replicative stress-generating conditions establishes ATR as a potential target for cancer therapy (Reaper et al., 2011; Toledo et al., 2011). There is no doubt that detailed knowledge of the molecular mechanism of ATR activation is a key for development of highly selective ATR inhibitors that can be used in combination with ionizing radiation and genotoxic drugs for treatment of p53-deficient tumors (Reaper et al., 2011; Toledo et al., 2011). In addition, it can be inferred from the above findings that the use of specific inhibitors of the ATM kinase could improve the efficacy and specificity of radio- and chemotherapy regimens for colorectal cancers associated with loss of MutSβ function (Peltomaki, 2001; Plaschke et al., 2004).

EXPERIMENTAL PROCEDURES

Antibodies, purified proteins, cell lines, DNA oligonucleotides and siRNAs

This information is provided in the Supplemental Experimental Procedures.

DR-GFP assay

DR-GFP reporter assays using HEK293/DR-GFP or U2OS/DR-GFP cells were performed as previously described (Bennardo et al., 2008; Gunn and Stark, 2012).

Laser microirradiation

In order to generate DSBs in defined nuclear compartments, a MMI CELLCUT system containing a 355 nm UVA laser (Molecular Machines & Industries) was used. Laser speed,

focus and intensity were all set to 50%. Prior to laser microirradiation, cells were grown on a 12 mm glass microscope coverslips (OmniLab) in a medium containing 10 μM bromodeoxyuridine (Sigma Aldrich) for 24 hours. The coverslips were transferred to microirradiation chambers (LAB-TEK) containing complete growth medium. After irradiation, cells were incubated at 37 °C for 30 min, fixed and immunostained as described below.

Immunofluorescence assays

Cells cultured on glass coverslips were fixed with 4 % (v/v) formaldehyde for 15 minutes at room temperature (RT) and subsequently permeabilized by soaking in 0.2 % (v/v) Triton X-100 for 5 minutes at RT, followed by a 30-min incubation in ice-cold methanol (only for laser-irradiated cells). Where required, before fixation, cells were pre-extracted for 5 min on ice in 25 mM HEPES (pH 7.4) containing 0.5 % (v/v) Triton X-100, 50 mM NaCl, 1 mM EDTA, 3 mM $MgCl_2$ and 0.3 M sucrose. Immunoflourescence staining and analysis were carried out as described in Supplemental Experimental Procedures.

Scan^R analysis

Automated image acquisition was performed using an Olympus IX70 microscope equipped with Scan^R imaging platform. 40×/1.3 NA objective was used. For RPA pSer4/8 intensity analysis, 225 images were acquired per sample. For RPA2 and ATRIP foci analysis, 10 z-stacks at a spacing of 0.3 μm were taken and 100 images were acquired for each sample. Analysis was performed using Scan^R analysis software based on signal intensity for RPA2 pSer4/8 or edge based sub-object counts for RPA2 and ATRIP foci. Nuclei were identified based on the DAPI signal. At least 1000 cells were analyzed for each condition.

In vitro kinase assays

Nuclear extracts were prepared as described in Supplemental Experimental Procedures. Reactions (15 µl) contained 10 µg of nuclear extract, 25-100 nM MutSβ or MutSα and 1 pmol of ssDNA (b90), and were started by addition of ATP to a final concentration of 1 mM. After incubation for 30 min at 37°C, reactions were stopped by addition of 4x SDS-PAGE loading buffer, boiled (5 min, 95 °C) and analyzed by western blotting.

Immunoprecipitation assays

HEK293 cells were transfected with pcDNA3.1-Flag-ATR (Tibbetts et al., 2000) and, 24 h later, with pLPCX-HA-ATRIP (Ball et al., 2005) using linear polyethyleneimine solution (Sigma). Cells were harvested 48 h after the first transfection and suspended in lysis buffer [50 mM Tris-HCl (pH 7.5), 150 mM NaCl, 10 mM β-glycerophosphate, 10 % (v/v) glycerol, 1 % (v/v) Tween-20, 0.1 % (v/v) Nonidet P-40, 2 mM $MgCl_2$] supplemented with protease and phosphatase inhibitors (Roche) and benzonase (50 U/ml; Merck). Cell lysates were sonicated and cleared by centrifugation at 16'000 g for 20 min at 4°C. Aliquots of the cell extracts containing 1 mg of protein were subjected to immunoprecipitation using anti-Flag M2 magnetic beads (10 µl; Sigma Aldrich) overnight at 4°C. Beads were washed 4 times with lysis buffer and bound proteins were eluted with SDS-PAGE loading buffer and analyzed by western blotting.

Affinity pull-down assays

Binding reactions (50 µl) were carried out in a buffer containing 50 mM Tris-HCl (pH 7.5), 120 mM NaCl and 0.1 % (v/v) Triton X-100. To form RPA-ssDNA complexes, 1 pmol of appropriate 5'-end-biotinylated oligonucleotide was incubated with 5 pmols of RPA for 30 min at RT. RPA or oligonucleotide alone were pre-incubated under the same conditions.

Reactions were then supplemented with indicated amounts of MutSα or MutSβ and incubated for one hour at 4°C. Finally Ni-NTA agarose beads (5 µl, Qiagen) or Streptavidin-coupled M280 Dynabeads (5 µl, Life Technologies) were added and incubation was continued for 30 min at 4°C. Beads were washed 4 times with binding buffer and bound proteins were eluted with SDS-PAGE loading buffer and analyzed by western blotting. Where indicated, ATP (2 mM), ATP-γ-S (2 mM) or ADP (2 mM) were added along with $MgCl_2$ (2 mM) at 60 min after MutSβ addition, and incubations were continued for 30 min at 4°C. EDTA was present at a concentration of 10 mM. In control reactions, MutSα/β was substituted with BSA.

For measurements of ATRIP binding to RPA-ssDNA, an extract of pLPCX-HA-ATRIP-transfected HEK293 cells was prepared as described for immunorecipitation assay except that $MgCl_2$ and benzonase were omitted in the lysis buffer. To form RPA-ssDNA complexes, Dynabeads (2.5 µl) pre-coated with 1 pmol of b90 oligonucleotide were incubated with 5 pmols of RPA for 30 min at RT. Where indicated, MutSβ was added and mixtures were incubated for additional 30 min at 4°C. Finally, the binding reactions were supplemented with HA-ATRIP-containing cell extract (250 µg of protein), and after incubation at 4°C for 30 min, beads were washed four times with lysis buffer. Bound proteins were eluted with SDS-PAGE loading buffer and analyzed by western blotting.

ACKNOWLEDGEMENTS

We thank Josef Jiricny, Jiri Bartek, Alessandro Sartori and Javier Pena Diaz for stimulating discussions and comments on the manuscript, David Cortez for pLPCX-HA-ATRIP construct, Randy Tibbetts for pcDNA3.1-Flag-ATR construct and Jeremy Stark for HEK293/DR-GFP and U2OS/DR-GFP cell lines. This work was supported by Czech Science Foundation (GAP305P305/10/0281), Oncosuisse (KLS-02344-02-2009), Novartis

Foundation for Medical and Biological Research (11A16), Cancer League of the Canton Zurich and Stiftung zur Krebsbekämpfung.

REFERENCES

Anantha, R.W., Vassin, V.M., and Borowiec, J.A. (2007). Sequential and synergistic modification of human RPA stimulates chromosomal DNA repair. J. Biol. Chem. *282*, 35910-35923.

Avemann, K., Knippers, R., Koller, T., and Sogo, J.M. (1988). Camptothecin, a specific inhibitor of type I DNA topoisomerase, induces DNA breakage at replication forks. Mol. Cell. Biol. *8*, 3026-3034.

Ball, H.L., Myers, J.S., and Cortez, D. (2005). ATRIP binding to replication protein A-single-stranded DNA promotes ATR-ATRIP localization but is dispensable for Chk1 phosphorylation. Mol. Biol. Cell. *16*, 2372-2381.

Balogun, F.O., Truman, A.W., and Kron, S.J. (2013). DNA resection proteins Sgs1 and Exo1 are required for G1 checkpoint activation in budding yeast. DNA Repair (Amst) *12*, 751-760.

Barlow, J.H., Lisby, M., and Rothstein, R. (2008). Differential regulation of the cellular response to DNA double-strand breaks in G1. Mol. Cell *30*, 73-85.

Bartek, J., and Lukas, J. (2003). Chk1 and Chk2 kinases in checkpoint control and cancer. Cancer Cell *3*, 421-429.

Bennardo, N., Cheng, A., Huang, N., and Stark, J.M. (2008). Alternative-NHEJ is a mechanistically distinct pathway of mammalian chromosome break repair. PLoS Genet. *4*, e1000110.

Bennardo, N., Gunn, A., Cheng, A., Hasty, P., and Stark, J.M. (2009). Limiting the persistence of a chromosome break diminishes its mutagenic potential. PLoS Genet. *5*, e1000683.

Britton, S., Coates, J., and Jackson, S.P. (2013). A new method for high-resolution imaging of Ku foci to decipher mechanisms of DNA double-strand break repair. J. Cell. Biol. *202*, 579-595.

Chen, W., and Jinks-Robertson, S. (1998). Mismatch repair proteins regulate heteroduplex formation during mitotic recombination in yeast. Mol. Cell. Biol. *18*, 6525-6537.

Choi, J.H., Lindsey-Boltz, L.A., Kemp, M., Mason, A.C., Wold, M.S., and Sancar, A. (2010). Reconstitution of RPA-covered single-stranded DNA-activated ATR-Chk1 signaling. Proc. Natl. Acad. Sci. USA *107*, 13660-13665.

Ciccia, A., and Elledge, S.J. (2010). The DNA damage response: making it safe to play with knives. Mol. Cell *40*, 179-204.

Cimprich, K.A., and Cortez, D. (2008). ATR: an essential regulator of genome integrity. Nat Rev Mol. Cell. Biol. *9*, 616-627.

Delacroix, S., Wagner, J.M., Kobayashi, M., Yamamoto, K., and Karnitz, L.M. (2007). The Rad9-Hus1-Rad1 (9-1-1) clamp activates checkpoint signaling via TopBP1. Genes Dev. *21*, 1472-1477.

Duursma, A.M., Driscoll, R., Elias, J.E., and Cimprich, K.A. (2013). A role for the MRN complex in ATR activation via TOPBP1 recruitment. Mol. Cell *50*, 116-122.

Fan, J., and Pavletich, N.P. (2012). Structure and conformational change of a replication protein A heterotrimer bound to ssDNA. Genes Dev. *26*, 2337-2347.

Franchitto, A., Pichierri, P., Piergentili, R., Crescenzi, M., Bignami, M., and Palitti, F. (2003). The mammalian mismatch repair protein MSH2 is required for correct MRE11 and RAD51 relocalization and for efficient cell cycle arrest induced by ionizing radiation in G2 phase. Oncogene *22*, 2110-2120.

Gamper, A.M., Rofougaran, R., Watkins, S.C., Greenberger, J.S., Beumer, J.H., and Bakkenist, C.J. (2013). ATR kinase activation in G1 phase facilitates the repair of ionizing radiation-induced DNA damage. Nucleic Acids Res. *41*, 10334-10344.

Gradia, S., Subramanian, D., Wilson, T., Acharya, S., Makhov, A., Griffith, J., and Fishel, R. (1999). hMSH2-hMSH6 forms a hydrolysis-independent sliding clamp on mismatched DNA. Mol. Cell *3*, 255-261.

Gravel, S., Chapman, J.R., Magill, C., and Jackson, S.P. (2008). DNA helicases Sgs1 and BLM promote DNA double-strand break resection. Genes Dev. *22*, 2767-2772.

Gunn, A., and Stark, J.M. (2012). I-SceI-based assays to examine distinct repair outcomes of mammalian chromosomal double strand breaks. Methods Mol. Biol. *920*, 379-391.

Habraken, Y., Sung, P., Prakash, L., and Prakash, S. (1996). Binding of insertion/deletion DNA mismatches by the heterodimer of yeast mismatch repair proteins MSH2 and MSH3. Curr. Biol. *6*, 1185-1187.

Hashimoto, Y., Tsujimura, T., Sugino, A., and Takisawa, H. (2006). The phosphorylated C-terminal domain of Xenopus Cut5 directly mediates ATR-dependent activation of Chk1. Genes Cells *11*, 993-1007.

Helmink, B.A., Tubbs, A.T., Dorsett, Y., Bednarski, J.J., Walker, L.M., Feng, Z., Sharma, G.G., McKinnon, P.J., Zhang, J., Bassing, C.H.*, et al.* (2011). H2AX prevents CtIP-mediated DNA end resection and aberrant repair in G1-phase lymphocytes. Nature *469*, 245-249.

Hong, Z., Jiang, J., Hashiguchi, K., Hoshi, M., Lan, L., and Yasui, A. (2008). Recruitment of mismatch repair proteins to the site of DNA damage in human cells. J. Cell. Sci. *121*, 3146-3154.

Jackson, S.P., and Bartek, J. (2009). The DNA-damage response in human biology and disease. Nature *461*, 1071-1078.

Jiricny, J. (2006). The multifaceted mismatch-repair system. Nat. Rev. Mol. Cell. Biol. *7*, 335-346.

Kumagai, A., Lee, J., Yoo, H.Y., and Dunphy, W.G. (2006). TopBP1 activates the ATR-ATRIP complex. Cell *124*, 943-955.

Kunkel, T.A., and Erie, D.A. (2005). DNA mismatch repair. Annu. Rev. Biochem. *74*, 681-710.

Lee, J., Kumagai, A., and Dunphy, W.G. (2007). The Rad9-Hus1-Rad1 checkpoint clamp regulates interaction of TopBP1 with ATR. J. Biol. Chem. *282*, 28036-28044.

Liu, Y., Fang, Y., Shao, H., Lindsey-Boltz, L., Sancar, A., and Modrich, P. (2009). Interactions of human mismatch repair proteins MutSalpha and MutLalpha with proteins of the ATR-Chk1 pathway. J. Biol. Chem. *285*, 5974-5982.

Marechal, A., Li, J.M., Ji, X.Y., Wu, C.S., Yazinski, S.A., Nguyen, H.D., Liu, S., Jimenez, A.E., Jin, J., and Zou, L. (2014). PRP19 transforms into a sensor of RPA-ssDNA after DNA damage and drives ATR activation via a ubiquitin-mediated circuitry. Mol. Cell *53*, 235-246.

Mordes, D.A., Glick, G.G., Zhao, R., and Cortez, D. (2008). TopBP1 activates ATR through ATRIP and a PIKK regulatory domain. Genes Dev. *22*, 1478-1489.

Namiki, Y., and Zou, L. (2006). ATRIP associates with replication protein A-coated ssDNA through multiple interactions. Proc. Natl. Acad. Sci. USA *103*, 580-585.

Pabla, N., Ma, Z., McIlhatton, M.A., Fishel, R., and Dong, Z. (2011). hMSH2 recruits ATR to DNA damage sites for activation during DNA damage-induced apoptosis. J. Biol. Chem. *286*, 10411-10418.

Palombo, F., Iaccarino, I., Nakajima, E., Ikejima, M., Shimada, T., and Jiricny, J. (1996). hMutSbeta, a heterodimer of hMSH2 and hMSH3, binds to insertion/deletion loops in DNA. Curr. Biol. *6*, 1181-1184.

Peltomaki, P. (2001). DNA mismatch repair and cancer. Mut. Res. *488*, 77-85.

Peterson, S.E., Li, Y., Wu-Baer, F., Chait, B.T., Baer, R., Yan, H., Gottesman, M.E., and Gautier, J. (2013). Activation of DSB processing requires phosphorylation of CtIP by ATR. Mol. Cell *49*, 657-667.

Pichierri, P., Franchitto, A., Piergentili, R., Colussi, C., and Palitti, F. (2001). Hypersensitivity to camptothecin in MSH2 deficient cells is correlated with a role for MSH2 protein in recombinational repair. Carcinogenesis *22*, 1781-1787.

Plaschke, J., Kruger, S., Jeske, B., Theissig, F., Kreuz, F.R., Pistorius, S., Saeger, H.D., Iaccarino, I., Marra, G., and Schackert, H.K. (2004). Loss of MSH3 protein expression is frequent in MLH1-deficient colorectal cancer and is associated with disease progression. Cancer Res. *64*, 864-870.

Reaper, P.M., Griffiths, M.R., Long, J.M., Charrier, J.D., Maccormick, S., Charlton, P.A., Golec, J.M., and Pollard, J.R. (2011). Selective killing of ATM- or p53-deficient cancer cells through inhibition of ATR. Nature Chem. Biol. *7*, 428-430.

San Filippo, J., Sung, P., and Klein, H. (2008). Mechanism of eukaryotic homologous recombination. Annu. Rev. Biochem. *77*, 229-257.

Sartori, A.A., Lukas, C., Coates, J., Mistrik, M., Fu, S., Bartek, J., Baer, R., Lukas, J., and Jackson, S.P. (2007). Human CtIP promotes DNA end resection. Nature *450*, 509-514.

Shiotani, B., Nguyen, H.D., Hakansson, P., Marechal, A., Tse, A., Tahara, H., and Zou, L. (2013). Two distinct modes of ATR activation orchestrated by Rad17 and Nbs1. Cell Rep. *3*, 1651-1662.

Symington, L.S., and Gautier, J. (2011). Double-strand break end resection and repair pathway choice. Annu. Rev. Genet. *45*, 247-271.

Tibbetts, R.S., Cortez, D., Brumbaugh, K.M., Scully, R., Livingston, D., Elledge, S.J., and Abraham, R.T. (2000). Functional interactions between BRCA1 and the checkpoint kinase ATR during genotoxic stress. Genes Dev. *14*, 2989-3002.

Toledo, L.I., Murga, M., Zur, R., Soria, R., Rodriguez, A., Martinez, S., Oyarzabal, J., Pastor, J., Bischoff, J.R., and Fernandez-Capetillo, O. (2011). A cell-based screen identifies ATR inhibitors with synthetic lethal properties for cancer-associated mutations. Nat. Struct. Mol. Biol. *18*, 721-727.

van Gent, D.C., and van der Burg, M. (2007). Non-homologous end-joining, a sticky affair. Oncogene *26*, 7731-7740.

van Oers, J.M., Edwards, Y., Chahwan, R., Zhang, W., Smith, C., Pechuan, X., Schaetzlein, S., Jin, B., Wang, Y., Bergman, A.*, et al.* (2013). The MutSbeta complex is a modulator of p53-driven tumorigenesis through its functions in both DNA double-strand break repair and mismatch repair. Oncogene.

Wang, H., Wang, H., Powell, S.N., Iliakis, G., and Wang, Y. (2004). ATR affecting cell radiosensitivity is dependent on homologous recombination repair but independent of nonhomologous end joining. Cancer Res. *64*, 7139-7143.

Wang, Y., and Qin, J. (2003). MSH2 and ATR form a signaling module and regulate two branches of the damage response to DNA methylation. Proc. Natl. Acad. Sci. USA *100*, 15387-15392.

Wilson, T., Guerrette, S., and Fishel, R. (1999). Dissociation of mismatch recognition and ATPase activity by hMSH2-hMSH3. J. Biol. Chem. *274*, 21659-21664.

Yoshioka, K., Yoshioka, Y., and Hsieh, P. (2006). ATR kinase activation mediated by MutSalpha and MutLalpha in response to cytotoxic O6-methylguanine adducts. Mol. Cell *22*, 501-510.

Yun, M.H., and Hiom, K. (2009). CtIP-BRCA1 modulates the choice of DNA double-strand-break repair pathway throughout the cell cycle. Nature *459*, 460-463.

Zou, L., Cortez, D., and Elledge, S.J. (2002). Regulation of ATR substrate selection by Rad17-dependent loading of Rad9 complexes onto chromatin. Genes Dev. *16*, 198-208.

Zou, L., and Elledge, S.J. (2003). Sensing DNA damage through ATRIP recognition of RPA-ssDNA complexes. Science *300*, 1542-1548.

FIGURE LEGENDS

Figure 1. Involvement of MSH2 and MSH3 in HR-mediated DSB repair. **(A)** Efficiency of HR-mediated repair of I-SceI-induced DSBs in HEK293/DR-GFP and U2OS/DR-GFP cells transfected with indicated siRNAs. Percentage of GFP-positive cells was measured by flow cytometry two days after transfection of I-SceI-expressing plasmid and taken as a measure of DSB repair efficiency. Values plotted represent relative repair efficiency calculated as a percentage of repair efficiency measured in mock-depleted cells (siLuc; 100%). The data are represented mean ± SEM. **(B)** Western blot analysis of extracts from HEK293/DR-GFP cells transfected with indicated siRNAs.

Figure 2. MSH2 is recruited to sites of DSBs during pre-synaptic phase of HR. **(A)** Indirect immunofluorescence imaging of MSH2, γ-H2AX and cyclin A in mock-, CtIP- and RAD51-depleted U2OS cells at 30 min after microirradiation with UVA laser. Cells were grown in the presence of 10 μM BrdU for 24 hours prior to laser microirradiation. Cells positive for cyclin A (dispersed nuclear staining) are in S/G2, whereas cells lacking cyclin A are in G1. DAPI was used to stain nuclei. **(B)** Quantitative analysis of immunofluorescence micrographs represented in (A). Percentage of irradiated cells (γ-H2AX lines) that contain RPA lines is plotted. **(C)** Indirect immunofluorescence imaging of MSH2, γ-H2AX and cyclin A in ATLD1 and ATLD1-MRE11 cells exposed to laser microirradiation. **(D)** Quantitative analysis of images represented in (C). For (B) and (D), the data are represented as mean ± SEM. In each experiment, at least 100 nuclei were analyzed.

Figure 3. Lack of MutSβ impairs ATR-dependent phosphorylation of RPA and CHK1 in response to replication-associated DSBs. **(A)** Formation of RPA2 foci in mock-, CtIP-,

MSH2-, MSH3- and MSH6-depleted U2OS cells treated with 1 μM camptothecin (CPT) for 1 h. *Left panel*: Representative images of mock-depleted (siLuc) cells positive (top) or negative (bottom) for γ-H2AX staining. *Right panel*: A graph showing percentage of γ-H2AX-positive cells with RPA foci determined for each sample using Olympus Scan^R screening station. Cells were subjected to Triton X-100 pre-extraction prior to formaldehyde fixation. DAPI was used to stain nuclei. **(B)** Western blot analysis of extracts of U2OS cells depleted of indicated proteins. Cells were either treated with 1 μM CPT for 1 hour (lane marked by "+") or left untreated. **(C)** Formation of Ser4/8-phophorylated form of RPA2 in mock-, CtIP-, MSH2-, MSH3- and MSH6-depleted U2OS cells after treatment with 1 μM CPT for 1 h. *Left panel*: Representative images of mock-depleted cells (siLuc) positive (top) or negative (bottom) for γ-H2AX staining. *Right panel*: A graph showing percentage of γ-H2AX-positive cells containing Ser4/8-phosphorylated RPA2 determined for each condition using Olympus Scan^R screening station. **(D)** Kinetics of CPT-induced phosphorylation of CHK1 in mock-, MSH3- and MSH6-depleted U2OS cells. Cells were treated with 1 μM CPT for indicated times. Whole cell extracts were analyzed by western blotting. **(E)** Effect of recombinant MutSα or MutSβ on ssDNA-induced phosphorylation of RPA and CHK1 in nuclear extract of HCT116 cells. MutSα and MutSβ were present at concentrations of 25, 50 and 100 nM, respectively. For (A) and (C), the data are represented as mean ± SEM.
See also Figure S1, S2 and S3.

Figure 4. MSH2 and MSH3 form complex with ATR and ATRIP and promote ATRIP recruitment to sites of DSBs in human cells. **(A)** Co-immunoprecipitation assay. HEK293 cells were transfected with plasmids expressing Flag-tagged ATR and HA-tagged ATRIP. Whole cell extracts from transfected and non-transfected cells were subjected to immunoprecipitation with anti-Flag M2 beads (α-Flag). Immunoprecipitates were analyzed

by western blotting using indicated antibodies. Bands corresponding to HA-ATRIP and endogenous ATRIP, respectively are indicated. **(B)** Formation of ATRIP foci in U2OS cells treated with 1 μM camptothecin (CPT) for 1 h. Representative images of cells that are positive (top) or negative (bottom) for γ-H2AX staining are shown. **(C)** Frequency of the formation of CPT-induced ATRIP foci in mock-, MSH2-, MSH3- and CtIP-depleted U2OS cells. Percentage of γ-H2AX-positive cells containing ATRIP foci was determined for each condition using Olympus Scan^R screening station. The data are represented as mean ± SEM. **(D)** Western blot analysis of extracts from U2OS cells transfected with indicated siRNAs.

See also Figure S4.

Figure 5. MutSβ binds to DNA secondary structures in RPA-ssDNA complexes and promotes ATRIP recruitment. **(A)** Binding of RPA (100 nM) to His-tagged MutSα or MutSβ (50 nM each) in the absence and the presence of 90-mer ssDNA (b90, 20 nM). RPA was preincubated with ssDNA before addition of MutS proteins. MutSα or MutSβ were captured with Ni-NTA beads and bound proteins were detected by western blotting. **(B)** Binding of MutSα or MutSβ (50 nM each) to biotinylated 90-mer ssDNA (b90, 20 nM) in the absence or the presence of RPA (100 nM). ssDNA oligonucleotide was incubated alone or pre-coated with RPA before addition of MutS proteins. ssDNA was captured with streptavidin beads and bound proteins detected by western blotting. **(C)** Effect of ATP on binding of MutSβ to RPA-coated ssDNA. Binding reactions were assembled and analyzed as in (B). ATP was present at a concentration of 2 mM. **(D)** Effect of MutSβ on binding of ATRIP to RPA-coated ssDNA. Biotinylated 90-mer ssDNA (b90, 20 nM) pre-coated with RPA (100 nM) was incubated with extract from HEK293 cells over-expressing HA-tagged ATRIP. Where indicated, MutSβ (25 nM) was added to RPA-ssDNA 30 min before the addition of the cell

extract. At indicated time points, protein-DNA complexes were isolated using streptavidin magnetic beads and analyzed by western blotting. **(E)** Graph showing data from quantitative analysis of ATRIP blots in (C), which was performed using Image J software. The values were normalized to the value obtained for the 30 min time point of binding reaction without MutSβ. The data are represented as mean ± SEM. **(F)** MutSβ (50 nM) binding to indicated biotinylated oligonucleoties (20 nM) precoated with RPA. Binding reactions were were carried and analyzed as in (C).

See also Figure S5 and S6.

Figure 6. Model for the role of MutSβ in ATR activation. MutSβ binds directly DNA hairpin structures persisting in RPA-coated single-stranded DNA (ssDNA) at sites of DNA damage and mediates recruitment of the ATR-ATRIP complex for its activation by TOPBP1. ATP binding by MutSβ triggers its dissociation from the complex allowing ATR-ATRIP to switch to a direct mode of binding to RPA-ssDNA, which is required for the retention of ATR-ATRIP at sites of DNA damage. ATR can be activated by TOPBP1 both before and after MutSβ dissociation.

Figure 1.

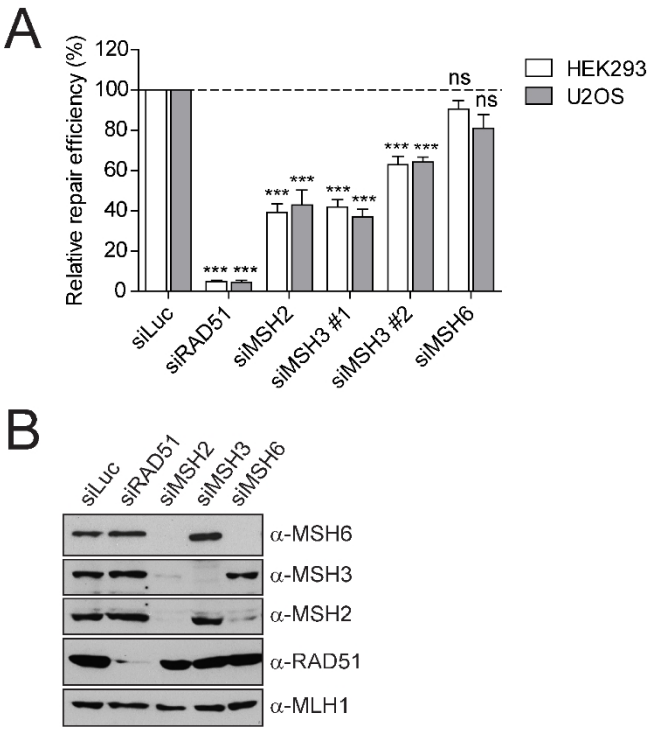
A
Relative repair efficiency (%)
120
100
80
60
40
20
0
HEK293
U2OS
ns
ns
***
siLuc
siRAD51
siMSH2
siMSH3 #1
siMSH3 #2
siMSH6
B
siLuc
siRAD51
siMSH2
siMSH3
siMSH6
α-MSH6
α-MSH3
α-MSH2
α-RAD51
α-MLH1

Figure 2.

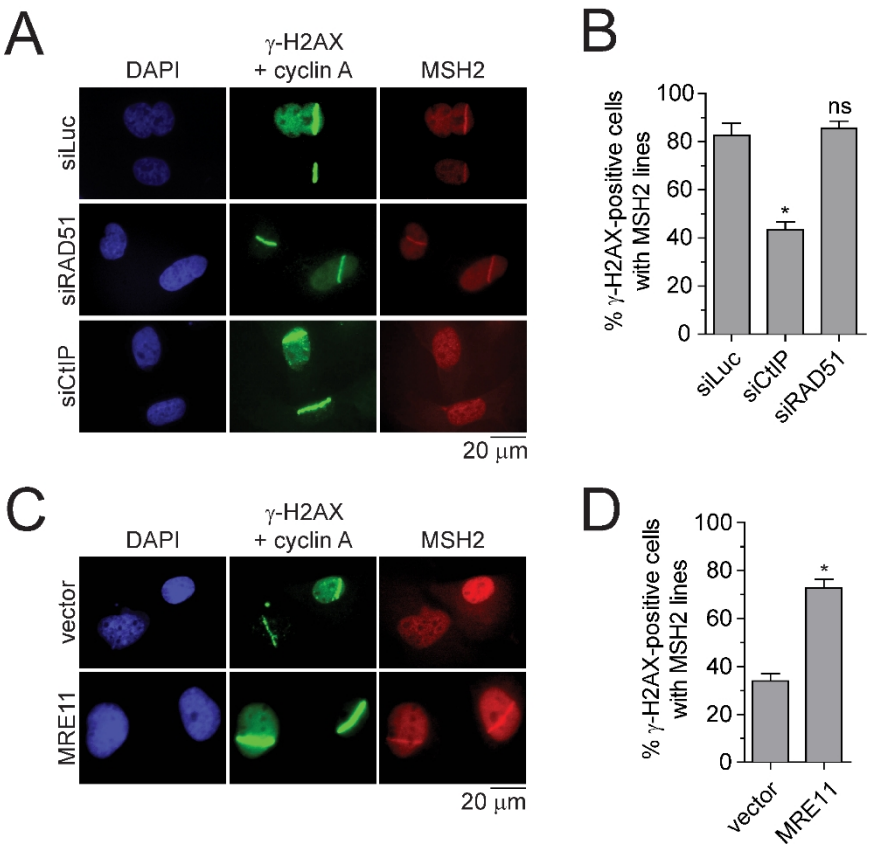
A
DAPI
γ-H2AX + cyclin A
MSH2
siLuc
siRAD51
siCtIP
20 μm
B
% γ-H2AX-positive cells with MSH2 lines
100
80
60
40
20
0
ns
*
siLuc
siCtIP
siRAD51
C
DAPI
γ-H2AX + cyclin A
MSH2
vector
MRE11
20 μm
D
% γ-H2AX-positive cells with MSH2 lines
100
80
60
40
20
0
*
vector
MRE11

Figure 3.

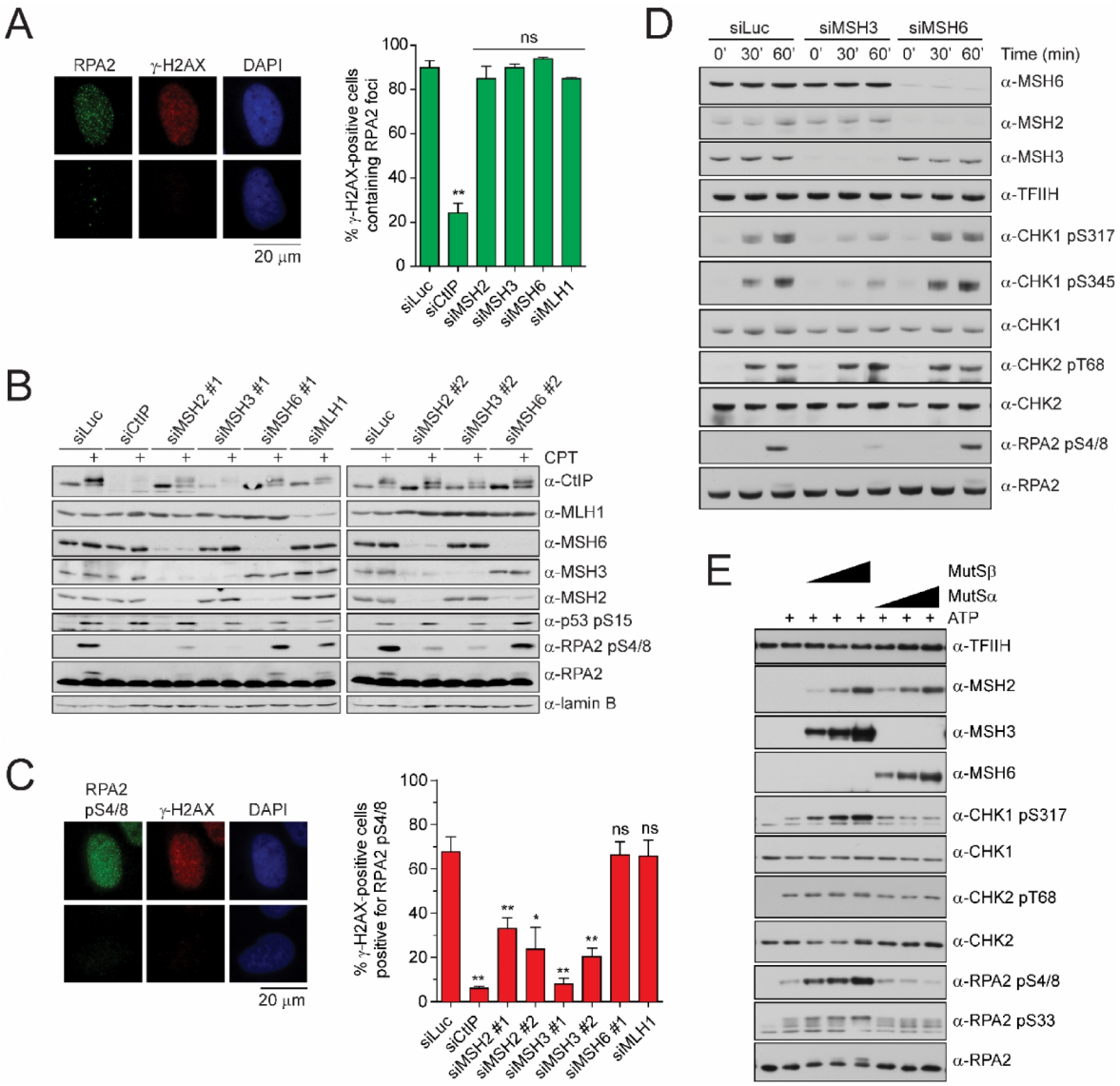
A
RPA2
γ-H2AX
DAPI
20 μm
% γ-H2AX-positive cells containing RPA2 foci
ns
siLuc
siCtIP
siMSH2
siMSH3
siMSH6
siMLH1
B
siLuc
siCtIP
siMSH2 #1
siMSH3 #1
siMSH6 #1
siMLH1
siMSH2 #2
siMSH3 #2
siMSH6 #2
CPT
α-CtIP
α-MLH1
α-MSH6
α-MSH3
α-MSH2
α-p53 pS15
α-RPA2 pS4/8
α-RPA2
α-lamin B
C
RPA2 pS4/8
γ-H2AX
DAPI
20 μm
% γ-H2AX-positive cells positive for RPA2 pS4/8
ns
D
siLuc
siMSH3
siMSH6
0' 30' 60' 0' 30' 60' 0' 30' 60'
Time (min)
α-MSH6
α-MSH2
α-MSH3
α-TFIIH
α-CHK1 pS317
α-CHK1 pS345
α-CHK1
α-CHK2 pT68
α-CHK2
α-RPA2 pS4/8
α-RPA2
E
MutSβ
MutSα
ATP
α-TFIIH
α-MSH2
α-MSH3
α-MSH6
α-CHK1 pS317
α-CHK1
α-CHK2 pT68
α-CHK2
α-RPA2 pS4/8
α-RPA2 pS33
α-RPA2

Figure 4.

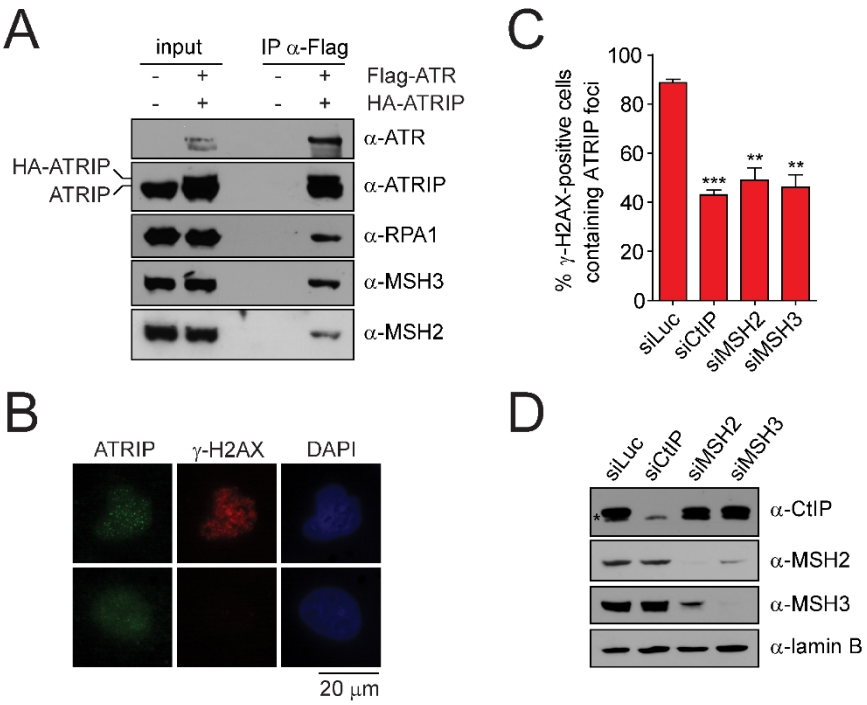
A
input
IP α-Flag
- + - +
Flag-ATR
- + - +
HA-ATRIP
HA-ATRIP
ATRIP
α-ATR
α-ATRIP
α-RPA1
α-MSH3
α-MSH2
C
% γ-H2AX-positive cells containing ATRIP foci
100
80
60
40
20
0
***
**
**
siLuc
siCtIP
siMSH2
siMSH3
B
ATRIP
γ-H2AX
DAPI
20 μm
D
siLuc
siCtIP
siMSH2
siMSH3
α-CtIP
α-MSH2
α-MSH3
α-lamin B

Figure 5.

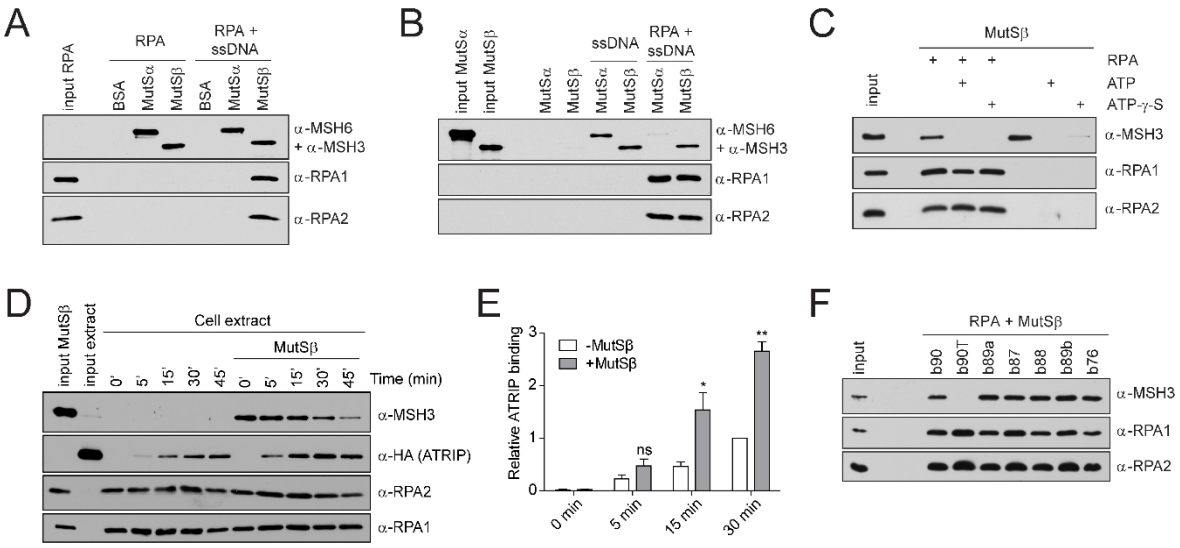
A
input RPA
RPA
RPA + ssDNA
BSA
MutSα
MutSβ
α-MSH6 + α-MSH3
α-RPA1
α-RPA2
B
input MutSα
input MutSβ
ssDNA
RPA + ssDNA
C
MutSβ
RPA
ATP
ATP-γ-S
input
α-MSH3
α-RPA1
α-RPA2
D
input MutSβ
input extract
Cell extract
MutSβ
Time (min)
α-MSH3
α-HA (ATRIP)
α-RPA2
α-RPA1
E
Relative ATRIP binding
-MutSβ
+MutSβ
ns
*
**
0 min
5 min
15 min
30 min
F
RPA + MutSβ
b90
b90T
b89a
b87
b88
b89b
b76

Figure 6.

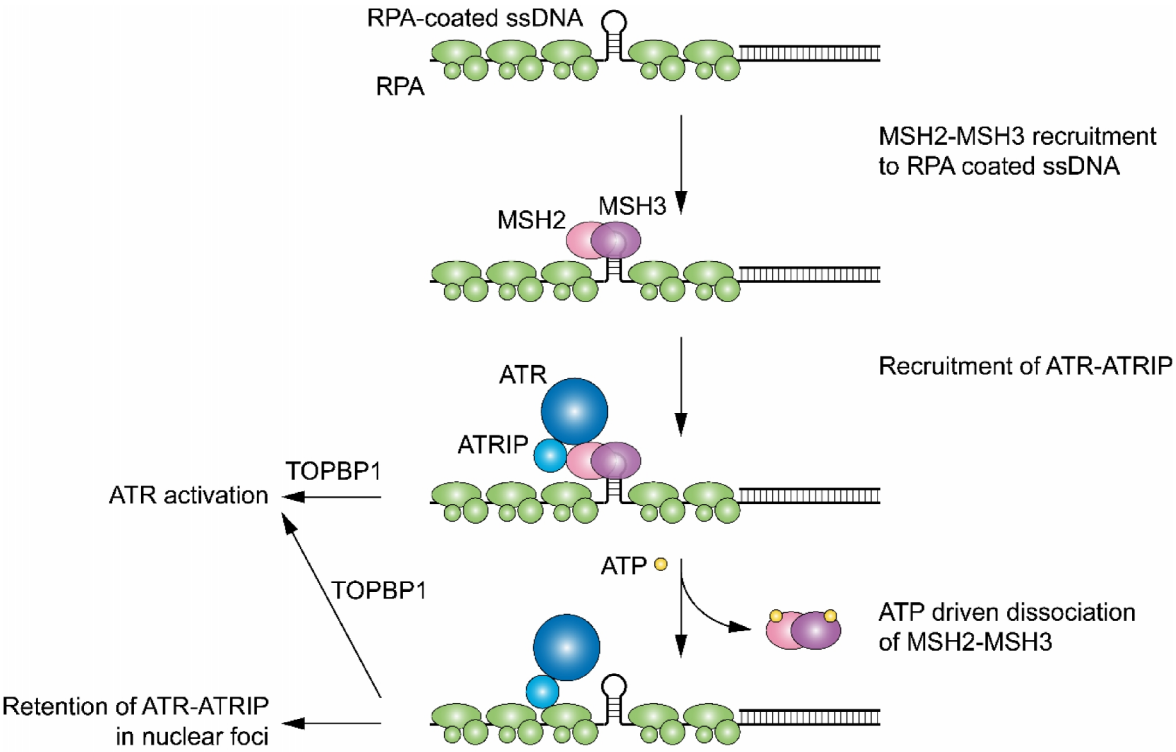
RPA-coated ssDNA
RPA
MSH2-MSH3 recruitment
to RPA coated ssDNA
MSH2
MSH3
Recruitment of ATR-ATRIP
ATR
ATRIP
TOPBP1
ATR activation
ATP
TOPBP1
ATP driven dissociation
of MSH2-MSH3
Retention of ATR-ATRIP
in nuclear foci

Supplemental Information

A role for the mismatch-binding factor MutSβ as a mediator of ATR activation in response to DNA double-strand breaks

Kamila Burdova, Boris Mihaljevic and Pavel Janscak

SUPPLEMENTAL INFORMATION INVENTORY

Burdova *et al.*, Figure S1

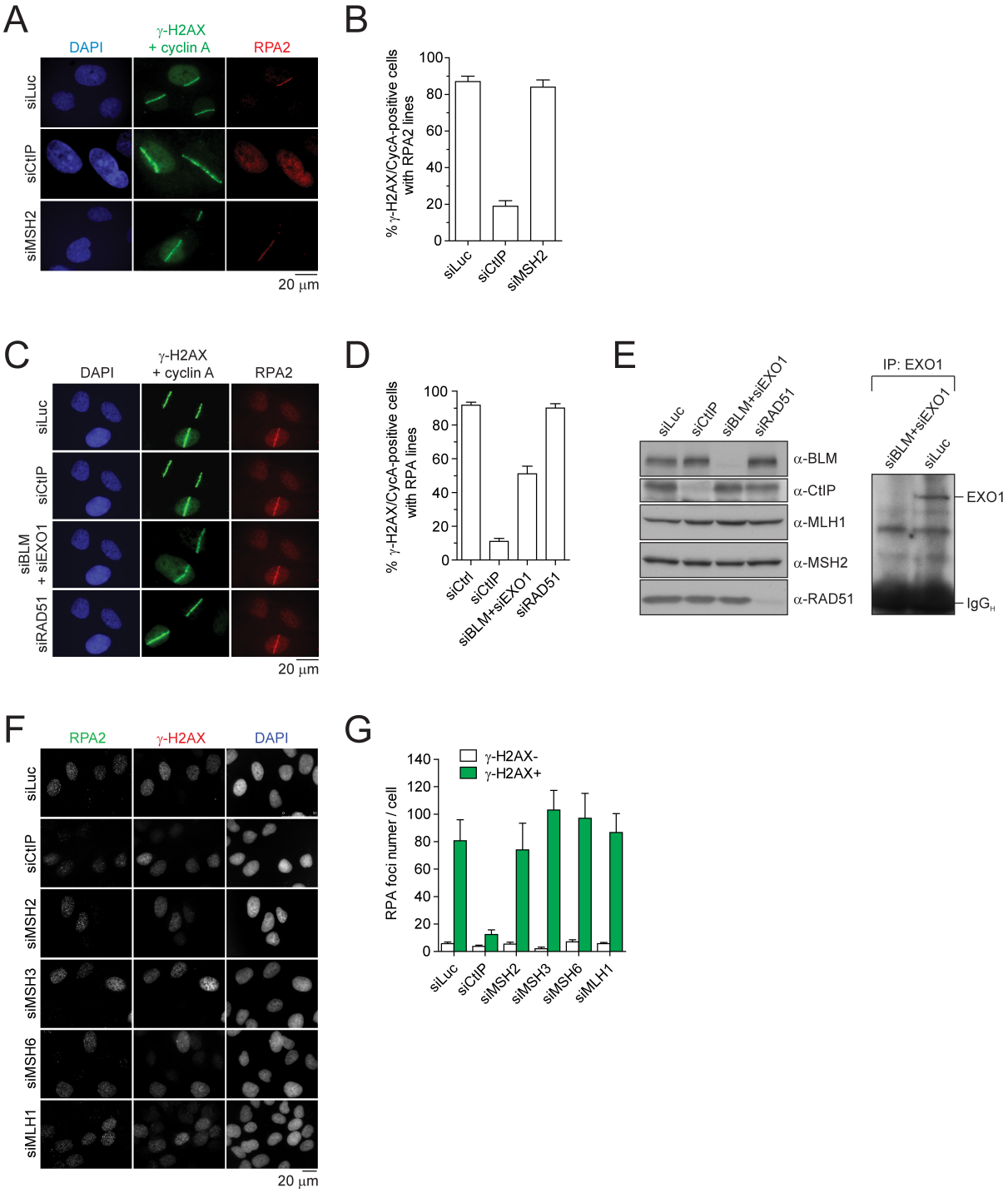

Burdova *et al.*, Figure S

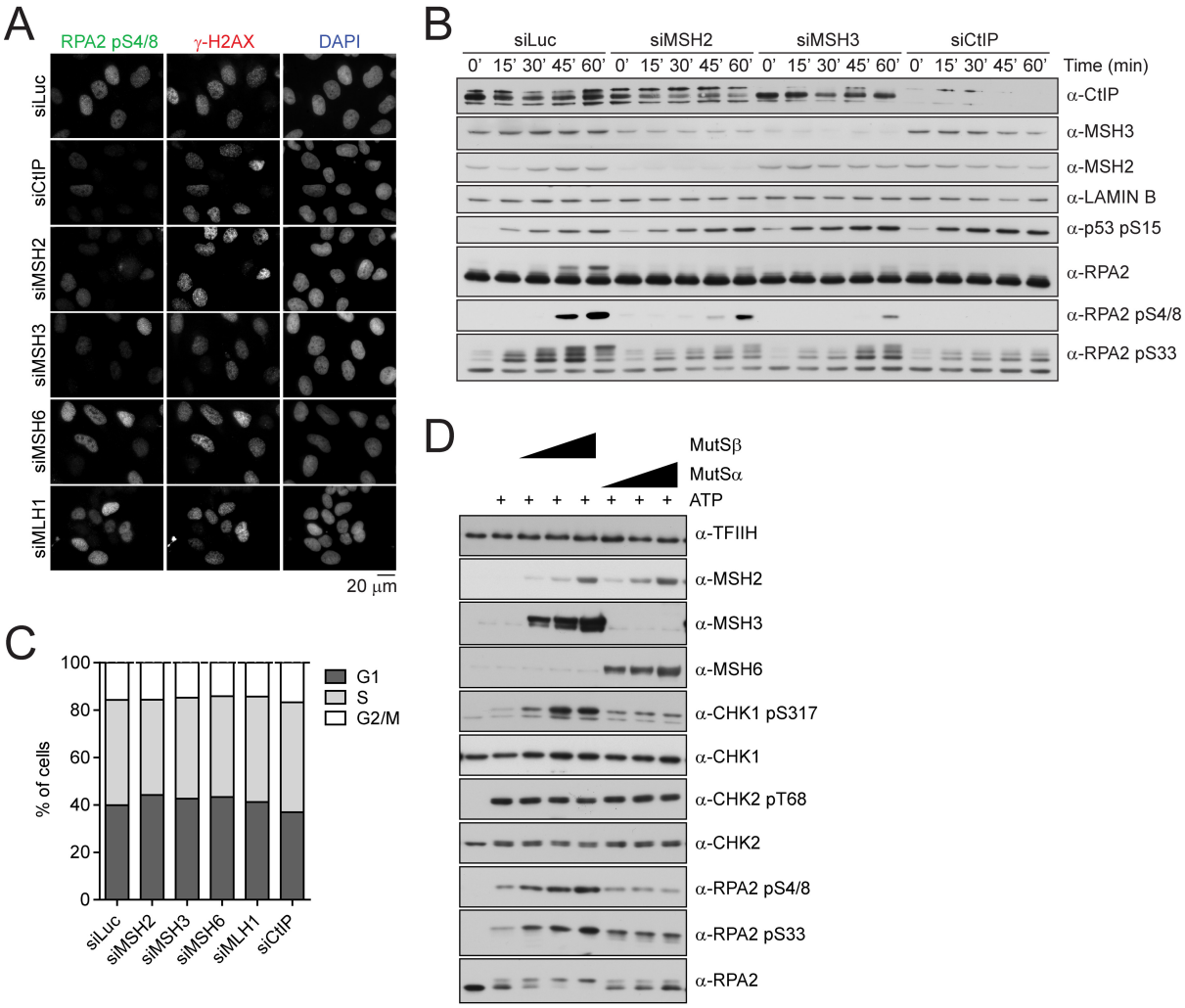

Burdova *et al.*, Figure S3

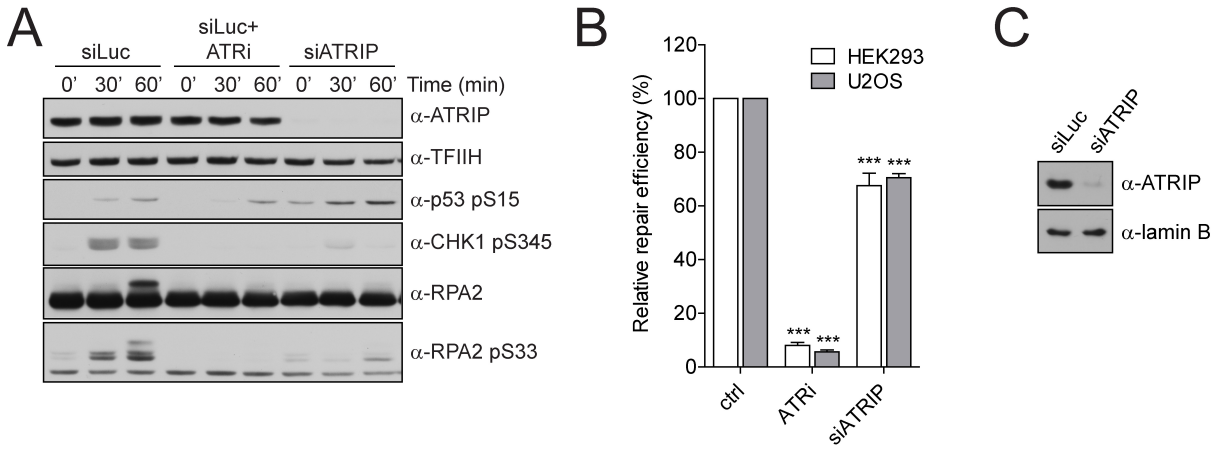

Burdova *et al.*, Figure S4

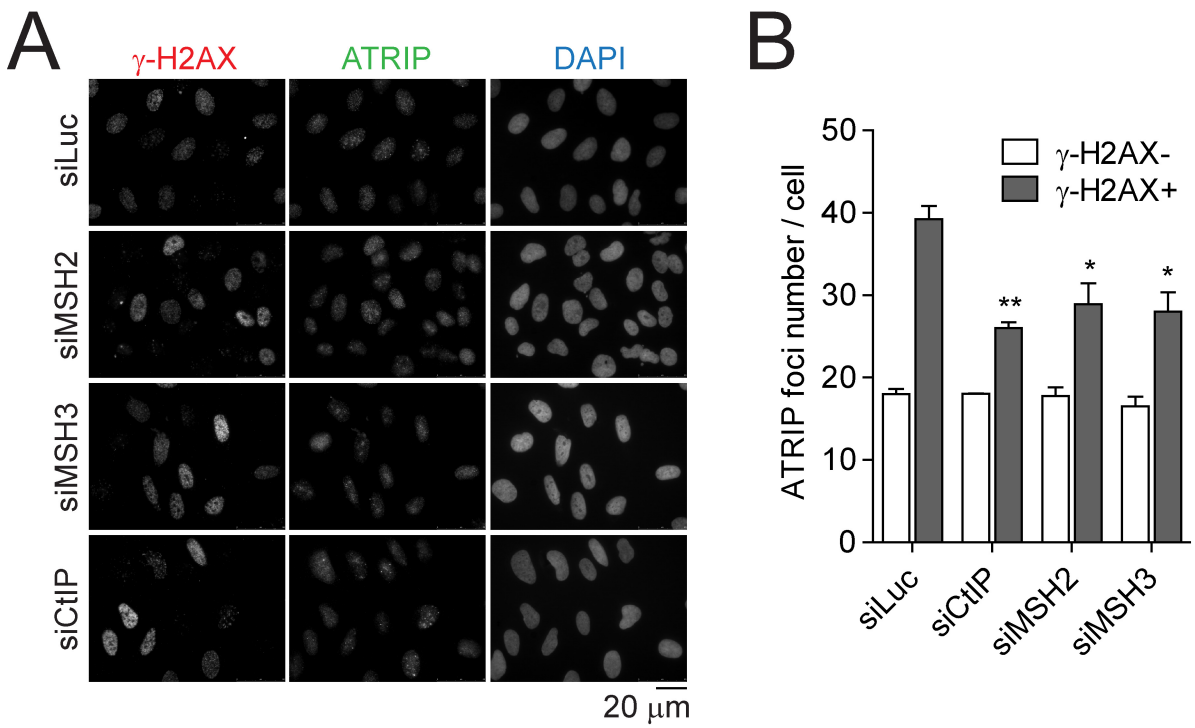

Burdova *et al.*, Figure S5

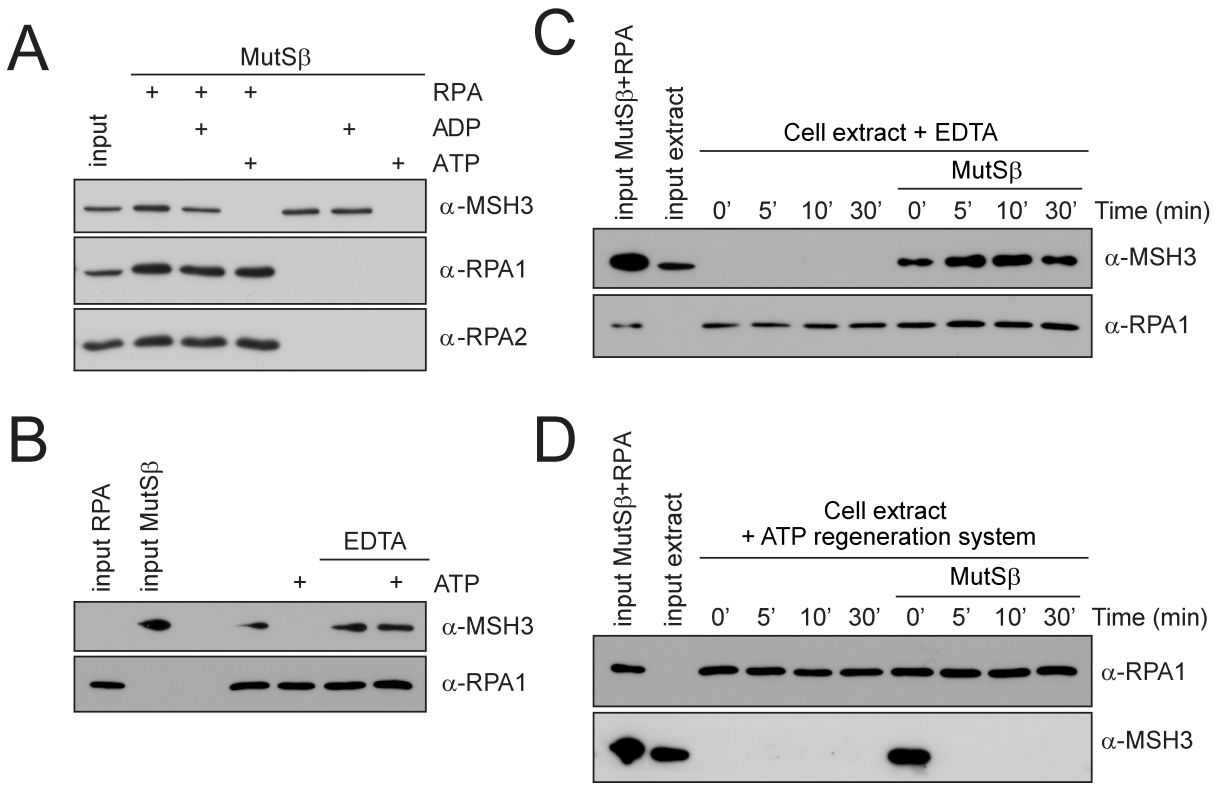

Burdova *et al.*, Figure S6

A

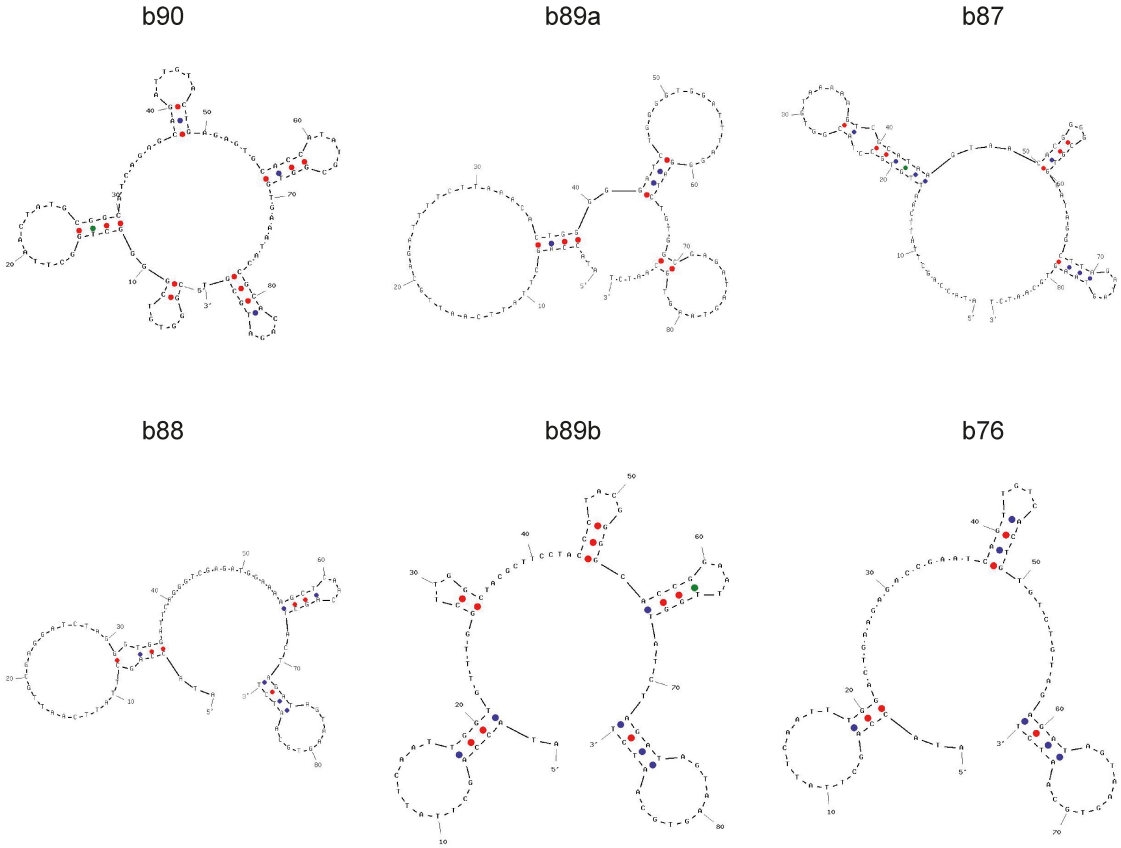

B

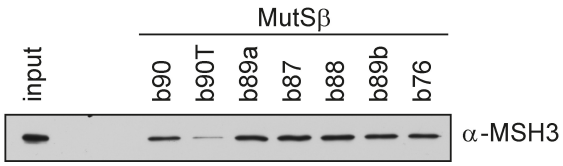

SUPLEMENTAL FIGURE LEGENDS

Figure S1. MMR proteins are not required for DSB end resection, related to Figure 3. (A) Indirect immunofluorescence imaging of RPA, γ-H2AX and cyclin A in U2OS cells subjected to laser microirradiation following siRNA-mediated depletion of CtIP (siCtIP), MSH2 (siMSH2) or mock-depletion (siLuc). DAPI was used to stain nuclei. (B) Graph showing data from quantitative analysis of immunofluorescence images represented in (A). Percentage of irradiated cells (γ-H2AX lines) that contain RPA lines is plotted. In each experiment, at least 100 nuclei were analyzed. (C) Indirect immunofluorescence imaging of RPA, γ-H2AX and cyclin A in U2OS cells subjected to laser microirradiation following depletion of CtIP (siCtIP), EXO1 and BLM (siEXO1+siBLM) or RAD51 (siRAD51), or following mock-depletion (siLuc). DAPI was used to stain nuclei. (D) Graph showing data from quantitative analysis of immunofluorescence images represented in (C). Percentage of irradiated cells (γ-H2AX lines) that contain RPA lines is plotted. At least 100 nuclei were analyzed in each experiment. (E) Western blot analysis of total extracts of U2OS cells (50 μg of protein) transfected with indicated siRNAs. Cells were harvested 72 hours post-transfection. EXO1 was concentrated by immunoprecipitation (IP, 1 mg of protein). (F) Representative immunofluorescence images of nuclei of mock-, CtIP-, MSH2-, MSH3- and MSH6-depleted U2OS cells stained for RPA and γ-H2AX after treatment with 1 μM CPT for 1 h. (G) Quantitative analysis of RPA foci in cells represented in (F). The number of RPA foci in γ-H2AX-negative and γ-H2AX-positive cells was determined using Olympus Scan^R screening station. For (B), (D) and (G), the data are represented as mean ± SEM.

Figure S2. MutSβ promotes ATR activation, related to Figure 3. (A) Representative immunofluorescence images of nuclei of mock-, CtIP-, MSH2-, MSH3- and MSH6-depleted

U2OS cells stained for pRPA Ser4/8 and γ-H2AX after treatment with 1 μM CPT for 1 h. A plot of data from quantitative analysis of these images is shown in Figure 3C. (B) Kinetics of CPT-induced phosphorylation of RPA in U2OS cells following siRNA-mediated depletion of MSH2, MSH3 or CtIP. Whole cell extracts were prepared and analyzed by western blotting using indicated antibodies. (C) Flow cytometry analysis of BrdU incorporation in U2OS cells transfected with indicated siRNAs. 10 μM BrdU was added 2 days after siRNA transfection for 30 minutes before cell fixation. BrdU incorporation was plotted against DNA content (propidium iodide) and cell cycle analysis was performed. The percentage of S phase (BrdU positive), G1 phase (BrdU negative, 2n) and G2-M phase (BrdU negative, 4n) cells is indicated. The data are represented as mean ± SEM. (D) Effect of recombinant MutSα (25-100 nM) or MutSβ (25-100 nM) on ssDNA-induced phosphorylation of RPA and CHK1 in nuclear extract of HeLa cells. *In vitro* kinase assay was performed as described under Experimental Procedures. Phosphorylation status of RPA, CHK1 and CHK2 was analyzed by western blotting using phosphospecific antibodies.

Figure S3. Loss of ATR function impairs checkpoint activation and HR-mediated DSB repair, related to Figure 3. (A) Effects of ATR inhibition and ATRIP depletion on CPT-induced phosphorylation of RPA and CHK1. U2OS cells were transfected either with control siRNA (siLuc) or with ATRIP siRNA (siATRIP) as described under Supplemental Experimental Procedures. Two days after second siRNA transfection, cells were treated with 1 μM CPT for 1 h. Where indicated, ATR inhibitor VE-821 (10 μM) was added 15 min prior to CPT. Total cell extracts were prepared and analyzed by western blotting using indicated antibodies. (B) Effect of ATR inhibition and ATRIP depletion on DSB repair by HR as determined by DR-GFP reporter assay. ATR inhibitor (10 μM) was added 15 min before transfection of I-SceI-expressing plasmid and present in the medium until harvest of cells.

The data are represented as mean ± SEM. (C) Western blot analysis of extracts from U2OS/DR-GFP cells transfected with indicated siRNAs. NT, non-treated; ATRi, ATR inhibitor, CPT, camptothecin.

Figure S4. MutSβ promotes ATRIP recruitment to sites of DSBs in human cells, related to Figure 4. (A) Representative immunofluorescence images of nuclei of mock-, MSH2-, MSH3-, CtIP-depleted U2OS cells stained for ATRIP and γ-H2AX after treatment with 1 μM CPT for 1 h. DAPI was used to stain nuclei. (B) Quantitative analysis of ATRIP foci in cells represented in (A). Number of ATRIP foci in nuclei of γ-H2AX-negative and γ-H2AX-positive cells was determined using Olympus Scan^R screening station. The data are represented as mean ± SEM.

Figure S5. MutSβ dissociation from RPA-coated ssDNA in the presence of ATP, related to Figure 5. (A) Effect of ATP and ADP on binding of MutSβ to RPA-coated ssDNA. Binding reactions were assembled and analyzed as in Figure 5C. ATP and ADP were present at a concentration of 2 mM. (B) ATP-induced dissociation of MutSβ from RPA-coated ssDNA is inhibited by EDTA. Biotinylated 90-mer oligonucleotide (b90, 20 nM) was pre-coated with RPA (100 nM) before addition of MutSβ complex. ssDNA was captured with streptavidin beads and supplemented or not with 10 mM EDTA before addition of 2 mM ATP. Bound proteins were detected by western blotting. (C) MutSβ binding to RPA-coated ssDNA in cell extracts is stabilized by EDTA. Biotinylated 90-mer oligonucleotide (b90, 20 nM) was pre-coated with RPA (100 nM) and incubated alone or with MutSβ (25 nM) before addition of extract from HEK293 cells supplemented with 10 mM EDTA. At indicated time points, protein-DNA complexes were isolated using streptavidin magnetic beads and analyzed by western blotting for the presence of MSH3 and RPA. (D) MutSβ dissociates

from RPA-coated ssDNA if ATP regeneration system is added to cell extract. Reactions were carried out and analyzed as in (C) except that cell extract was supplemented with 12 mM creatine phosphate, 10 U/ml creatine phosphokinase, 2 mM $MgCl_2$.

Figure S6. MutSβ binds preferentially to ssDNA forming secondary structures, related to Figure 5. (A) Schematic representation of the most probable hairpin structures formed by the oligonucleotides used in this study. DNA sequences were analyzes at http://eu.idtdna.com/analyzer/Applications/OligoAnalyzer/. (B) MutSβ (50 nM) binding to indicated biotinylated oligonucleoties (20 nM). Reactions were were carried out as decribed in Experimental Procedures. Bound proteins were detected by western blotting.

SUPPLEMENTAL EXPERIMENTAL PROCEDURES

Antibodies

Primary antibodies used for immunoblotting are as follows: mouse monoclonal anti-MSH2 (NA27, Oncogene); rabbit polyclonal anti-MSH3 (provided by Dr. Giancarlo Marra); mouse monoclonal anti-MSH6 (610919, BD Transduction Laboratories); mouse monoclonal anti-MLH1 (554073, BD Pharmingen); goat polyclonal anti-CtIP (Santa Cruz Biotechnology); rabbit polyclonal anti-CtIP (A300-488A, Bethyl Laboratories); rabbit polyclonal anti-RAD51 (sc-8349, Santa Cruz Biotechnology); rabbit polyclonal anti-RPA1 (A300-241A, Bethyl Laboratories); mouse monoclonal anti-RPA2 (NA19, Calbiochem); rabbit polyclonal anti-p53 pSer15 (#9284, Cell Signaling); rabbit polyclonal anti-RPA2 pSer4/8 (A300-245A, Bethyl Laboratories); rabbit polyclonal anti-RPA2 pSer33 (NB100-544, Novus); rabbit polyclonal anti-CHK1 pSer317 (#2344, Cell Signaling); rabbit polyclonal anti-CHK1 pSer345 (#2341, Cell Signaling); mouse monoclonal anti-CHK1 (sc-8408, Santa Cruz); mouse monoclonal anti-CHK2 (sc-17748, Santa Cruz); rabbit polyclonal anti-TFIIH (sc-293, Santa Cruz Biotechnology); mouse monoclonal anti-lamin B (NA12, Calbiochem); rabbit polyclonal anti-ATRIP (07-625, Millipore); mouse monoclonal anti-HA (mms-101R, Covance). Rabbit polyclonal anti-EXO1 antibody used for immunoprecipitation and immunoblotting was previously described (El-Shemerly et al., 2005). Primary and secondary antibodies used for immunofluorescence staining are listed at the end of this section.

Purified proteins

RPA was produced in bacteria and purified as described (Henricksen et al., 1994). MutSα and MutSβ heterodimers carrying a hexahistidine tag on MSH6 and MSH3, respectively, were produced in Sf9 insect cells by means of baculovirus system. Harvested cells were disrupted by Dounce homogenization in buffer A [50 mM Tris-HCl (pH 7.5), 0.25 M NaCl, 0.1 % (v/v)

Nonidet P-40, 10 % (v/v) glycerol] supplemented with 20 mM imidazole and protease inhibitors (cOmplete, Roche). MutSα and MutSβ were isolated from cell extracts using Ni-NTA beads (Qiagen). Bound proteins were eluted with 250 mM imidazol in buffer A and dialyzed against buffer B [50 mM Tris-HCl (pH 7.5), 0.2 M NaCl, 1 mM DTT, 0.1 mM EDTA, 25 % (v/v) glycerol].

Oligonucleotides

The 5'-end-biotinylated oligonucleotides used in this study were synthesized and PAGE-purified at Microsynth AG or Sigma. The sequences these oligonucleotides are shown in the following table:

Name	Length (nt)	Sequence (5' – 3')
b90	90	CGGGTGTCGGGGCTGGCTTAACTATGCGGCATCAGAGCAGATTGTACTGAGAGTGCACCATATGCGGTGTGAAATACCGCACAGATGCGT
b90dT	90	TTTTTTTTTTTTTTTTTTTTTTTTTTTTTTTTTTTTTTTTTTTTTTTTTTTTTTTTTTTTTTTTTTTTTTTTTTTTTTTTTTTTTTTTT
b87	87	ATACCAGCTTATTCAATTGTGCCTACGGTGTAAAAAGTCGCATAAGTAACACGGGGCGTGGATAGGCTTAGATAGTAAGTGCAATCT
b88	88	ATACCAGCTTATTCAATTGCGAGGATCTAGGGTGGATTCAGGGTCGAGATGGAAAAGCTCAACAGCTACTAGATAGTAAGTGCAATCT
b89a	89	ATACCAGCTTATTCAATTGCAGATTTTCTTAAACACTGGGGGATCTGGGGTGGATTTAGGGATCTGTGGCGAGATAGTAAGTGCAATCT
b89b	89	ATACCAGCTTATTCAATTGGTGTTTGGCTTGGCTACGCTTCCTACCCTACGGGGCACCGGAATTGGTATCTAGATAGTAAGTGCAATCT
b87	87	ATACCAGCTTATTCAATTACTACGGGGGCTTGCGGCTGCGCCGGGACTATCGCAAATAGTTGGGCGGGAAGATAGTAAGTGCAATCT
b76	76	ATACCAGCTTATTCAATTTGGACTGAAGAGACCGAATCAGTTGTCACTGTGTCTGTAGAGATAGTAAGTGCAATCT

Cell culture

U2OS, HeLa, HCT116 and HEK293 cells were grown in Dulbecco modified Eagle's medium (DMEM, Sigma Aldrich) supplemented with 10 % fetal calf serum (FCS, Life Technologies or Gibco) and streptomycin/penicillin (100 U/ml, Sigma Aldrich). Immortalized ATLD1 cells harboring retrovirus expressing wild-type MRE11 cDNA (ATLD1-MRE11) or corresponding empty vector were grown in DMEM supplemented with 20 % FCS, streptomycin/penicillin antibiotics (100 U/mL) and 1 μg/mL puromycin (Sigma Aldrich) (Carson et al., 2003). HCT116 cells carry homozygous frameshift mutations of the $[A]_8$ repeat in the exon 7 of the *MSH3* gene (Haugen et al., 2008).

siRNA and transfections

All small-interfering RNA (siRNA) oligoduplexes used in this study were purchased from Microsynth. The sequences of the sense strands of these siRNAs are shown below:

siCtrl: 5'-CGUACGCGGAAUACUUCGAdTdT-3'

siCtIP: 5'-UCCACAACAUAAUCCUAAUdTdT-3'

siRAD51: 5'-AAGGGAAUUAGUGAAGCCAAAdTdT-3'

siMSH2 #1: 5'-AAUCUGCAGAGUGUUGUGCUUdTdT-3'

siMSH2 #2: 5'-UCCAGGCAUGCUUGUGUUGAAdTdT-3'

siMSH3 #1: 5'-UCGAGUCGAAAGGAUGGAUAAdTdT-3'

siMSH3 #2: 5'-CAGCAAGGAGUUAUGGAUUAAdTdT-3'

siMSH6 #1: 5'-AUCGCCAUUGUUCGAGAUUUAdTdT-3'

siMSH6 #2: 5'-CAGCAGGGCUAUAAUGUAUGAdTdT-3'

MLH1: 5'-GUGGCUCAUGUUACUAUUACAdTdT-3'

siATRIP: 5'-AAGGUCCACAGAUUAUUAGAUdTdT-3'

Transfection of siRNA oligonucleotides (40 nM) was carried out using Lipofectamine RNAiMAX (Invitrogen) according to manufacturer's instructions. Cells were analyzed 48-72 h after siRNA transfection. For siATRIP, cells were re-transfected with 20 nM siRNA at 44 h after first transfection to enhance protein depletion efficiency.

Immunofluorescence staining and analysis

Cells cultured on glass coverslips were fixed with 4 % (v/v) formaldehyde for 15 minutes at room temperature (RT) and subsequently permeabilized by soaking in 0.2 % (v/v) Triton X-100 for 5 minutes at RT, followed by a 30-min incubation in ice-cold methanol (only for laser-irradiated cells). Where required, before fixation, cells were pre-extracted for 5 min on ice in 25 mM HEPES (pH 7.4) containing 0.5 % (v/v) Triton X-100, 50 mM NaCl, 1 mM EDTA, 3 mM $MgCl_2$ and 0.3 M sucrose. After blocking in PBS containing 10 mg/ml BSA for 30 min at RT, coverlips were incubated overnight at 4°C (laser-irradiated cells) or 2 hours at RT (CPT-treated cells) with appropriate primary antibodies. Incubations with secondary antibodies were carried out for 1-2 hours at RT. Coverslips were mounted using Vectashield containing DAPI (Vector Laboratories) and images were captured on an Olympus IX81 fluorescence microscope (laser-irradiated cells) or Leica DM6000 fluorescence microscope (CPT-treated cells).

Preparation of nuclear extracts

Nuclear extracts were prepared as previously described (Vidal-Eychenie et al., 2013). Briefly, HCT116 or HeLa cells were grown to near confluency and harvested by scraping to PBS. Cells were collected by centrifugation, resuspended in 5 volumes of hypotonic buffer A [10 mM HEPES-KOH (pH 7.9), 10 mM KCl, 1.5 mM $MgCl_2$, 0.5 mM DTT] supplemented with protease and phosphatase inhibitors (Roche) and incubated on ice for 5 min. Cells were spun

down, resuspended in 2 volumes of buffer A and lysed by Dounce homogenization using a tightly fitting pestle. Nuclei were collected by centrifugation at 4'000 g for 5 min at 4°C, resuspended in 1 volume of buffer B [20 mM HEPES-KOH (pH 7.9), 600 mM KCl, 1.5 mM $MgCl_2$, 0.2 mM EDTA, 25 % (v/v) glycerol, 0.5 mM DTT], supplemented with protease and phosphatase inhibitors (Roche) and kept at 4°C with over-head rotation for 30 min. After centrifugation (16'000 g for 15 min at 4 °C), supernatant was diluted using buffer C [20 mM HEPES-KOH (pH 7.9), 1.5 mM $MgCl_2$, 0.2 mM EDTA, 0.5 mM DTT] supplemented with protease and phosphatase inhibitors to a final KCl concentration of 100 mM. Extracts were incubated at 4°C for 30 min and cleared by centrifugation at 16'000 g for 30 min at 4 °C. Resulting nuclear fraction was aliquoted, snap freezed in liquid nitrogen and kept at -80 °C before use.

DR-GFP assay

HEK293/DR-GFP or U2OS/DR-GFP cells (Bennardo et al., 2008; Gunn and Stark, 2012) were transfected with 40 nM siRNA using Lipofectamine RNAiMAX. After 24 hours, siRNA-transfected cells were transferred into a 12-well plate, with 200'000 cells per well for HEK293/DR-GFP cell line and 150'000 cells per well for U2OS/DR-GFP cell line, respectively. At 44 hours after siRNA transfection, cells were transfected with 0.6 µg of the I-SceI expression vector pCBASce (Richardson et al., 1998) using linear polyethyleneimine solution (1 mg/ml), and 6 hours later with appropriate siRNA at a final concentration of 20 nM using standard calcium phosphate method. At 52 hours after I-SceI transfection, cells were harvested and subjected to FACS analysis using LSRII (BD Biosciences) and FlowJo software (Tree Star) to determine the percentage of GFP-positive cells.

BrdU incorporation analysis

BrdU was added to media to a final concentration of 10 μM for 30 min before harvesting the cells. Staining with FITC-conjugated α-BrdU antibody (347583, BD Biosciences) was done according to manufacturer's protocol. Flow cytometry analysis was performed using LSRII (BD Biosciences) and FlowJo software (Tree Star). BrdU incorporation was plotted against DNA content (propidium iodide) and the percentage of S phase (BrdU positive), G1 phase (BrdU negative, 2n) and G2-M phase (BrdU negative, 4n) cells was analyzed.

Statistical analysis

Data were analyzed in GraphPad Prism by two-tailed paired t-test with confidence interval of 95%. P-values smaller than 0.05 were marked *, p-values smaller than 0.005 were marked ** and p-values smaller than 0.0005 were marked ***.

List of antibodies used for immunofluorescence staining

Primary antibodies	**Secondary antibodies**
Camptothecin-treated cells	
Mouse monoclonal anti-RPA2 (NA19, Calbiochem) Rabbit monoclonal anti-γ-H2AX (#9718, Cell Signaling)	Alexa Fluor 488-conjugated goat anti-mouse IgG (A11029, Life Technologies) Texas Red-conjugated sheep anti-rabbit IgG (ab6793, Abcam)
Rabbit polyclonal anti-RPA2 pSer4/8 (A300-245A, Bethyl Laboratories) Mouse monoclonal anti-γ-H2AX (05-636, Millipore)	Alexa Fluor 488-conjugated goat polyclonal anti-rabbit (A11034, Life Technologies) Texas Red-conjugated sheep anti-mouse IgG (ab6806, Abcam)
Rabbit polyclonal anti-ATRIP (07-625, Millipore) Mouse monoclonal anti-γ-H2AX (05-636, Millipore)	Alexa Fluor 488-conjugated goat polyclonal anti-rabbit (A11034, Life Technologies) Alexa Fluor 568-conjugated goat polyclonal anti-mouse (A11031, Life Technologies)
Laser-microirradiated cells	
Mouse monoclonal anti-RPA2 (NA19, Calbiochem) Rabbit monoclonal anti-γ-H2AX (#9718, Cell Signaling)	Texas Red-conjugated anti-mouse IgG (Jackson Immunoresearch) FITC-conjugated anti-rabbit IgG (Jackson Immunoresearch)
Mouse monoclonal anti-MSH2 (NA27, Oncogene) Rabbit polyclonal anti-cyclin A (sc-751, Santa Cruz Biotechnology) Rabbit monoclonal anti-γ-H2AX (#9718, Cell Signaling)	Texas Red-conjugated anti-mouse IgG (Jackson Immunoresearch) FITC-conjugated anti-rabbit IgG (Jackson Immunoresearch)

SUPPLEMENTAL REFERENCES

Bennardo, N., Cheng, A., Huang, N., and Stark, J.M. (2008). Alternative-NHEJ is a mechanistically distinct pathway of mammalian chromosome break repair. PLoS Genet *4*, e1000110.

Carson, C.T., Schwartz, R.A., Stracker, T.H., Lilley, C.E., Lee, D.V., and Weitzman, M.D. (2003). The Mre11 complex is required for ATM activation and the G2/M checkpoint. EMBO J. *22*, 6610-6620.

El-Shemerly, M., Janscak, P., Hess, D., Jiricny, J., and Ferrari, S. (2005). Degradation of human exonuclease 1b upon DNA synthesis inhibition. Cancer Res. *65*, 3604-3609.

Gunn, A., and Stark, J.M. (2012). I-SceI-based assays to examine distinct repair outcomes of mammalian chromosomal double strand breaks. Methods Mol. Biol. *920*, 379-391.

Haugen, A.C., Goel, A., Yamada, K., Marra, G., Nguyen, T.P., Nagasaka, T., Kanazawa, S., Koike, J., Kikuchi, Y., Zhong, X.*, et al.* (2008). Genetic instability caused by loss of MutS homologue 3 in human colorectal cancer. Cancer Res. *68*, 8465-8472.

Henricksen, L.A., Umbricht, C.B., and Wold, M.S. (1994). Recombinant replication protein A: expression, complex formation, and functional characterization. J. Biol. Chem. *269*, 11121-11132.

Richardson, C., Moynahan, M.E., and Jasin, M. (1998). Double-strand break repair by interchromosomal recombination: suppression of chromosomal translocations. Genes Dev. *12*, 3831-3842.

Vidal-Eychenie, S., Decaillet, C., Basbous, J., and Constantinou, A. (2013). DNA structure-specific priming of ATR activation by DNA-PKcs. J. Cell. Biol. *202*, 421-429.

4 DISCUSSION

4.1 HUMAN RECQ HELICASES IN DNA REPAIR

4.1.1 Role of WRN Helicase in Oxidative Damage Repair

Oxidative damage of DNA is one of the most common problems that the cells have to deal with. The steady state level of 8-oxo-G lesions has been estimated to be about 10^3 lesions per cell per day (Klungland et al., 1999). Majority of oxidative DNA lesions are repaired by base excision repair. There is evidence that WRN helicase plays a role in oxidative damage repair as cells derived from Werner syndrome patients accumulate 8-oxo-G (Das et al., 2007; Von Kobbe et al., 2004). However, the function of WRN in oxidative damage repair has not been defined.

We show that in cells treated with hydrogen peroxide WRN accumulates on chromatin. Moreover, we found that WRN is recruited to 8-oxo-G sites in S phase cells by Polλ. Recruitment of both WRN and Polλ was replication dependent and was significantly decreased after depletion of MUTYH glycosylase that initiates repair of 8-oxo-G:A mispairs (van Loon and Hubscher, 2009). In agreement with previous studies, cells depleted of Polλ were sensitive to hydrogen peroxide (Braithwaite et al., 2010). Additionally, cells depleted of WRN exhibited about the same sensitivity to hydrogen peroxide as Polλ-depleted cells. This sensitivity was rescued by co-depletion of MUTYH, suggesting that WRN with Polλ are involved in MUTYH initiated 8-oxo-G:A mispairs repair.

Interestingly, the function of WRN in repair of oxidative DNA damage does not rely on its helicase or exonuclease activities, which is in concordance with the WRN mutation spectrum found in Werner syndrome patients (Kamath-Loeb et al., 2007). WRN was found to physically interact with FEN1 and stimulate FEN1-catalysed cleavage of 5'-flap structures that are formed after strand displacement synthesis by Polλ (Brosh et al., 2001). Similarly, we found that WRN physically interacts with Polλ and stimulates the bypass of 8-oxo-G by Polλ on gapped DNA duplex *in vitro*. Importantly, while Polλ is readily recruited to lesion-free and 8-oxo-G-containing substrates, WRN is bound only to latter substrate in a manner dependent on Polλ. Thus it is possible that there is a conformational change in the structure of Polλ upon its binding 8-oxo-G containing substrates that enables binding of WRN.

Cells derived from Werner syndrome patients display genomic instability. It has been suggested that telomere shortening is the main reason for genomic instability in these cells (Crabbe et al., 2007). Moreover, telomere shortening has been found to be accelerated after oxidative stress (von Zglinicki, 2002). Recently, Ogg1 knockout embryonic mouse fibroblasts were found to accumulate oxidative guanine lesions in telomeric region upon oxidative stress supporting the hypothesis that telomere integrity is compromised through induction of oxidative base damage (Wang et al., 2010). Thus it is possible that accelerated telomere shortening in cells derived from Werner syndrome patients also arise from decreased repair efficiency of oxidative damage.

4.1.2 RECQ5 Helicase Promotes SDSA subpathway in HR

HR in an important DNA damage repair pathway for maintenance of genome integrity to prevent chromosomal rearrangements or insertions/deletions induced by DSB repair pathways that do not rely on homology (e.g. NHEJ). However, HR can also lead to chromosomal rearrangements if the final step of double Holiday junction resolution leads to CO formation. Recent studies show that SDSA is the preferred subpathway of HR yielding only NCOs (Matos et al., 2011; Mitchel et al., 2010). The process of regulation of HR subpathway choice is well described in yeast but poorly understood in humans.

Srs2 and Mph1 helicases were found to promote SDSA in yeast (Ira et al., 2003; Krejci et al., 2003). There are two proposed human helicases that could play role in SDSA promotion: FBH1 and RECQ5. We firstly evaluated the effect of depletion of these proteins in cell-based reporter assay for monitoring efficiency of HR. In this system, only NCO events are seen as successful DSB repair by HR. Interestingly, only RECQ5 depletion resulted in decreased repair efficiency, while FBH1 depletion increased HR repair efficiency. Because the SSA repair pathway resembles postsynaptic stage of SDSA, we evaluated the roles of RECQ5, RAD51 and BRCA2 in this pathway again using cell-based reporter system. Depletion of BRCA2 or RAD51 resulted in increased SSA repair efficiency showing a direct inhibitory effect of RAD51 on SSA. Interestingly, RECQ5 depletion decreased SSA repair efficiency only in cells containing RAD51.

RECQ5 has been shown to physically interact with RAD51 having the ability to disrupt the ATP-bound form of RAD51-ssDNA filament (Hu et al., 2007; Schwendener et al., 2010).

For SDSA to proceed, extended D-loop has to be disrupted by action of DNA helicase, Srs2 or Mph1 in yeast (Ira et al., 2003; Krejci et al., 2003). It has been shown in yeast that presence of Rad51 inhibits annealing of DNA complementary strands even in the presence of Rad52 and RPA (Wu et al., 2008). We examined the effect of RAD51 on RAD52-mediated DNA annealing using human recombinant proteins and also saw inhibitory effect of RAD51. This inhibitory effect of RAD51 was opposed after addition of RECQ5, suggesting that RECQ5 might be involved in disruption of illegitimate RAD51 nucleofilaments formed after unwinding of D-loop, thus promoting repair by SDSA. Consistent with our finding, mouse *Recq5-/-* cells show persistence of Rad51 foci after camptothecin treatment (Hu et al., 2009; Hu et al., 2007). In agreement with observation that disruption of Recq5 in mice leads to increased levels chromosomal rearrangements, we observed increased number of SCEs in CPT-treated cell (Hu et al., 2007). Moreover, co-depletion of RECQ5 with BLM lead to further increase in number of SCEs implying that they act in two different pathways for suppression of CO formation. Our data suggest that RECQ5 promotes SDSA, possibly by disrupting illegitimate post-synaptic RAD51-ssDNA filaments. We propose that RECQ5 is the functional ortholog of Srs2 in human cells.

4.1.3 WRN Interacts with DNA2 during Long-Range Resection of DNA Ends at DSB Sites

Resection of DNA ends at sites of DSBs has been widely studied in yeast but the knowledge of human proteins involved in this process is limited. In the current model, there are two steps of 5’ to 3’ resection of DNA DSB ends. Firstly, ends of DNA are trimmed by the MRN/X complex in conjunction with CtIP/Sae2 (Longhese et al., 2010; Sartori et al., 2007). In this step, up to 100 bases are resected creating a 3’ overhang that inhibits NHEJ (Symington and Gautier, 2011). Two pathways mediate the second step of resection, reffered to as long-range resection. In yeast, these pathways involve Exo1 and Dna2 in conjunction with the Sgs1-Top3-Rmi1 complex, respectively (Cejka et al., 2010a; Mimitou and Symington, 2008; Nimonkar et al., 2011). In human cells, BLM has been suggested to be functional ortholog of Sgs1 in long-range resection (Nimonkar et al., 2011). However, depletion of WRN helicase in human cells was also found to negatively influence ssDNA

formation after ionizing irradiation (Tomimatsu et al., 2012). Experiments in *Xenopus laevis* extracts revealed stimulation of xDNA2 by xWRN helicase promoting DNA end resection (Liao et al., 2008; Toczylowski and Yan, 2006; Yan et al., 2005).

In contrast to study published by Kowalczykowski group that has shown that BLM but not WRN acts in conjunction with DNA2 in long range resection, we observed a more efficient 5' to 3' DNA end resection with WRN-DNA2 than with BLM-DNA2 complex (Nimonkar et al., 2011). As expected, this activity was dependent on the helicase activity of WRN and the endonuclease activity of DNA2. Moreover, we found that WRN physically interacts with DNA2 with about the same affinity as BLM.

To investigate the role of WRN and BLM helicases in DNA end resection in human cells, we employed cell based reporter system for detection of SSA repair efficiency as in this system, there is a need to resect 2.7 kb for repair to take place (Bennardo et al., 2008; Gunn and Stark, 2012). Depletion of DNA2, WRN, BLM and EXO1 resulted in decreased SSA repair efficiency in U2OS cells showing the role of these proteins in DNA end resection. In agreement with previous study, we saw that DNA2 and EXO1 work in two independent pathways of DNA resection (Karanja et al., 2012). Moreover, we found that either WRN or BLM act in conjunction with DNA2 in this process in U2OS cells. We also show, consistently with finding in yeast, that the helicase activity of BLM in DNA-catalyzed DNA end resection in stimulated by the TRR complex although this stimulation was only modest under our experimental conditions (Cejka et al., 2010a; Niu et al., 2010; Zhu et al., 2008). Interestingly, depletion of BLM in HEK293 cells led to an increase in SSA repair efficiency suggesting that BLM in complex with TRR could act as SSA suppressor in these cells. When comparing HEK293 and U2OS cells, we observed that BLM protein levels in HEK293 are much higher than in U2OS. Therefore it seems that BLM in complex with TRR suppresses SSA if its concentration exceeds certain threshold.

4.2 Mismatch-Repair Proteins in Double Strand Break Repair

Mismatch repair proteins have been previously shown to be present at DSBs induced by laser micro-irradiation. However, the role of MMR proteins in process of double strand break repair have not been investigated in detail (Hong et al., 2008; Liberti et al., 2010). It

has been demonstrated that Msh2 knock-out cells are hypersensitive to camptothecin (CPT) treatment and γ-irradiation (Franchitto et al., 2003; Pichierri et al., 2001). Moreover, Msh2 complementation in mouse knock-out cells increased DSB repair efficiency by HR (Bennardo et al., 2009). However, MSH2 protein is bound in two different complexes in human cells: with MSH3 and MSH6, and which of these complexes is involved in HR remains unclear. We have shown that MSH2 in complex with MSH3 stimulates repair of DSBs by HR. This result is supported by evidence that there is persistence of γ-H2AX foci after γ - irradiation in MSH3 knock-out cells (Takahashi et al., 2011; van Oers et al., 2013).

In yeast, Msh2-Msh3 complex has been shown to be involved in 3'ssDNA tail removal during SSA (Dowen et al., 2010). On the other hand, complementation of Msh2 knock-out cells had no effect on SSA efficiency in mouse embryonic fibroblasts (Bennardo et al., 2009). We have shown that in human cells, MSH2-MSH3 complex is recruited to DSBs during presynaptic stage of HR thus excluding the possibility that MSH2-MSH3 complex would only play role in 3'ssDNA tail removal.

To study the role of MSH2-MSH3 complex in HR, we employed CPT treatment as CPT induces DSBs specifically in replicating cells, and these are repaired exclusively by HR (Britton et al., 2013; Huang et al., 2008; Palitti, 1993). Using RNA interference, we demonstrated that MSH2 depletion does not affect DNA end resection at DSBs after CPT treatment or laser micro-irradiation. Interestingly, depletion of MSH2 and MSH3, but not MSH6, impaired RPA2 phosphorylation at Ser4/8 and Ser33 after CPT treatment. Moreover, we demonstrated that purified MSH2-MSH3, but not MSH2-MSH6, complex stimulated RPA phosphorylation in nuclear extracts prepared from HCT116 cells lacking MSH3 protein (Kantelinen et al., 2010). Phosphorylation of RPA in DSB repair has been shown to be a sequential process leading to hyper-phosphorylation of RPA2 subunit changing its DNA binding properties and preventing replication to continue in presence of DSBs (Anantha et al., 2007; Vassin et al., 2009; Vassin et al., 2004). Cyclin-dependent kinases are the first to phosphorylate RPA2 at S23 and T29 that are then followed by phosphorylation of S33 by ATR (Anantha et al., 2007; Olson et al., 2006). Finally, RPA is hyperphosphorylated at S4/8 by DNA-PKcs or ATM kinase (Liu et al., 2012). As we saw decreased phosphorylation at S33 in cells depleted for MSH2 and MSH3, we tested also phosphorylation status of other ATR substrates after DNA damage. Indeed, we found defect in phosphorylation of CHK1 at S345

and S317 but no difference in phosphorylation of CHK2 at T68 after CPT treatment. Moreover, purified MSH2-MSH3 complex could also stimulate CHK1 phosphorylation at S345 and S317 but not CHK2 phosphorylation at T68 in nuclear extracts. Role of MMR proteins in CHK1 and CHK2 phosphorylation has been studied before after treatment with different DNA damaging agents (Franchitto et al., 2003; Jiang et al., 2010; Pabla et al., 2011). It has been shown that MSH2 is necessary for both CHK1 and CHK2 phosphorylation after curcumin treatment but is dispensable for CHK1 phosphorylation after cis-platin treatment (Jiang et al., 2010; Pabla et al., 2011).

Consistent with finding that ATR-ATRIP complex interacts with MSH2 and that MSH2 is necessary for ATR foci formation after N-methyl-N'-nitro-N-nitrosoguanidine and cis-platin treatment, we found that MSH2-MSH3 complex interacts with ATR-ATRIP complex and is involved ATRIP foci formation after CPT treatment (Pabla et al., 2011; Wang and Qin, 2003).

Finally we found that MSH2-MSH3 complex but not MSH2-MSH6 binds specifically to DNA hairpin structures persisting in RPA-ssDNA complexes and stimulates ATRIP recruitment to RPA-coated ssDNA *in vitro*.

We proposed a model in which the MSH2-MSH3 complex binds to DNA secondary structrures formed in RPA-coated ssDNA generated by DNA end resection during HR, stimulate ATR/ATRIP recruitment and thus promote ATR activation.

5 CONCLUSIONS

5.1 WRN STIMULATES REPAIR OF 8-OXO-G:A MISPAIRS

Polλ recruits WRN to 8-oxo-G:A mispairs *in vitro*. WRN localizes to sites of oxidative damage in S phase cells and interacts with Polλ. Co-depletion of MUTYH glycosylase rescues sensitivity of WRN and Polλ depleted cells to hydrogen peroxide. WRN stimulates DNA repair synthesis activity of Polλ.

My contribution to this work: I performed cell fractionation and flow cytometry analysis of cell cycle.

5.2 RECQ5 PROMOTES SDSA SUBPATWAY OF HR IN HUMAN CELLS

RECQ5 promotes non-crossover product formation during HR in human cells. RECQ5 helicase counteracts the inhibitory effect of RAD51 on RAD52-mediated ssDNA annealing *in vitro*. Depletion of RECQ5 leads to accumulation of RAD51 at chromatin flanking the sites of DSBs.

My contribution to this work: I did some of the cell based reporter assays to monitor DNA damage repair and cell cycle analysis.

5.3 WRN INTERACTS WITH DNA2 DURING DNA END RESECTION AT DSBS

WRN-DNA2 resects DNA ends more efficiently than BLM-DNA2 *in vitro*. The helicase function of WRN and endonuclease activity are necessary for DNA end resection. WRN and DNA2 form complex *in vivo* and *in vitro*. Two long-range resection pathways exist in HEK293 cells: EXO1 and WRN-DNA2. BLM acts mainly as an antirecombinase in HEK293 cells. In U2OS cells, DNA2 cooperates with WRN or BLM in long-range resection. TopIIIα-RMI1-RMI2 complex stimulates BLM-DNA2 mediated DNA end resection *in vitro* and *in vivo*.

My contribution to this work: I performed the immunoprecipitation experiments from human cell extracts and all other cell based experiments (cell based reporter assays, immunoblotting, RNA isolation, qRT-PCR, and immunofluorescence staining followed fluorescence microscopy).

5.4 MSH2-MSH3 Complex Promotes ATR Activation and Repair of DNA Double-Strand Breaks

MSH2-MSH3 complex is involved in DSB repair by HR. MSH2-MSH3 interacts with ATR-ATRIP complex. MSH2-MSH3 stimulates ATR activation and promotes ATRIP foci formation after DNA damage. MSH2-MSH3 binds to DNA secondary structures in RPA-ssDNA complexes and promotes ATRIP recruitment.

My contribution to this work: I did all the experiments except for laser-microirradiation.

6 LIST OF METHODS

- Cloning and standard molecular biology techniques
- Recombinant protein expression and purification
- Tissue cultures, transfections, preparation of stable cell lines
- Cell based reporter assays
- Cell fractionation
- Kinase assays
- Immunocytochemistry and fluorescence microscopy
- Flow cytometry
- SDS-PAGE and immunoblotting
- Co-immunoprecipitations and pull-downs
- RNA isolation, cDNA synthesis and quantitative RT-PCR

7 REFERENCES

Anantha, R.W., Vassin, V.M., and Borowiec, J.A. (2007). Sequential and synergistic modification of human RPA stimulates chromosomal DNA repair. The Journal of biological chemistry *282*, 35910-35923.

Avkin, S., and Livneh, Z. (2002). Efficiency, specificity and DNA polymerase-dependence of translesion replication across the oxidative DNA lesion 8-oxoguanine in human cells. Mutation research *510*, 81-90.

Baynton, K., Otterlei, M., Bjoras, M., von Kobbe, C., Bohr, V.A., and Seeberg, E. (2003). WRN interacts physically and functionally with the recombination mediator protein RAD52. The Journal of biological chemistry *278*, 36476-36486.

Bennardo, N., Cheng, A., Huang, N., and Stark, J.M. (2008). Alternative-NHEJ is a mechanistically distinct pathway of mammalian chromosome break repair. PLoS genetics *4*, e1000110.

Bennardo, N., Gunn, A., Cheng, A., Hasty, P., and Stark, J.M. (2009). Limiting the persistence of a chromosome break diminishes its mutagenic potential. PLoS genetics *5*, e1000683.

Bernstein, K.A., Gangloff, S., and Rothstein, R. (2010). The RecQ DNA helicases in DNA repair. Annual review of genetics *44*, 393-417.

Bothmer, A., Rommel, P.C., Gazumyan, A., Polato, F., Reczek, C.R., Muellenbeck, M.F., Schaetzlein, S., Edelmann, W., Chen, P.L., Brosh, R.M., Jr.*, et al.* (2013). Mechanism of DNA resection during intrachromosomal recombination and immunoglobulin class switching. The Journal of experimental medicine *210*, 115-123.

Braithwaite, E.K., Kedar, P.S., Stumpo, D.J., Bertocci, B., Freedman, J.H., Samson, L.D., and Wilson, S.H. (2010). DNA polymerases beta and lambda mediate overlapping and independent roles in base excision repair in mouse embryonic fibroblasts. PloS one *5*, e12229.

Britton, S., Coates, J., and Jackson, S.P. (2013). A new method for high-resolution imaging of Ku foci to decipher mechanisms of DNA double-strand break repair. J Cell Biol *202*, 579-595.

Brosh, R.M., Jr., von Kobbe, C., Sommers, J.A., Karmakar, P., Opresko, P.L., Piotrowski, J., Dianova, I., Dianov, G.L., and Bohr, V.A. (2001). Werner syndrome protein interacts with human flap endonuclease 1 and stimulates its cleavage activity. The EMBO journal *20*, 5791-5801.

Bugreev, D.V., Yu, X., Egelman, E.H., and Mazin, A.V. (2007). Novel pro- and anti-recombination activities of the Bloom's syndrome helicase. Genes Dev *21*, 3085-3094.

Cannavo, E., Cejka, P., and Kowalczykowski, S.C. (2013). Relationship of DNA degradation by Saccharomyces cerevisiae exonuclease 1 and its stimulation by RPA and Mre11-Rad50-Xrs2 to DNA end resection. Proc Natl Acad Sci U S A *110*, E1661-1668.

Cejka, P., Cannavo, E., Polaczek, P., Masuda-Sasa, T., Pokharel, S., Campbell, J.L., and Kowalczykowski, S.C. (2010a). DNA end resection by Dna2-Sgs1-RPA and its stimulation by Top3-Rmi1 and Mre11-Rad50-Xrs2. Nature *467*, 112-116.
Cejka, P., Plank, J.L., Bachrati, C.Z., Hickson, I.D., and Kowalczykowski, S.C. (2010b). Rmi1 stimulates decatenation of double Holliday junctions during dissolution by Sgs1-Top3. Nat Struct Mol Biol *17*, 1377-1382.
Chapman, J.R., Barral, P., Vannier, J.B., Borel, V., Steger, M., Tomas-Loba, A., Sartori, A.A., Adams, I.R., Batista, F.D., and Boulton, S.J. (2013). RIF1 is essential for 53BP1-dependent nonhomologous end joining and suppression of DNA double-strand break resection. Mol Cell *49*, 858-871.
Choi, J.H., Lindsey-Boltz, L.A., Kemp, M., Mason, A.C., Wold, M.S., and Sancar, A. (2010). Reconstitution of RPA-covered single-stranded DNA-activated ATR-Chk1 signaling. Proc Natl Acad Sci U S A *107*, 13660-13665.
Cimprich, K.A., and Cortez, D. (2008). ATR: an essential regulator of genome integrity. Nature reviews. Molecular cell biology *9*, 616-627.
Cooper, M.P., Machwe, A., Orren, D.K., Brosh, R.M., Ramsden, D., and Bohr, V.A. (2000). Ku complex interacts with and stimulates the Werner protein. Genes Dev *14*, 907-912.
Crabbe, L., Jauch, A., Naeger, C.M., Holtgreve-Grez, H., and Karlseder, J. (2007). Telomere dysfunction as a cause of genomic instability in Werner syndrome. Proc Natl Acad Sci U S A *104*, 2205-2210.
Croteau, D.L., Popuri, V., Opresko, P.L., and Bohr, V.A. (2014). Human RecQ helicases in DNA repair, recombination, and replication. Annual review of biochemistry *83*, 519-552.
Das, A., Boldogh, I., Lee, J.W., Harrigan, J.A., Hegde, M.L., Piotrowski, J., de Souza Pinto, N., Ramos, W., Greenberg, M.M., Hazra, T.K.*, et al.* (2007). The human Werner syndrome protein stimulates repair of oxidative DNA base damage by the DNA glycosylase NEIL1. The Journal of biological chemistry *282*, 26591-26602.
Decottignies, A. (2013). Alternative end-joining mechanisms: a historical perspective. Frontiers in genetics *4*, 48.
Delacroix, S., Wagner, J.M., Kobayashi, M., Yamamoto, K., and Karnitz, L.M. (2007). The Rad9-Hus1-Rad1 (9-1-1) clamp activates checkpoint signaling via TopBP1. Genes Dev *21*, 1472-1477.
Di Virgilio, M., Callen, E., Yamane, A., Zhang, W., Jankovic, M., Gitlin, A.D., Feldhahn, N., Resch, W., Oliveira, T.Y., Chait, B.T.*, et al.* (2013). Rif1 prevents resection of DNA breaks and promotes immunoglobulin class switching. Science *339*, 711-715.
Dowen, J.M., Putnam, C.D., and Kolodner, R.D. (2010). Functional studies and homology modeling of Msh2-Msh3 predict that mispair recognition involves DNA bending and strand separation. Molecular and cellular biology *30*, 3321-3328.
Duursma, A.M., Driscoll, R., Elias, J.E., and Cimprich, K.A. (2013). A role for the MRN complex in ATR activation via TOPBP1 recruitment. Mol Cell *50*, 116-122.

Escribano-Diaz, C., Orthwein, A., Fradet-Turcotte, A., Xing, M., Young, J.T., Tkac, J., Cook, M.A., Rosebrock, A.P., Munro, M., Canny, M.D.*, et al.* (2013). A cell cycle-dependent regulatory circuit composed of 53BP1-RIF1 and BRCA1-CtIP controls DNA repair pathway choice. Mol Cell *49*, 872-883.

Fortini, P., and Dogliotti, E. (2007). Base damage and single-strand break repair: mechanisms and functional significance of short- and long-patch repair subpathways. DNA repair *6*, 398-409.

Franchitto, A., Pichierri, P., Piergentili, R., Crescenzi, M., Bignami, M., and Palitti, F. (2003). The mammalian mismatch repair protein MSH2 is required for correct MRE11 and RAD51 relocalization and for efficient cell cycle arrest induced by ionizing radiation in G2 phase. Oncogene *22*, 2110-2120.

Fugger, K., Mistrik, M., Danielsen, J.R., Dinant, C., Falck, J., Bartek, J., Lukas, J., and Mailand, N. (2009). Human Fbh1 helicase contributes to genome maintenance via pro- and anti-recombinase activities. J Cell Biol *186*, 655-663.

Goodarzi, A.A., Jeggo, P., and Lobrich, M. (2010). The influence of heterochromatin on DNA double strand break repair: Getting the strong, silent type to relax. DNA repair *9*, 1273-1282.

Goodarzi, A.A., and Jeggo, P.A. (2013). The repair and signaling responses to DNA double-strand breaks. Advances in genetics *82*, 1-45.

Gravel, S., Chapman, J.R., Magill, C., and Jackson, S.P. (2008). DNA helicases Sgs1 and BLM promote DNA double-strand break resection. Genes Dev *22*, 2767-2772.

Gunn, A., and Stark, J.M. (2012). I-SceI-based assays to examine distinct repair outcomes of mammalian chromosomal double strand breaks. Methods Mol Biol *920*, 379-391.

Hashimoto, Y., Tsujimura, T., Sugino, A., and Takisawa, H. (2006). The phosphorylated C-terminal domain of Xenopus Cut5 directly mediates ATR-dependent activation of Chk1. Genes to cells : devoted to molecular & cellular mechanisms *11*, 993-1007.

Hayashi, H., Tominaga, Y., Hirano, S., McKenna, A.E., Nakabeppu, Y., and Matsumoto, Y. (2002). Replication-associated repair of adenine:8-oxoguanine mispairs by MYH. Current biology : CB *12*, 335-339.

Hazra, T.K., Das, A., Das, S., Choudhury, S., Kow, Y.W., and Roy, R. (2007). Oxidative DNA damage repair in mammalian cells: a new perspective. DNA repair *6*, 470-480.

Heyer, W.D., Ehmsen, K.T., and Liu, J. (2010). Regulation of homologous recombination in eukaryotes. Annual review of genetics *44*, 113-139.

Hoeijmakers, J.H. (2001). Genome maintenance mechanisms for preventing cancer. Nature *411*, 366-374.

Hong, Z., Jiang, J., Hashiguchi, K., Hoshi, M., Lan, L., and Yasui, A. (2008). Recruitment of mismatch repair proteins to the site of DNA damage in human cells. J Cell Sci *121*, 3146-3154.

Hu, Y., Lu, X., Barnes, E., Yan, M., Lou, H., and Luo, G. (2005). Recql5 and Blm RecQ DNA helicases have nonredundant roles in suppressing crossovers. Molecular and cellular biology *25*, 3431-3442.
Hu, Y., Lu, X., Zhou, G., Barnes, E.L., and Luo, G. (2009). Recql5 plays an important role in DNA replication and cell survival after camptothecin treatment. Molecular biology of the cell *20*, 114-123.
Hu, Y., Raynard, S., Sehorn, M.G., Lu, X., Bussen, W., Zheng, L., Stark, J.M., Barnes, E.L., Chi, P., Janscak, P.*, et al.* (2007). RECQL5/Recql5 helicase regulates homologous recombination and suppresses tumor formation via disruption of Rad51 presynaptic filaments. Genes Dev *21*, 3073-3084.
Huang, M., Miao, Z.H., Zhu, H., Cai, Y.J., Lu, W., and Ding, J. (2008). Chk1 and Chk2 are differentially involved in homologous recombination repair and cell cycle arrest in response to DNA double-strand breaks induced by camptothecins. Mol Cancer Ther *7*, 1440-1449.
Ira, G., Malkova, A., Liberi, G., Foiani, M., and Haber, J.E. (2003). Srs2 and Sgs1-Top3 suppress crossovers during double-strand break repair in yeast. Cell *115*, 401-411.
Islam, M.N., Paquet, N., Fox, D., 3rd, Dray, E., Zheng, X.F., Klein, H., Sung, P., and Wang, W. (2012). A variant of the breast cancer type 2 susceptibility protein (BRC) repeat is essential for the RECQL5 helicase to interact with RAD51 recombinase for genome stabilization. The Journal of biological chemistry *287*, 23808-23818.
Jacobs, A.L., and Schar, P. (2012). DNA glycosylases: in DNA repair and beyond. Chromosoma *121*, 1-20.
Jiang, Z., Jin, S., Yalowich, J.C., Brown, K.D., and Rajasekaran, B. (2010). The mismatch repair system modulates curcumin sensitivity through induction of DNA strand breaks and activation of G2-M checkpoint. Mol Cancer Ther *9*, 558-568.
Jiricny, J. (2006). The multifaceted mismatch-repair system. Nature reviews. Molecular cell biology *7*, 335-346.
Kamath-Loeb, A.S., Lan, L., Nakajima, S., Yasui, A., and Loeb, L.A. (2007). Werner syndrome protein interacts functionally with translesion DNA polymerases. Proc Natl Acad Sci U S A *104*, 10394-10399.
Kantelinen, J., Kansikas, M., Korhonen, M.K., Ollila, S., Heinimann, K., Kariola, R., and Nystrom, M. (2010). MutSbeta exceeds MutSalpha in dinucleotide loop repair. British journal of cancer *102*, 1068-1073.
Karanam, K., Kafri, R., Loewer, A., and Lahav, G. (2012). Quantitative live cell imaging reveals a gradual shift between DNA repair mechanisms and a maximal use of HR in mid S phase. Mol Cell *47*, 320-329.
Karanja, K.K., Cox, S.W., Duxin, J.P., Stewart, S.A., and Campbell, J.L. (2012). DNA2 and EXO1 in replication-coupled, homology-directed repair and in the interplay between HDR and the FA/BRCA network. Cell cycle *11*, 3983-3996.

Karmakar, P., Snowden, C.M., Ramsden, D.A., and Bohr, V.A. (2002). Ku heterodimer binds to both ends of the Werner protein and functional interaction occurs at the Werner N-terminus. Nucleic acids research *30*, 3583-3591.
Kass, E.M., and Jasin, M. (2010). Collaboration and competition between DNA double-strand break repair pathways. FEBS letters *584*, 3703-3708.
Klungland, A., Rosewell, I., Hollenbach, S., Larsen, E., Daly, G., Epe, B., Seeberg, E., Lindahl, T., and Barnes, D.E. (1999). Accumulation of premutagenic DNA lesions in mice defective in removal of oxidative base damage. Proc Natl Acad Sci U S A *96*, 13300-13305.
Krejci, L., Van Komen, S., Li, Y., Villemain, J., Reddy, M.S., Klein, H., Ellenberger, T., and Sung, P. (2003). DNA helicase Srs2 disrupts the Rad51 presynaptic filament. Nature *423*, 305-309.
Kumagai, A., Lee, J., Yoo, H.Y., and Dunphy, W.G. (2006). TopBP1 activates the ATR-ATRIP complex. Cell *124*, 943-955.
Lee, J., Kumagai, A., and Dunphy, W.G. (2007). The Rad9-Hus1-Rad1 checkpoint clamp regulates interaction of TopBP1 with ATR. The Journal of biological chemistry *282*, 28036-28044.
Li, B., and Comai, L. (2000). Functional interaction between Ku and the werner syndrome protein in DNA end processing. The Journal of biological chemistry *275*, 28349-28352.
Liao, S., Toczylowski, T., and Yan, H. (2008). Identification of the Xenopus DNA2 protein as a major nuclease for the 5'->3' strand-specific processing of DNA ends. Nucleic acids research *36*, 6091-6100.
Liberti, S.E., Andersen, S.D., Wang, J., May, A., Miron, S., Perderiset, M., Keijzers, G., Nielsen, F.C., Charbonnier, J.B., Bohr, V.A.*, et al.* (2010). Bi-directional routing of DNA mismatch repair protein human exonuclease 1 to replication foci and DNA double strand breaks. DNA repair *10*, 73-86.
Lieber, M.R. (2010). The mechanism of double-strand DNA break repair by the nonhomologous DNA end-joining pathway. Annual review of biochemistry *79*, 181-211.
Lisby, M., Barlow, J.H., Burgess, R.C., and Rothstein, R. (2004). Choreography of the DNA damage response: spatiotemporal relationships among checkpoint and repair proteins. Cell *118*, 699-713.
Liu, S., Opiyo, S.O., Manthey, K., Glanzer, J.G., Ashley, A.K., Amerin, C., Troksa, K., Shrivastav, M., Nickoloff, J.A., and Oakley, G.G. (2012). Distinct roles for DNA-PK, ATM and ATR in RPA phosphorylation and checkpoint activation in response to replication stress. Nucleic acids research *40*, 10780-10794.
Liu, Y., and Wilson, S.H. (2012). DNA base excision repair: a mechanism of trinucleotide repeat expansion. Trends in biochemical sciences *37*, 162-172.
Longhese, M.P., Bonetti, D., Manfrini, N., and Clerici, M. (2010). Mechanisms and regulation of DNA end resection. The EMBO journal *29*, 2864-2874.
Lyndaker, A.M., and Alani, E. (2009). A tale of tails: insights into the coordination of 3' end processing during homologous recombination. Bioessays *31*, 315-321.

Maga, G., Crespan, E., Wimmer, U., van Loon, B., Amoroso, A., Mondello, C., Belgiovine, C., Ferrari, E., Locatelli, G., Villani, G.*, et al.* (2008). Replication protein A and proliferating cell nuclear antigen coordinate DNA polymerase selection in 8-oxo-guanine repair. Proc Natl Acad Sci U S A *105*, 20689-20694.

Maga, G., Villani, G., Crespan, E., Wimmer, U., Ferrari, E., Bertocci, B., and Hubscher, U. (2007). 8-oxo-guanine bypass by human DNA polymerases in the presence of auxiliary proteins. Nature *447*, 606-608.

Matos, J., Blanco, M.G., Maslen, S., Skehel, J.M., and West, S.C. (2011). Regulatory control of the resolution of DNA recombination intermediates during meiosis and mitosis. Cell *147*, 158-172.

McVey, M., and Lee, S.E. (2008). MMEJ repair of double-strand breaks (director's cut): deleted sequences and alternative endings. Trends in genetics : TIG *24*, 529-538.

Mimitou, E.P., and Symington, L.S. (2008). Sae2, Exo1 and Sgs1 collaborate in DNA double-strand break processing. Nature *455*, 770-774.

Mitchel, K., Zhang, H., Welz-Voegele, C., and Jinks-Robertson, S. (2010). Molecular structures of crossover and noncrossover intermediates during gap repair in yeast: implications for recombination. Mol Cell *38*, 211-222.

Mladenov, E., and Iliakis, G. (2011). Induction and repair of DNA double strand breaks: the increasing spectrum of non-homologous end joining pathways. Mutation research *711*, 61-72.

Mordes, D.A., Glick, G.G., Zhao, R., and Cortez, D. (2008). TopBP1 activates ATR through ATRIP and a PIKK regulatory domain. Genes Dev *22*, 1478-1489.

Nassif, N., Penney, J., Pal, S., Engels, W.R., and Gloor, G.B. (1994). Efficient copying of nonhomologous sequences from ectopic sites via P-element-induced gap repair. Molecular and cellular biology *14*, 1613-1625.

Nimonkar, A.V., Genschel, J., Kinoshita, E., Polaczek, P., Campbell, J.L., Wyman, C., Modrich, P., and Kowalczykowski, S.C. (2011). BLM-DNA2-RPA-MRN and EXO1-BLM-RPA-MRN constitute two DNA end resection machineries for human DNA break repair. Genes Dev *25*, 350-362.

Niu, H., Chung, W.H., Zhu, Z., Kwon, Y., Zhao, W., Chi, P., Prakash, R., Seong, C., Liu, D., Lu, L.*, et al.* (2010). Mechanism of the ATP-dependent DNA end-resection machinery from Saccharomyces cerevisiae. Nature *467*, 108-111.

Olson, E., Nievera, C.J., Klimovich, V., Fanning, E., and Wu, X. (2006). RPA2 is a direct downstream target for ATR to regulate the S-phase checkpoint. The Journal of biological chemistry *281*, 39517-39533.

Pabla, N., Ma, Z., McIlhatton, M.A., Fishel, R., and Dong, Z. (2011). hMSH2 recruits ATR to DNA damage sites for activation during DNA damage-induced apoptosis. The Journal of biological chemistry *286*, 10411-10418.

Palitti, F. (1993). Mechanism of induction of chromosomal aberrations by inhibitors of DNA topoisomerases. Environ Mol Mutagen *22*, 275-277.

Paques, F., and Haber, J.E. (1999). Multiple pathways of recombination induced by double-strand breaks in Saccharomyces cerevisiae. Microbiology and molecular biology reviews : MMBR *63*, 349-404.
Parvathaneni, S., Stortchevoi, A., Sommers, J.A., Brosh, R.M., Jr., and Sharma, S. (2013). Human RECQ1 interacts with Ku70/80 and modulates DNA end-joining of double-strand breaks. PloS one *8*, e62481.
Petermann, E., and Helleday, T. (2010). Pathways of mammalian replication fork restart. Nature reviews. Molecular cell biology *11*, 683-687.
Pichierri, P., Franchitto, A., Piergentili, R., Colussi, C., and Palitti, F. (2001). Hypersensitivity to camptothecin in MSH2 deficient cells is correlated with a role for MSH2 protein in recombinational repair. Carcinogenesis *22*, 1781-1787.
Sallmyr, A., Tomkinson, A.E., and Rassool, F.V. (2008). Up-regulation of WRN and DNA ligase IIIalpha in chronic myeloid leukemia: consequences for the repair of DNA double-strand breaks. Blood *112*, 1413-1423.
San Filippo, J., Sung, P., and Klein, H. (2008). Mechanism of eukaryotic homologous recombination. Annual review of biochemistry *77*, 229-257.
Sartori, A.A., Lukas, C., Coates, J., Mistrik, M., Fu, S., Bartek, J., Baer, R., Lukas, J., and Jackson, S.P. (2007). Human CtIP promotes DNA end resection. Nature *450*, 509-514.
Schwendener, S., Raynard, S., Paliwal, S., Cheng, A., Kanagaraj, R., Shevelev, I., Stark, J.M., Sung, P., and Janscak, P. (2010). Physical interaction of RECQ5 helicase with RAD51 facilitates its anti-recombinase activity. The Journal of biological chemistry *285*, 15739-15745.
Shiotani, B., Nguyen, H.D., Hakansson, P., Marechal, A., Tse, A., Tahara, H., and Zou, L. (2013). Two distinct modes of ATR activation orchestrated by Rad17 and Nbs1. Cell Rep *3*, 1651-1662.
Simandlova, J., Zagelbaum, J., Payne, M.J., Chu, W.K., Shevelev, I., Hanada, K., Chatterjee, S., Reid, D.A., Liu, Y., Janscak, P.*, et al.* (2013). FBH1 helicase disrupts RAD51 filaments in vitro and modulates homologous recombination in mammalian cells. The Journal of biological chemistry *288*, 34168-34180.
Singleton, M.R., Dillingham, M.S., and Wigley, D.B. (2007). Structure and mechanism of helicases and nucleic acid translocases. Annual review of biochemistry *76*, 23-50.
Sinicrope, F.A., and Sargent, D.J. (2012). Molecular pathways: microsatellite instability in colorectal cancer: prognostic, predictive, and therapeutic implications. Clinical cancer research : an official journal of the American Association for Cancer Research *18*, 1506-1512.
Sugawara, N., Ira, G., and Haber, J.E. (2000). DNA length dependence of the single-strand annealing pathway and the role of Saccharomyces cerevisiae RAD59 in double-strand break repair. Molecular and cellular biology *20*, 5300-5309.
Symington, L.S., and Gautier, J. (2011). Double-strand break end resection and repair pathway choice. Annual review of genetics *45*, 247-271.

Takahashi, M., Koi, M., Balaguer, F., Boland, C.R., and Goel, A. (2011). MSH3 mediates sensitization of colorectal cancer cells to cisplatin, oxaliplatin, and a poly(ADP-ribose) polymerase inhibitor. The Journal of biological chemistry *286*, 12157-12165.
Takao, M., Zhang, Q.M., Yonei, S., and Yasui, A. (1999). Differential subcellular localization of human MutY homolog (hMYH) and the functional activity of adenine:8-oxoguanine DNA glycosylase. Nucleic acids research *27*, 3638-3644.
Thorslund, T., McIlwraith, M.J., Compton, S.A., Lekomtsev, S., Petronczki, M., Griffith, J.D., and West, S.C. (2010). The breast cancer tumor suppressor BRCA2 promotes the specific targeting of RAD51 to single-stranded DNA. Nat Struct Mol Biol *17*, 1263-1265.
Toczylowski, T., and Yan, H. (2006). Mechanistic analysis of a DNA end processing pathway mediated by the Xenopus Werner syndrome protein. The Journal of biological chemistry *281*, 33198-33205.
Tomimatsu, N., Mukherjee, B., Deland, K., Kurimasa, A., Bolderson, E., Khanna, K.K., and Burma, S. (2012). Exo1 plays a major role in DNA end resection in humans and influences double-strand break repair and damage signaling decisions. DNA repair *11*, 441-448.
Uringa, E.J., Youds, J.L., Lisaingo, K., Lansdorp, P.M., and Boulton, S.J. (2011). RTEL1: an essential helicase for telomere maintenance and the regulation of homologous recombination. Nucleic acids research *39*, 1647-1655.
van Gent, D.C., and van der Burg, M. (2007). Non-homologous end-joining, a sticky affair. Oncogene *26*, 7731-7740.
van Loon, B., and Hubscher, U. (2009). An 8-oxo-guanine repair pathway coordinated by MUTYH glycosylase and DNA polymerase lambda. Proc Natl Acad Sci U S A *106*, 18201-18206.
van Loon, B., Markkanen, E., and Hubscher, U. (2010). Oxygen as a friend and enemy: How to combat the mutational potential of 8-oxo-guanine. DNA repair *9*, 604-616.
van Oers, J.M., Edwards, Y., Chahwan, R., Zhang, W., Smith, C., Pechuan, X., Schaetzlein, S., Jin, B., Wang, Y., Bergman, A.*, et al.* (2013). The MutSbeta complex is a modulator of p53-driven tumorigenesis through its functions in both DNA double-strand break repair and mismatch repair. Oncogene.
Vassin, V.M., Anantha, R.W., Sokolova, E., Kanner, S., and Borowiec, J.A. (2009). Human RPA phosphorylation by ATR stimulates DNA synthesis and prevents ssDNA accumulation during DNA-replication stress. J Cell Sci *122*, 4070-4080.
Vassin, V.M., Wold, M.S., and Borowiec, J.A. (2004). Replication protein A (RPA) phosphorylation prevents RPA association with replication centers. Molecular and cellular biology *24*, 1930-1943.
Von Kobbe, C., May, A., Grandori, C., and Bohr, V.A. (2004). Werner syndrome cells escape hydrogen peroxide-induced cell proliferation arrest. FASEB journal : official publication of the Federation of American Societies for Experimental Biology *18*, 1970-1972.
von Zglinicki, T. (2002). Oxidative stress shortens telomeres. Trends in biochemical sciences *27*, 339-344.

Wang, W., Seki, M., Narita, Y., Nakagawa, T., Yoshimura, A., Otsuki, M., Kawabe, Y., Tada, S., Yagi, H., Ishii, Y.*, et al.* (2003). Functional relation among RecQ family helicases RecQL1, RecQL5, and BLM in cell growth and sister chromatid exchange formation. Molecular and cellular biology *23*, 3527-3535.
Wang, Y., and Qin, J. (2003). MSH2 and ATR form a signaling module and regulate two branches of the damage response to DNA methylation. Proc Natl Acad Sci U S A *100*, 15387-15392.
Wang, Z., Rhee, D.B., Lu, J., Bohr, C.T., Zhou, F., Vallabhaneni, H., de Souza-Pinto, N.C., and Liu, Y. (2010). Characterization of oxidative guanine damage and repair in mammalian telomeres. PLoS genetics *6*, e1000951.
Wechsler, T., Newman, S., and West, S.C. (2011). Aberrant chromosome morphology in human cells defective for Holliday junction resolution. Nature *471*, 642-646.
Wu, L., Davies, S.L., Levitt, N.C., and Hickson, I.D. (2001). Potential role for the BLM helicase in recombinational repair via a conserved interaction with RAD51. The Journal of biological chemistry *276*, 19375-19381.
Wu, L., and Hickson, I.D. (2003). The Bloom's syndrome helicase suppresses crossing over during homologous recombination. Nature *426*, 870-874.
Wu, Y., Kantake, N., Sugiyama, T., and Kowalczykowski, S.C. (2008). Rad51 protein controls Rad52-mediated DNA annealing. The Journal of biological chemistry *283*, 14883-14892.
Yan, H., McCane, J., Toczylowski, T., and Chen, C. (2005). Analysis of the Xenopus Werner syndrome protein in DNA double-strand break repair. J Cell Biol *171*, 217-227.
Yang, H., Clendenin, W.M., Wong, D., Demple, B., Slupska, M.M., Chiang, J.H., and Miller, J.H. (2001). Enhanced activity of adenine-DNA glycosylase (Myh) by apurinic/apyrimidinic endonuclease (Ape1) in mammalian base excision repair of an A/GO mismatch. Nucleic acids research *29*, 743-752.
Zhu, Z., Chung, W.H., Shim, E.Y., Lee, S.E., and Ira, G. (2008). Sgs1 helicase and two nucleases Dna2 and Exo1 resect DNA double-strand break ends. Cell *134*, 981-994.
Zimmermann, M., and de Lange, T. (2014). 53BP1: pro choice in DNA repair. Trends in cell biology *24*, 108-117.
Zimmermann, M., Lottersberger, F., Buonomo, S.B., Sfeir, A., and de Lange, T. (2013). 53BP1 regulates DSB repair using Rif1 to control 5' end resection. Science *339*, 700-704.
Zou, L., Cortez, D., and Elledge, S.J. (2002). Regulation of ATR substrate selection by Rad17-dependent loading of Rad9 complexes onto chromatin. Genes Dev *16*, 198-208.
Zou, L., and Elledge, S.J. (2003). Sensing DNA damage through ATRIP recognition of RPA-ssDNA complexes. Science *300*, 1542-1548.